Targeting AMACR to treat castrate-resistant prostate cancer

Lee, Guat Ling

Award date:
2016

Awarding institution:
University of Bath

Targeting AMACR to treat castrate-resistant prostate cancer

Guat Ling Lee

A thesis submitted for the degree of Doctor of Philosophy

University of Bath
Department of Pharmacy and Pharmacology

March 2016

Table of contents

List of Figures

List of Schemes

List of Tables

Acknowledgement

I would like to express my immense gratitude to my supervisors, Dr Matthew Lloyd and Dr Timothy Woodman. I am very thankful for their advice in my work, training and guidance in laboratories and constant support throughout my PhD. I would also like to thank my group member, Dr Maksim Yevglevskis for helpful discussions and assistance in the laboratory. I am grateful for helpful advice from Dr Gyles Cozier regarding site-directed mutagenesis and valuable discussions with Professor Michael Threadgill and Dr Amit Nathubhai regarding synthetic chemistry.

I would like to acknowledge Professor Paul Groundwater, Dr Maksim Yevglevskis, Dr Daniel Darley and Dr Xiaolong Sun for compounds that they have provided for my PhD work. I appreciate the generosity of those allowing my access to equipments in their labs, including Professor Rex Tyrrell for his GeneGenius bio-imaging system, Dr Ian Eggleston for his freeze dryer (first year of my PhD), Dr Paul De Bank for his freeze dryer (second and third year of my PhD) and his plate reader, Professor Stephen Husbands for his CombiFlash automated purification system (and Dr Gerta Cami-Kobeci for the training), Professor Tony James for his fluorescence spectrometer and the Chemical Engineering Department for the dynamic light scattering analyser.

I appreciate the help of Dr Anneke Lubben regarding mass spectrometry queries. I would like to thank 4th year MPharm project students (Jean Monaghan and Simon Vas) and summer placement students (Ella Nash, Becky Walshe, Shiyi Zhou, Nicolas Christodoulou and Yoana Petrova) for their input to my work. I am very grateful to receive the University of Bath Overseas Research Scholarship so that I can complete my PhD.

I would like to thank my parents and my brothers who always believe in me and have been nothing other than supportive. Finally, a big thank you to my wonderful husband, Starkey Chan, who is so loving, has gone through many ups and downs with me and always stood by me. Without him, I could not have done this. This thesis is dedicated to my family and my husband.

Abstract

Levels of the enzyme α-methylacyl-CoA racemase (AMACR) are increased *ca.* 9-fold in prostate cancer cells. AMACR is a very promising novel drug target as reducing AMACR levels converts castrate-resistant prostate cancer cells to androgen-dependent cells which will respond to androgen-deprivation. Despite the importance of AMACR in prostate and other cancers, there are very limited numbers of AMACR inhibitors described to-date. This is mainly due to the absence of a high-throughput assay for the screening of inhibitors against AMACR. The active-site residues and catalytic mechanism of human AMACR are still unknown, which make the rational design of drugs targeting AMACR very difficult. A range of novel potential inhibitors were synthesised using a rational drug design approach to explore the structure-activity relationship (SAR) on the side-chains of AMACR inhibitors. Their potencies were assessed using the fluoride elimination assay based on ^{1}H and ^{19}F NMR. Potency, mode of binding and kinetic parameters of these inhibitors were assessed using the multi-well colorimetric assay, which is the first AMACR high-throughput continuous assay reported to-date. A site-directed mutagenesis study was carried out to identify the active-site residues and catalytic mechanism of human AMACR. His-122, Asp-152, Met-184 and Glu-237 were identified as potential active-site residues, so the cDNA was mutated and expressed. The activity of wild-type and mutant AMACR enzymes were assessed using the deuterium wash-in, fluoride elimination and multi-well colorimetric assays. Results from these assays showed that human AMACR does not operate using a 'two-base' mechanism. Instead, it operates using a 'one-base' mechanism, most likely *via* water molecules acting as intermediaries within the hydrogen-bondings network in the active site. The knowledge obtained from this research informs rational drug design for this castrate-resistant prostate cancer target.

List of abbreviations

2-APA	2-Arylpropanoic acid
ACOT	Acyl-CoA thioesterase
AMACR	α-Methylacyl-CoA racemase a.k.a. P504S
ANS	8-Anilino-1-naphthalenesulfonic acid
BPH	Benign prostatic hyperplasia
CD	Circular dichroism
CDI	1,1'-Carbonyldiimidazole
CoA	Coenzyme A
COSY	Correlation spectroscopy
COX	Cyclooxygenase
DAST	(Diethylamino)sulfur trifluoride
dATP	2' Deoxyadenosine 5'-triphosphate
DCC	Dicyclohexylcarbodiimide
DCM	Dichloromethane
DEAD	Diethyl azodicarboxylate
DIBAL	Diisobutylaluminum hydride
DHT	5α-Dihydrotestosterone
DLS	Dynamic light scattering
DMAP	4-(Dimethylamino)pyridine
DME	1,2-Dimethoxyethane
DMF	*N*,*N*-Dimethylformamide
DMPMB	2-(2,5-Dihydroxy-4-methylphenyl)-5-methyl benzene-1,4-diol
DMSO	Dimethyl sulfoxide
dNTPs	Deoxyribonucleotide triphosphates
DRE	Digital rectal examination
EBRT	External beam radiotherapy
E. coli	*Escherichia coli*
EDTA	Ethylenediaminetetraacetic acid
ESI-TOF	Electrospray ionisation time-of-flight
Et_2O	Diethyl ether
EtOAc	Ethyl acetate
FDA	Food and Drug Administration
GLC	Gas-liquid chromatography
GnRH	Gonadotrophin-releasing hormone
HEPES	4-(2-Hydroxyethyl)piperazine-1-ethanesulfonic acid
HMBC	Heteronuclear multiple bond correlation spectroscopy
HPLC	High-performance liquid chromatography
HSQC	Heteronuclear single-quantum correlation spectroscopy
IGF-1	Insulin-like growth factor 1

IPTG	Isopropyl β-*D*-1-thiogalactopyranoside
IR	Infra-red
KLD	Kinase, ligase and *Dpn*I
KOAc-HOAc	Potassium acetate-acetic acid
LB	Lennox Luria-Bertani media
LacI	Lac repressor
LACS	Long-chain acyl-CoA synthetase
LHRH	Luteinising hormone-releasing hormone
MCR	2-Methylacyl-CoA racemase from *Mycobacterium tuberculosis*
Me	Methyl
NMR	Nuclear magnetic resonance
NOESY	Nuclear Overhauser effect spectroscopy
NSAID	Non-steroidal anti-inflammatory drug
PCR	Polymerase chain reaction
PE	Petroleum ether 40-60 °C
PET	Photoinduced electron transfer
pMFE-1	Peroxisomal multifunctional enzyme type 1
PMSF	Phenylmethanesulfonyl fluoride
PSA	Prostate-specific antigen
PTS1	Peroxisomal targeting signal-1
r.p.m.	Revolutions per minute
rt	Room temperature
SAR	Structure-activity relationship
SDS	Sodium dodecyl sulfate
SDS-PAGE	Sodium dodecyl sulfate-polyacrylamide gel electrophoresis
SNP	Single nucleotide polymorphism
SPE	Solid phase extraction
T2WI	T2-weighted magnetic resonance imaging
TAE	Tris-acetate-EDTA
TBAF	Tetrabutylammonium fluoride
TBDPSCl	*tert*-Butyl(chloro)diphenylsilane
TCA	Trichloroacetic acid
TEMED	Tetramethylethylenediamine
THCA	Trihydroxycholestanoic acid
THF	Tetrahydrofuran
TLC	Thin layer chromatography
Tris	Tris(hydroxymethyl)aminomethane
UV	Ultraviolet
WT	Wild-type

Description of the AMACR ‘racemisation’ reaction

Conventionally racemisation refers to the process of converting an enantiomerically pure compound to a racemic mixture of *R*- and *S*-compounds. AMACR is an enzyme that catalyses the conversion of a single chiral centre (at the 2-methyl position) of *R*- or *S*- configuration to a near 1:1 mixture of ‘epimers’,[1, 2] while all other chiral centres of the acyl-CoA moiety are unaffected. The conventional definition of racemisation would require production of a 1:1 mixture of all chiral centres, which is clearly not that case for AMACR. However, the AMACR catalysed reaction should not be called epimerisation either because even though only one chiral centre is involved, it is not converted to the opposite configuration (from *R*- to *S*- configuration or *vice versa*); rather the end product is a nearly 1:1 racemic mixture. Hence, the reaction performed by AMACR is referred to as ‘racemisation’,[3] implying change of stereochemical configuration only at the centre bearing the 2-methyl group and will be used as such in this thesis.

Syn- and *anti*- terminology

The *syn*- and *anti*- terminology refer to the relative orientations of the fluorine atom and methyl group of 3-fluoro-2-methyldecanoyl-CoAs. *Syn*- refers to these two groups at the same direction, whilst *anti*- refers to them at the opposite direction.

1 Introduction

1.1 The prostate

The prostate is a tubulo-alveolar gland that belongs to the male reproductive system. Following the production of testosterone from the foetus's testes at the 8th week of gestation, the prostate forms 2 weeks later. The prostate starts from solid outgrowths of the urethral epithelium upon signalling by 5α-dihydrotestosterone (DHT).[4] These solid outgrowths develop into specialised tissues with distinct functions in the prostate and continue developing during gestation. The prostate weighs a few grams at birth and continues to grow to approximately 20 g in a young male adult.[5]

The prostate has a 'walnut' shape and is located at the neck of the bladder (Figure 1.1). The urethra runs from the bladder and goes through the centre of the prostate. During ejaculation, the prostate secretes its contents into the urethra which mixes with the sperm and secretions from the seminal vesicle.[6]

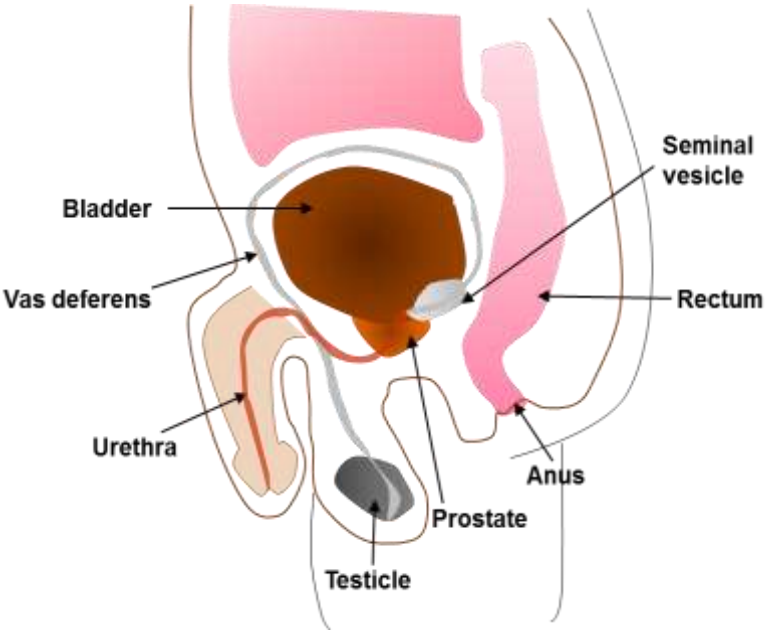

Figure 1.1: The location of the prostate as part of the male reproductive system. This diagram is not to actual scale but an illustration of the approximate positions of the organs.

1.2 Functions of the prostate

The prostate plays an important role in facilitating fertility. It produces a range of molecules and enzymes including fibrinolysin and coagulase which are

involved in the coagulation of the ejaculate[5] and proteases such as prostate-specific antigen (PSA) which help to break down the seminal coagulum.[6] As the seminal fluid is slightly alkaline, it neutralises the acidity of the urethra and vagina, and ensures the survival of spermatozoa.[5] Glycoproteins in the seminal fluid have a lubricating property which could improve sperm motility.[6] The prostatic fluid also has a high zinc content which acts as an antibacterial agent. The acid phosphatase enzyme produced by the prostate is involved in the conversion of phosphorylcholine to choline, which is a nutrient source for spermatozoa.[5] As the urethra passes through the prostate, it also plays a role in the transmission of seminal fluid and in controlling urine output (which can result in urinary problems with the enlargement of prostate). The prostate also has an endocrine function, where its 5α-reductase enzyme converts testosterone to DHT, a more potent hormone with a greater affinity for androgen receptors.[5, 7]

1.3 Prostate conditions

There are some common prostate problems, such as prostatitis, benign prostatic hyperplasia (BPH) and prostate cancer.

1.3.1 Prostatitis

Prostatitis refers to the inflammation of the prostate. This condition affects about 10% of the male population with the majority of those affected in their 40s.[8] Prostatitis can be classified into four categories, where category I is acute bacterial prostatitis; category II is chronic bacterial prostatitis; category III is chronic pelvic pain syndrome which is sub-divided into IIIa (inflammatory) and IIIb (non-inflammatory) and lastly category IV which is asymptomatic inflammatory prostatitis.[9] Acute bacterial prostatitis can be easily treated with antibiotics.[8, 9] The first line treatment for chronic prostatitis is an α-adrenergic antagonist such as tamsulosin and alfuzosin for patients with slow urinary flow.[10] The choice of antibiotics will depend on the species of bacterial present in cultures and their antibiotic sensitivities.[10] Analgesics are often used for pain management.[10]

1.3.2 Benign prostatic hyperplasia (BPH)

BPH refers to the non-malignant enlargement of the prostate due to overgrowth of periurethral prostatic tissue.[11, 12] As mentioned previously, the urethra runs through the prostate, so that when the surrounding tissue of the prostate overgrows, it exerts extra pressure on the urethra and causes resistance to urinary flow. This leads to lower urinary tract symptoms such as difficulty in urination, a frequent urge to urinate and nocturia.[11] BPH is age-related; only 8% of men in their 30s experience it but about 90% of those aged 90 years do.[11] It can be managed medically with α-adrenergic antagonists (*e.g*. tamsulosin) or 5-α-reductase inhibitors (*e.g*. finasteride).[13] In severe cases, prostatectomy can be performed.[13]

1.3.3 Prostate cancer

Prostate cancer is the most common cancer in males in most developed countries including the U.K. and is the second most common cancer worldwide.[14] Developed countries have a six times higher incidence of prostate cancer (56.2 cases per 100 000 population) in comparison to less developed countries (9.4 cases per 100 000 population).[14] In 2012, over 1.11 million men were diagnosed with prostate cancer worldwide and *ca.* 417 000 new diagnoses were in Europe alone.[15] After lung cancer, prostate cancer is the leading cause of cancer death in men.[15, 16] It caused 92 300 deaths in Europe in 2012[15] and 29 480 deaths in the U.S.A. in 2014.[16] Approximately one in six men will be diagnosed with prostate cancer in their lifetime.[17] The 5-year survival rate for men diagnosed with prostate cancer in England and Wales is 85% according to data from 2010-11.[15] As prostate cancer is an age-related condition, all men will eventually get histological prostate cancer if they live long enough.[18] Older men (66 years old and above) with localised prostate cancer are more likely to die with prostate cancer rather than die from prostate cancer.[19]

1.4 Risk factors of prostate cancer

Risk factors of developing prostate cancer include age, ethnicity, family history, genetics, diet and androgen hormone signalling.

1.4.1 Age

Prostate cancer is relatively rare in younger men, with the risk of 0.005% for those below 39 years old.[20] The risk increases with age, from 2.2% (40-59 years old) to 13.7% (60-79 years old).[20] Most cases (~85%) are diagnosed in patients over 65 years old.[21]

1.4.2 Ethnicity

African Americans have the highest risk of developing prostate cancer. Their risk of having prostate cancer is 61% higher than Caucasians, 68% higher than Hispanics and 72% higher than Asians.[22] African Americans are twice as likely to die from prostate cancer compared with Caucasians[23] and 5 times as likely compared with Asians.[22] It is not known whether the differences are purely due to an inherent difference from ethnicity, or whether cultural differences and socioeconomic status play a role.[23]

1.4.3 Family history and genetics

The risk of a man developing prostate cancer is increased by 2 times if one of his first-degree relatives (a father or brother) has a history of prostate cancer.[22, 24] This risk increases with the increase in the number of affected first-degree relatives. The man will have 5 to 11 times higher risk if 2 or 3 of his first-degree relatives have been affected.[24] Men also tend to develop prostate cancer at an earlier age (6-7 years earlier) when they have first-degree relatives with a history of prostate cancer compared to those without such family history.[22]

To determine whether genetics play a role, studies have been conducted to compare the concordance rates of prostate cancer (rates of both twins affected by prostate cancer) in monozygotic twins and dizygotic twins.[25, 26] It has been found that monozygotic twins tend to have a higher concordance rate (~27%) in comparison to dizygotic twins (~7%), suggesting that there are hereditary influences[25]

1.4.4 Diet

Japanese Americans have a higher risk of prostate cancer compared to Japanese males who live in their native land due to the influence of their diet.[22] The Western diet with high red meat intake and high dairy product consumption increase their risk of developing prostate cancer.[22] Red meats and dairy products are a rich source of branched-chain fatty acids and dietary levels are linked to the α-methylacyl-CoA racemase (AMACR) enzyme that is up-regulated in prostate cancer (*vide infra*).[21, 22] It has also been hypothesised that the preparation and cooking of meat at a high temperature could result in the production of carcinogens such as heterocyclic amines, which may increase the risk of developing prostate cancer.[21]

1.4.5 Hormones

Androgens are a class of hormones that bind to androgen receptors and include testosterone and its more potent metabolite, dihydrotestosterone (DHT).[27, 28] Androgen receptors are usually located at the cytoplasm.[29] Upon binding with the androgen, the receptor translocates into the nucleus and binds to the promoter region of the target genes.[29] The activation of the androgen receptor is important to allow cell proliferation during the growth of a normal prostate.[30]

However, increased androgen receptor activity has been associated with prostate cancer.[7, 29] It has been found that the receptor can bind to the promoter region of the TMPRSS2 gene.[31] This causes the rearrangement of the chromosome where the promoter region of TMPRSS2 gene fuses with oncogenic genes (ERG or ETV1).[31] The ERG and ETV1 transcription factors are over-expressed and lead to the progression of prostate cancer.[32, 33] Animal models have also shown that testosterone and DHT can induce the growth of prostate cancer.[21] The use of androgen-deprivation therapy supports the finding that prostate cancer cells are androgen-dependent in the early stages of the disease.[23, 34]

Insulin-like growth factor 1 (IGF-1) also plays a role in cancer cell proliferation and differentiation.[21] High levels have been associated with an increased risk

of prostate cancer.[35, 36] The activation of the IGF-1 receptor alters the phosphorylation state of the androgen receptor.[37] This assists the translocation of the androgen receptor from the cytoplasm into the nucleus for it to stimulate the growth of prostate cancer.[37]

1.5 Screening and diagnosis of prostate cancer

Initial examination of prostate cancer may involve the use of prostate cancer biomarkers and digital rectal examination.[38] Imaging and biopsy will be used to diagnose prostate cancer, and the biopsy will be staged and graded.[39, 40]

1.5.1 Prostate cancer biomarkers

Prostate-specific antigen (PSA) is a serine protease secreted by epithelial cells of the prostate.[6, 41] The function of PSA is to liquefy the seminal coagulum upon ejaculation.[6] Together with digital rectal examination, PSA has been an approved screening tool for prostate cancer in the U.S.A since 1994.[38] As PSA levels vary among men and change with age, there is no single PSA value that is considered to be the 'normal' value. As a rule of thumb, serum PSA levels that are below 4 ng mL^{-1} are considered as normal and elevated levels may indicate prostate cancer.[38, 41] Even though PSA is still the most common biomarker for the detection of prostate cancer, it carries a few limitations. Some patients may have prostate cancer even though their serum PSA levels are below 4 ng $mL^{-1.}$ With PSA levels of 1.1-2.0 ng mL^{-1}, patients have 17% prostate cancer risk, and this risk is increased to 24% with PSA levels of 2.1-3.0 ng mL^{-1} and 27% with PSA levels of 3.1-4.0 ng mL^{-1}.[42, 43] Increased PSA levels are not specific to prostate cancer and may be raised in non-malignant conditions such as BPH and prostatitis.[38] PSA levels are increased in only 20% of prostate cancer cases but high levels are detected in 30-50% of BPH cases.[38] To make the matter worse, a large proportion of prostate cancers detected are microscopic and may not result in a clinically significant condition.[41] If treatment is merely based on raised PSA levels, it will result in over-diagnosis and unnecessary treatment. Routine screening of prostate cancer using PSA has been controversial as there has been a high number of over-diagnosed prostate cancer cases in Western countries, such as the

U.S.A.[44, 45] PSA screening is currently not recommended in Europe as the risks outweigh the benefits.[42]

Other potential prostate cancer markers include the urokinase plasminogen activator (a protein that is involved in metastasis by degrading the extracellular matrix),[38] human kallikrein 2 (a serine protease that is closely related to PSA), transforming growth factor-beta 1 (a growth factor that is involved in the proliferation and differentiation of cancer cells) and interleukin-6 (a cytokine that is involved in immune responses).[46] Even though these proteins have been shown to be involved in cancer mechanisms and could be potential biomarkers for prostate cancer, they have not been extensively validated and are not currently used in clinical settings.[46]

Another very promising prostate cancer marker is the enzyme α-methylacyl-CoA racemase (AMACR; P504S). AMACR levels are increased *ca.* 9-fold in prostate cancer cells compared to normal cells at both protein and mRNA levels.[47-49] Immunocytochemical analysis conducted by Jiang *et al.* showed 100% positive staining for P504S in prostate cancer cells and only 12% of benign prostate cells were stained positive for P504S.[50] Honma *et al.* subsequently showed positive staining in *ca.* 70% of prostate cancer cells and negative staining in normal cells (Figure 1.2).[51] As P504S is not raised in benign prostate conditions, it is a better prostate cancer biomarker compared to PSA.[50, 51] It is highly sensitive and specific, and has been used clinically to help with prostate cancer diagnosis. Immunostaining of P504S on prostate needle biopsy (*vide infra*) can be used as an adjuvant diagnostic tool for ambiguous specimens, to differentiate between malignant prostate cancer from benign lesions.[52-55]

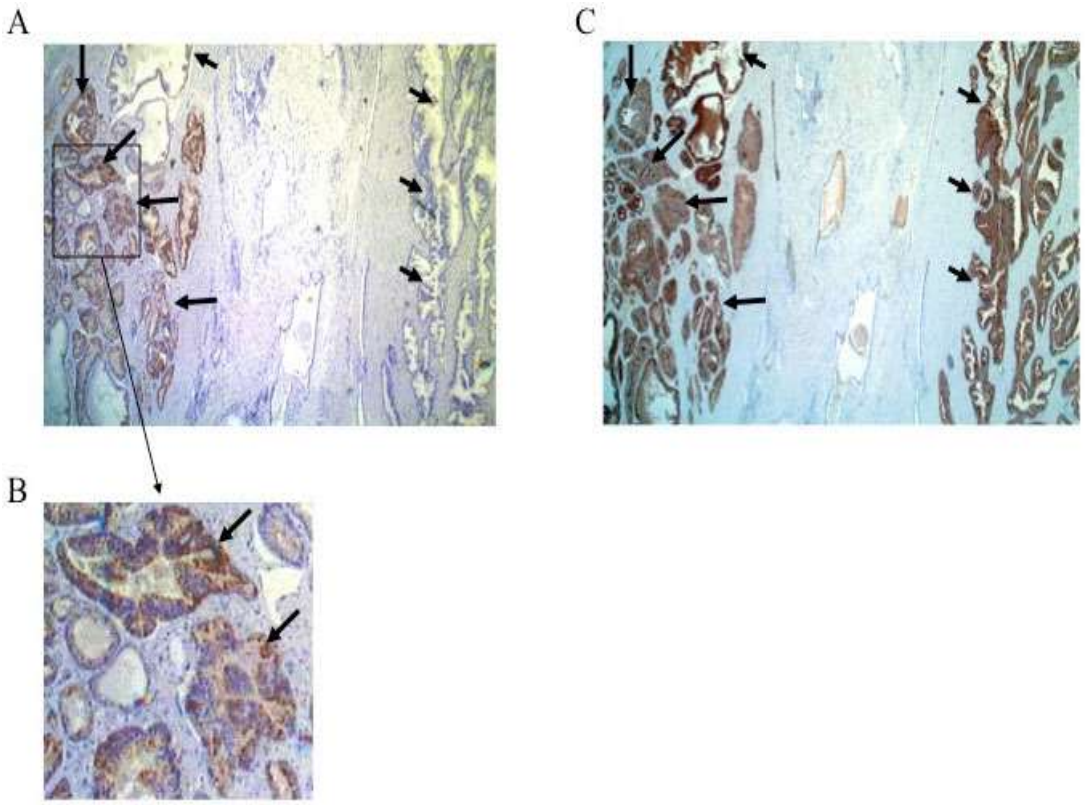

Figure 1.2: Immunostaining performed by Honma *et al*.[51]: panel A was stained with anti-AMACR antibody and positive staining was shown in cancerous cells (long arrows) but negative staining was shown in non-cancerous cells (short arrows). Panel B was the magnified picture for cancerous cells stained positive by anti-AMACR antibody. Panel C was stained with anti-PSA antibody and both cancerous cells (long arrows) and non-cancerous cells (short arrows) were stained.

1.5.2 Digital rectal examination (DRE)

Examination of the prostate is carried out by inserting the index finger into the rectum and each lobe of prostate (anterior, posterior, medial and two lateral lobes) is physically examined for any irregularities.[56] This method of detection is relatively insensitive as early-stage cancer is usually small and not easily palpated.[56, 57] When DRE is combined with PSA, the detection rate improves.[58] However, the screening does not reduce the mortality rate from prostate cancer.[42]

1.5.3 Imaging and biopsy

If prostate cancer is suspected due to raised PSA levels and/or abnormal DRE results, a transrectal ultrasound (TRUS)-guided, systematic needle biopsy will

be performed.[59] The TRUS-guided biopsy has been proven to be a superior biopsy method compared to digital-guided biopsy and it is currently the standard method for the diagnosis of prostate cancer.[59] The procedure is performed under local anaesthetic and a set of systematic, laterally directed biopsy (at least 10-core biopsies) are taken and sent for analysis.[42, 59] These samples will be graded and assigned a Gleason score (*vide infra*).[42] A 10-core biopsy misses about 22% cases of cancer and a re-biopsy still misses about 10% cases of cancer.[59] The T2-weighted magnetic resonance imaging (T2WI) gives good anatomical images of the gland and improves the performance of prostate cancer examination.[60] Dynamic contrast-enhanced imaging and diffusion-weighted imaging has been used to augment T2WI to give a more accurate diagnosis.[60, 61]

1.6 Staging and grading

The tumour, node, and metastasis (TNM) classification system by the American Joint Committee on Cancer (AJCC) is commonly used to stage prostate cancer.[39] All three categories, T, N and M are given a score where the higher the score is, the more advanced the disease is. The T category is to determine the local extent of a prostate tumour: T1 is a tumour that is not detectable clinically or *via* imaging while T4 is a tumour that invades adjacent tissues.[39, 41] The N category is to decide the involvement of regional lymph nodes: N0 is when regional lymph nodes are not involved and N3 is when metastasis occurs in a lymph node and is greater than 5 cm.[39] The M category is to decide whether there is distant metastasis: M0 is when there is no distant metastasis and M1 is when a distant metastasis occurs.[39] Most categories are divided into sub-categories (a, b and c) in order further classify the tumour.[39] It is essential to stage the disease in order to predict the prognosis of the disease and to decide the best treatment option for the patient.[41]

Prostate cancer biopsy samples will be graded with Gleason score based on their histologic features examined under microscopes. Gleason scores range from 1 to 5, where 1 corresponds to uniform and very well differentiated cancerous cells and 5 corresponds to the most poorly differentiated cells.[40] Pattern 3 (moderately differentiated cancerous cells) is the most commonly

observed pattern.[40] The most prevalent pattern in the biopsy will be graded as the primary pattern and the second most prevalent pattern will be graded as the secondary pattern. The primary and secondary pattern numbers will be combined to give a final Gleason score, which ranges from 2 to 10.[40] If multiple-core needle biopsies show different scores, they are now reported separately and the highest score is used to decide the treatment option.[62] The Gleason score correlates strongly with cancer survival where higher scores are associated with poorer prognosis.[40, 63]

1.7 Management of prostate cancer

The management of prostate cancer will be quite different, depending on the stage and prognosis of the cancer.

1.7.1 Active survelliance

Routine PSA screening has led to an increase in the number of prostate cancer cases detected. However, screening has also contributed to *ca.* 27-56% incidences of over-detection, where the disease is clinically insignicant and patient will usually have no symptoms even the condition is left untreated.[64] Elderly men that present a localised and low-grade tumour may be offered active survelliance instead of radical treatments.[64] This will prevent unnecesary treatments that do not increase their survival but lead to side-effects such as impotence and urinary incontinence.[65] These patients will be actively monitored and treatments will be commenced if their tumours show signs of disease progression (when there are increases in PSA levels or changes in the Gleason scores of biopsy samples).[64, 65]

1.7.2 Surgery

Radical prostatectomy is a common surgery for localised tumours (grade ≤T2c)[66] and involved the removal of the prostate, the seminal vesical and the ampulla of the vas.[41] High-risk prostate cancer patients will significantly benefit from radical prostatectomy as the 10-year cancer-specific mortality rate was only 5.2% after they have undergone the surgery.[67] This rate was significantly lower than the observation cohort which has a 12.8% cancer-specific mortality rate.[67] Modern technologies have reduced the mortality rate from the surgery

to as low as 0.3%.[41] However, erectile dysfunction and urinary incontinence are very common side-effects, affecting 30-70% of patients.[41]

1.7.3 Radiotherapy

Radical radiotherapy which includes external beam radiotherapy (EBRT) and brachytherapy is an alternative to radical prostatectomy for localised prostate cancer.[68] EBRT is effective for patients with prostate-confined disease but can also be used for patients with advanced disease (T3-T4) that has not metastasised.[68] The success rate correlates with the tumour stage where 72% of T1 patients but only 22% of T2 b and c patients been tumour-free after 12-year follow up.[41] While conventional radiotherapy delivers 60-70 Gy doses to the prostate, seminal vesicle and surrounding tissues, higher doses (160 Gy) can be delivered *via* brachytherapy.[41] Brachytherapy uses radioactive seeds (^{125}I or ^{103}Pd) which target prostate cancer cells directly and spare the surrounding normal tissues.[68] Hormonal therapy can be used as an adjunct to radiotherapy in order to shrink the tumour before radiotherapy and minimise toxicity caused by high radiation dose.[68]

1.7.4 Hormonal therapy

Hormonal therapy, also known as androgen-deprivation therapy, is the main form of treatment for advanced stage prostate cancer.[34] Orchiectomy is a surgical castration procedure where both testicles are removed to reduce the production of testesterone.[34] Castration can also be performed chemically where drugs such as anti-androgens, luteinising hormone-releasing hormone (LHRH) agonists and gonadotrophin-releasing hormone (GnRH) antagonists are used.[69] Anti-androgens are androgen receptor antagonists and they can be steroidal (such as cyproterone acetate) or non-steroidal (such as bicatulamide and flutamide).[69] LHRH agonists reduce the release of pitutary hormones which in turn reduce the production of testesterone. Examples of LHRH agonists include buserelin, goserelin and triptorelin.[69] They are usually given by subcutaneous or intramuscular injection every one to four months.[69] LHRH agonists can induce testosterone surges in the first two weeks of treatment and cause tumour flare.[69, 70] GnRH antagonists, such as degarelix,[71] represents the newest drug class and has the advantage of not inducing

tumour flare.[69] These treatments are not curative but they can induce remission in 80-90% cases of advanced stage prostate cancer.[34] Prostate cancer will develop a castrate-resistant phenotype usually within 2 to 3 years of treatment.[72] The prognosis of castrate-resistant prostate cancer is very poor and patients only live for 9 to 13 months if they have metastatic disease.[73]

1.7.5 Treatments for castrate-resistant prostate cancer

Chemotherapeutic agents such as docetaxel and cabazitaxel[72] and newer agents such as Sipuleucel-T, a cell-based cancer vaccine[74] are used for castrate-resistant prostate cancer. Drug resistance emerges rapidly and the condition will progress despite treatment.[72] Two-third of patients are reported to receive palliative care instead of active treatments.[73] Bisphosphonates, opioids and radiotherapy are used to manage skeletal-related pain.[73]

1.8 AMACR as a drug target for castrate-resistant prostate cancer

AMACR was identified as a drug target for castrate-resistant prostate cancer more than a decade ago.[47, 75] AMACR levels are increased *ca.* 9-fold in prostate cancer compared to normal cells.[47, 48] Increased levels of AMACR protein is associated with androgen-independent growth of prostate cancer but its exact mechanism is unknown.[48] It has been postulated that AMACR is involved in lipid metabolism (*vide infra*) and hence provides an alternative energy source for the growth of prostate cancer.[76] Another postulation is its role in peroxisomal β-oxidation which produces reactive oxygen species that damage DNA.[77]

Besides being over-expressed in prostate cancer, AMACR is also over-expressed in other types of cancer such as breast,[78, 79] colon,[80] ovarian[81] and renal cancers.[82, 83] It is unknown whether the over-expression of AMACR causes the occurrence or progression of these cancers.

It has been shown that inhibiting the activity of AMACR causes a significant change in the phenotype of castrate-resistant prostate cancer. A siRNA study was used to reduce the protein levels and it targeted AMACR 1A, which is the active spliced variant of AMACR (*vide infra*). The study showed that the

androgen receptor and B-cell translocation gene I protein levels were up-regulated when AMACR expression was suppressed.[84] Castrate-resistant prostate cancer cells reverted to being androgen-dependent and responsive to androgen-deprivation treatments again.[84] AMACR inhibition also slows down cancer cell growth,[85] which may be due to reduced expression of genes associated with cancer progression (such as IGF-1 and platelet-derived growth factor alpha).[84] This makes AMACR a very good drug target as a combination of anti-AMACR therapy with androgen-deprivation therapy could convert castrate prostate cancer into a more 'normal' phenotype and potentially cure the cancer or at least make it more treatable.[48, 84] In comparison to the traditional cytotoxic chemotherapy that kills all fast-growing cells, inhibiting AMACR shows a better treatment prospect due to it being a specific molecular target.

1.9 Subcellular distribution of AMACR

AMACR belongs to the family III CoA transferase.[86] The class III family can be broadly divided into CoA transferases or racemases, and AMACR belongs to the latter.[87-89] Besides humans,[90] AMACR has also been discovered in many other mammalian species such as rat[91] and mouse.[92] AMACR is highly conserved; for example, mouse and rat enzymes are 89.7% identical,[93] whilst the human enzyme is 81% and 77% identical to rat and mouse enzymes, respectively.[94]

The subcellular distributions of AMACR may vary depending on species even though the reasons for such variations are still unknown. 2-Arylpropionyl-CoA epimerase (which was later shown to be identical to AMACR)[95, 96] was reported to be localised in the cytosol and mitochondria of rats.[97] Later studies showed that even though the activity mainly comes from mitochondria, peroxisomes also contribute to some of the activity in rats.[98, 99] In mice, the enzyme is found to be distributed in both peroxisomes and mitochondria.[92] In humans, it has a preferential distribution in the peroxisome (75-90%) with the remainder found in mitochondria.[90] The C-terminus of human AMACR possesses the amino acid sequence KASL (Appendix 1), which is a peroxisomal targeting signal-1 (PTS1).[98] The N-terminus may be responsible

for targeting the mitochondria, but the exact targeting sequence has not been determined.[98, 100, 101] Zellweger's syndrome results from a defect in peroxisome biogenesis (*i.e*., peroxisomes are not formed).[102-105] The peroxisome-deficient cells retain 10-30% of AMACR activity, which is contributed by the mitochondria instead of peroxisomes, consistent with the observed distribution.[90]

Homologous enzymes of human AMACR have been found in bacteria and invertebrates. The 2-methylacyl-CoA racemase (MCR) from *Mycobacterium tuberculosis* (*vide infra*) shares 43% sequence identity with human AMACR (Appendix 1)[76, 85, 86] and has been used in many studies as a model for human AMACR.[106-108] A homologous enzyme was also found in the secretions of the larvae of a parasitic worm, *Anisakis simplex*.[109] The enzyme appears to play an important role in energy production to support the growth and development of the larvae.[109]

1.10 Function of AMACR in the body

AMACR is found in mitochondria and peroxisomes in humans[101] and is involved in the metabolism of branched-chain fatty acids.[110] Red meats such as beef and dairy products in the diet contain an abundance of phytanic acid (3*R*,*S*,7*R*,11*R*,15-tetramethylhexadecanoic acid), a branched-chain fatty acid.[111, 112] Phytanic acid is turned into phytanoyl-CoA **1** and is shortened by a one-carbon unit *via* α-oxidation to give pristanoyl-CoA (2*R*,*S*,6*R*,10*R*,14-tetramethylpentadecanoyl-CoA) (**2** and **3**) which undergoes further metabolism.[91, 111-113] Dehydrogenases in both peroxisomes and mitochondria that are involved in the subsequent β-oxidation pathway have been shown to have an absolute requirement for substrates to have *S*-stereochemical configuration at the centre bearing the 2-methyl group.[99, 114-117] The 2-methyl fatty acyl-CoA ester (pristanoyl-CoA) produced by α oxidation is a racemic mixture of *R*- and *S*- configurations at carbon-2 bearing the methyl group.[93] Pristanoyl-CoA with 2*S*-configuration **3** can be directly β-oxidised whilst those with 2*R*-configuration **2** have to undergo a change in chiral configuration to 2*S*- before metabolism. The 2*R*- **2** to 2*S*- **3** conversion of chiral configuration is performed by AMACR (Scheme 1.1).[91, 93]

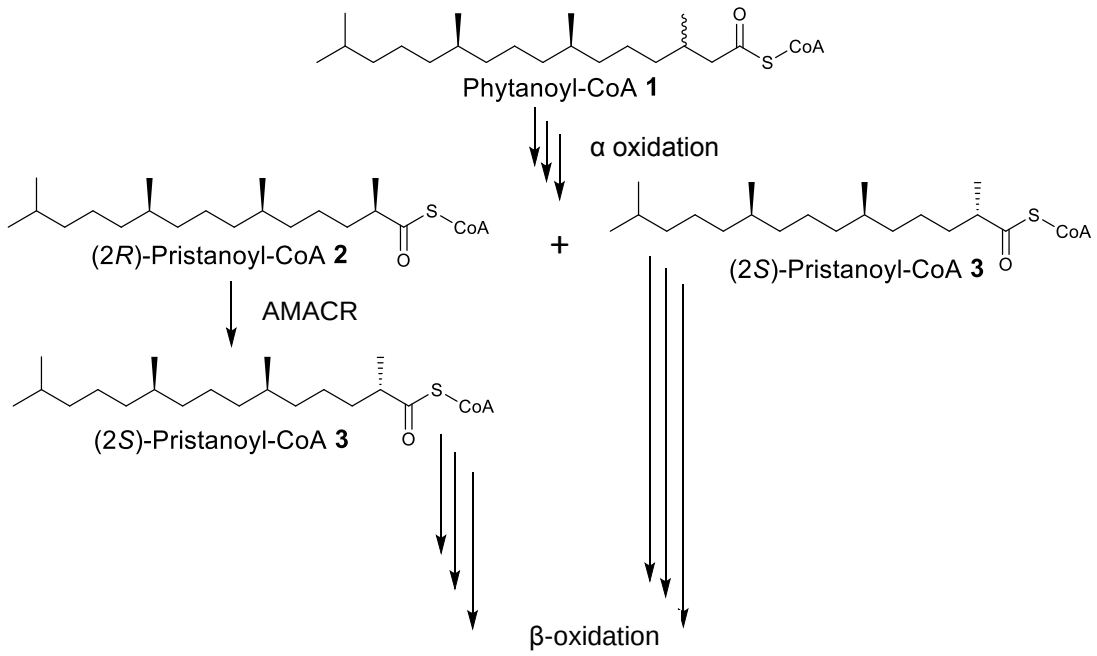

Scheme 1.1: The role of AMACR in the metabolism of branched-chain fatty acids.[111, 112]

AMACR also plays a part in the synthesis of bile acids. Bile acid intermediates such as trihydroxycholestanoic acid (THCA) are produced from cholesterol *via* complex bile acid biosynthetic pathways.[118] Mitochondrial oxidation produces a product with its α-carbon (position 25 in the conventional numbering of cholesterol) that is exclusively in the *R*- configuration but the subsequent β-oxidation requires that the substrate possesses *S*- configuration.[93, 119] The 25*R*- bile acid intermediate is activated as its acyl-CoA ester and AMACR catalyses the 25*R*- **4** to 25*S*- **5** conversion (Scheme 1.2).[93, 118]

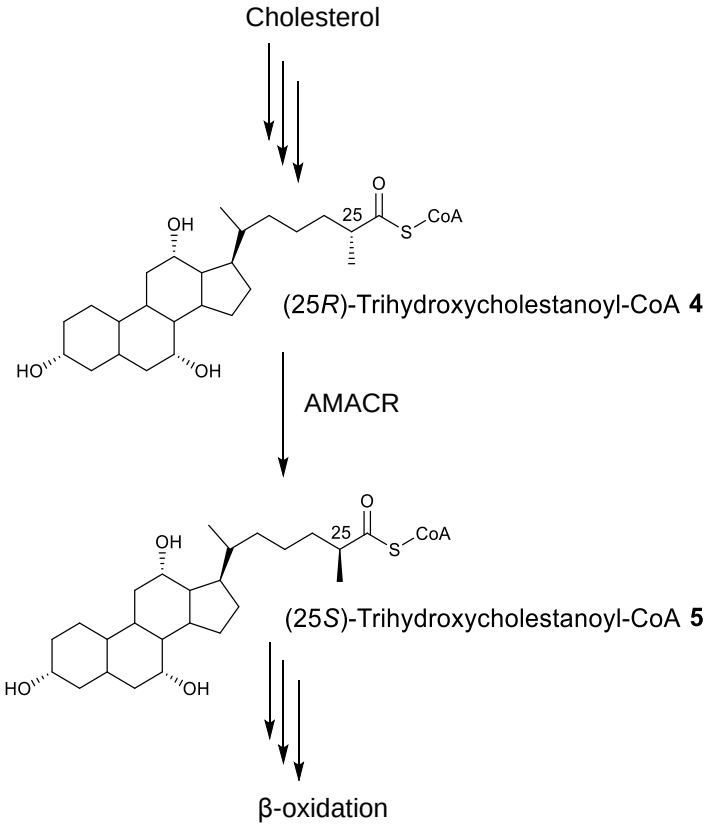

Scheme 1.2: The role of AMACR in bile acid synthesis where it converts (25*R*)-THC-CoA **4** to (25*S*)-THC-CoA **5**.[118]

AMACR 'racemises' branched-chain fatty acids and bile acid intermediates to give a 1:1 mixture of *R*- **6** and *S*- **8** products *via* a deprotonation/reprotonation mechanism (Scheme 1.3).[1, 2] The *S*- product **8** will be taken by the downstream β-oxidation pathway and the *R*- product **6** will be recycled by AMACR.

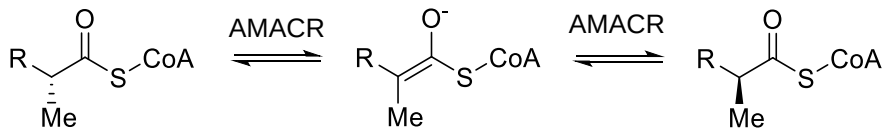

R-2-methylacyl-CoA **6** Enolate Intermediate **7** *S*-2-methylacyl-CoA **8**

Scheme 1.3: Chiral inversion of an *R*-2-methylacyl-CoA ester **6** to the corresponding *S*-2-methylacyl-CoA ester **8** catalysed by AMACR *via* a deprotonation/reprotonation mechanism.

Sensory motor neuropathy has been reported in patients with AMACR deficiency due to accumulation of *R*-pristanic acid and bile-acid intermediates.[94, 120] The neurological problem could potentially be a serious side-effect if AMACR is inhibited. However, an AMACR knock-out study in

mouse has shown that as long as dietary intake of branched-chain fatty acids is restricted, the neurological disorder will not occur.[121] The body will adapt to the inhibition of AMACR and develop an alternative AMACR-independent route to synthesise bile acids, presumably mediated by peroxisomal multifunctional enzyme type 1 (pMFE-1), CYP3A11 and CYP46A1.[121]

1.11 Role of AMACR in the metabolism of 2-arylpropanoic acids (2-APAs)

Many non-steroidal anti-inflammatory drugs (NSAIDs) such as ibuprofen **9**, fenoprofen **10** and flurbiprofen **11** have a common 2-arylpropanoic acid (2-APA) structure (Figure 1.3).[122] 2-APAs exert their anti-inflammatory activity by inhibition of cyclooxygenase-1 and -2 (COX-1 and -2) enzymes and thereby the inhibition of the synthesis of prostaglandin.[123, 124]

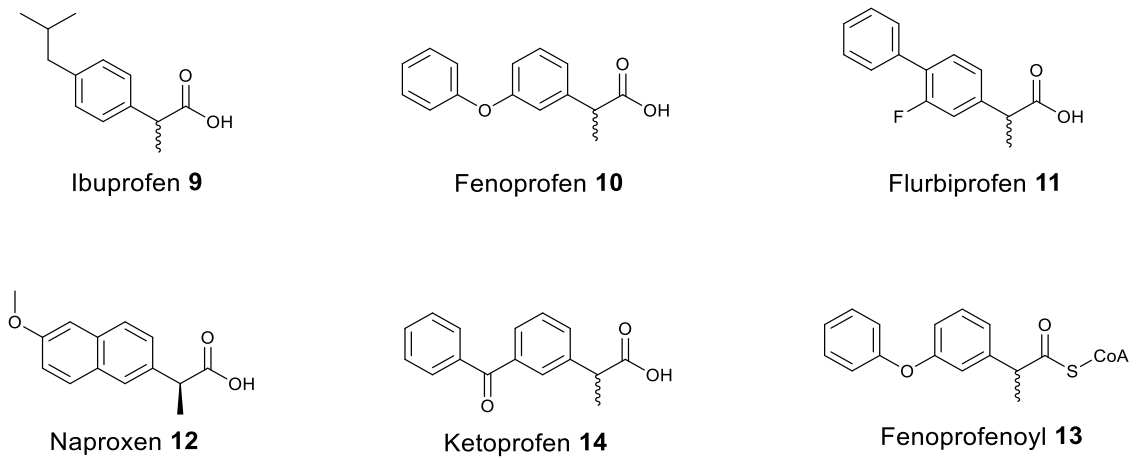

Figure 1.3: Examples of 2-APA drugs (compound **9**, **10**, **11**, **12** and **14**) and the best AMACR substrate **13** reported to-date.

2-APAs (except naproxen **12**) are usually administered to patients as a racemic mixture but only the *S*-enantiomer is the pharmacologically-active form in inhibiting COX enzymes.[125, 126] AMACR is responsible for the chiral inversion of these drugs into its active *S*-isomer. First, the 2-APA is coupled to coenzyme A by the long-chain acyl-CoA synthetase (LACS) to form a 2-APA-CoA ester (Scheme 1.4).[122, 127-129] The product is a substrate for AMACR, which is responsible for catalysing the chiral inversion of the ester from the *R*- to the *S*- isomer (Scheme 1.4).[130, 131] The *S*-2-APA-CoA ester is subsequently

hydrolysed by human acyl-CoA thioesterases (ACOTs),[132, 133] possibly ACOT-1 and ACOT-2[131] to give the *S*-2-APA, which is the active entity (Scheme 1.4). The chiral inversion of 2-APAs is uni-directional *in vivo*[129] even though AMACR has been shown to 'racemise' both *R*- and *S*- isomers *in vitro*.[1, 2] This is because only the *R*-2-APA-CoA ester but not the *S*-2-APA-CoA ester is produced by LACS as it has a stereospecific substrate requirement.[128, 129, 134] Even though flurbiprofenoyl-CoA has been shown as a substrate of AMACR *in vitro*,[2] flurbiprofen **11** is not a substrate for the chiral inversion pathway in humans,[135, 136] presumably because the acid is not being converted to acyl-CoA ester by LCAS.[137]

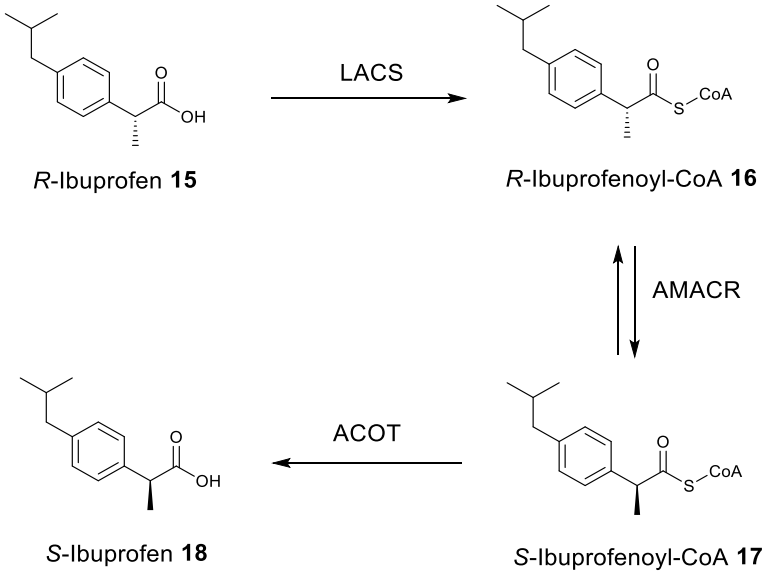

R-Ibuprofen **15** — *R*-Ibuprofenoyl-CoA **16**

S-Ibuprofen **18** — *S*-Ibuprofenoyl-CoA **17**

Scheme 1.4: The *in vivo* chiral inversion pathway of 2-APAs using ibuprofen as an example.

AMACR has been shown to be able to chirally invert 2-APAs but it has different affinities for them.[2] The best substrate for AMACR reported to-date is fenoprofenoyl-CoA **13** (Figure 1.3; *vide supra*) with a reported K_m value to 2.3 μM.[2] Regular use of 2-APAs has been associated with a reduced risk of prostate cancer.[138, 139] This chemo-preventive effect may be due to the anti-inflammatory effect of NSAIDs[140, 141] but the inhibitory effect of 2-APAs on AMACR activity may also play a role in reducing cancer risk.[142] *R*-Ibuprofenoyl-CoA **16** has been shown to be a moderate AMACR inhibitor,

which inhibits the 'racemisation' of (25*S*)-THC-CoA **5**, with a K_i value of 5.4 μM.[143]

1.12 AMACR inhibitors reported in the literature

Very few AMACR inhibitors have been synthesised in the past 15 years since the enzyme was first identified as a prostate cancer target.[47, 75, 76] Even though this novel target has attracted researchers' interest in designing molecules to inhibit it, progress has been slow due to the lack of a convenient and high-throughput assay to measure their potency.[76]

The very first inhibitors were reported by Carnell *et al*. in 2007,[143] and were designed using AMACR's natural substrate, a 2-methyl-branched fatty acyl-CoA ester (Figure 1.4). The inhibitors were modified by adding one or more fluorine atoms to the structure. Among all the variations, the most potent structure is the inhibitor **19** containing a α-trifluoromethyl group, which has a reported K_i value of 0.9 μM. The inhibitor **20** containing a α-difluoromethyl group has a 22 times larger K_i value of 20 μM. A single fluorine atom that is in the β-position relative to the acyl-CoA ester results in inhibitors with low K_i values, such as compounds **21**, **22** and **23** having K_i values of 1.3, 2.3 and 3.8 μM, respectively. Adding a fluorine atom next to the α-proton will reduce the pK_a of α-proton. This may ease the deprotonation step in forming the enolate intermediate, and hence make the compound a good competitive inhibitor. Carnell *et al.* also hypothesised that these compounds could undergo fluoride elimination but concluded that it was unlikely.[143]

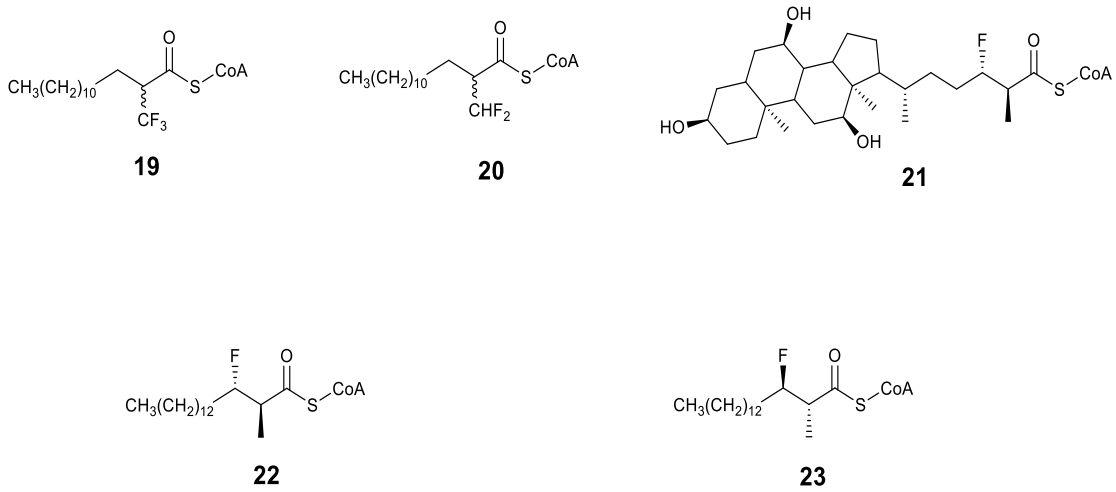

Figure 1.4: Inhibitors reported by Carnell *et al* in 2007.[143]

These inhibitors may be administered to cells as carboxylic acid pro-drugs as they have been shown to be converted into acyl-CoA esters when incubated with rat liver homogenate or purified microsomes.[143] The activation of these pro-drugs is not surprising as *R*-2-APAs have also be shown to be converted stereoselectively *in vivo* by LACS to their corresponding acyl-CoA esters (*vide supra*).[129] LACS could be responsible for esterifying the pro-drugs of these inhibitors as well.[143]

The carboxylic acid precursor of inhibitor **19** has been shown to be cytotoxic to several prostate cancer cell lines (PC3, Du145 and CWR22Rv1) when tested using the MTT cell proliferation assay. It was least toxic to the CWR22Rv1 cell line, which also has the lowest expression levels of AMACR, suggesting that the cytotoxic effect may be due to AMACR inhibition.[143]

In 2011, a series of AMACR competitive inhibitors (compounds **24**, **25** and **26**) with a 2-methylene functional group replacing the 2-methyl group were reported (Figure 1.5).[144] These reported inhibitors are not more potent than the compound **19** reported by Carnell *et al.*[143] in 2007. However, these inhibitors have the potential of being developed into a diagnostic tool for prostate cancer. One of the inhibitors, (*E*)-13-iodo-2-methylenetridec-12-enoyl-CoA **26** with K_i value of 19.0 μM, was further studied. The acid form of the inhibitor was labelled with radioactive ^{131}I in order to study its uptake by

AMACR-positive prostate cancer cell lines (LNCaP, LNCaP C4-2wt and DU145). The acid was hypothesised to be taken up by fatty acid transporters and thioesterified by LACS in the cells to form acyl-CoA ester **27**. AMACR-positive prostate cancer cells showed four times higher radioactivity compared to benign prostate cells due to the accumulation of compound **27** by binding to AMACR. As compound **27** is radioactive and has preferential accumulation in AMACR-positive prostate-cancer cells, it is a potential imaging tool for prostate cancer.[144]

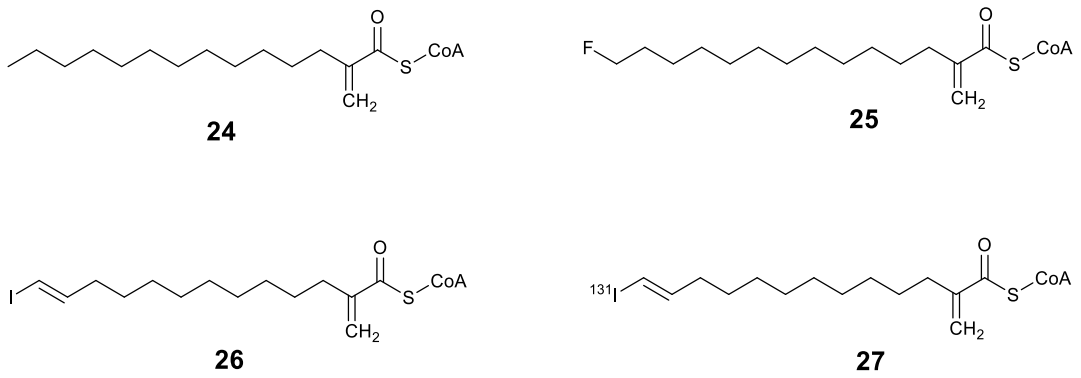

Figure 1.5: AMACR competitive inhibitors with a 2-methylene group and the ^{131}I-labelled compound.[144]

In 2013, Carnell *et al.* published a second paper on rationally designed AMACR inhibitors (Figure 1.6).[145] α–Fluoroibuprofenoyl-CoA **28** and 2-chloro-2-(4-isobutylphenyl)acetyl-CoA **29** are inhibitors with structures designed based on ibuprofenoyl-CoA. Even though inhibitor **28** has its α-proton replaced by fluorine and hence is not enolisable, it still shows a very promising K_i value (K_i = 0.32 μM). This suggests that enolisability is not essential for a compound to be an AMACR inhibitor. Inhibitor **29** can potentially be enolised as it does have a α-proton, but its methyl group is replaced by chlorine. Replacing the methyl group with an electron withdrawing atom such as chlorine may assist enolisation and it is notable that the compound is a good inhibitor (K_i = 0.58 μM).[145]

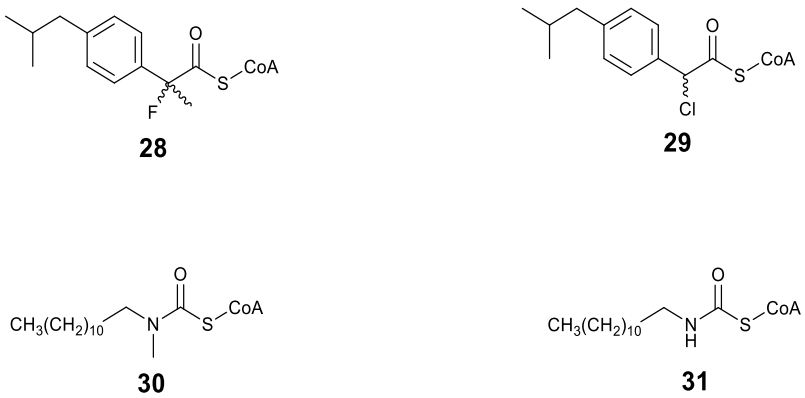

Figure 1.6: Examples of inhibitors reported by Carnell *et al.* in 2013.[145]

N-Dodecyl-*N*-methylcarbamoyl-CoA **30** and *N*-dodecylcarbamoyl-CoA **31** are inhibitors designed to mimic the enolate intermediate **7**.[145] Substrates of AMACR are hypothesised to be deprotonated by the enzyme to form enolate intermediates **7** (Scheme 1.3; *vide supra*). The thiocarbamate structure with a methylamide group **32** is an isoelectronic and isoelectric mimic **33** of the AMACR-bound enolate intermediate **7** (Figure 1.7). The thiocarbamate structure makes inhibitor **30** the most potent inhibitor reported to-date with a K_i value in the nanomolar range (K_i = 98 nM). However, this inhibitor cannot be used in cells as the pro-drug will spontaneously decompose by decarboxylation. Inhibitor **31** with a hydrogen atom instead of a methyl group attached to the thiocarbamate is nearly 10 times less potent (K_i = 1 µM) than inhibitor **30**, confirm the importance of the 2-methyl group to fit into the binding pocket of AMACR.[145, 146]

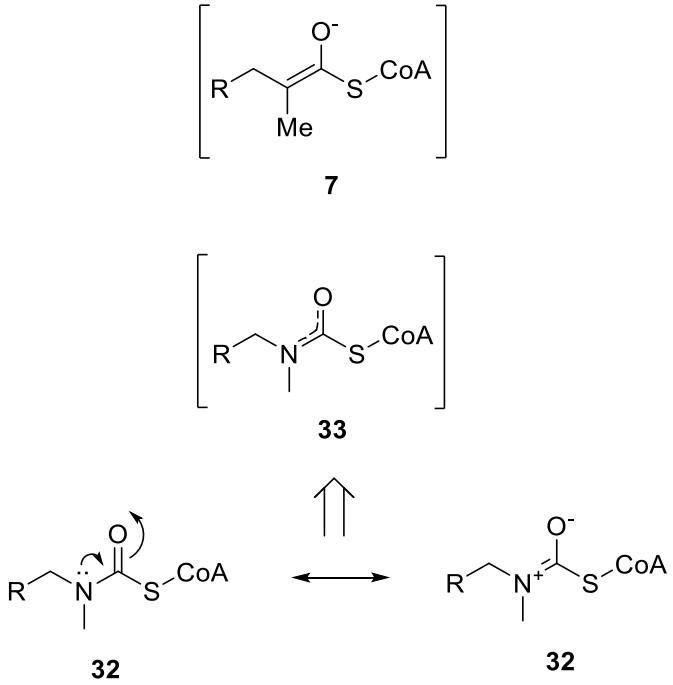

Figure 1.7: AMACR inhibitor with thiocarbamate structure that isoelectronically mimics AMACR-bound enolate intermediate.[145]

Besides rational drug design, drug screening using a medium-throughput assay has been used to look for AMACR inhibitors. Several inhibitors that are not substrate-based have been identified, including ebselen **34** (IC_{50} = 2.79 µM), ebselen oxide **35** (IC_{50} = 0.80 µM), 2-(2,5-dihydroxy-4-methylphenyl)-5-methyl benzene-1,4-diol (DMPMB) **36** (IC_{50} = 4.34 µM) and rose bengal **37** (IC_{50} = 10.0 µM) (Figure 1.8). The inhibition of AMACR by these inhibitors was not reversible upon removal of inhibitors by dialysis. Ebselen **34** has been postulated to alkylate the His-122 residue of AMACR to cause an irreversible inhibition. Ebselen **34** and DMPBM **36** were tested in prostate cancer cells lines and the cancer cell survival was dependent on the level of expression of AMACR. For ebselen, the kill (quoted in LD_{50}) was five times greater in AMACR-expressing cells (LNCaP) than low-expressing cells (WPMY1). This is the first ever screening study reported and it managed to screen nearly 5000 compounds.[85] The details of the screening will be discussed further in next section.

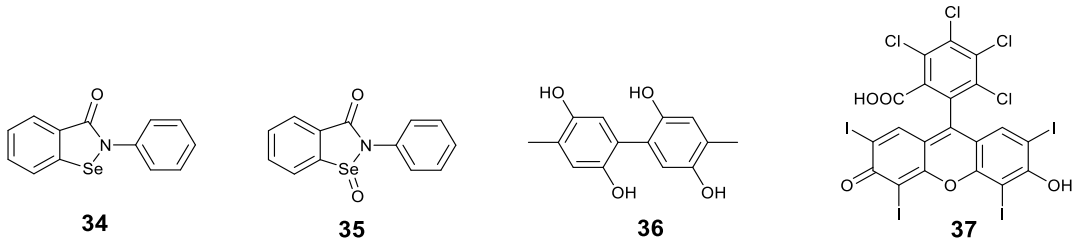

Figure 1.8: AMACR inhibitors found by drug screening.[85]

1.13 Current assays to measure AMACR activity and drug potency

There are several AMACR assays reported, including the wash-out of tritium from substrate[85] and wash-in or wash-out of deuterium into or from substrate.[1] There are also assays involving the use of high-performance liquid chromatography (HPLC),[145] gas-liquid chromatography (GLC)[90, 91] or circular dichroism (CD).[106] Some of these assays have been developed just to measure AMACR activity whilst others can also be used to screen for AMACR inhibitors.

1.13.1 Detection of radioactivity from tritium release

The method of detecting tritium release was first done as an end-point assay[91] before it was adapted by Wilson *et al* as a screening assay for drugs.[85] AMACR was incubated with a potential inhibitor in a 96-well plate before the [2,3-^{3}H] pristanoyl-CoA substrate was added. As AMACR deprotonates the substrate, the radioactive α-proton is released into the reaction buffer. A solid phase extraction (SPE) plate is used to separate the unreacted substrate from the buffer containing the released tritium. The eluent with $^{3}H_2O$ is transferred to a reading plate for its radioactivity to be measured by a 96-well scintillation detector. The lower the radioactivity detected, the higher the potency of the inhibitor. This is because the deprotonation of the α-proton is inhibited and hence the tritium release is reduced.[85]

Even though the study claimed to be a high-throughput screening, it could only be used to screen a small to medium library, so at most, it is a medium throughput assay. A considerable level of manipulation is required before the radioactivity can be measured. The SPE plate has to be first conditioned using methanol or acetonitrile and washed twice with the reaction buffer before it can

be used. The AMACR reaction in the 96-well plate has to be quenched with acid and then neutralised with base before it can be eluted from the SPE plate into a collection plate. Then, it has to be transferred from the collection plate into a reading plate in order for radioactivity to be measured by the scintillation detector. In addition to the laborious preparation of samples for radioactivity measurement, there is also the safety concern of possible exposure to radioactivity if spillage occurs.[85]

1.13.2 ^{1}H nuclear magnetic resonance (NMR) spectroscopy

The enzyme activity of AMACR towards substrates can be explored in the presence of $^{2}H_2O$. Substrates such as *S*-2-methyldecanoyl-CoA **38** would be 'racemised' by AMACR through deprotonation and reprotonation steps.[1] As this reaction occurs in $^{2}H_2O$, the α-proton would be exchanged for deuterium (Scheme 1.5).[1] The loss of the α-proton could be observed using ^{1}H nuclear magnetic resonance (NMR) as the α-methyl peak of the substrate **38** with the chemical shift at 1.00 ppm would change from a doublet to a single peak.[1] At the same time, the peak for the α-proton at δ 2.60 ppm would be reduced and would eventually disappear at high substrate conversions.[1] The same method has been used to test various AMACR substrates such as acyl-CoA esters of 2-APA[2] and straight-chain acyl-CoA esters.[147]

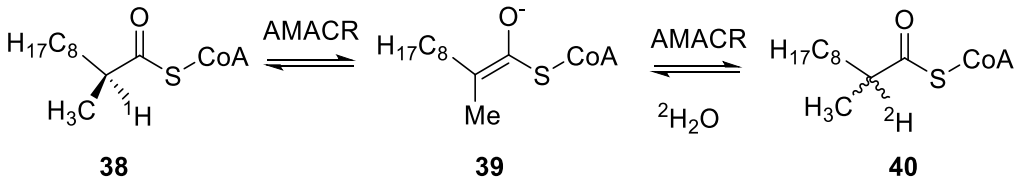

38 **39** **40**

Scheme 1.5: 'Racemisation' of *S*-2-methyldecanoyl-CoA by AMACR in $^{2}H_2O$.

However, the ^{1}H NMR-based method suffers the problem of low sensitivity. The lower the concentration of substrate, the greater the acquisition time is required. Even though ^{1}H NMR can measure a substrate concentration in the micromolar range, it will have difficulty in accurately detecting concentrations below 10-20 μM. In addition, only a single sample can be investigated at a time. Hence, if this method were to be translated into an inhibition assay, it will

be laborious and low throughput. Moreover, the use of deuterated water is likely to result in a solvent kinetic isotope effect.[1, 106]

1.13.3 High-performance liquid chromatography (HPLC) and gas-liquid chromatography (GLC)

'Racemisation' by AMACR can be followed using HPLC[148] or GLC.[90, 91] After the *R*- or *S*- substrate is incubated with AMACR, the reaction is quenched with acid.[90, 91] The acyl-CoA ester product is hydrolysed to form an acid product of unknown chirality.[90, 91] The resulting acid is coupled with a chiral molecule such as *R*-1-phenylethylamine to form a diastereomeric derivative which can be analysed by a HPLC or GLC method.[90, 91, 148]

This method can be adapted for use in AMACR inhibition studies. The enzyme is incubated with the *S*-ibuprofenoyl-CoA **17** and a potential inhibitor. An aliquot is taken from the mixture at an interval of 3 min and quenched with acid. Instead of an extra step of coupling the hydrolysed product with a chiral molecule to form a diastereomer, the aliquot from the reaction can be directly analysed by a HPLC with a chiral column. A chiral column will differentiate the *S*-isomer from the *R*- isomer as it contains a chiral stationary phase. Multiple time points and various inhibitor concentrations will need to be analysed in an inhibition assay.[145] It will be very time-consuming in analysing multiple samples using HPLC as it is low throughput method.

1.13.4 Continuous assay using circular dichroism (CD)

CD can be used as a continuous assay to detect the rate of 'racemisation' of substrates possessing a chromophoric side-chain by AMACR. The reported study used MCR from *M. tuberculosis*,[106] which is a homologous enzyme of human AMACR.[86] The MCR enzyme was incubated with the substrate (*R*- **15** or *S*- ibuprofenoyl-CoA **16**) and the 'racemisation' followed continuously using a CD spectrometer at a constant temperature of 37 °C.[106] The molar ellipticities of *R*-ibuprofenoyl-CoA **16** and *S*-ibuprofenoyl-CoA **17** are equal in magnitude but opposite in sign[106] because the chiral molecules absorb the left- (L) and right-handed (R) circular polarised light differently.[149] The changes of molar

ellipticity correspond with the changes of stereochemical configuration when the substrate is 'racemised' and this process can be followed with time.[106]

The main problem in measuring the 'racemisation' reaction of AMACR is because the end product is very similar to the initial substrate as the only change is that the one chiral centre is 'racemised'. The CD assay offers the advantage of recognising the difference in the *R*- and *S*- configuration without the use of isotopes such as deuterium or tritium. This avoids the complications of kinetic isotope effects in the assay.[106] Moreover, continuous assays offer the advantage of following the reaction in real time and it is unnecessary to stop the reaction before measurement, which is required in all end-point assays.[106] The reported study only measured the 'racemisation' of ibuprofenoyl-CoA but it has the potential in AMACR inhibitor screening.[106] However, it has a limitation in terms of sample absorbance where high concentration of sample will result in high absorbance and hence excessive noise.[106, 149] In addition, acyl-CoA inhibitors with aromatic side-chain are likely to be 'racemised' by AMACR, which will lead to very complicated ellipticity readings.[149] Assays based on CD have been used to study various racemases,[150-152] but all of them suffer from a common problem, which is low-throughput.

1.14 The proposed mechanism of human AMACR catalysed reaction

AMACR is proposed to catalyse the 'racemisation' of substrates by a deprotonation/reprotonation mechanism.[146] The deprotonation was studied using a ^{13}C and ^{2}H doubly-labelled substrate **41** (Scheme 1.6).[1] The wash-out of deuterium label by AMACR was followed using a ^{13}C NMR spectroscopy. The triplet (at δ 47.11) of the substrate **41** slowly disappears with the loss of the α-^{2}H. A new singlet (at δ 47.55) of the product **43** appears as the ^{2}H is exchanged to ^{1}H.

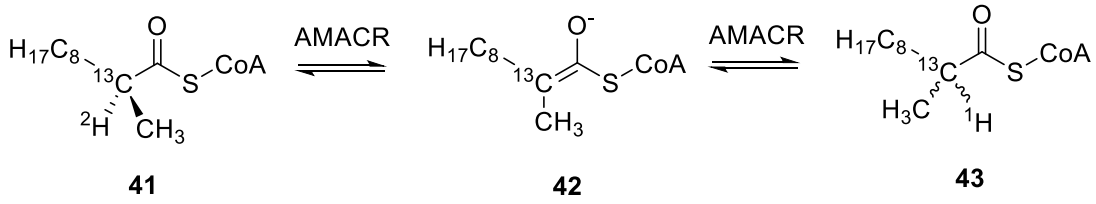

41 **42** **43**

Scheme 1.6: The deprotonation and reprotonation of *S*-2-methyl-2-[^{13}C]-2-[^{2}H]-decanoyl-CoA **41**.

Use of isotopic labelling allows the study of the reprotonation step. An unlabelled *R*- **44** or *S*- 2-methyl-decanoyl-CoA **38** was 'racemised' by AMACR in the presence of $^{2}H_2O$ (Scheme 1.5; *vide supra*). The product was in a nearly 1:1 racemic mixture regardless of whether the substrate was initially in a *R*- or *S*-configuration.[1] Similar experiments were performed on the acyl-CoA esters of 2-APA and consistent results of 1:1 racemic product were obtained.[2]

The study from Darley *et al.* also showed that the deprotonation rate was almost twice the rate of chiral inversion and the resulting product was a near racemic mixture.[1] The stereochemical outcomes is suggestive of a planar intermediate, with non-steroselective reprotonation (*i.e.*, from both faces of the molecule). An enol or enolate **39** is the most plausible intermediate compared with other possible intermediates such as a carbanion **45** or a ketene **46** (Scheme 1.7).[107, 108] A carbanion **45** has a tetrahedral structure, so would not be so easily converted into a racemic mixture. A ketene **46** is also unlikely as quantum chemical modellling on MCR has shown that the intermediate's C-S bond was lengthened (from 1.80 Å to 1.87 Å) but was not broken.[107] A ketene intermediate would require the C-S bond to be broken. The observation where the oxygen atom of the carbonyl became more negatively charged (from -0.487 to -0.651) with the removal of the α-proton supports the hypothesis of the intermediate being an enolate.[107]

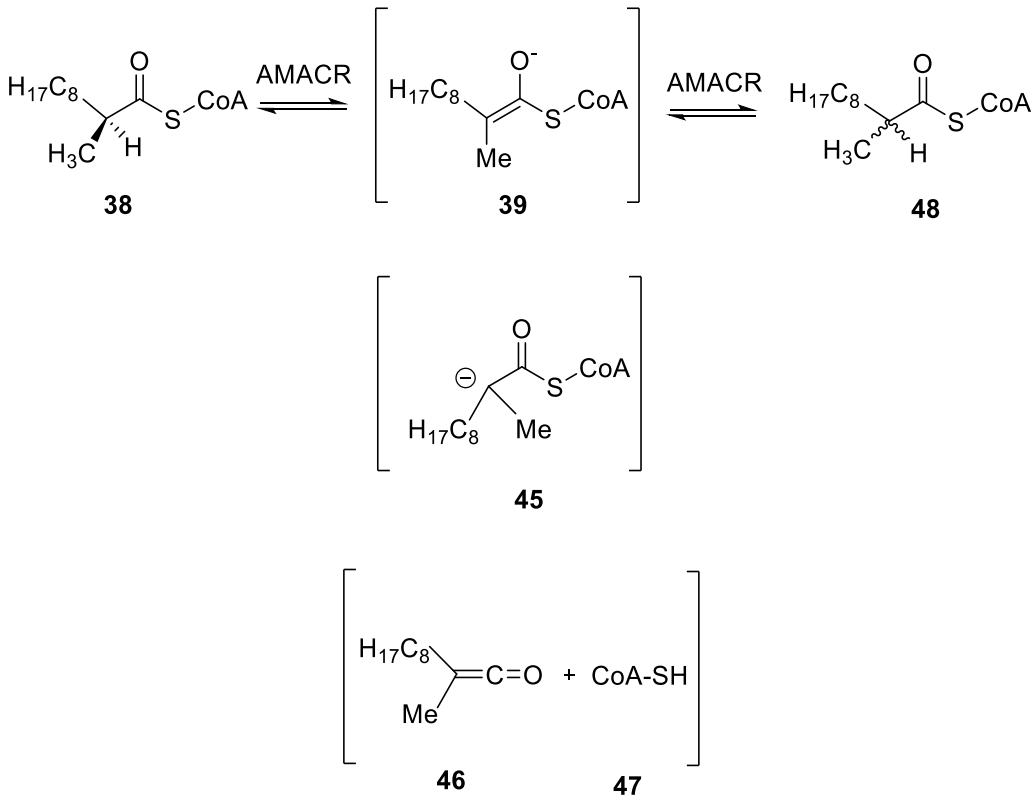

Scheme 1.7: The proposed intermediates in the reaction catalysed by AMACR.

To date, the structure of mammalian AMACR has not been determined but the X-ray crystal structures of its homologue MCR from *M. tuberculosis*, have been reported (Figure 1.9).[146, 153, 154] These homologous structures have always been used to investigate the mechanism of human AMACR by analogy.[77, 106]

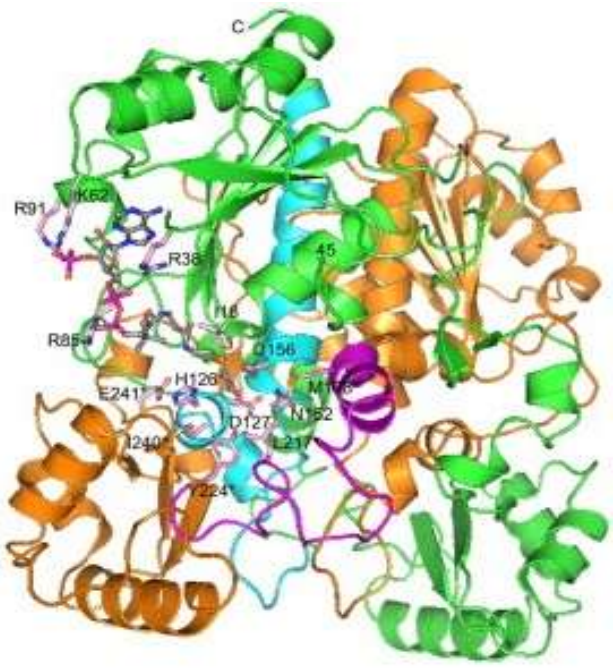

Figure 1.9: MCR dimer complexed with a substrate molecule reported by Bhaumik *et al*.[146]

The X-ray crystal structure and the site-directed mutagenesis study on bacterial MCR have identified the catalytic residues of MCR as His-126, Asp-156 and Glu-241.[86, 108, 146] The crystal structure of MCR showed that the enzyme is a tight interlocked dimer (Figure 1.9). Each monomer has a large domain at the N-terminus followed by a linker, a small domain, a second linker and a C-terminus that goes toward its large domain (Figure 1.10).The active site is at the interface of the dimer between the large and small domain. The active site is contributed by both subunits of the dimer where the His-126 and Asp-156 residues are situated at the large domain, within α5 and α7 respectively, while the Glu-241 residue is situated within the α9 of the small domain. Hence, each dimer contains two independent catalytic centres.[86]

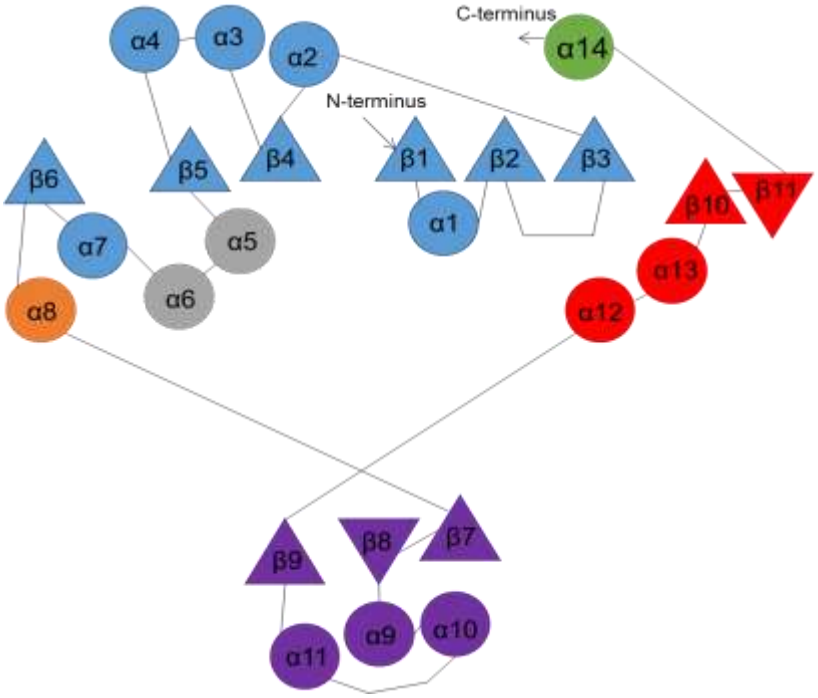

Figure 1.10: A simplified diagram of the MCR showing a monomer with a large domain (blue), a small domain (purple), two protruding helices (grey), two linkers (orange and red) and its C-terminus (green).[86]

Using the MCR data, it has been proposed that the Asp-152 residue of human AMACR 1A deprotonates the *R*-substrate to form an enolate intermediate (Scheme 1.8).[76, 86, 146] The enolate intermediate is non-stereoselectively reprotonated to give the *R* and *S*-product in a *ca.*1:1 ratio.[1] It is unknown if this proton is donated by the enzyme catalytic residues (His-122/Glu-237 dyad) or by the bulk solvent.[1] The His-122 and Glu-237 residues are paired by a hydrogen bond and work as a dyad to deprotonate the *S*-substrate.[86, 146] Again, the reprotonation of the intermediate could be by the Asp-152 residue or the bulk solvent.[1]

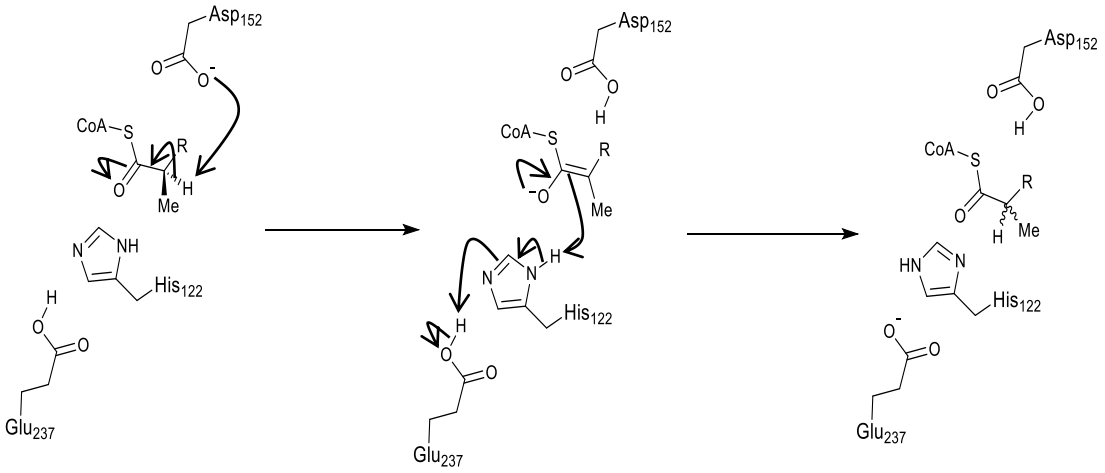

Scheme 1.8: The proposed catalytic mechanism of AMACR, showing the deprotonation of *R*-2-methylacyl-CoA ester to form an enolate intermediate and reprotonation to give a racemic mixture.[76, 86, 146]

The X-ray crystal structure of MCR has shown that the enolate intermediate is stabilised in an oxyanion hole (Figure 1.11). The negatively charged oxygen forms hydrogen bonds with His-126, Asp-156 and the backbone of Asp-127. His-126 is further stabilised by forming a hydrogen bond with Glu-241 from the small domain of the second subunit. The sulfur atom of Met-188 interacts with the side-chain of Asp-156 and further stabilises the intermediate.[107, 108, 146]

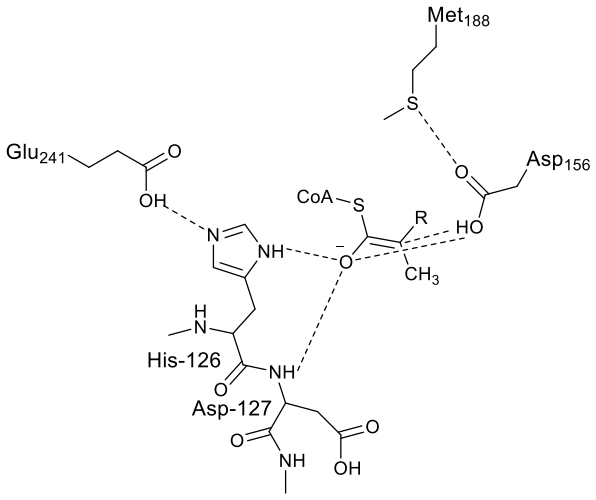

Figure 1.11: The enolate intermediate stabilised in the oxyanion pocket of MCR.[107, 108, 146]

It has been shown that the side-chains of *R*-substrate and *S*-substrate bind in different pockets within the MCR.[146] The pockets are hydrophobic in nature[146]

and allow binding of a broad spectrum of side-chains (Figure 1.12).[1, 2, 90] There is a methionine-rich hydrophobic site (between residues 195 to 223) that allows the substrate sliding from *R*- to S- pocket and *vice versa*.[146] The methyl group has a separate binding pocket between the large and small domain and the position of methyl group binding is fixed.[146] The methyl binding pocket is small and prefers methyl groups and its isosteres,[146] which explains the preference of the enzyme for 2-methylacyl-CoA substrates.[90, 147]

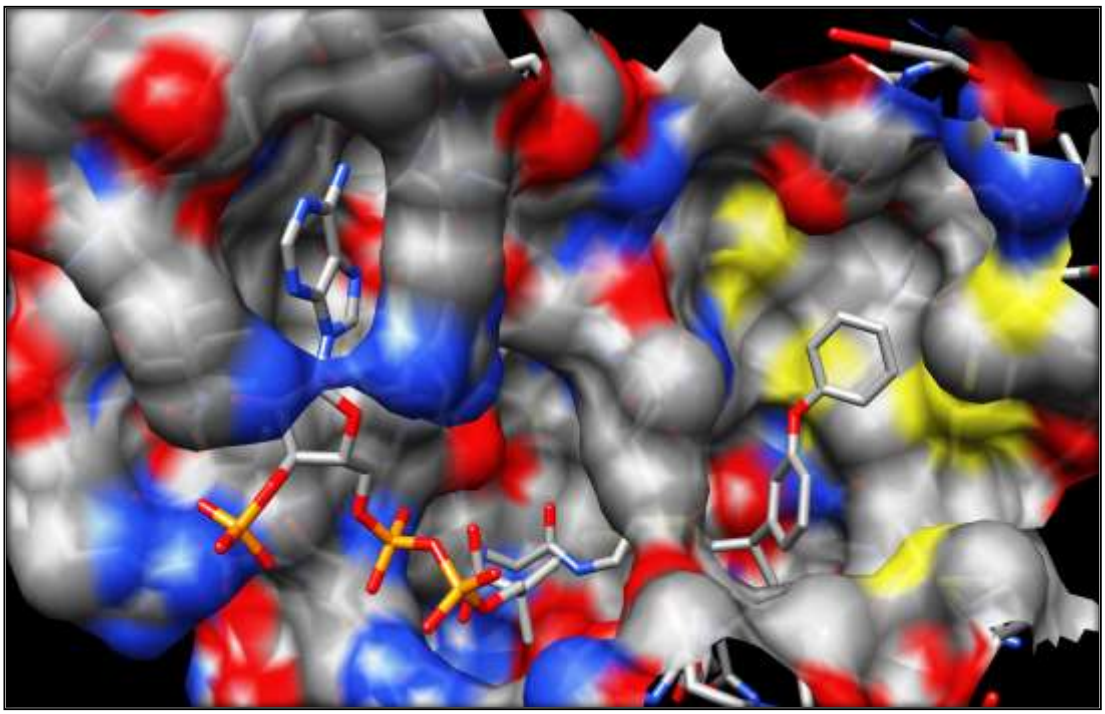

Figure 1.12: Modelled structure of *R*-fenoprofenoyl-CoA docked into the active-site of MCR. The CoA moiety is in the pocket shown on the left, the carbonyl oxygen, α-proton, and α-methyl are situated in the catalytic site in the middle while the acyl side- chain is situated at the methionine-rich surface (yellow) shown on the right.[2]

Understanding the mechanism of enzymes using a X-ray crystal structure is a commonly used method, but it has its limitations. The two obvious problems are that MCR is not AMACR even though they are quite similar. The second problem is that the cystal structure is not necessarily representative of what happens in solution.[155, 156]

1.15 Different spliced variants of AMACR

More than one form of AMACR are present in prostate cancer cells. The gene encoded for human AMACR is located on the short arm of chromosome 5 at position 13 (5p13)[157] but alternative splicing has resulted in different spliced variants from a single gene locus.[158] There have been 10 different spliced variants reported (Figure 1.13),[158-161] but one recently discovered spliced variant (IAs; Genbank accession number: CR618063) was subsequently removed from the database.[158]

The spliced variants can be divided into type I and II variants, where type I have an intact exon 5 while type II have an alternative splicing of exon 5.[158, 159] The splice variants can also be sub-divided into classes A and B where A has an intact exon 3 whilst B has a deleted an exon 3.[158, 160] Even though AMACR 1A is the most abundant in prostate cancer, other spliced variants (in descending order: IB > IAdel > IIA = IBLi > IIAs) are also up-regulated.[158, 161]

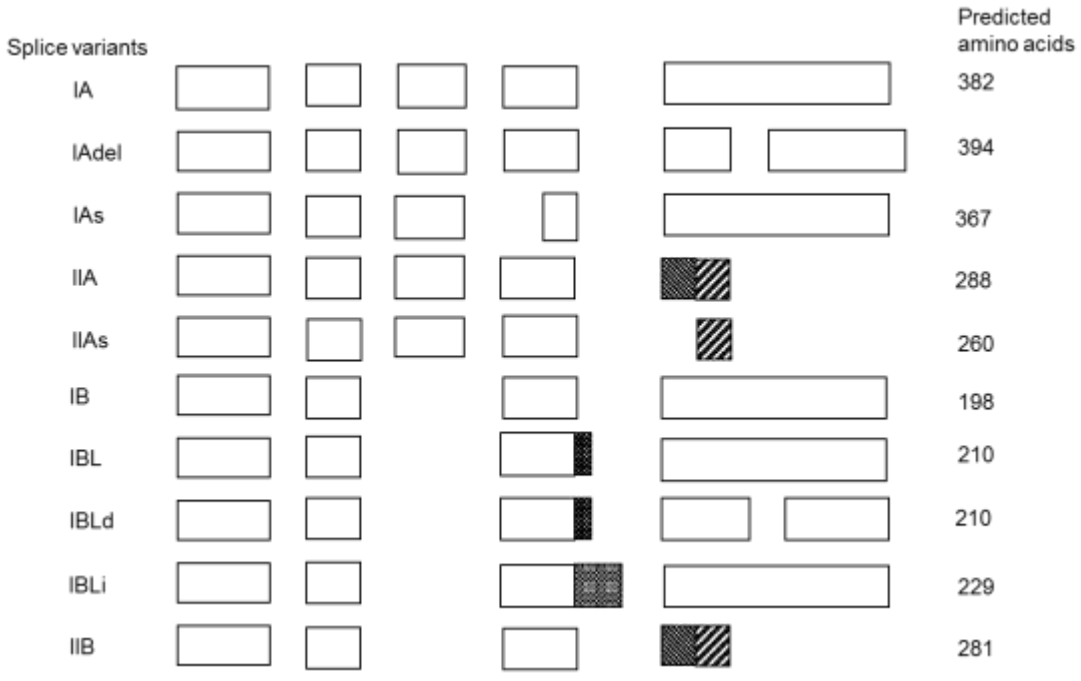

Figure 1.13: The 10 different spliced variants of AMACR.[158-161] Spliced variant IAs has been recently removed from the Genbank database.

The active site residues of bacterial MCR, His-126 (His-122 for human AMACR), Asp-156 (Asp-152 for human AMACR) and Glu-241 (Glu-237 for

human AMACR) are encoded on exons 2, 3 and 4, respectively.[86, 158] Hence, for the enzyme to be catalytically active, it must have intact exons 2, 3 and 4. All variants B are proposed to be inactive as they do not have exon 3 and hence some catalytic residues are missing.[158] Theoretically, all variants A are active except variant IAs where part of exon 4 is missing.[158] However, an intact C-terminus is needed for dimerization to give the active enzyme,[86] so variants with a truncated C-terminus (IIA and IIAs) are also predicted to be inactive. Spliced variant IAdel is likely to be catalytically active but differs from 1A in having a C-terminal extension and this removes the PTS1 motif.[161] Without the PTS1 sequence, the enzyme will not be localised in peroxisomes.[98] As AMACR 1A is the most abundant and active form of AMACR, all the work done in this thesis is on AMACR 1A.

1.16 Single nucleotide polymorphisms of AMACR

Single nucleotide polymorphisms (SNPs) of AMACR have been shown to affect the risk of developing prostate cancer.[162-166] The frequencies of occurrence of the M9V, D175G, S201L and K277E SNPs have been found to be significantly different in patients with hereditary prostate cancer compared to the control group.[162] Of all of the SNPs, the M9V variant and the haplotype of M9V and D175G (the combination of these two SNPs) show the strongest association with prostate cancer.[162, 163] However, a later study showed that the association of M9V and D175G is more significant in sporadic prostate cancer instead of hereditary prostate cancer.[166]

A study by Daugherty *et al*. showed that the risk of prostate cancer is not affected by the occurrence of allele variants but the behaviour of their carriers.[142] Carriers of M9V, D175G, S201L and K277E variants who regularly use ibuprofen have a lower risk of prostate cancer.[142] Since ibuprofenoyl-CoA has been shown to be an inhibitor of AMACR,[91, 143] it may also have an effect on these allelic variants of AMACR. The 2-APA-CoA may modulate the activity of these variants by competing with their natural substrates and hence confer a protective effect against prostate cancer. This protective effect of ibuprofen also implies that prostate cancer risk may be linked with higher enzymatic

activity and not just protein levels *per se*, and that the disease-linked SNPs give rise to higher enzymatic activity.

1.17 Conclusions

Inhibiting AMACR in castrate-resistant prostate cancer is a very good treatment strategy because it complements the clinically accepted androgen-deprivation therapy and enhanced the response of the cancer to these conventional treatments.[48, 84] However, very few inhibitors of AMACR have been described in the literature to-date.[85, 143-145] So far only one drug (trifluoroibuprofen) has been tested *in vivo*[167] and no drug has entered clinical trials. One of the reasons for this may be that the enzyme is a racemase. It is difficult to assay the activity of a racemase as the substrate and the product are difficult to distinguish.[1]

There is an urgent need to design better and more potent drugs against human AMACR but the bottleneck is not having a convenient and high-throughput assay. Even though there has been substantial studies on the crystal structure and mechanism of MCR (the homologue of human AMACR),[86, 108, 146, 154] there are significant limitations when translating the data to human AMACR.[168, 169] It is paramount to understand the active-site of human AMACR in order to rationally design drugs against it.

2 Aims and objectives

2.1 Aims

A range of novel compounds will be synthesised using a rational drug design approach to explore the SAR of the side-chains of AMACR inhibitors. These compounds will be tested using different assays with the aim of developing a high-throughput and convenient AMACR assay. The AMACR enzyme will be studied using a site-directed mutagenesis in order to identify active-site residues and to further understand its catalytic mechanism.

2.2 Objectives

2.2.1 The development of AMACR inhibitors using the rational drug design approach

In order to explore the SAR of the side-chains of AMACR inhibitors, a range of novel compounds will be designed based on the structure of fenoprofenoyl-CoA **13**, the best substrate of AMACR. Both electron-withdrawing groups and electron-donating groups at the β-position will be introduced in order to study whether a substrate mimic or a transition-state mimic is a better inhibitor. The side-chain will be designed to have a *meta*- or *para*- substituents to explore the optimal structure for side-chain binding. The 2-methyl group will be designed to have the *R*- or *S*- stereochemical configuration to explore if there is a spatial preferential binding.

2.2.2 Inhibitor testing and the development of high-throughput assay

The inhibitors will be tested with the deuterium wash-in assay and fluorescent-binding assay to study their binding to AMACR. As AMACR has been recently described to catalyse the elimination of 3-fluoro-2-methylacyl-CoA esters, the development of this reaction into a high-throughput assay to measure the potency of inhibitors will be investigated. In order to validate the fluoride-elimination assay, novel compounds described above and a number of known AMACR ligands will be assessed using ^{1}H NMR and ^{19}F NMR. The novel inhibitors and known AMACR ligands will be characterised using a multi-well colorimetric assay.

2.2.3 Site-directed mutagenesis on AMACR

To study the catalytic mechanism of the enzyme to assist drug design, site-directed mutagenesis will be performed. Potential AMACR active-site residues will be identified using the X-ray crystal structure of MCR, a homologous bacterial enzyme. Primers to produce the mutant will be designed and each of AMACR residues His-122, Asp-152, Met-184, and Glu-237 will be mutated. His-tag wild-type and mutant AMACR proteins will be expressed using *E. coli* and purified by metal-chelate chromatography.

2.2.4 The characterisation of mutant enzymes and enzyme assays

The effects of the above mutations on the protein structure will be investigated using dynamic light scattering (DLS), CD and fluorescence study using 8-anilino-1-naphthalenesulfonic acid (ANS). The wild-type and mutant enzymes will be tested using the deuterium wash-in assay and fluoride elimination assays to study changes in enzyme activity. The multi-well colorimetric assay will be used to determine kinetic parameters for substrate coversion by these enzymes.

3 Results and discussion for potential AMACR inhibitors

3.1 Design of potential AMACR inhibitors

To date, no SAR on the side-chains of AMACR inhibitors have been performed. Even though there are some rationally designed inhibitors against AMACR, limited numbers of each type of inhibitor have been designed and tested.[143-145]

In order to have better understanding of the SAR, a rational approach was used to design potential inhibitors of AMACR based on known substrate structures and mechanistic information. All the inhibitors designed have an acyl-CoA-ester moiety (Figure 3.1, blue) as the group is absolutely required for binding to the enzyme.[144] The 2-methyl moiety (Figure 3.1, red) was also included as it enhances the binding of substrates to AMACR.[145-147] The presence of the 2-methyl group will prevent binding to other enzymes metabolising straight-chain acyl-CoA esters, thereby enhancing selectivity for the target and reducing off-target effects. The side-chains (Figure 3.1, green) were varied in order to study their influence on binding affinity and the inhibitory effect on the enzyme.

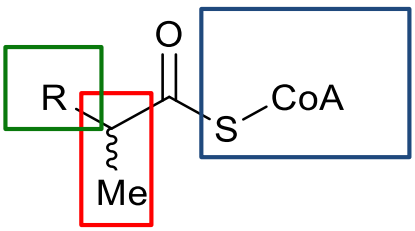

Figure 3.1: Design of potential inhibitors with an acyl-CoA ester, a methyl group and a varied side-chain.

Fenoprofenoyl-CoA **13** has been shown to be the best substrate of AMACR (Figure 3.2), with a K_m value to 2.3 μM.[2] Hence, to design an inhibitor that competitively binds to AMACR, fenoprofenoyl-CoA **13** was chosen as the initial structure on which to base inhibitor design. It was thought that the extended aromatic rings increase the hydrophobicity of the compound and would enhance interactions with the methionine-rich surface of AMACR.[146]

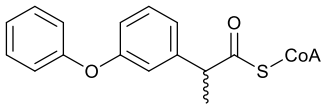

13

Figure 3.2: Structure of fenoprofenoyl-CoA, the best substrate of human AMACR 1A.[2]

To turn a compound into an inhibitor, sulfide (**49** and **50**) and sulfone (**51** and **52**) groups were added adjacent to the 2-methyl group (Figure 3.3). These electron-withdrawing groups will increase the acidity of the α-proton, promoting the removal of α-proton to form a stable enolate intermediate.[143] The propensity of an inhibitor to forming a stable intermediate allows the inhibitor to compete well with the enzyme's natural substrate.[143]

A phenoxyphenol side-chain was also designed (Figure 3.3), resulting in compounds (**53**, **54**, **55** and **56**) with an oxygen at the β-position. Having an electron-donating oxygen atom next to the 2-methyl group would suppress the formation of an enolate. Hence, the inhibitor would be a poorly enolisable substrate. If the inhibition of AMACR is mediated by substrate analogues which block the active site instead of transition-state analogues, a poorly enolisable compound will be a better inhibitor.

No systematic SAR study on AMACR inhibitor structure has been undertaken and the binding of the substrate side-chain (Figure 3.1, green) to AMACR is thought to occur at a non-specific hydrophobic surface, which does not have a specific side-chain binding pocket. A series of analogues with modified side-chains at both *para*- and *meta*- position (Figure 3.3) were produced in order to examine this hypothesis. If the orientation of the side-chain has an effect on inhibitor potency, it would provide an insight into the structure of the binding pocket. This could be useful in designing further inhibitors to explore optimal binding in the side-chain pocket.

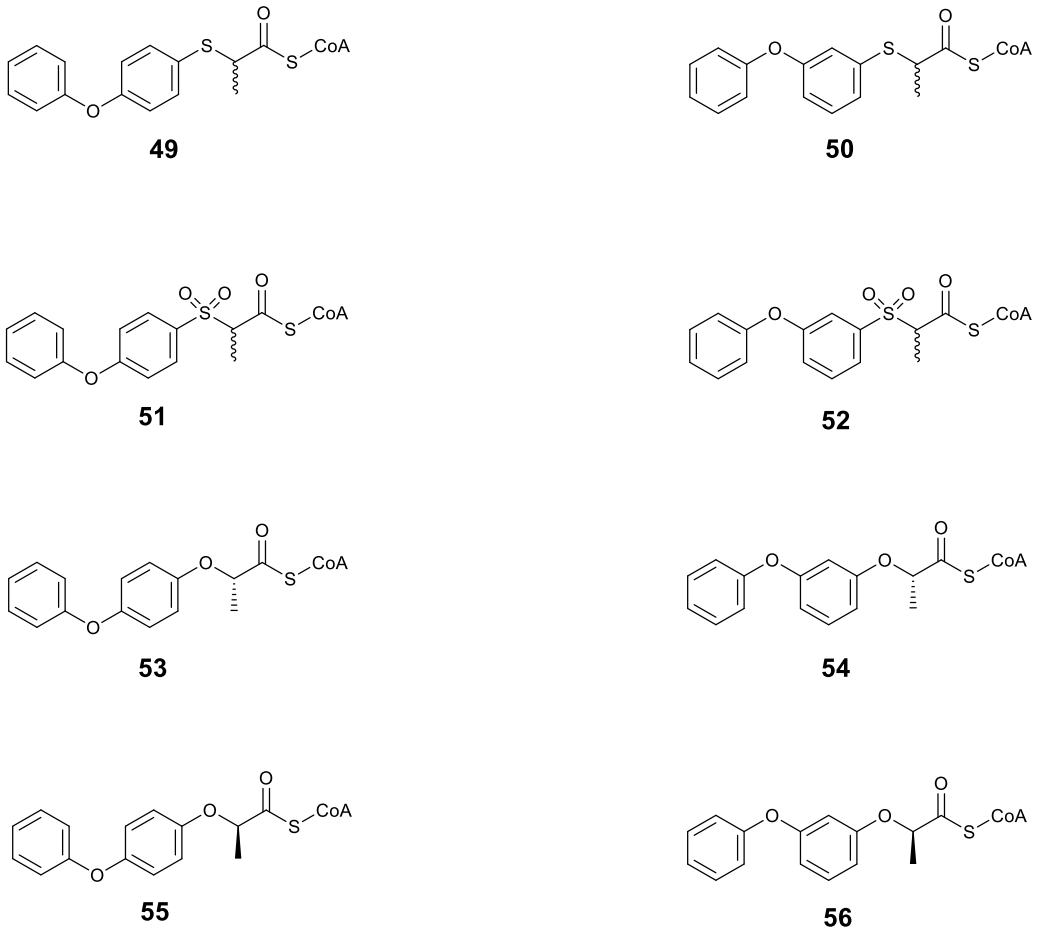

Figure 3.3: Structures of potential inhibitors of AMACR.

3.2 Synthesis of the proposed inhibitor structures

3.2.1 Synthesis of 3-sulfide inhibitors

Synthesis of the proposed 3-sulfide inhibitor **49** was attempted by converting the aromatic amine **57** to the corresponding thiophenol **58**. The thiophenol **58** could be reacted with ethyl 2-bromopropanoate followed by deprotection and conversion to the acyl-CoA ester **49** (Scheme 3.1).

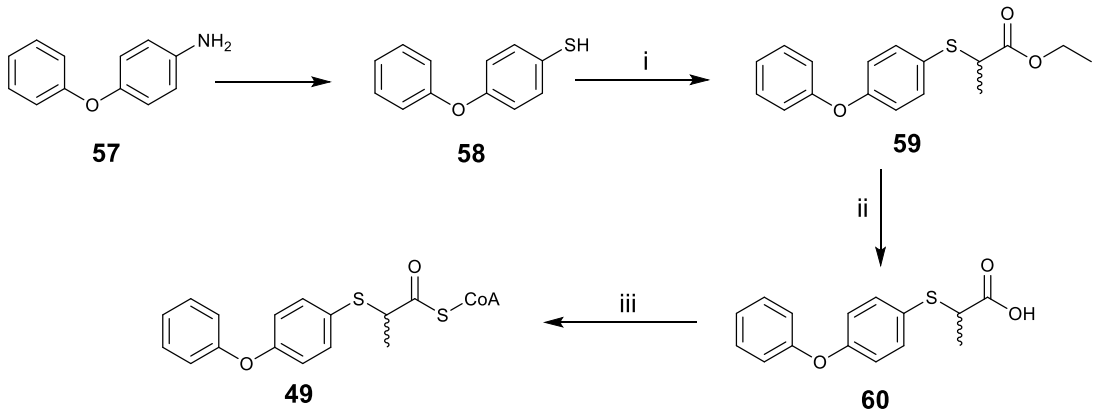

Scheme 3.1: Attempted synthesis of 3-sulfide inhibitor **49** using an aromatic amine. Reagents and conditions: i) K_2CO_3, MeCN, -45 °C, 15 min, then ethyl 2-bromopropionate, rt, 20 h; ii) 2.5 M NaOH $_{aq.}$, MeOH, rt, 1.5 h; iii) DCM, CDI, rt, 1 h, then THF, 0.1 M $NaHCO_3$ $_{aq.}$, CoA-Li_3, rt, 18 h.

The synthesis of the thiophenol **58** was attempted with the Sandmeyer reaction (Scheme 3.2). The nucleophilic substitution of aromatic amine **57** occurred *via* the formation of a diazonium salt intermediate[170] **61** which was reacted with potassium ethyl xanthate.[171] The dithioester **62** was hydrolysed and subsequently acidified. Instead of giving the predicted thiophenol **58**, the reaction produced a complex mixture without any of the desired compound. As thiophenol **58** is easily oxidised, it is possible that the product had been oxidised into acid **63** and/or into a dimer **64** during the reaction.

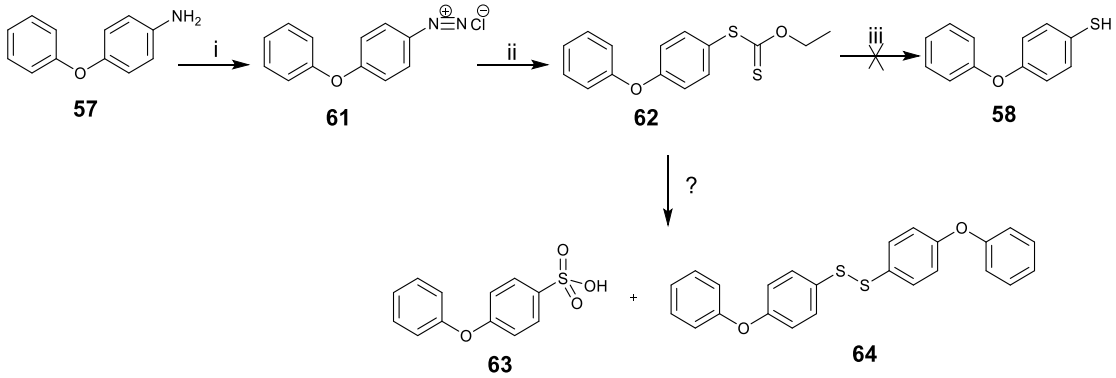

Scheme 3.2: Attempted synthesis of thiophenol **58** using the Sandmeyer reaction. Reagents and conditions: i) DME, conc. H_2SO_4 $_{aq.}$, $NaNO_2$ $_{aq.}$, 0 °C, 30 min, ii) potassium ethyl xanthate, 0 °, 10 min, iii) KOH $_{aq.}$, ethanol, reflux, 14 h.

To test if the Sandmeyer reaction had worked, the reaction was repeated with the conventional nucleophile, NaI, instead of potassium ethyl xanthate (Scheme 3.3). The desired iodo-product **65** (75%) was obtained together with a by-product **66** (25%). This showed that potassium ethyl xanthate is not a very good nucleophile compared to NaI and could not be utilised in this reaction.

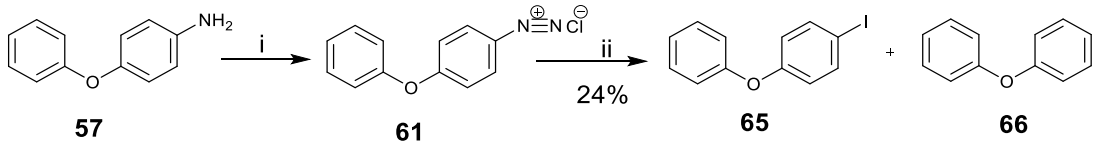

Scheme 3.3: Synthesis of iodinated aromatic compound **65** using the Sandmeyer reaction. Reagents and conditions: i) DME, conc. $H_2SO_{4\ aq.}$, $NaNO_{2\ aq.}$, 0 °C, 30 min, ii) $NaI_{\ aq.}$, 0 °, 10 min.

As the attempts to synthesize thiophenol **58** using the Sandmeyer reaction failed, a new route was investigated. The phenol **67** was first coupled to *N*,*N*-dimethylthiocarbamoyl chloride to form thiocarbamate **68** which was then heated to allow thermal rearrangement to form carbamothioate **69** (Scheme 3.4).[38, 39]

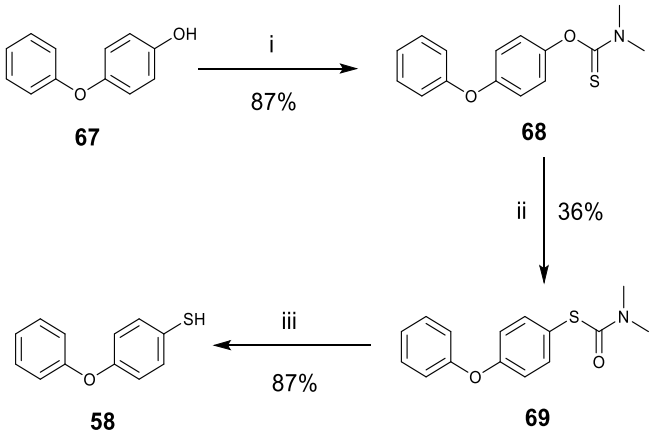

Scheme 3.4: Synthesis of thiophenol **58** using the Newman-Kwart reaction. Reagents and conditions: i) NaH, DMF, 10 °C, then *N*,*N*-dimethylthiocarbamoyl chloride, 70 °C, 21 h; ii) argon atmosphere, 280 °C, 1.7 h; iii) 2.5 M $NaOH_{\ aq.}$, MeOH, reflux, 4 h.

The rearrangement from thiocarbamate **68** to carbamothioate **69** is named the Newman-Kwart reaction, in which the compound is heated to a very high

temperature to allow intra-molecular rearrangement of oxygen and sulfur atoms (Scheme 3.5).[172, 173] The conversion was initially trialled at 260 °C following the protocol described by Brown *et al*.[174] However, no conversion was observed at this temperature. The temperature was increased to 300 °C which resulted in some product formation but in very low yield (3%). The temperature was optimised and it was found that 280 °C gave the best conversion (36%) whilst minimising decomposition.

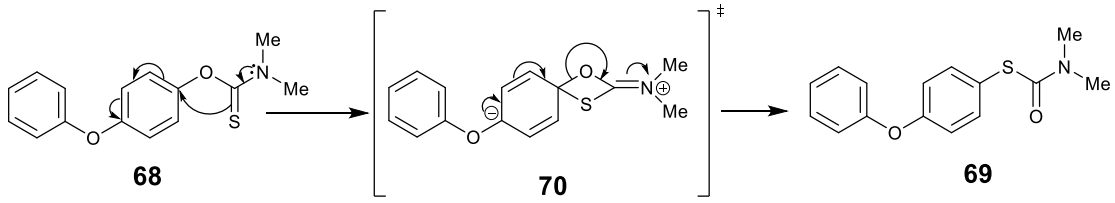

Scheme 3.5: The proposed mechanism of the Newman-Kwart reaction.[172, 173]

The carbamothioate **69** from the Newman-Kwart reaction was hydrolysed at reflux in methanol to obtain the thiophenol **58,** which was purified by column chromatography to *ca.* 90% purity. Unfortunately, the thiophenol **58** was rapidly oxidised and it proved impossible to obtain the product in 100% purity and it was used without further purification. Later experiments showed that purification was unnecessary as long as the crude thiophenol **58** was used immediately to form the ester **59**. The ester **59** was deprotected by reacting with a strong base to form the acid **60**. The deprotected acid **60** was activated with CDI to form a carbonylimidazole intermediate **72** before being coupled to CoA-Li_3 to form the corresponding acyl-CoA ester **49** (Scheme 3.6). The acyl-CoA ester **49** was purified using solid phase extraction. The *meta*- acyl-CoA-ester **50** was synthesised by an analogous route starting from *meta*-phenoxyphenol **73** (Scheme 3.7).

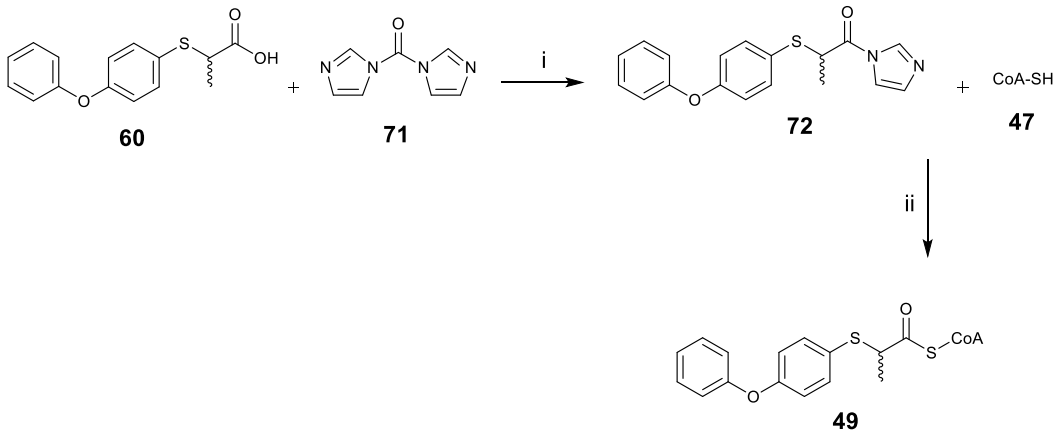

Scheme 3.6: Synthesis of acyl-CoA ester **49** from its deprotected acid **60**. Reagents and conditions: i) DCM, rt, 1 h; ii) THF, 0.1 M $NaHCO_{3\ aq.}$, rt, 18 h.

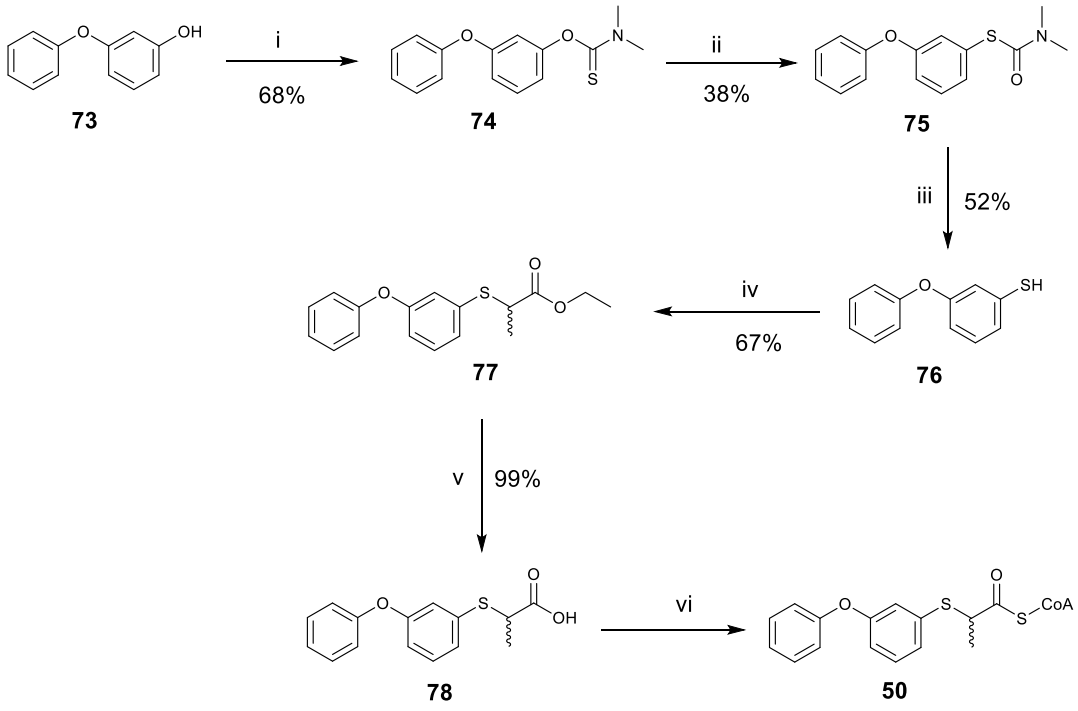

Scheme 3.7: Synthesis of *meta*- acyl-CoA-ester **50** from *meta*- phenoxyphenol **73**. Reagents and conditions: i) NaH, DMF, 10 °C, then *N*,*N*-dimethylthiocarbamoyl chloride, 70 °C, 21 h; ii) argon atmosphere, 280 °C, 1.7 h; iii) 2.5 M $NaOH_{\ aq.}$, MeOH, reflux, 4 h; iv) K_2CO_3, MeCN, -45 °C, 15 min, then ethyl 2-bromopropionate, rt, 20 h; v) 2.5 M $NaOH_{\ aq.}$, MeOH, rt, 1.5 h; vi) DCM, CDI, rt, 1 h, then THF, 0.1 M $NaHCO_{3\ aq.}$, CoA-Li_3, rt, 18 h.

3.2.2 Synthesis of 3-sulfone inhibitors

To synthesise *para*- sulfone **51**, H_2O_2 was first used as an oxidising agent to convert the sulfide **59** to sulfone **79** (Scheme 3.8).[41] The desired product was obtained but was mixed with *ca.* 40% of an unknown impurity which could not be separated. It was postulated that H_2O_2 is not a sufficiently strong enough oxidising agent to fully oxidise the sulfide.

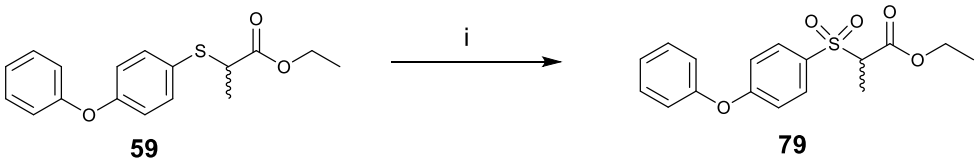

Scheme 3.8: Attempted synthesis of *para*- sulfone **79**. Reagents and conditions: i) cyanuric chloride, MeCN, 30% (w/w) $H_2O_{2\ aq.}$, rt, 22 h.

Another oxidising agent, OXONE® was tried and gave a yield of 82% of sulfone **79** (Scheme 3.9).[175] The synthetic routes for both *para*- and *meta*- sulfone were similar, with the reaction time being the only variation. The formation of *para*- sulfone **79** took only 4 hours (Scheme 3.9), whilst the reaction to produce the *meta*- sulfone **80** took 21 hours (Scheme 3.10) to go to completion. The resulting *para*- and *meta*- sulfones (**79** and **80** respectively) were deprotected to form their corresponding acids (**81** and **82**, respectively).

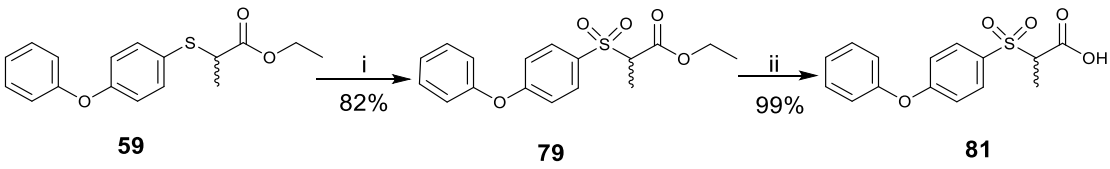

Scheme 3.9: Synthesis of *para*- sulfone **79** and its deprotection. Reagents and conditions: i) OXONE®, MeOH/THF (1:1), rt, 4 h; ii) 2.5 M $NaOH_{aq.}$, MeOH, rt, 2 h.

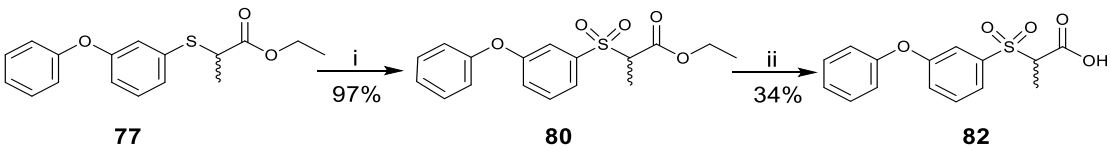

Scheme 3.10: Synthesis of *meta*- sulfone **80** and its deprotection. Reagents and conditions: i) OXONE®, MeOH/THF (1:1), rt, 21 h; ii) 2.5 M $NaOH_{aq.}$, MeOH, rt, 2 h.

The *para*- deprotected acid **81** was coupled with CoA-Li_3 to form acyl-CoA ester **51** (Scheme 3.11). A significant amount of uncoupled free CoA was found at the end of the reaction and the yield of *para*- acyl-CoA ester **51** was relatively low. The same procedure of CoA coupling was repeated on the *meta*- deprotected acid **82** and none of the *meta*- acyl-CoA ester **52** was found. A ^{1}H NMR experiment (reaction followed with ^{1}H NMR over time) showed that the imidazole derivative did not form. The coupling reaction was repeated using a standard acid (naproxen **12**)[2] and the imidazole derivative **84** formed with reasonable (71%) yield (Scheme 3.12). This suggested that the procedure of activating acids using carbonyldiimidazole worked but in this case the sulfone electron-withdrawing group might render the starting material less reactive to behave as a nucleophile. It seems that the electron-withdrawing effect was more significant with a sulfone possessing a *meta*- substituted aromatic side-chain compared to a sulfone possessing a *para*- substituted aromatic side-chain. Hence a low yield of the *para*- acyl-CoA ester **51** and zero yield of *meta*- acyl-CoA ester **52** were observed.

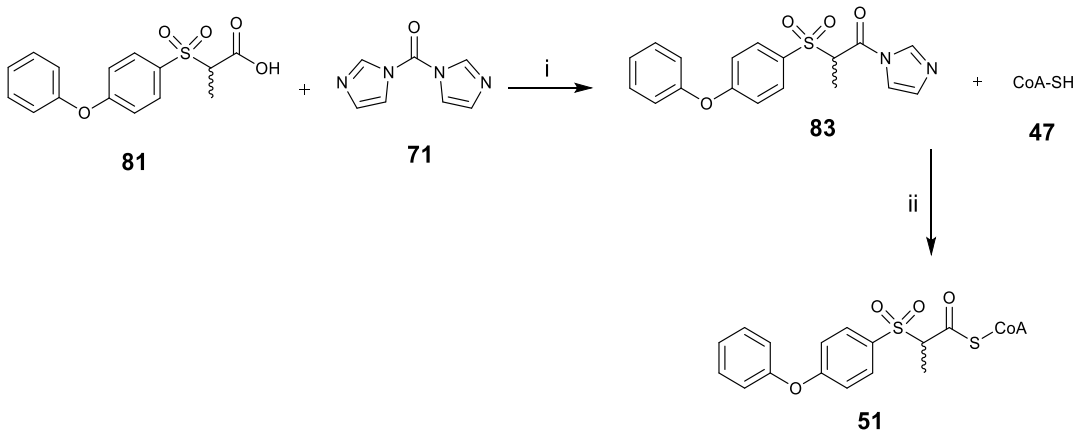

81 71 83 47 51

Scheme 3.11: Synthesis of *para*- acyl-CoA ester **51** from its deprotected acid. Reagents and conditions: i) DCM, rt, 1 h; ii) THF, 0.1 M $NaHCO_{3\ aq.}$, rt, 18 h.

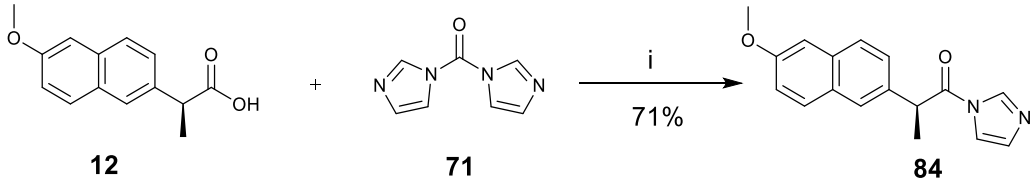

12 71 84

Scheme 3.12: Coupling of naproxen with CDI. Reagents and conditions: i) DCM, rt, 1h.

Instead of activating the acid with carbonyldiimidazole **71**, the activation of acid **81** was attempted with ethyl chloroformate **85** (Scheme 3.13), which is another standard method of producing acyl-CoA esters.[1, 176, 177] However, this method did not result in the formation of desired acyl-CoA ester **51**.

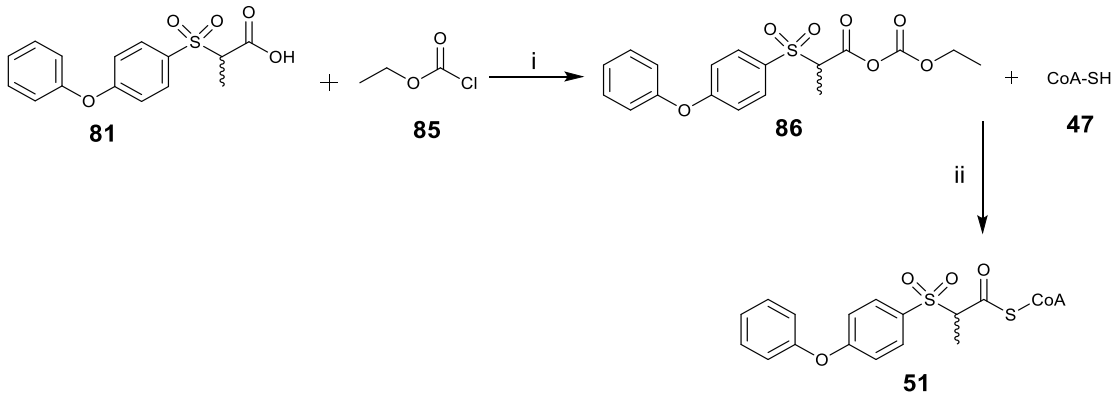

81 85 86 47 51

Scheme 3.13: Attempted synthesis of acyl-CoA ester **51**. Reagents and conditions: i) THF, triethylamine, ethyl chloroformate, rt. 0.5 h; ii) THF, 0.1 M $NaHCO_{3\ aq.}$, rt, 66 h.[1]

3.2.3 Synthesis of phenoxyphenol side-chain inhibitors

Instead of a 3-sulfide or 3-sulfone group, the 3-position was replaced with an oxygen atom (Figure 3.4) to investigate the effect of an electron-donating group on inhibitor potency. It has been shown that the side-chains of the *R*- and *S*- substrate binds to slightly different hydrophobic surface within the enzyme active site of MCR.[146] Carnell *et al.* has also suggested that the *R*-ibuprofenoyl-CoA **16** may be a more potent inhibitor of human AMACR (K_i = 5.4 µM) than the *S*-ibuprofenoyl-CoA **17** (K_i = 19.2 µM).[143] Hence, the 2-methyl group was arranged in both the *R*- and *S*- stereochemical configurations (Figure 3.4) to investigate any differences in competing with the natural substrate. The phenoxyphenol side-chain was arranged in a *meta*- or *para*-position (Figure 3.4) to investigate if it could bind differently to the enzyme and exhibit different potency.

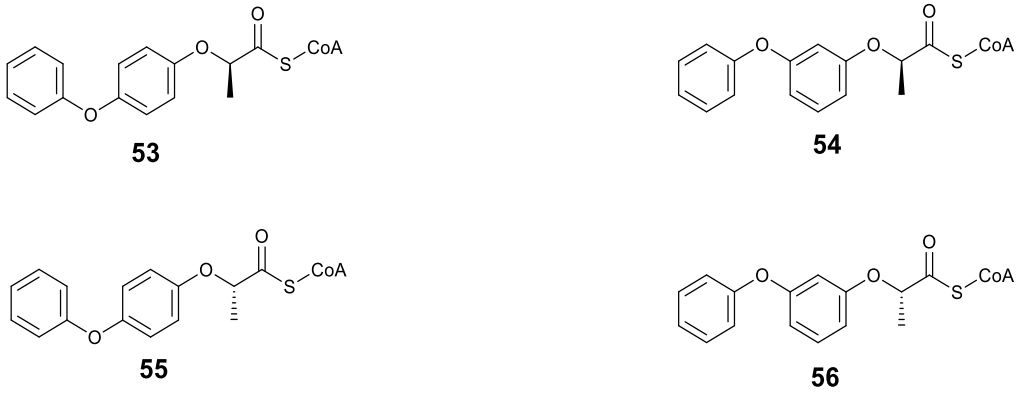

Figure 3.4: Potential AMACR inhibitors with a phenoxyphenol side-chain.

The synthesis of the proposed inhibitors (Figure 3.4) was started by reacting the appropriate methyl lactate with a phenoxyphenol to produce the corresponding methyl ester. The methyl ester was hydrolysed to form the corresponding acid. The acid was coupled with CoA-Li_3 using the standard carbonyldiimidazole method (*vide supra*). The whole reaction scheme starting from phenoxyphenol to the final acyl-CoA ester was shown in Scheme 3.14. Only one example of the acyl-CoA ester **53** is shown as all of them followed the same route.

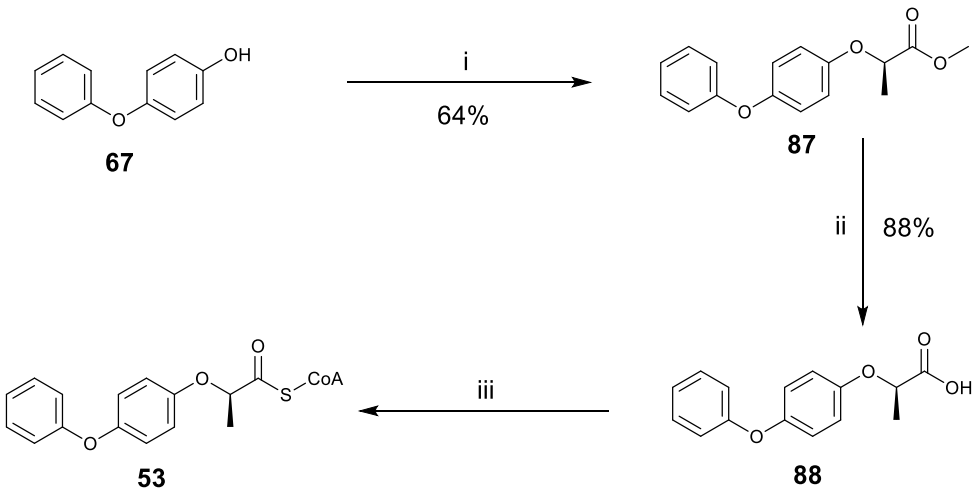

Scheme 3.14: Synthesis of acyl-CoA ester **53** from its corresponding phenoxyphenol. Reagents and conditions: i) Triphenylphosphine, methyl *S*-lactate, THF, DEAD, rt, 24 h; ii) 2.5 M $NaOH_{aq.}$, MeOH, rt, 2.5 h; iii) DCM, CDI, rt, 1 h, then THF, 0.1 M $NaHCO_{3\ aq.}$, CoA-Li_3, rt, 18 h.

A 4-phenoxyphenol **67** and 3-phenoxyphenol **73** were used to produce a methyl ester with a *para*- (**87** and **91**) and *meta*- (**93** and **95**) side-chains, respectively. The phenoxyphenol could either react with a methyl *S*-lactate **89** to form the *R*-methyl esters (**87** and **93**) or a methyl *R*-lactate **90** to form the *S*-methyl esters (**91** and **95**). Methyl esters (**87**, **91**, **93** and **95**) were hydrolysed to form the corresponding acids (**88**, **92**, **94** and **96**, respectively) (Scheme 3.15).

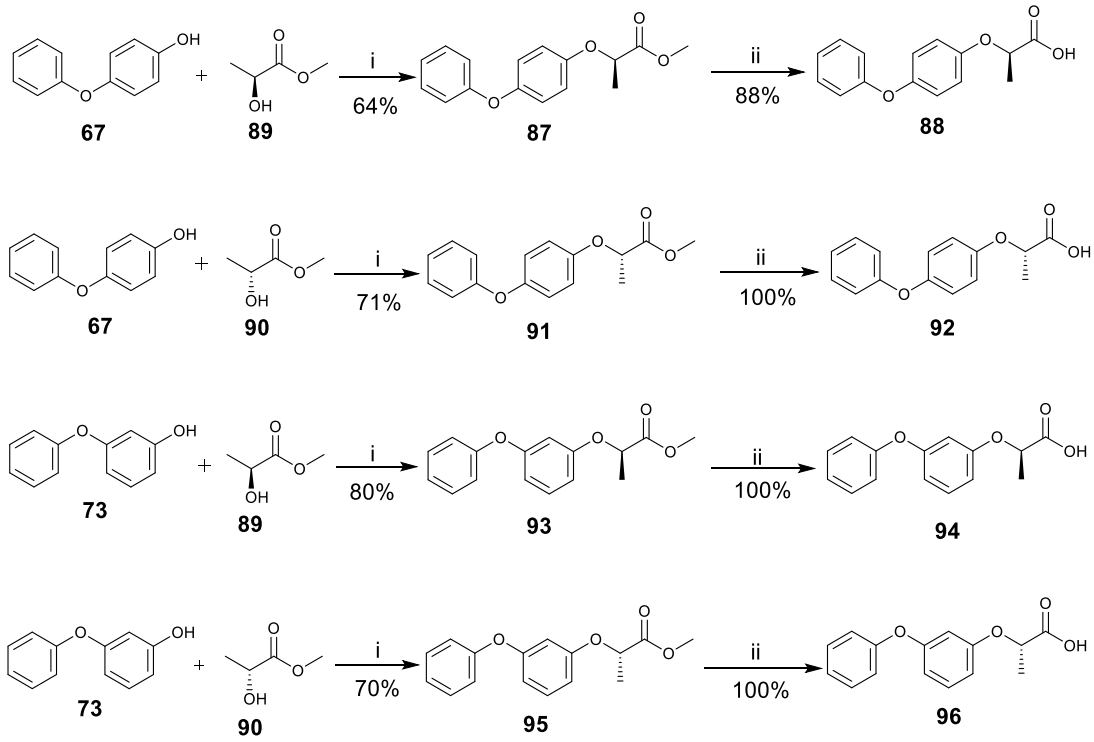

Scheme 3.15: Various combinations of phenoxyphenol and methyl lactate to produce methyl esters with a *para*- or *meta*- side-chain and *R*- or *S*- stereochemical configuration. These were hydrolysed to form the corresponding acids. Reagents and conditions: i) Triphenylphosphine, THF, diethyl azodicarboxylate (DEAD), rt, 24 h; ii) 2.5 M $NaOH_{aq.}$, MeOH, rt, 2.5 h.

The reaction of phenoxyphenol and methyl lactate was performed using the Mitsunobu reaction (Scheme 3.16).[178-180] Triphenylphosphine **97** first reacted with the diethyl azodicarboxylate (DEAD) **98** to produce an intermediate **99** that would deprotonate the phenol **67**. The OH group from the methyl lactate **89** attacks the positively charged phosphorus atom to produce an oxonium **105**. The phenoxide **100** reacted with the resulting oxonium cation **105**. This

is substituted using an S_N2 reaction which led to the formation of a methyl ester **87** with inversion of stereochemical configuration.

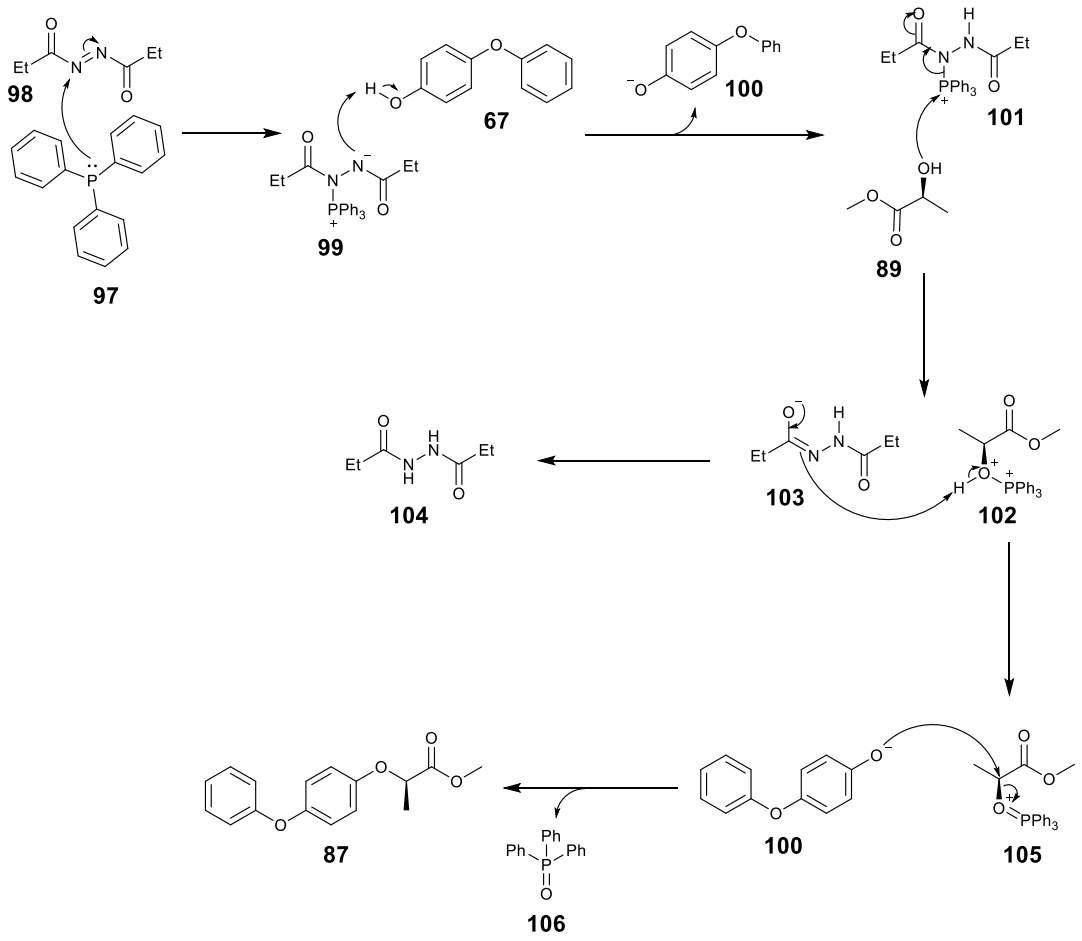

Scheme 3.16: The mechanism of the Mitsunobu reaction.[178-180]

3.2.4 Synthesis of long-chain inhibitors

In addition to substrates with a sulfide and sulfone group at β-position, these groups were also placed at the γ-position. It would be interesting to see if having these group at γ-position has any electron-withdrawing effect to the α-proton, and whether they could affect the enolisability of the compound. If they could improve the enolisability, the compound would mimic the transition-state analogues better and could potentially increase the inhibitor potency. As Dr Daniel Darley from the MDL group has already prepared long-chain acids with sulfide **107** and sulfone **108** at the γ-position, no further acids were synthesised. These acids were analysed to confirm their identity and purity, and subsequently coupled with CoA-Li_3 to produce the corresponding acyl-CoA esters **109** and **110** (Scheme 3.17).

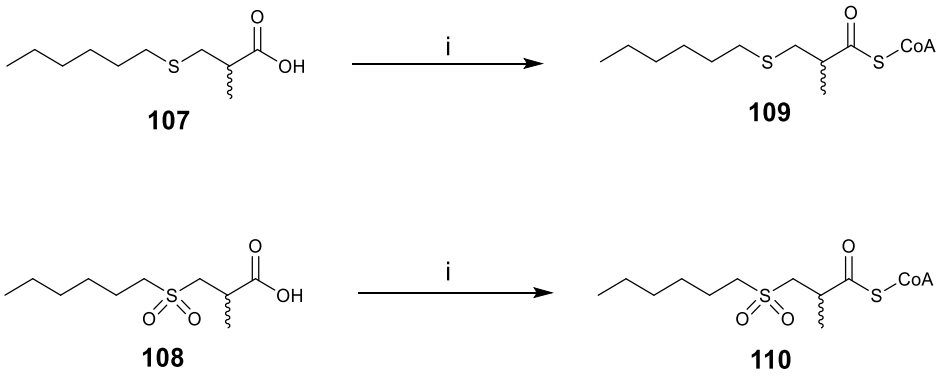

Scheme 3.17: Synthesis of long-chain inhibitors from their corresponding acids. Reagents and conditions: i) DCM, CDI, rt, 1 h, then THF, 0.1 M $NaHCO_{3\ aq.}$, CoA-Li_3, rt, 18 h.

3.3 Limitations of the currently reported assays

Attempts to measure the activity of AMACR and to test the potency of AMACR inhibitors are hampered by the limited number of convenient assays available.[1, 85, 106, 145] This is mainly due to the enzyme being a racemase. AMACR 'racemises' the 2-methyl group from one stereochemical configuration to another while the remaining structure of substrate remains unchanged.[1] This makes the substrate and product almost indistinguishable from one another by most analytical methods except by measurements of chirality which are insensitive and time-consuming. Another draw-back is that acyl-CoA inhibitors can potentially undergo 'racemisation' as they are structurally similar to substrate.Therefore, it might be difficult to determine if it is substrate or inhibitor 'racemisation' that is been measured. Hence, it is very tricky to develop an assay to measure the change from the substrate to the product (*i.e.*, enzyme activity) or to measure the suppression of such a change (*i.e.*, drug potency). Assays for other racemases also suffer from the same problems, and a very limited number of assays, especially high-throughput assays, have been developed.[181-183]

Currently, there are AMACR assays that are based on the use of hydrogen isotopes such as the exchange of hydrogen with deuterium which can be measured with ^{1}H NMR[1, 2, 147, 184] or the measurement of radioactivity due to the release of tritium from a ^{3}H-labelled substrate.[85, 91] These methods

measure α-proton exchange and not 'racemisation' and a kinetic isotope effect is probably also present, which complicates analyses. There are also HPLC or GLC methods for measuring AMACR activity[91, 145] as well as a CD assay[106] to study the changes in chirality between the substrate and the product. However, each assay has its own flaws and as they are not high-throughput, the measurements are very time consuming.

3.4 Assay to determine binding of potential AMACR inhibitors to the enzyme

A limited number of compounds were designed as potential AMACR inhibitors in this current study. The number of compounds synthesised might not be sufficient to fully explore the SAR of AMACR inhibitors, but they serve as a good starting point to allow parallel study of inhibitor design as well as the development of a more convenient AMACR assay.

To characterise the potential inhibitors which were synthesised, they were first tested using the deuterium wash-in assay.[1, 2] If AMACR catalyses α-proton exchange, it shows that the compound binds to the enzyme and is a substrate, and therefore potentially of use as a competitive inhibitor. If the compound is a substrate of AMACR, it will probably also be 'racemised' by the enzyme (for a definite confirmation of 'racemisation', a derivatisation of products has to be performed).[1]

Inhibitor acyl-CoA esters were dissolved in $^{2}H_2O$ and the concentrations of the stock solutions were determined by ^{1}H NMR.[2] These acyl-CoA esters were incubated with AMACR in the presence of $^{2}H_2O$. Heat-inactivated AMACR was used as a negative control. After 1 h of incubation at 30 °C, the enzyme was heat inactivated and ^{1}H NMR was used to measure the levels of α-proton exchange.

When acyl-CoA ester **49** was incubated with active AMACR, its α-proton was exchanged for deuterium. As a result, the 2-methyl peak turned from a doublet (at 1.34 ppm) to an unresolved triplet (appeared as a single peak at 1.33 ppm) as it was next to a deuterium instead of a proton and is no longer split by a

proton (Figure 3.5 C). The doublet of the compound when incubated with heat-inactivated enzyme (Figure 3.5 B) and the single peak resulted from the action of live enzyme on the compound (Figure 3.5 C) were integrated. These integrals were used to calculate the percentage of exchange. A limited amount of non-enzymatic exchange occurrs, as shown by the spectrum from the incubation of the compound with the heat-inactivated enzyme (Figure 3.5 B). This may be due to the electron-withdrawing properties of the sulfide which reduces the pK_a of the α-proton and makes the deprotonation event occur more readily. After taking into account the non-enzymatic exchange, acyl-CoA ester **49** seemed to have undergone 88% of enzyme-catalysed deuterium exchange.

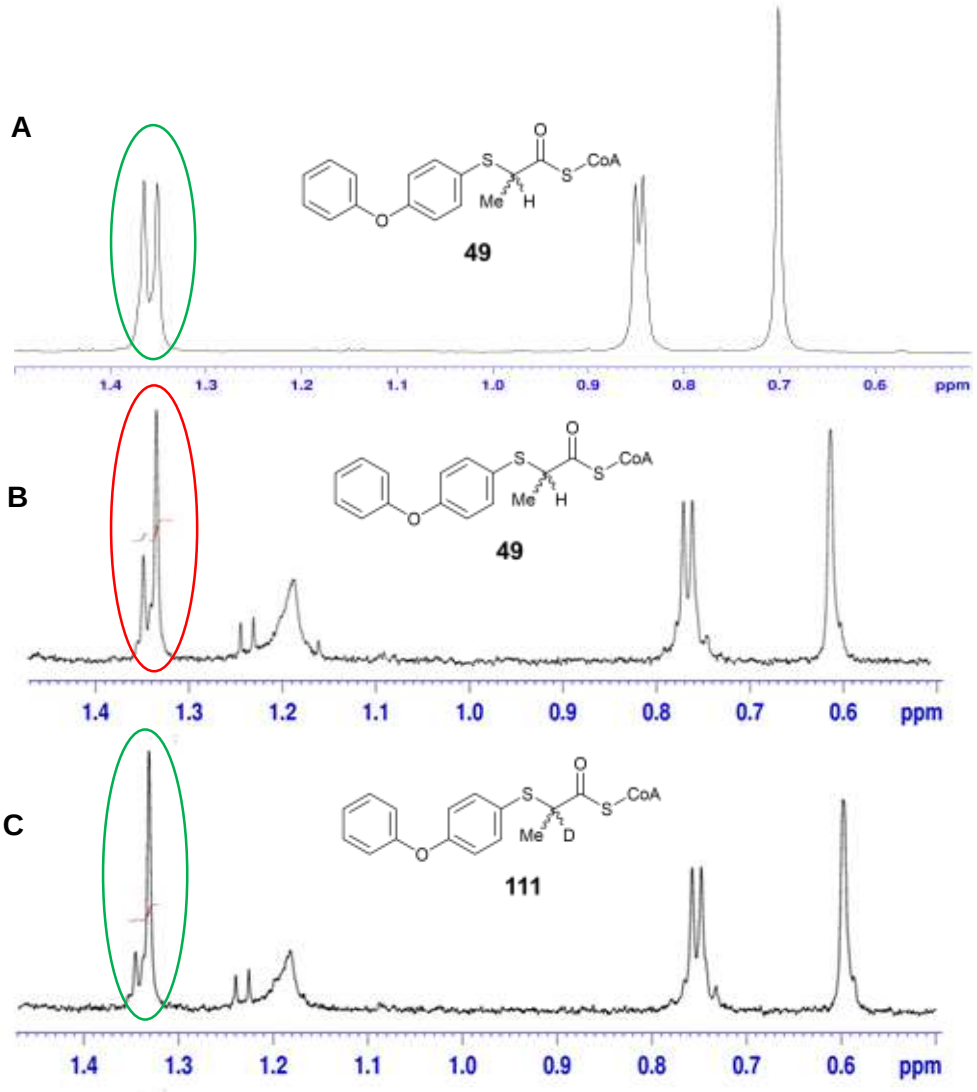

Figure 3.5: Different splitting patterns of 2-methyl peak at *ca.* 1.35 ppm of potential inhibitor **49** on ^{1}H NMR spectra. A) The compound was dissolved in $^{2}H_2O$ prior to the enzyme assay; B) The compound (final assay concentration 100 µM) incubated with heat-inactivated AMACR (final assay concentration 0.18 mg mL^{-1}; 3.82 µM); C) The compound (final assay concentration 100 µM) incubated with active AMACR (final assay concentration 0.18 mg mL^{-1}; 3.82 µM).

With acyl-CoA ester **50**, an extensive non-enzymatic exchange has occurred, resulted in very similar spectra for both the samples containing heat-inactivated enzyme (Figure 3.6 B) and active enzyme (Figure 3.6 C). More than 70% deuterium exchange has occurred in the sample containing heat-inactivated enzyme, showing that exchange of the α-proton in this compound is very facile.

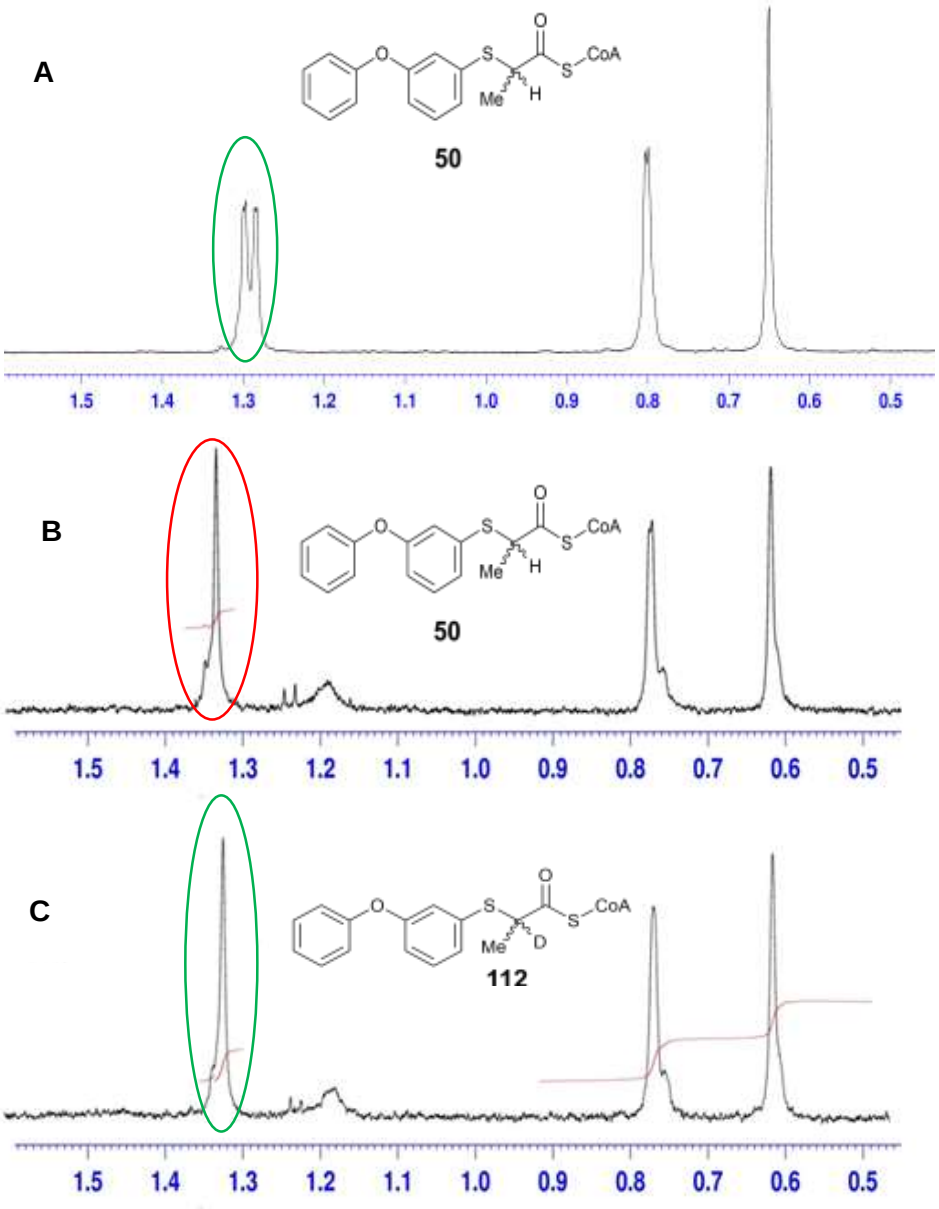

Figure 3.6: Different splitting patterns of 2-methyl peak at *ca.* 1.30 ppm of potential inhibitor **50** on ^{1}H NMR spectra. A) The compound was dissolved in $^{2}H_2O$ prior to the enzyme assay; B) The compound (final assay concentration 100 µM) incubated with heat-inactivated AMACR (final assay concentration 0.18 mg mL^{-1}; 3.82 µM); C) The compound (final assay concentration 100 µM) incubated with active AMACR (final assay concentration 0.18 mg mL^{-1}; 3.82 µM).

The deuterium wash-in assay was only used to investigate a couple of the potential inhibitors which were synthesised. It aimed to prove that the manipulation of the side-chain of acyl-CoA ester would still allow the binding of the compound to AMACR and it predicts that these compounds would behave as competitive inhibitors. The results came back as predicted; the

compounds tested have been shown to be substrates of AMACR and underwent α-proton exchange. This was not surprising as AMACR has been shown to accept a spectrum of substrates with a number of different types of side-chains structures.[2, 76, 146]

This assay could be used to test whether a compound is a substrate for AMACR but would not be useful as an inhibitor assay for several reasons. Both the substrate and the potential inhibitor of AMACR have a 2-methyl group which has a chemical shift of *ca.* 1.00 ppm.[1] To observe deuterium exchange by integrating the change from doublet to single with overlapping peaks would be very difficult if not impossible. In addition, the involvement of deuterium in both substrate and inhibitor might complicate the results due to the operation of a solvent kinetic isotope effect.

3.5 Fluoride elimination assay

As the deuterium wash-in assay was unsuitable for measuring the potency of the compounds as AMACR inhibitors, an alternative assay method was sought. Yevglevskis *et al.* reported that *syn*- **113** and *anti*- 3-fluoro-2-methyldecanoyl-CoA **114** could undergo an elimination reaction catalysed by AMACR (Figure 3.7).[3] This was the first report that AMACR could perform a reaction other than 'racemisation' on one of its substrates.[3]

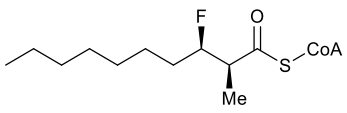

113

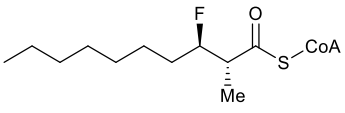

114

Figure 3.7: *Syn*- and *anti*- 3-fluoro-2-methyldecanoyl-CoA substrates reported by Yevglevskis *et al.*[3]

As discussed previously, the analysis of ^{1}H NMR can be complicated by multiple peaks from the substrate and the product. In addition, to probe the substrates stereochemical configuration entailed a derivatisation step, which can be tricky on the small amount of material involved. The 3-fluoro-2-methyldecanoyl-CoA esters were originally synthesised with the aim of overcoming these problems. If the ester was 'racemised' by AMACR, it would

produce diastereomers (Scheme 3.18) which have different chemical shifts in the ^{1}H and ^{19}F NMR spectra. Since the only peaks in the ^{19}F spectra would be from the substrate (*i.e*., no background peaks as fluorine is relatively rare, unlike in the ^{1}H spectrum), it would be easier to analyse the reaction mixture as only two peaks of diastereotopic fluorine would be expected.[3]

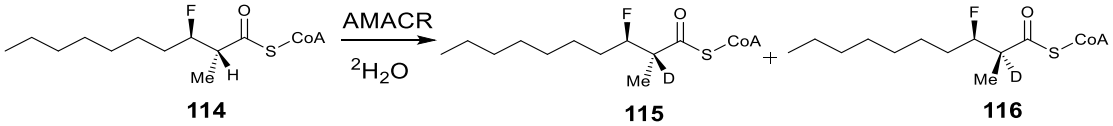

Scheme 3.18: The expected 'racemisation' reaction catalysed by AMACR.[3]

However, the results showed that instead of being 'racemised' by AMACR, the 3-fluoro-2-methyldecanoyl-CoA esters **114** underwent elimination. In the ^{1}H NMR spectrum, the 2-methyl peak did not convert from a doublet into an unresolved triplet. Instead the 2-methyl doublet at *ca.* 1.10 ppm diminished with time (Figure 3.8). A new peak at *ca.* 1.75 ppm also appeared and increased in intensity over time (Figure 3.8). This new peak corresponded to a methyl peak next to a double bond, suggesting that the saturated substrate was converted into an unsaturated product. When the reaction was analysed by ^{19}F NMR spectrum, the organic fluorine peak at *ca*. -181 ppm disappeared and a peak that corresponded to the inorganic fluoride anion at *ca.* -122 ppm appeared. This showed that *anti*-3-fluoro-2-methyldecanoyl-CoA **114** underwent an elimination reaction catalysed by AMACR to form an unsaturated product **117** and inorganic fluoride **118** (Figure 3.8). The identity of the unsaturated product **117** was confirmed by the synthesis of an authentic product.[3] The same elimination reaction was observed with *syn*-3-fluoro-2-methyldecanoyl-CoA **113** but as this was less stable, it underwent a significant non-enzymatic elimination reaction.[3] The AMACR-catalysed elimination reaction was irreversible as the incubation of the unsaturated compound **117** with AMACR and inorganic fluoride did not produce the saturated ester **113** or **114**.[3]

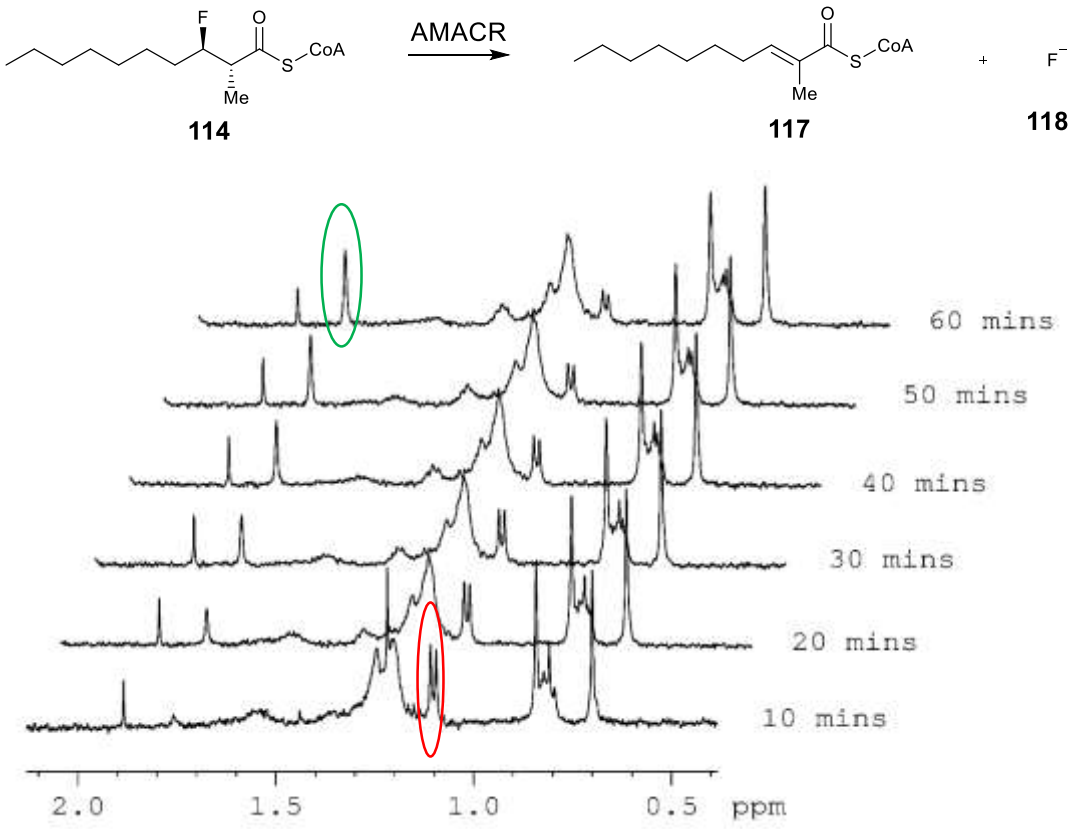

Figure 3.8: ^{1}H NMR time course of (2*R*,3*R*)-3-fluoro-2-methyldecanoyl-CoA **114** (final assay concentration 100 µM) when incubated with AMACR (final assay concentration 0.12 mg mL^{-1}; 2.55 µM) over 60 min. The saturated substrate decreased over time (shown by diminished peak at *ca*. 1.10 ppm) and the unsaturated product increased over time (shown by the formation of peak at *ca.* 1.75 ppm).

3.5.1 Evaluation of potential AMACR inhibitors using fluoride elimination assay

The fluoride elimination assay could be used to test for potential AMACR inhibitors as the methyl peaks of the substrate and the product have significantly different chemical shifts (at *ca.* 1.10 and 1.75 ppm respectively). Non-overlapping peaks make it much easier to quantify the extent of substrate conversion. As the *anti*-acyl-CoA ester **114** has been shown to be more stable than the *syn*- ester **113**,[3] (2*R*,3*R*)-3-fluoro-2-methyldecanoyl-CoA **114** (*anti*-) was chosen for use in the fluoride elimination assay. If a compound was an inhibitor of AMACR, it would inhibit the elimination reaction of the (2*R*,3*R*)-3-fluoro-2-methyldecanoyl-CoA **114**, and this would be reflected by a reduction in conversion as measured by integration of the peaks at *ca.* 1.10 and 1.75 ppm (Figure 3.9).

In the absence of an inhibitor, around 50% of (2*R*,3*R*)-3-fluoro-2-methyldecanoyl-CoA **114** substrate was converted to product after 1 h in the presence of active enzyme. The spectrum shows almost equal integration for the doublet at *ca.* 1.10 ppm and singlet at *ca.* 1.75 ppm (Figure 3.9 B). In the presence of an inhibitor, the level of elimination will be reduced to an extent depending on the potency of the inhibitor. Hence, there is less conversion from the doublet to the singlet (Figure 3.9 C). In the negative control (heat-inactivated enzyme), there was only non-enzymatic background elimination so the spectrum shows mostly a doublet with a minimal amount of singlet (<10% conversion) (Figure 3.9 D). The inhibitor *N*-dodecyl-*N*-methylcarbamoyl-CoA **30** at 100 μM almost completely abolished the enzyme activity as shown by peaks in the sample with active enzyme (Figure 3.9 B), inhibitor (Figure 3.9 C) and the negative control (Figure 3.9 D).

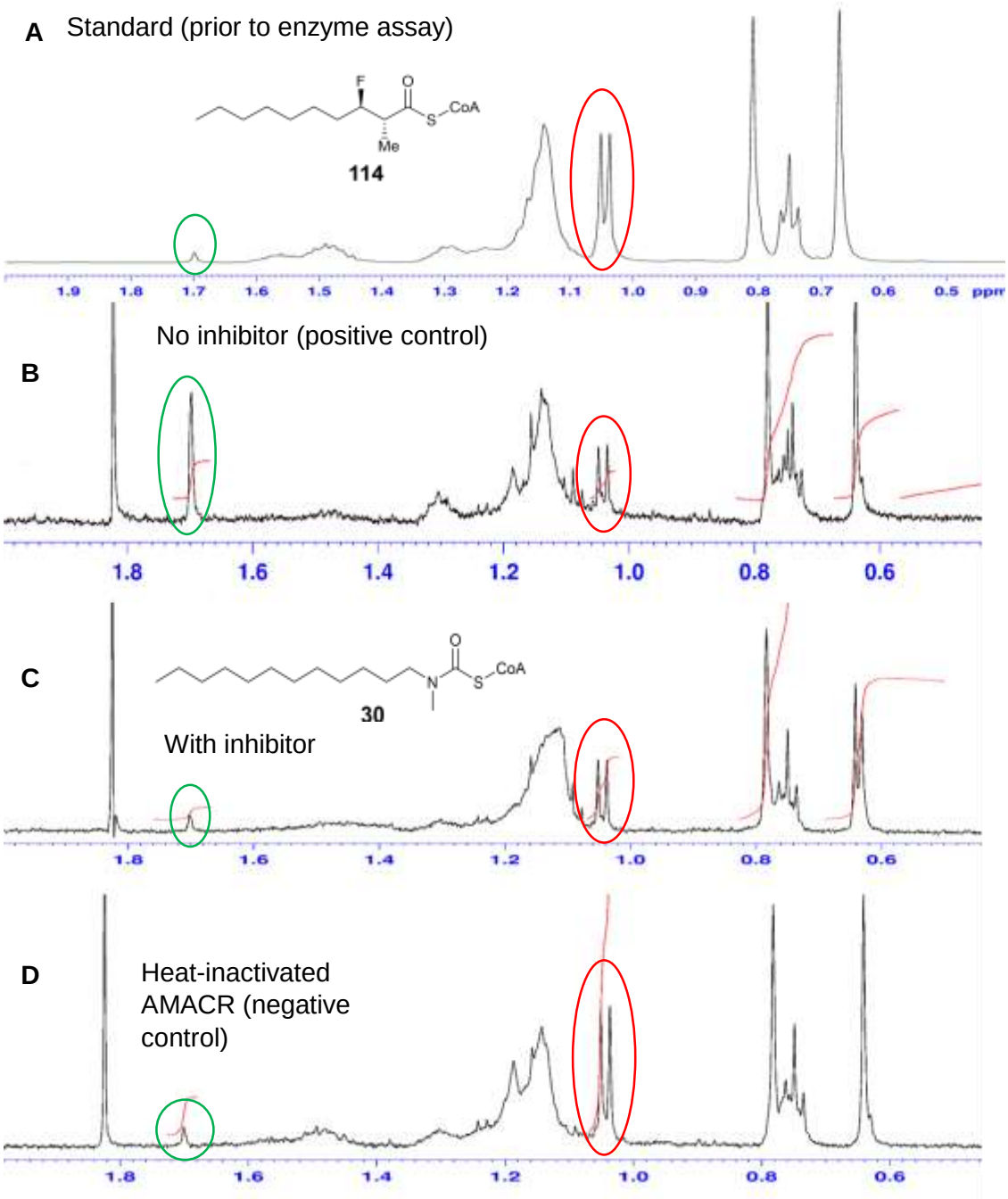

Figure 3.9: ^{1}H NMR spectra of the fluoride elimination assay using (2*R*,3*R*)-3-fluoro-2-methyldecanoyl-CoA **114** (final assay concentration 100 µM) as the substrate, incubated with AMACR (final assay concentration 0.12 mg mL^{-1}; 2.55 µM). The red circles show the doublet at *ca.* 1.10 ppm of the 2-methyl group from the saturated substrate **114** and the green circles show the singlet at *ca.* 1.75 ppm of the 2-methyl group from the unsaturated product **117**. A) Substrate **114** in $^{2}H_2O$ prior to the enzyme assay; B) Positive control without any inhibitor; C) Reaction in the presence of an inhibitor (*N*-dodecyl-*N*-methylcarbamoyl-CoA **30** at 100 µM); D) Negative control containing heat-inactivated AMACR.

To quantify the level of elimination, the doublet at *ca.* 1.10 ppm and the singlet at *ca.* 1.75 ppm were integrated. Enzymatic conversion was calculated by correcting for background elimination in the negative control. The elimination of the substrate in the absence of an inhibitor was used as a comparison standard to allow a 'rank order' of compounds to be produced between different experiments. The percentage of elimination in the presence of an inhibitor was calculated by subtracting the integration from the negative control and was normalised to positive control. The measurements were done in duplicates and average values and standard deviations were calculated.

^{19}F NMR was also run to detect the presence of inorganic fluoride anion. In the positive control, both the organic fluorine peak at *ca.* -181 ppm and inorganic fluoride peak at *ca*. -122 ppm were observed as ~50% of the substrate had undergone elimination after 1 h (Figure 3.10 B). In the presence of an inhibitor, this elimination was much reduced and less fluoride anion was produced as was shown by a smaller integration at peak of *ca.* -122 ppm (Figure 3.10 C). No significant elimination occurred in the negative control containing heat-inactivated enzyme, so no peak at *ca*. -122 ppm was observed (Figure 3.10 D). These results are consistent with those obtained by ^{1}H NMR.

A Standard (prior to enzyme assay)

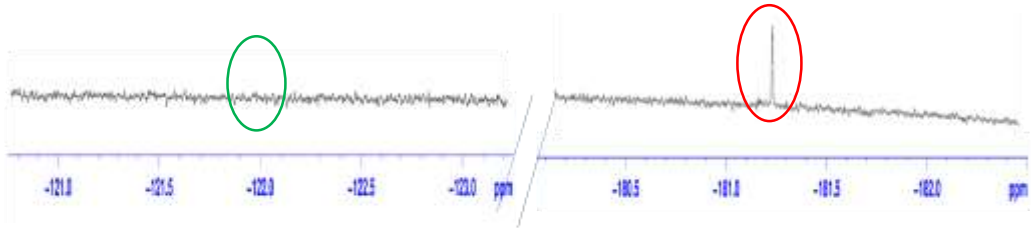

B No inhibitor (positive control)

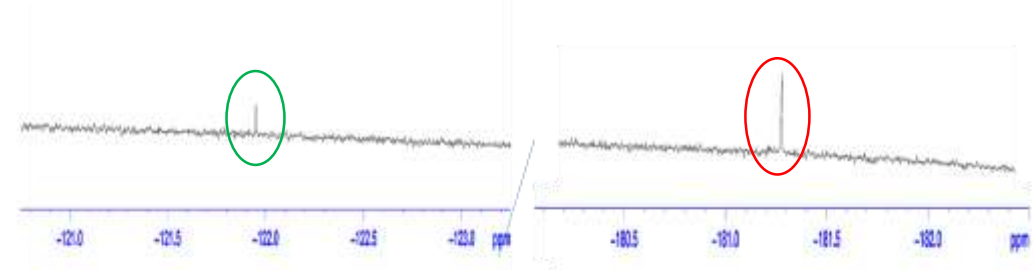

C With inhibitor

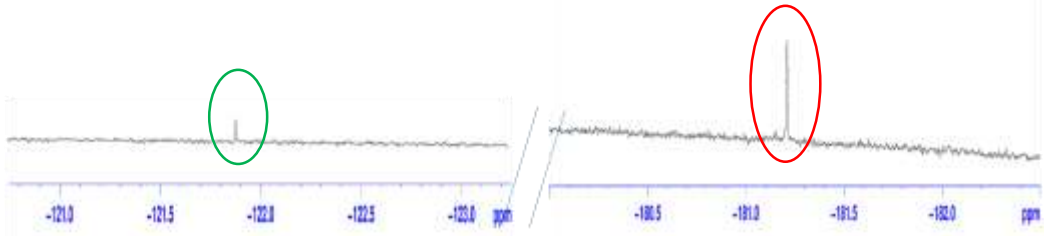

D Heat-inactivated enzyme (negative control)

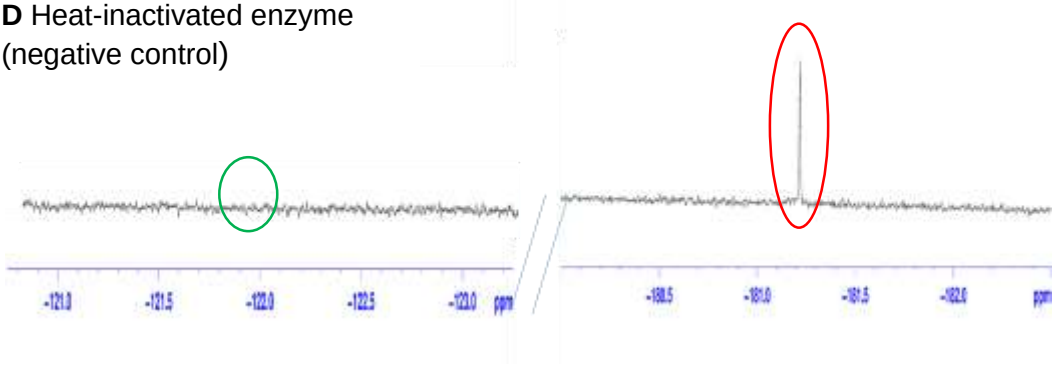

Figure 3.10: ^{19}F NMR spectra of fluoride elimination assay using (2*R*,3*R*)-3-fluoro-2-methyldecanoyl-CoA **114** (final assay concentration 100 µM) as the substrate, incubated with AMACR (final assay concentration 0.12 mg mL^{-1}; 2.55 µM). A) Substrate **114** in $^{2}H_2O$ prior to the enzyme assay; B) Positive control in the absence of an inhibitor; C) Reaction in the presence of an inhibitor (final assay concentration 100 µM); D) Negative control containing heat-inactivated AMACR. The red circles show the organic fluorine peak from the substrate while the green circles show the inorganic fluoride anion peak formed from the elimination reaction. Please note that the regions at -181 and -122 ppm were expanded and the spectra were not continuous (as indicated by the double lines).

The initial protocol involved adding the substrate and the potential AMACR inhibitor at the same time to the enzyme. The percentage conversion was calculated using ^{1}H NMR based on the integration of the 2-methyl peaks from the substrate and the product. The inhibitor was first tested at a final concentration of 50 μM. It was found that the inhibition was minimal especially for a weak inhibitor and this could result in large errors due to the difficulty in quantifying small changes. The final concentration of inhibitor was therefore set at 100 μM for subsequent tests.

All the potential AMACR inhibitors that had been synthesised were tested using the fluoride elimination assay and the results are shown in Table 3.1. Except for compound **55** which showed almost no inhibition of AMACR (<5%), all of the novel compounds (**49**, **50**, **51**, **53**, **54**, **56**, **109** and **110**) were moderate inhibitors of the enzyme (15-38% inhibition). In addition to the novel compounds, some known compounds were also tested. Ibuprofenoyl-CoA **119** has previously been shown to be an inhibitor of AMACR with K_i value of 56 μM.[91] It was tested in this assay and gave a positive result, inhibiting the elimination of the substrate by 24%, consistent with previous findings[91, 143] that it was a moderate AMACR inhibitor. Darley *et al.* reported that *R*- **44** and *S*-2-methyldecanoyl-CoA **38** were substrates of AMACR with K_m values of 1.2 mM for both of them.[1] These substrates are expected to behave as competitive inhibitors of AMACR. They were tested in the fluoride elimination assay and showed moderate to weak inhibition on AMACR (19% for *R*-acyl-CoA ester **44** and 11% for *S*-acyl-CoA ester **38**).

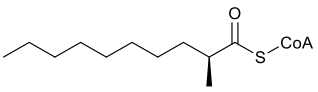

38

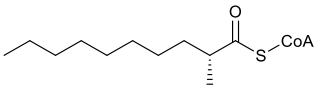

44

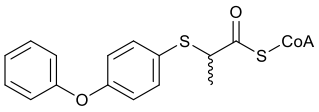

49

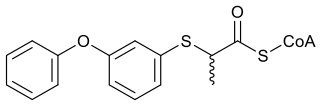

50

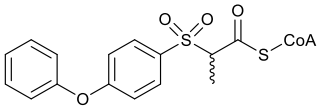

51

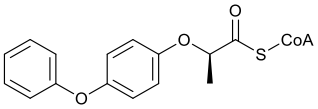

53

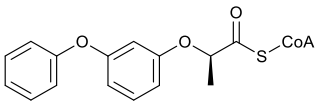

54

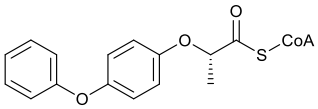

55

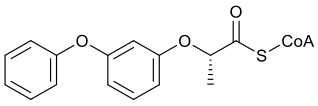

56

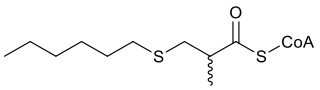

109

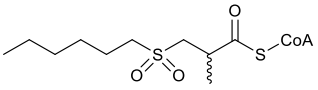

110

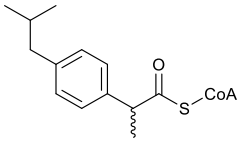

119

Compound	Relative conversion compared to no inhibitor	Reduction in conversion compared to no inhibitor
No inhibitor	100%	0%
38	88.9 ± 6.4%	11.1%
44	80.9 ± 5.3%	19.1%
49	78.1 ± 10.4%	21.9%
50	76.1 ± 0.5%	23.9%
51	75.0 ± 1.7%	25.0%
53	61.8 ± 7.1%	38.2%
54*	84.6 ± 15.0%	15.4%
55	>95%	<5%
56*	61.8 ± 3.4%	38.2%
109	72.0 ± 5.5%	28.0 %
110	80.5 ± 5.8%	19.5%
119	76.1 ± 0.2%	23.9%

Table 3.1: Fluoride elimination assay. (2*R*,3*R*)-3-Fluoro-2-methyldecanoyl-CoA **114** substrate (final assay concentration 100 µM) and potential inhibitor were added to AMACR (final assay concentration 0.12 mg mL^{-1}; 2.55 µM) at the same time and incubated with the enzyme for 1 h. The results show the percentage of elimination after correction for non-enzymatic conversion and are normalised to the positive control (100%). The results are quoted as average values (2 replicates) ± standard deviation. All inhibitors tested were in final concentration of 100 µM except those with an asterisk which were tested at 50 µM.

The problem with adding the inhibitor and substrate to the enzyme at the same time is that the inhibitor may not have a chance to bind to the enzyme before it competes for binding with the substrate. The relative kinetics and binding affinities of substrate compared to inhibitor could affect the results. This is usually not a problem for a classical reversible inhibitor that associates and dissociates from the enzyme at a rate much faster than the formation of the product.[185] If a compound is a slow-binding inhibitor, not pre-incubating it with the enzyme would underestimate the potency of the inhibitor and potentially could give a false negative result. A slow-binding inhibitor will bind in a time-dependent fashion, so sufficient pre-incubation time allows it to bind to the binding site of the enzyme to compete with the substrate.[186] Hence, the

protocol was modified to incorporate a 10-min pre-incubation time of inhibitor and enzyme in order to identify time-dependent inhibitors. The final concentration of inhibitor was the same as the previous protocol (100 μM) to allow comparisons between protocols.

The results using the protocol involving pre-incubation (Table 3.2) were generally improved compared to the previous protocol. The best inhibitors from the previous protocol was **53** and **56** with 38% inhibition. The percentage inhibition was markedly increased to 51% for inhibitor **53** but there was no change for **56** (38%). This suggests that inhibitor **53** could be a slowly binding but a potent inhibitor and pre-incubation allowed it to bind to the enzyme to compete with the substrate. On the other hand, compound **56** was a fast binding inhibitor. Binding reached equilibrium rapidly so pre-incubation made no significant difference to its ability in inhibiting the enzyme. The previous protocol also gave a false negative result with compound **55** which showed <5% inhibition (*vide supra*). Using the pre-incubation protocol, compound **55** was shown to be a moderate inhibitor where it inhibited the elimination of the substrate by 27%. The differences in results could be due to the relative kinetics of inhibitor binding compared to the substrate.

Known compounds were also tested as inhibitors using the pre-incubation protocol. The most potent inhibitor reported to-date is *N*-dodecyl-*N*-methylcarbamoyl-CoA **30** with K_i value of 98 nM.[145] Using the fluoride elimination assay, *N*-dodecyl-*N*-methylcarbamoyl-CoA **30** was shown to inhibit the enzyme by 83%, consistent with the finding that it was a potent inhibitor. The acyl-CoA esters of 2-APA drugs were also tested as they are known substrates of AMACR.[2] Presumably, they would behave as competitive inhibitors of the elimination reaction. Fenoprofenoyl-CoA **13** and ibuprofenoyl-CoA **119** showed moderate inhibition to AMACR, at 25% and 26%, respectively. Ketoprofenoyl-CoA **120**, naproxenoyl-CoA **121** and flurbiprofenoyl-CoA **122** each showed *ca.* 10% reduction in conversion, showing that they were modest inhibitors.

Ebselen **34**, ebselen oxide **35** and rose bengal **37** have been identified as inhibitors of AMACR by Wilson *et al*.[85] Ebselen oxide **35** was the most potent inhibitor reported in their assays, with an IC_{50} value of 0.80 µM, while ebselen **34** had an IC_{50} of 2.79 µM and rose bengal **37** had an IC_{50} of 10.0 µM.[85] Surprisingly, the fluoride elimination assay shows that of these 3 inhibitors, ebselen oxide **35** was the least potent, only inhibiting the elimination by 12%. In contrast, ebselen **34** and rose bengal **37** inhibited the elimination by more than 95%. As ebselen **34** covalently binds to the histidine residue to inactivate the enzyme,[85] measuring IC_{50} values is an inappropriate method of determining the potency of irreversible inhibitors. Rose bengal **37** is not a conventional reversible inhibitor. Its ability to inactive the enzyme appears to be mediated by the production of singlet oxygen followed by oxidative damage of the enzyme[187-189] and hence its effects are not pharmacologically tractable.[190] Hence, the results of fluoride elimination assay are not directly comparable to the previous study.

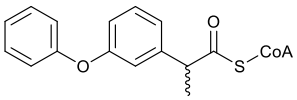

13

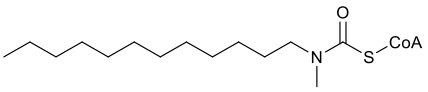

30

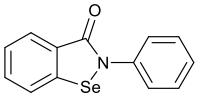

34

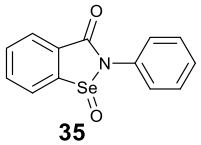

35

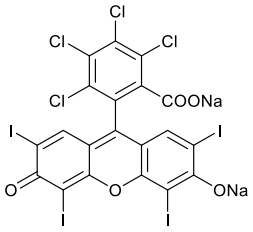

37

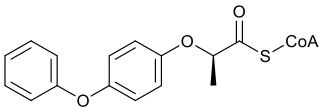

53

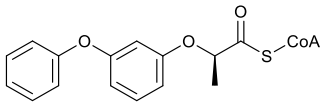

54

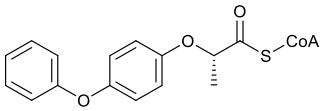

55

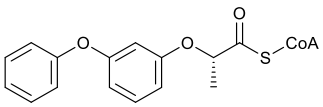

56

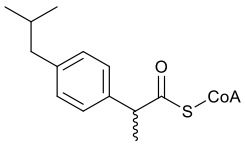

119

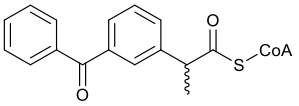

120

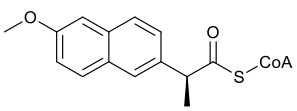

121

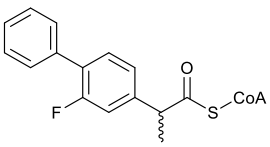

122

Compound	Relative conversion compared to no inhibitor	Reduction in conversion compared to no inhibitor
No inhibitor	100%	0%
13	75.0 ± 0.4%	25.0%
30	16.8 ± 1.9%	83.2%
34	<5%	>95%
35	88.2 ± 5.4%	11.8%
37	<5%	>95%
53	49.2 ± 0.9%	50.8%
54	68.2 ± 1.9%	31.8%
55	72.8 ± 0.9%	27.2%
56	62.1 ± 5.5%	37.9%
119	74.1 ± 7.2%	25.9%
120	92.0 ± 8.6%	8.0%
121	88.8 ± 4.0%	11.2%
122	91.6 ± 2.0%	8.4%

Table 3.2: Fluoride elimination assay. Potential AMACR inhibitors (final assay concentration 100 µM) were pre-incubated with human AMACR (final assay concentration 0.12 mg mL^{-1}; 2.55 µM) for 10 min before (2*R*,3*R*)-3-fluoro-2-methyldecanoyl-CoA **114** substrate (final assay concentration 100 µM) was added to the enzyme/inhibitor mixture. The results show the percentage of elimination after correction for non-enzymatic conversion and are normalised to the positive control (100%). Data are quoted as average values (2 replicates) ± standard deviation.

A range of small molecules were sent to our lab by Professor Paul Groundwater from the University of Sydney, Australia for testing using the fluoride elimination assay (Table 3.3). These molecules had been identified as potential inhibitors by structure-based design using the MCR crystal structures. These drug-like molecules have small molecular weights (ranging between 200-350 Da.) and do not have the CoA moiety which is bulky and highly charged. They were first tested using a final concentration of 100 µM for both substrate and inhibitor. None of the compounds showed any inhibition to the enzyme under these assay conditions.

The K_m of the (2*R*,3*R*)-3-fluoro-2-methyldecanoyl-CoA **114** substrate has been shown to be 21 µM.[3] As the concentration of substrate used in the assay is nearly 5 times the K_m value, competitive inhibition could be overcome by high concentration of substrate. Hence, the small reduction in activity by a weak competitive inhibitor would be difficult to observe. To investigate if the inhibition was masked by the high concentration of substrate, the concentration of (2*R*,3*R*)-3-fluoro-2-methyldecanoyl-CoA **114** was lowered to 20 µM.

The experiment was re-run with 100 µM of potential inhibitor and 20 µM of substrate (Table 3.3). Except for compound **123** which still did not show any inhibition, the other four compounds showed some inhibition of the enzyme at 20 µM substrate. The most promising compound was **124**, which inhibited the enzyme by 44%. The other compounds **125**, **126** and **127** inhibited the enzyme by 16%, 23% and 6% respectively. The level of inhibition was still significantly lower than that of the novel fenoprofenoyl-CoA analogue **56** which inhibited the enzyme by 38% in assays containing 100 µM substrate and 69% in assays containing 20 µM substrate.

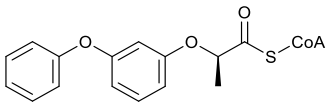

56

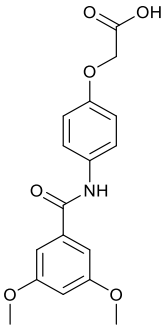

123

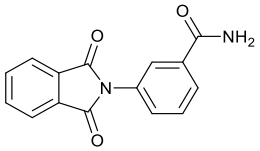

124

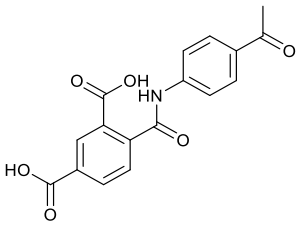

125

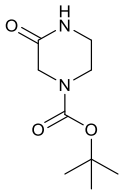

126

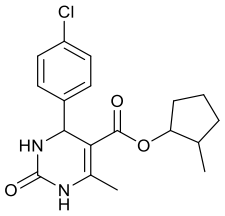

127

Compound	Relative conversion compared to no inhibitor	Reduction in conversion compared to no inhibitor
No inhibitor	100%	0%
56	31.3 ± 8.5%	68.7%
123	>95%	<5%
124	56.1 ± 2.4%	43.9%
125	83.6 ± 3.6%	16.4%
126	76.6 ± 8.2%	23.4%
127	94.1 ± 14.7%	5.9%

Table 3.3: Fluoride elimination assay on small molecules designed by Professor Paul Groundwater. The compounds (final assay concentration 100 µM) were pre-incubated with human AMACR (final assay concentration 0.01 mg mL^{-1}; 0.21 µM) for 10 min before (2*R*,3*R*)-3-fluoro-2-methyldecanoyl-CoA **114** substrate (final assay concentration 20 µM) was added to the enzyme/inhibitor mixture. The results show the percentage of elimination after correction for non-enzymatic conversion and are normalised to the positive control (100%). Data are quoted as average values (2 replicates) ± standard deviation.

3.5.2 Attempts to develop a high-throughput assay based on fluoride elimination

The fluoride elimination assay offers advantages compared to the deuterium wash-in assay, as product formation is irreversible and the peaks of substrate and product are non-overlapping. However, using ^{1}H NMR to quantify the conversion is still a laborious method which is time-consuming and low-throughput. The aim was to turn this assay into a high-throughput multi-well assay to allow efficient screening of potential AMACR inhibitors. This can be done by the use of sensors to quantify the levels of the fluoride product. The fluoride anion **118** released from the fluoro-substrate **114** (Scheme 3.19) could be detected by a fluoride sensor and could potentially be developed into a multi-well high-throughput assay.

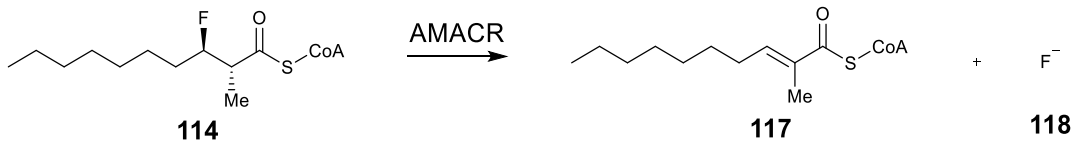

114 **117** **118**

Scheme 3.19: Irreversible elimination of fluoride from (2*R*,3*R*)-3-fluoro-2-methyldecanoyl-CoA **114** substrate by AMACR.

3.5.2.1 *tert*-Butyldimethylsilyl-protected fluorescein as a fluoride sensor

Rydzik *et al.* reported a fluorescent assay based on fluoride release to measure the activity of γ-butyrobetaine hydroxylase and to screen for potential inhibitors.[191] The fluoride anions removed the silyl-protecting group from *tert*-butyldimethylsilyl-protected fluorescein **128** (Scheme 3.20) and the fluorescence intensity of the fluorescein **129** is proportional to the enzyme activity.[191] The protected fluorescein **128** could be used in organic/aqueous environment and should be ideal for AMACR which needs a buffer system but can tolerate DMSO (*vide infra*). This fluoride sensor **128** was investigated to see if it was suitable in detecting the fluoride anion released by AMACR.

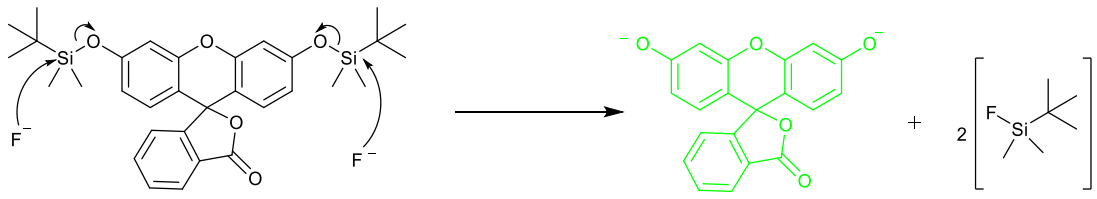

128 **129** **130**

Scheme 3.20: The released fluoride anions react with the protected fluorescein to yield fluorescence at 520 nm.

The *tert*-butyldimethylsilyl-protected fluorescein **128** was synthesised using the same method described by Rydzik *et al.*[191] To quantify the enzyme activity, the fluorescence intensity requires a linear relationship with the concentration of fluoride anion. Fluorescence intensity as a function of fluoride anion concentration was therefore determined.

Different concentrations of fluoride (up to 20 µM) were incubated with protected fluorescein in a mixture of DMSO and NaH_2PO_4-NaOH buffer. The buffer was prepared using highly purified water in order to prevent fluoride contamination from the water source. The fluorescence intensity was measured and plotted against fluoride concentration. No linear relationship was observed, and in fact, the results seemed quite erratic despite several attempts to repeat the experiment.

The buffer system was changed to Tris-HCl as this buffer was reported to give less background noise.[191] The concentration of fluoride was increased to a much higher range than what was reported previously.[191] The result shows an almost linear relationship (hyperbolic curve) between fluorescence intensity and high concentrations of fluoride (Figure 3.11). However, very high levels of scatter in the data was observed at low concentrations of fluoride, which are similar to the concentrations anticipated to be found in the enzyme assay (Figure 3.12). As the assay was intended to be used to screen for potential AMACR inhibitor, it is important to have a linear relationship at low concentrations of fluoride. High levels of scatter make it difficult to determine the residual enzyme activity, which is required to measure potency. There could be a number of reasons for high levels of scatter; could be due to fluoride

contamination from external sources, spontaneous decomposition of the sensor or aggregation of the sensor, *etc*. High scatter in this range of concentrations made it very unreliable when correlating fluorescence with enzyme activity, and hence this method was not developed further.

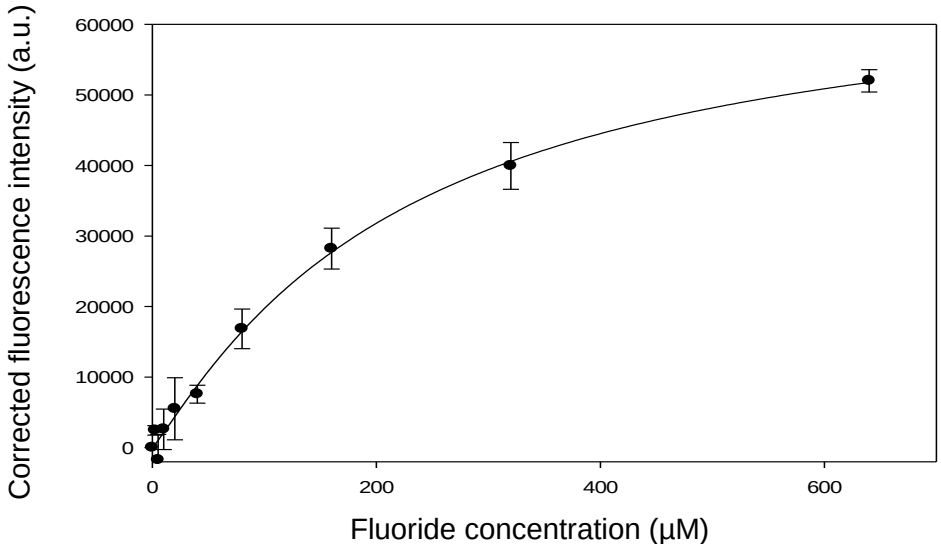

Figure 3.11: The calibration curve of corrected fluorescence intensity against fluoride concentration. The hyperbolic curve shows an almost linear relationship between 40 µM to 320 µM of fluoride and reaches saturation at higher concentrations. Large scatter in the data is observed at low concentrations of fluoride.

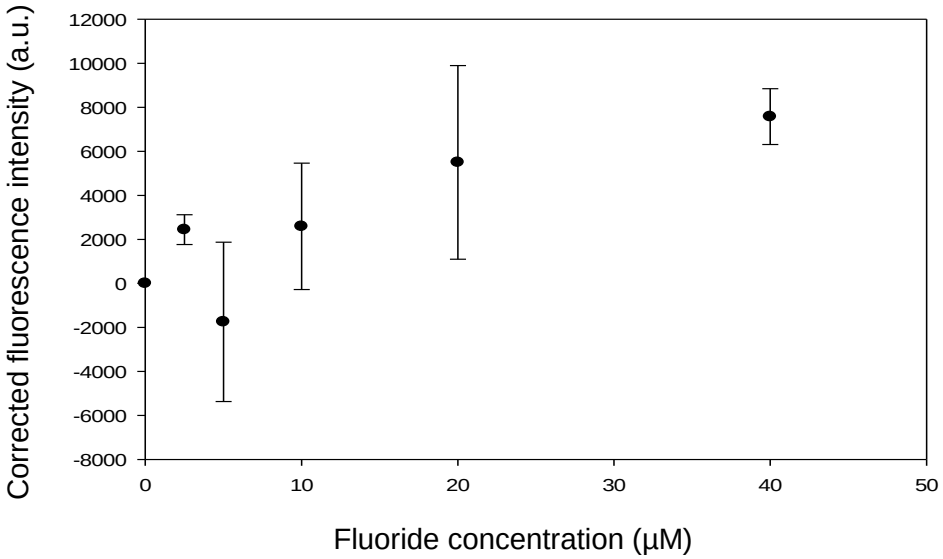

Figure 3.12: The expansion of the calibration curve from Figure 3.11. Corrected fluorescence intensity was plotted against 0 µM to 40 µM of fluoride. Large scatter in the data is observed in this concentration range. The results are quoted as average values (n = 12) ± standard deviation.

3.5.2.2 Boronate-based fluorescent probe as a fluoride sensor

A large scatter in data was observed at low concentrations of fluoride when using a fluoride sensor that was turned on by fluoride anions (silyl-protected fluorescein). In order to reduce the error margin, a “turn-off” sensor was tried. Sun *et al.* reported a boronate-based fluorescent sensor **131** that could be switched off by a strong nucleophile and was used for the detection of peroxynitrite, a strong oxidant in cells.[192] Fluoride, just like peroxynitrite, is a strong nucleophile, and was expected to interact with the sensor in the same way.

The boronate-based fluorescent sensor **131** has extended planar aromatic rings and is strongly fluorescent (Scheme 3.21 A). As boron is an electron-deficient atom, it forms a strong interaction with the nitrogen atom. Hence, the lone pair of the nitrogen is not available to the fluorophore (extended planar aromatic rings) to cause photoinduced electron transfer (PET). Fluoride anion is a strong nucleophile and can bind to the electron-deficient boron to release the nitrogen lone pair of electrons (Scheme 3.21 B). The lone pair of the nitrogen can now act as an electron donor to the fluorophore which has its electron in the excited state.[193] This process is called PET where it quenches the fluorescence and “turns off” the probe. The higher the concentration of fluoride anions, the greater the quenching effect due to PET. The fluorescence intensity is thus inversely related to the concentration of fluoride anion.

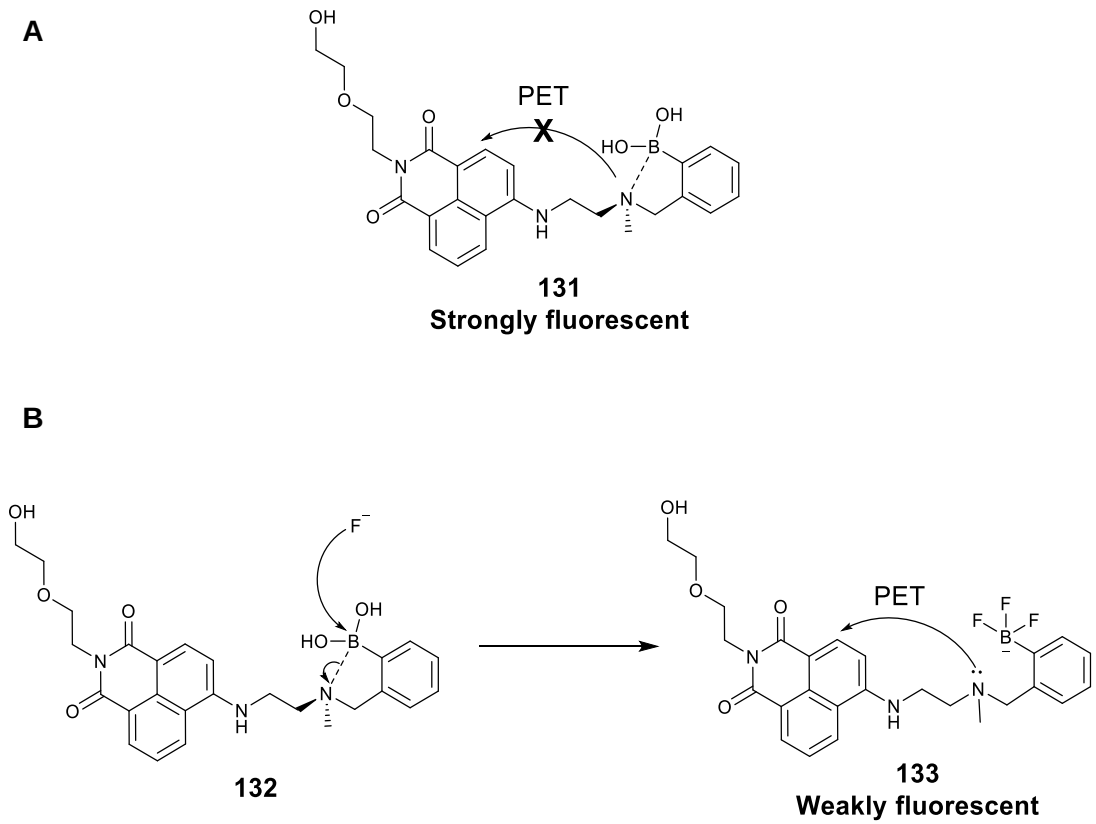

Scheme 3.21: Boronate-based fluorescent probe as a fluoride sensor: A) Strongly-fluorescent sensor in the absence of fluoride anions; B) The proposed mechanism of fluorescence quenching by photoinduced electron transfer (PET) where fluoride anions release the lone pair of the nitrogen and make them available to cause fluorescence quenching.

A sample of the boronate-based fluorescence sensor **131** was obtained from Dr Xiaolong Sun[192] to be tested with fluoride anions. A standard calibration curve of fluorescence intensity against fluoride concentration was plotted. As the probe has been shown to work well between pH 3.0 and pH 8.0,[192] the usual buffer for AMACR, NaH_2PO_4-NaOH, pH 7.4, was used. The experiments were initially performed in 80% (v/v) acetonitrile and 20% (v/v) buffer. An overall trend of decreasing fluorescence intensity with increasing fluoride concentration was observed (Figure 3.13). However, the fluorescence readings fluctuated with very large scatter of the data at low concentrations of fluoride, even with multiple repeats.

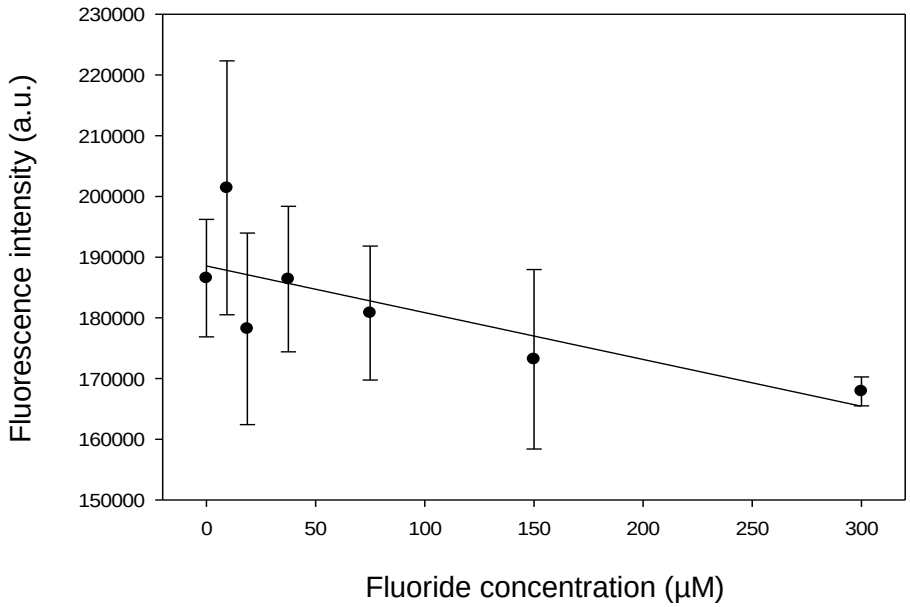

Figure 3.13: The calibration curve of fluorescence intensity against fluoride concentration in a reaction mixture in 80% (v/v) acetonitrile.

The assay was repeated using 100% (v/v) acetonitrile where tetrabutylammonium fluoride (TBAF) was used as the fluoride source. The result showed an inverse standard linear curve reaching saturation at 75 µM fluoride (Figure 3.14). The promising result obtained using a pure organic solvent system suggested that the large scatter of the data in the previous experiment might be due to high amount of aqueous buffer in the final assay. Further experiments were attempted by increasing the concentration of organic solvent to 95% (v/v). The first experiment using 95% (v/v) acetonitrile showed a promising inversely linear relationship at low concentrations of fluoride (0-50 µM) (Figure 3.15). Unfortunately, the result was not reproducible. Variable readings were recorded in subsequent experiments under the same conditions.

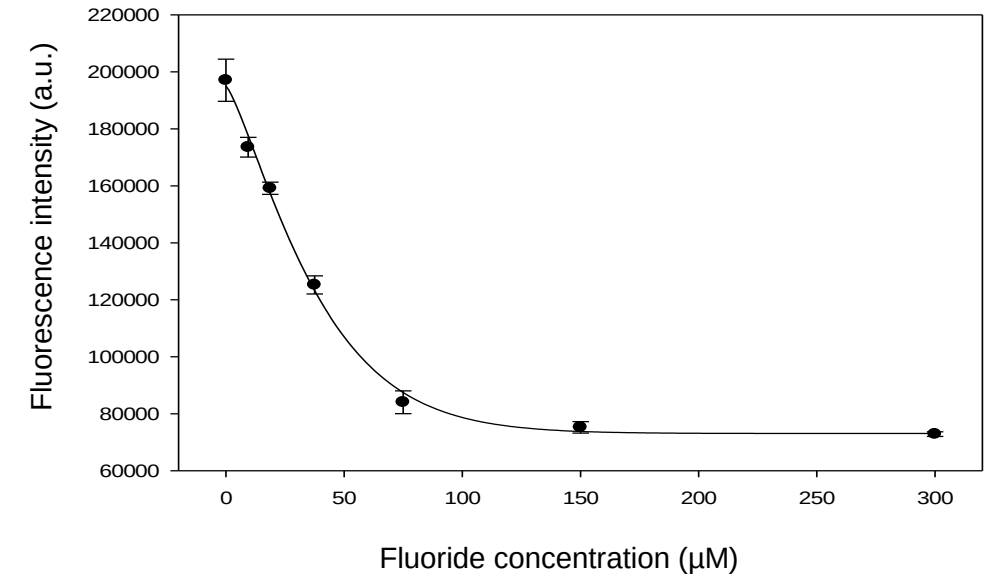

Figure 3.14: The calibration curve of fluorescence intensity against fluoride concentration in a reaction mixture in 100% (v/v) acetonitrile.

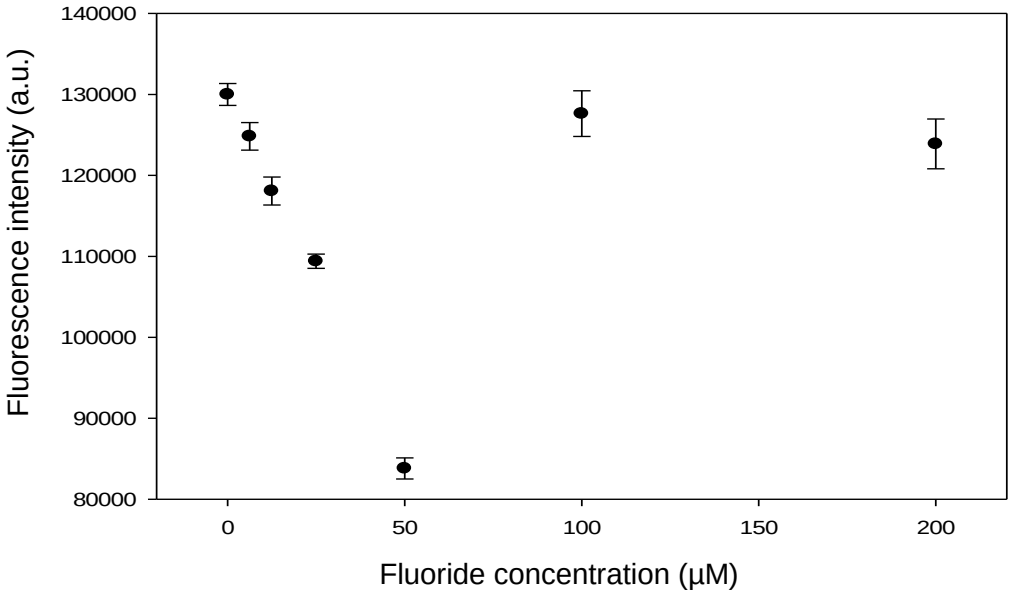

Figure 3.15: The calibration curve of fluorescence intensity against fluoride concentration in a reaction mixture in 95% (v/v) acetonitrile.

The results showed that reaction has to be performed in organic solvent to obtain an inversely linear curve. The presence of small amounts of buffer solution distorts the result, possibly caused by variable levels of hydration of the fluoride anion in water, resulting in a variable amount of nucleophile available for the reaction. Hence, the probe is not suitable for testing the

elimination of fluoride from the substrate by AMACR. The system would need to be able to tolerate an aqueous solution as the fluoride would be released by the AMACR in a buffer solution. In addition, it would need to have a linear/inverse linear relationship at low concentrations of fluoride in order to measure enzyme activity at low concentrations of substrate.

3.6 Fluorescence-based competitive binding assay

Even though fluoride detection using a fluoride sensor has the potential to be developed into a multi-well assay, it has been difficult to create a working system that gives accurate and reproducible data. An alternative was to measure the inhibitor potency using a fluorescence-based competitive binding assay. A fluorescent ligand **134** of AMACR was synthesised by Dr Maksims Yevglevskis.[194] The ligand has two domains; the acyl-CoA ester binds to the enzyme acting as an enolate-intermediate analogue, and the extended aromatic rings are the fluorophore (Figure 3.16).[194] The fluorescence intensity is different depending on whether ligand **134** is bound to the enzyme or exists freely in a solution.[194] The binding constant of the fluorescent ligand **134** was measured as 3 µM.[194]

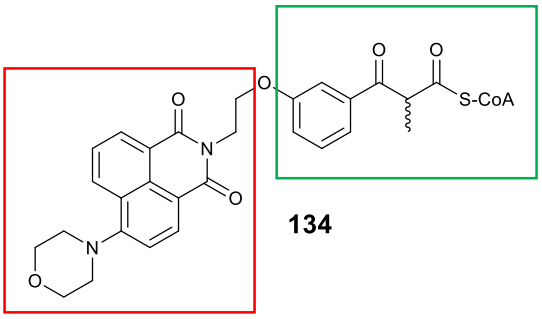

134

Figure 3.16: Fluorescent ligand synthesised by Dr Maksims Yevglevskis.[194]

A sample of the fluorescent ligand was obtained from Dr Maksims Yevglevskis to measure the potency of AMACR inhibitors. The fluorescent ligand was allowed to bind to the enzyme and the inhibitor was added after 10 min. The fluorescence intensity decreased with increasing concentrations of inhibitor as the fluorescent ligand was displaced by the inhibitor. IC_{50} and K_i values of the inhibitors were calculated (Table 3.4). A number of compounds produced random data that did not fit to a standard IC_{50} curve. They were assumed to have IC_{50} values of more than 1000 µM (Table 3.4). The experiment was

repeated but unfortunately, all of the data were not re-producible. Further investigations showed that fluorescent quenching had occurred even though the sample was incubated in the dark, suggesting that the ligand might be prone to rapid degradation.

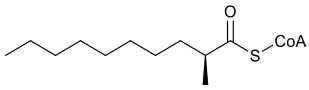

38

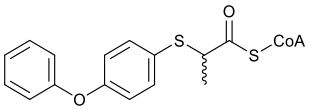

49

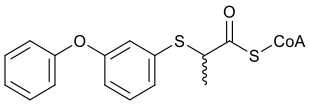

50

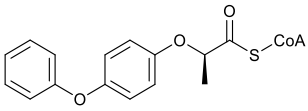

53

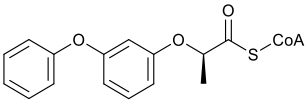

54

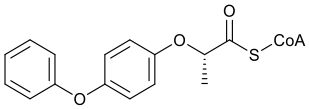

55

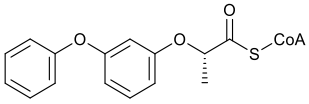

56

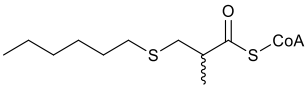

109

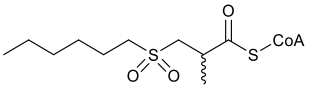

110

Compound	IC_{50} value (µM)	K_i value (µM)
38	6.6	2.3
49	>1000	-
50	169.6	63.0
53	3.1	1.0
54	15.6	5.6
55	451.9	168.2
56	>1000	-
109	5.1	1.7
110	>1000	-

Table 3.4: IC_{50} and K_i values of compounds tested with the fluorescence-based competitive binding assay. K_i values were calculated using the K_i calculator (website: http://sw16.im.med.umich.edu/software/calc_ki/).[195, 196]

In considering potential differences in relative kinetics and binding affinities of substrate compared to inhibitors (*vide supra*), an alternative protocol where

the potential inhibitor was pre-incubated with AMACR before addition of the fluorescent ligand was also attempted. However, there was large scatter in the data and no correlation between fluorescence intensity and the concentrations of several inhibitors was found. Sensible IC_{50} values could not be obtained. Multiple attempts on the fluorescent-binding assay were unsuccessful.

3.7 Multi-well colorimetric assay

Instead of having an external probe that detects the product from an enzyme's reaction (for example, a sensor that detects fluoride anion from the elimination of the fluoro substrate **114**), Dr Maksims Yevglevskis has developed an alternative substrate of AMACR, 3-(2,4-dinitrophenoxy)-2-methylpropanoyl-CoA **135** (Figure 3.17).[197] A colour is produced directly by the action of AMACR on this substrate, so no derivatisation is required to detect the product.

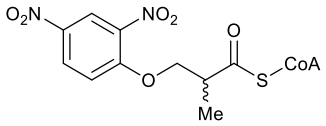

135

Figure 3.17: Substrate of AMACR that allows *in situ* detection of AMACR reaction.[197]

The α-proton of the substrate **135** is deprotonated by catalytic bases of the enzyme to form an enolate intermediate (Scheme 3.22). The enolate intermediate **136** produces 2,4-dinitrophenolate **137** by elimination of the substrate side-chain (Scheme 3.22), in a similar way to the fluoride anion been eliminated from (2*R*,3*R*)-3-fluoro-2-methyldecanoyl-CoA **114**. The enolate intermediate of substrate undergoes elimination as it has a moderate leaving group, 2,4-dinitrophenolate **137** (pK_a value of the acid is 4.1).[198] Unlike the fluoride anion which needs to be detected with a fluoride sensor, the product, 2,4-dinitrophenolate **137** absorbs in the UV range so it can be directly measured. The substrate **135** is developed into a multi-well assay where its UV absorbance is measured by a plate reader.

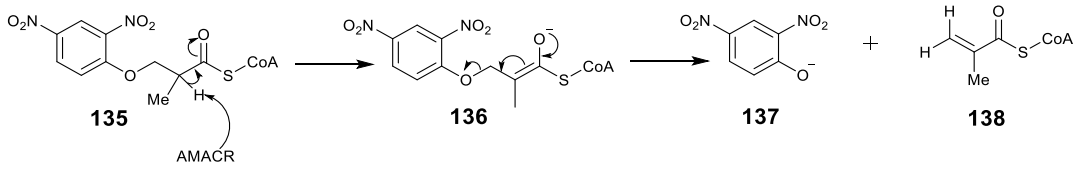

Scheme 3.22: The proposed mechanism of the elimination of 3-(2,4-dinitrophenoxy)-2-methylpropanoyl-CoA **135** to form 2,4-dinitrophenolate **137**, which absorbs at 354 nm (ε = 15.3 mM^{-1} cm^{-1}).[199]

A sample of 3-(2,4-dinitrophenoxy)-2-methylpropanoyl-CoA **135** was obtained from Dr Maksim Yevglevskis and used to measure the potency of potential AMACR inhibitors in a 96-well plate assay. An AMACR inhibitor was expected to reduce the production of 2,4-dinitrophenolate **137** and hence decrease the UV absorbance. The product **137** has a peak absorbance at 354 nm so the UV absorbance was measured at this wavelength. However, some aromatic inhibitors might have an UV absorbance with a maximum absorbance near to this wavelength, so a secondary absorbance at 390 nm was recorded as an alternative. The K_m value of the substrate (58 µM) was used to decide the final concentration of the substrate in the assay. The average absorbance reading against the concentration of inhibitor was plotted to obtain the IC_{50} value of the inhibitor (Figure 3.18). For competitive inhibitors, K_i values (binding affinity of inhibitor) were calculated from IC_{50} values using the Cheng-Prusoff equation:[200]

$$K_i = \frac{IC_{50}}{1 + ([S]/K_m)}$$

where IC_{50} is the concentration of the inhibitor at which the inhibition is 50%, [S] is the substrate concentration used in the experiment and K_m is substrate concentration to produce half of the maximal enzyme activity (58 µM).

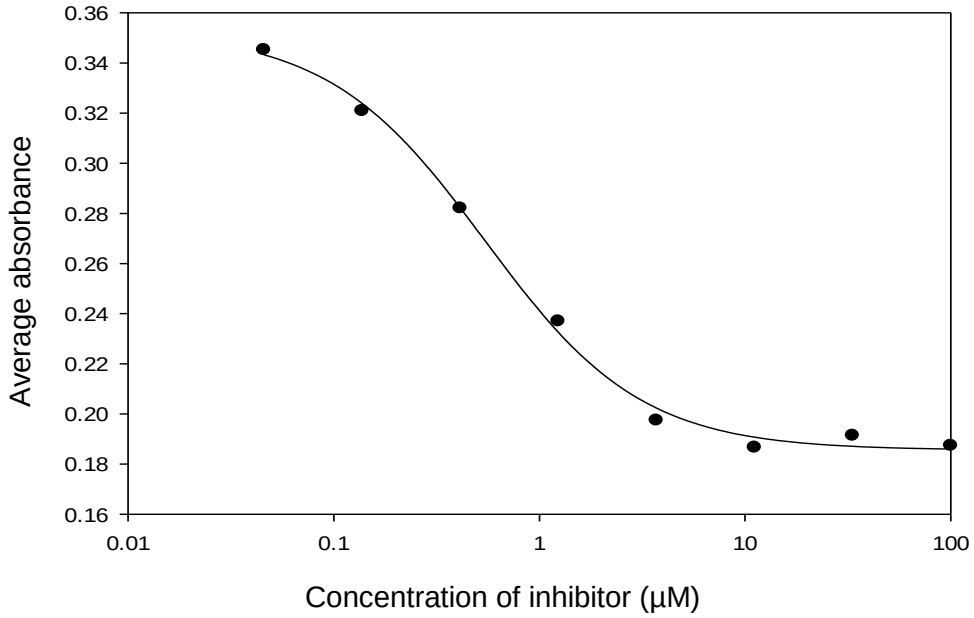

Figure 3.18: A typical IC_{50} curve of an AMACR inhibitor.

Even though Carnell *et al.* reported that *R*-ibuprofenoyl-CoA **16** was about four times more potent than *S*-ibuprofenoyl-CoA **17** (K_i = 5.4 µM *vs*. 19.2 µM),[143] such a trend was not observed in the novel fenoprofenoyl-CoA analogues (Table 3.5). *R*-inhibitors (**53**and **54**) and *S*- inhibitors (**55** and **56**) did not show significantly different IC_{50} and K_i values (Table 3.5). No significant difference in the potency of inhibitors with a *para*- or *meta*- aromatic side-chains (**49**, **53** and **55** compared with **50**, **54** and **56**, respectively) was observed. It is unknown why the acyl-CoA ester with a 3-sulfone group **51** has a six-times higher K_i value than the one with a 3-sulfide group **49** (479 nM *vs*. 80 nM). A sulfone group was expected to be more electron withdrawing and thus allow easier enolization and make the compound a better competitive inhibitor. The relatively high K_i value might be due to the steric hindrance by a bulky sulfone group compared to sulfide. The active site of AMACR seemed to be quite restricted around the area binding the 2-methyl group according to the modelling of the AMACR active site based on the MCR crystal structure.[2, 108, 146] Hence a large bulky group next to the 2-methyl group might affect the binding of the inhibitor in the active site of the enzyme.

All novel aromatic compounds showed quite similar K_i values and their differences were not greater than 10-fold. No specific structural features that improved the K_i value significantly were observed. The obtained data did not allow defining of the features resulting in higher potency in order to determine structural-activity relationships. This lack of selectivity in inhibitors binding to the enzyme is probably due to the side-chains binding to the methionine-rich hydrophobic surface which accepts a wide variety of structures. Aromatic rings seem to bind well to this region to give K_i values in nanomolar range (50- 480 nM) (Table 3.5). Long alkyl-chain inhibitors **109** and **110** bind less well, as shown by their K_i values, which are in the low micromolar range (2 and 11 μM respectively) instead of nanomolar range (Table 3.5). The results suggest that π-interactions from aromatic rings could be important for binding.

The novel fenoprofenoyl-CoA analogues were shown to be moderate AMACR inhibitor using the multi-well colorimetric assay and the results were consistent with the fluoride elimination assay (*vide supra*). Even though these novel compounds were not significantly more potent than the acyl-CoA ester of the 2-APA (Table 3.6), the assay has shown that these inhibitors bind to AMACR. It is a promising start for the rational design of AMACR inhibitors as further exploration of the SAR of side-chains and other regions is now possible with this newly developed multi-well assay.

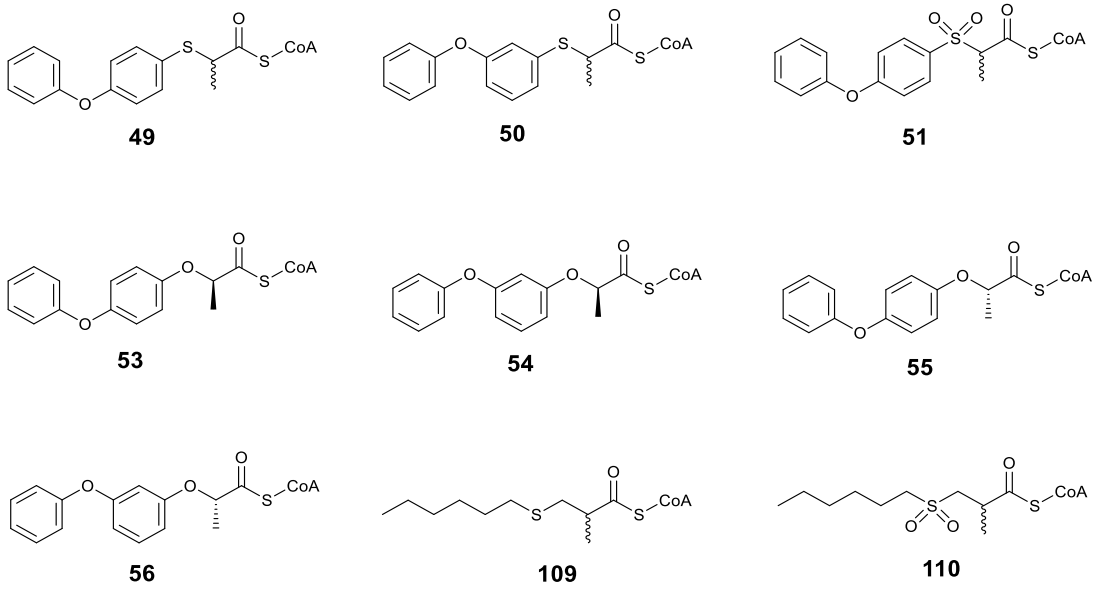

Compound	IC_{50} value (nM)	K_i value (nM)
49	135.0	79.9
50	89.8	53.2
51	809.8	479.2
53	189.8	112.3
54	515.1	304.8
55	543.9	321.8
56	283.3	167.6
109	3331	1971
110	18670	11050

Table 3.5: IC_{50} and K_i values of novel compounds tested with the multi-well colorimetric assay.

The results showed that having an electron-donating group (oxygen) or electron-withdrawing groups (sulfide and sulfone) next to the α-proton did not make a siginificant difference in the potency of fenoprofenoyl-CoA analogues (Table 3.5). The most potent fenoprofenoyl-CoA analogue with an electron withdrawing group was **50** with K_i value of 53 nM while the one with an electron donating group was **53** with a K_i value of 112 nM. Their K_i values were different by just 2-fold and such difference is probably not statistically significant.

The small molecules designed by Professor Paul Groundwater (Figure 3.19) were also tested using the multi-well colorimetric assay. They did not inhibit

the elimination of 3-(2,4-dinitrophenoxy)-2-methylpropanoyl-CoA **135** sufficiently to give any sensible IC_{50} value. These results were consistent with the fluoride elimination assay (*vide supra*) where they did not show any inhibition at 100 µM substrate and very limited inhibition at 20 µM substrate.

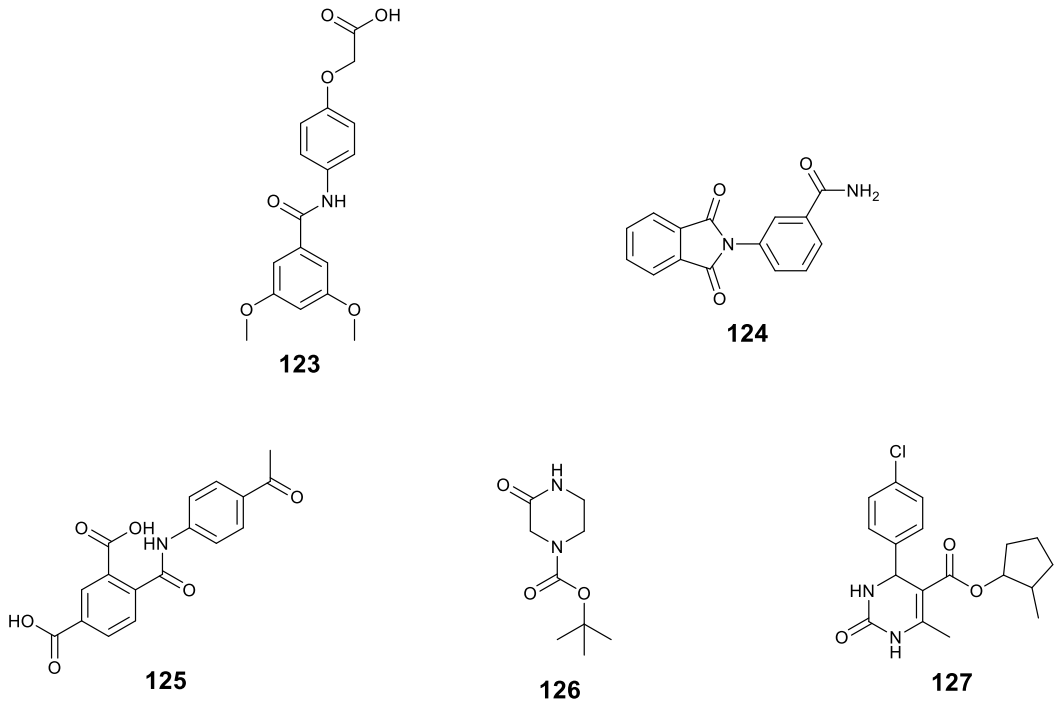

Figure 3.19: Small molecules designed by Professor Paul Groundwater.

A range of known compounds were also tested as AMACR inhibitors using the multi-well colorimetric assay (Table 3.6). The K_i values of acyl-CoA esters of several 2-APAs were similar and the most potent of them was fenoprofenoyl-CoA **13** with K_i value of 168 nM. It was followed by ketoprofenoyl-CoA **120**, flurbiprofenoyl-CoA **122**, ibuprofenoyl-CoA **119** and naproxenoyl-CoA **121** (K_i values = 177, 216, 235 and 291 nM respectively) (Table 3.6). The results were largely similar to the fluoride elimination assay except for ibuprofenoyl-CoA **119** which showed greater inhibition in the fluoride elimination assay compared to ketoprofenoyl-CoA **120** (Table 3.2; *vide supra*). However, the relative inhibition from the fluoride elimination assay was a single-point assay and so the results using the two assays are not directly comparable. Both assays gave consistent results showing that the acyl-CoA esters of 2-APA were moderate AMACR inhibitors.

Ibuprofenoyl-CoA **119** has been reported as an inhibitor of AMACR with K_i value of 56 μM,[91] which was much higher compared to the current data (K_i = 235 nM). However, the previous assay used AMACR from rat liver and the multi-well colorimetric assay in this study used human recombinant AMACR. These two enzymes only shared 81% amino acid homology.[94] As they are not identical enzymes, ibuprofenoyl-CoA **119** may exhibit different degree of inhibition to both enzymes. It is noteworthy that the rat liver enzyme is a native enzyme whilst the human AMACR is a recombinant enzyme expressed using a bacterial system and different levels of activity between native enzyme and recombinant enzyme is not uncommon.

The data from the multi-well colorimetric assay has shown consistent lower K_i values compared to previous studies. *N*-Dodecyl-*N*-methylcarbamoyl-CoA **30**, the most potent AMACR inhibitor reported to-date has a K_i value of 98 nM according to Carnell *et al*.[145] The results from this study showed that *N*-dodecyl-*N*-methylcarbamoyl-CoA **30** is still the most potent inhibitor, but the K_i value obtained was much lower, 0.4 nM (Table 3.6). Carnell *et al.* used human AMACR expressed using a mammalian cells (HEK293 kidney cell culture)[145] while the enzyme used in this study was expressed using a bacterial cells (*E. coli*). Enzymes expressed by different systems would have considerably different level of activity and it is difficult to compare data across studies. In addition, an end-point assay was used by Carnell *et al.* to study *N*-dodecyl-*N*-methylcarbamoyl-CoA **30**[145] whilst a continuous assay was used in this study to examine its potency. The latter is usually more accurate than the former.

Alkyl acyl-CoA esters with various chain-lengths were also tested as AMACR inhibitors (Table 3.6). Acetyl-CoA **139** has a K_i value of 18 μM. Butyryl-CoA **140** was a poor AMACR inhibitor and its data could not be fitted in a standard curve to obtain a sensible IC_{50} value. Hexanoyl-CoA **141**, octaboyl-CoA **142** and decanoyl-CoA **143** have K_i values of 5, 4 and 1 μM, respectively (Table 3.6). The results showed that the longer the chain-length, the lower the IC_{50} and K_i values. This observation was consistent with the data reported by Sattar *et al.* who showed that the longer the chain-length, the higher the conversion rate experienced by the alkyl acyl-CoA esters (*i.e.*, they were better

substrates).[147] With longer side-chain, these alkyl acyl-CoA esters have a higher level of hydrophobicity, and hence also behave as better competitive inhibitors.[147] Long-chain alkyl compounds still have higher K_i values than aromatic compounds, such as acyl-CoA esters of 2-APA. The tight binding exhibited by aromatic compounds could be due to greater hydrophobicity or stronger π-interactions from the aromatic rings.

In contrary to the data from Sattar *et al*.,[147] *iso*-butyryl-CoA **144** was a better AMACR inhibitor than butyryl-CoA **140** even though it has the same number of carbon units. This probably is because *iso*-butyryl-CoA **144** has a 2-methyl group which fits into the specific methyl-pocket in the enzyme and binds more tightly.[146] The same trend was observed with 2-methyldecanoyl-CoA and decanoyl-CoA **143**. Decanoyl-CoA **143** has a K_i of 1164 nM while *R*-2-methyldecanoyl-CoA **44** has a K_i of 263 nM and *S*-2-methyldecanoyl-CoA **38** has a K_i value of 379 nM, both significantly lower than decanoyl-CoA **143**. Having a 2-methyl group improved the K_i value by 3-fold for the *S*-acyl-CoA ester **38** and more than 4-fold for *R*-acyl-CoA ester **44**. This observation was consistent with the data reported by Sattar *et al.* who observed the exchange efficiency of S-2methyldecanoyl-CoA **38** to be three times greater than decanoyl-CoA **143**.[147] Having a 2-methyl group improved the specificity and made it a better substrate and a more potent competitive inhibitor.

The acyl-CoA ester of *S*-mandelic acid (*S*-2-hydroxy-2-phenylacetyl-CoA **145**) has been previously proposed to be substrate of AMACR just like the acyl-CoA esters of 2-APA.[201] It was later proven not to be the case by Yevglevskis *et al.* who showed that both *S*- **145** and *R*- 2-hydroxy-2-phenylacetyl-CoA **146** were not substrates of AMACR.[184] The 2-hydroxyl group was thought to prevent binding to AMACR.[184] These acyl-CoA esters of *S*- **145** and *R*-mandelic acid **146** were tested to see if they could be inhibitors of AMACR. The results showed that these two compounds were poorer inhibitors compared to acyl-CoA esters of 2-APA (Table 3.6). The K_i values were 0.84 µM for *R*-inhibitor **146** and 0.45 µM for S-inhibitor **145**. This was not unexpected, as the presence of a hydrophilic 2-hydroxyl group might fit poorly in the hydrophobic 2-methyl pocket in the enzyme,[184] and hence made it a

poor competitive inhibitor. However, limited binding might still occur as the compound has an aromatic side-chain and acyl-CoA moiety which could occupy the appropriate binding sites in AMACR, allowing it to inhibit the enzyme to some extent.

3-Fluoro-2-methyldecanoyl-CoA, the substrate used in fluoride elimination assay was also tested as an inhibitor using the multi-well colorimetric assay. Both the *R*- **114** and *S*- compounds **147** were very good AMACR inhibitors with K_i values in the low nanomolar range (Table 3.6). However, the results were complicated by the fact that these compounds undergo fluoride elimination reaction catalysed by AMACR and the product might also be an inhibitor of different potency, giving variable inhibition with time. As they were not simple reversible inhibitors, it was not appropriate to quote IC_{50} values in discussing their potency.

The IC_{50} of ebselen **34**, ebselen oxide **35** and rose bengal **37** were also measured using the multi-well colorimetric assay. The IC_{50} value of ebselen **34** was about 20-fold smaller than ebselen oxide **35** (Table 3.6) and these results were consistent with the fluoride elimination assay (Table 3.2; *vide supra*). However, these inhibitors have been proposed to inhibit the enzyme by covalent modification or other mechanisms and are not simple reversible inhibitors.[85, 187-189] Their mode of binding to AMACR should be studied and confirmed (*vide infra*) as IC_{50} would not be an accurate representation of potency for irreversible inhibitors.

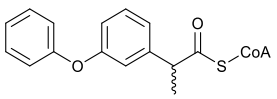

13

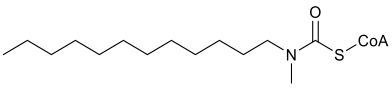

30

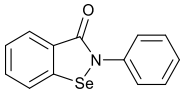

34

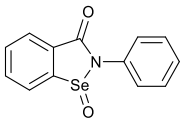

35

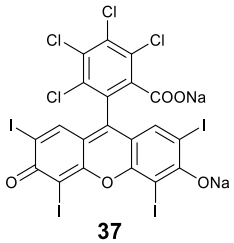

37

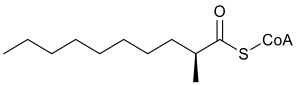

38

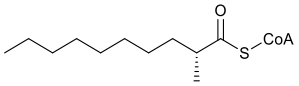

44

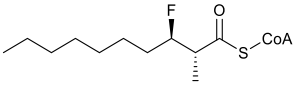

114

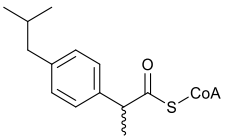

119

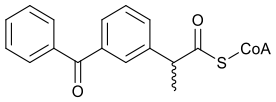

120

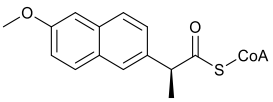

121

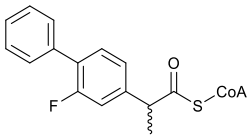

122

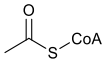

139

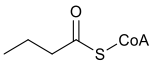

140

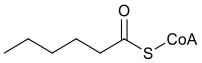

141

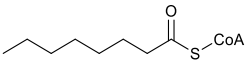

142

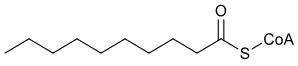

143

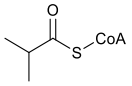

144

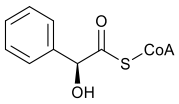

145

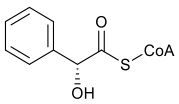

146

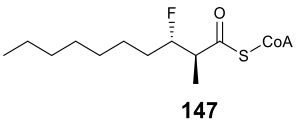

147

Compound	IC_{50} value (nM)	K_i value (nM)
13	283.1	167.5
30	0.7	0.4
34	41.3	24.4
35	872.4	-
37	1612	953.8
38	640.0	378.7
44	445.0	263.3
114	65.1	38.5
119	397.6	235.3
120	298.4	176.6
121	492.0	291.1
122	364.6	215.7
139	29960	17730
140	>1000000	-
141	8294	4908
142	7241	4285
143	1967	1164
144	42230	24990
145	1457	862
146	2702	1599
147	205.3	121.5

Table 3.6: IC_{50} and K_i values of known compounds tested with the multi-well colorimetric assay. The K_i value of ebselen oxide **35** was not calculated using the Cheng-Prusoff equation as it is not a competitive inhibitor (*vide infra*).

3.7.1 Mode of binding of inhibitors

The multi-well colorimetric assay can also be used to study the mode of binding of inhibitors, and to examine the compound to see if it is a reversible or irreversible inhibitor. Three separate experiments should be performed to study the mode of binding. They will be simplified here as experiment 1, experiment 2 and experiment 3. Experiment 1 and experiment 3 were intended to study association of the inhibitor with the enzyme. Experiment 1 involved a pre-incubation of the inhibitor with AMACR while experiment 3 did not. A

simple reversible inhibitor would show no difference in the absorbance reading in both experiment 1 and 3 because the binding is fast (equilibrim achieved in ~1 seconds) so pre-incubation should not make a difference to the observed potency (Figure 3.20). However, a slow-binding, tight-binding or irreversible inhibitor would show greater inhibition in experiment 1 compared to experiment 3 as pre-incubation allowed the inhibitor either to bind to the enzyme (slow and tight-binding inhibitors) or inactivate the enzyme (irreversible inhibitors) (Figure 3.22). Experiment 2 used a small volume but high concentration of enzyme (100× final concentration) and inhibitor (20× IC_{50}) during pre-incubation phase. On dilution, the enzyme concentration was the same as experiment 1 but the inhibitor concentration was 0.4× IC_{50}. Experiment 2 was used to study whether the enzyme activity could be restored upon dilution of the inhibitor. A fast reversible inhibitor or a slow-binding but fast-release inhibitor would dissociate rapidly from the enzyme and the enzyme activity would be restored (Figure 3.20 and 3.21); whilst a tight-binding inhibitor could have a time-dependent dissociation. Covalent inhibitors which irreversibly modify the enzyme are predicted to show no recovery of activity under these conditions (Figure 3.22).

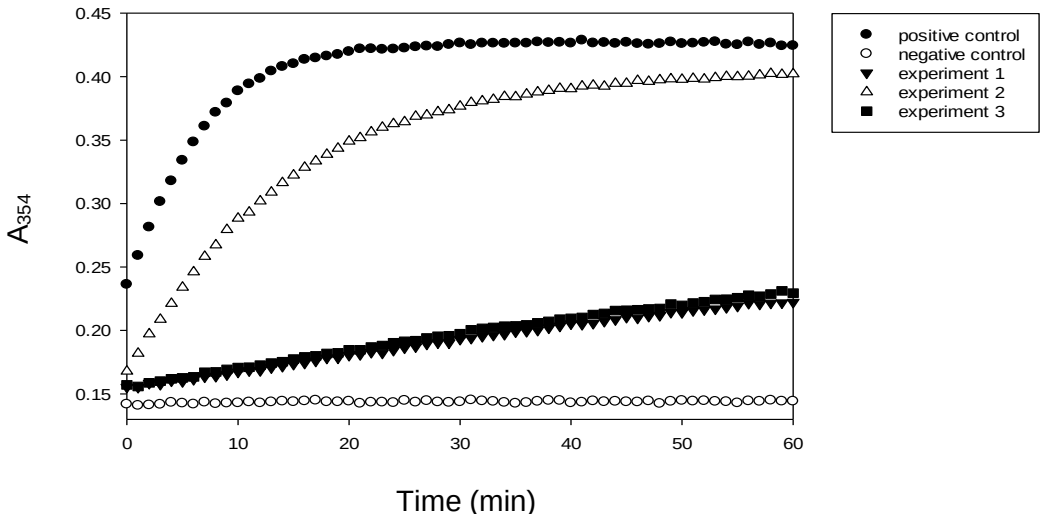

Figure 3.20: Mode of binding experiment for a fast reversible inhibitor (ibuprofenoyl-CoA **119**). Experiment 1 and 3 show rapid binding as the observed absorbance readings are the same with or without pre-incubation; experiment 1 and 2 show that the reaction is reversible as the activity is restored upon dilution of the inhibitor. The positive control lacked an inhibitor while the negative control lacked active AMACR.

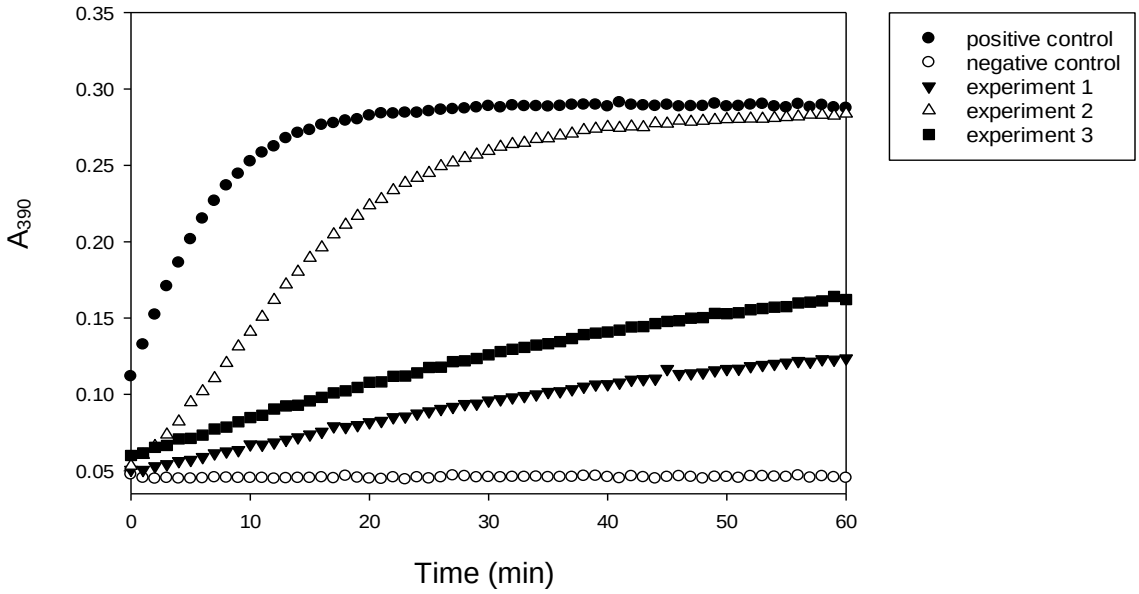

Figure 3.21: Mode of binding experiment for a slow-binding/fast release inhibitor (ebselen **34**). Experiment 1 and 3 show that the binding is slow as the absorbance is lower (lower enzyme activity) with pre-incubation; experiment 1 and 2 show that the reaction is reversible and the release of inhibitor is fast as the activity is restored upon dilution of the inhibitor. The positive control lacked an inhibitor while the negative control lacked an active AMACR. Wavelength at 390 nm instead of 354 nm was measured as ebselen **34** has a maximal UV absorbance near 354 nm.

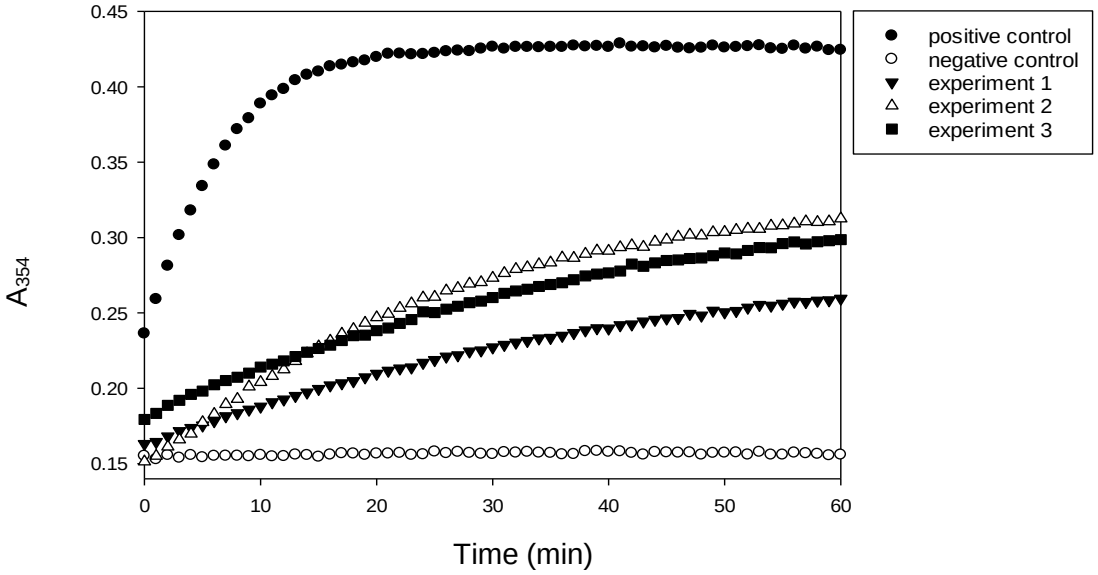

Figure 3.22: Mode of binding experiment for an irreversible inhibitor (ebselen oxide **35**). Experiment 1 and 2 show the reaction is probably irreversible as there is very limited recovery of activity upon dilution of the inhibitor. The positive control lacked an inhibitor while the negative control lacked an active AMACR.

A selection of novel synthesised compounds and known compounds were tested to examine their mode of binding to AMACR and the results were shown in Table 3.7. The results showed that ibuprofenoyl-CoA **119** was a fast reversible inhibitor, and hence all acyl-CoA esters of 2-APA are also likely to be fast reversible inhibitors. This is consistent with them been known as alternative substrates.[2] All novel fenoprofenoyl-CoA analogues are probably fast reversible inhibitors, as represented by **49** and **53**. Long alkyl acyl-CoA esters such as 3-(hexylsulfanyl)-2-methylpropanoyl-CoA **109** and *R*-2-methyldecanoyl-CoA **44** were also shown to be fast reversible inhibitors. It was not surprising as they were meant to mimic the natural substrate of AMACR and act as competitive inhibitors.

Even though ebselen **34** and rose bengal **37** were predicted to be irreversible inhibitors of AMACR, they were shown to be slow-binding inhibitors in this study. Ebselen oxide **35** was shown to be an irreversible inhibitor which bound to the enzyme and did not dissociate upon dilution (Figure 3.22). To confirm that it reacted the enzyme irreversibly, the Kitz-Wilson analysis was performed to determine whether the inactivation was time-dependent (which is characteristic of an irreversible inhibitor).

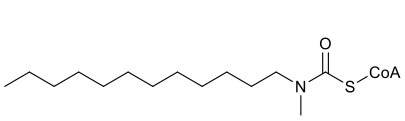

30

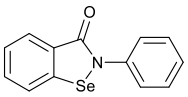

34

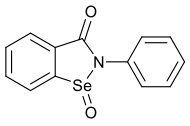

35

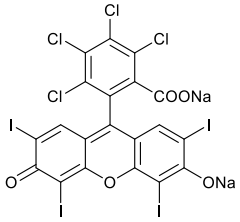

37

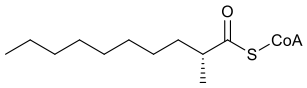

44

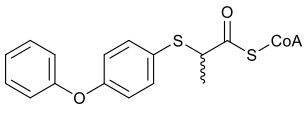

49

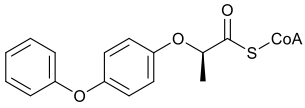

53

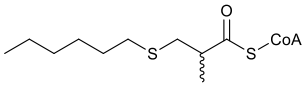

109

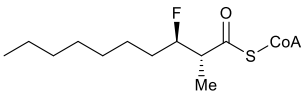

114

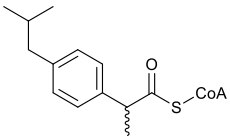

119

Compound	Mode of binding
30	Fast reversible
34	Slow binding but fast release
35	Irreversible
37	Slow binding but fast release
44	Fast reversible
49	Fast reversible
53	Fast reversible
109	Fast reversible
114	Fast reversible
119	Fast reversible

Table 3.7: Mode of binding of inhibitors tested using the multi-well colorimetric assay.

3.7.2 Kitz-Wilson analysis

In order to confirm ebselen oxide **35** was an irreversible inhibitor, Kitz-Wilson analysis[85, 202] was carried out. AMACR was pre-incubated with ebselen oxide **35** at concentrations 10 times higher than the final concentrations in the assay. High inhibitor concentrations during the pre-incubation phase allowed the irreversible inhibitor to inactivate the enzyme before the substrate was added. Ebselen oxide **35** inactivated the enzyme during pre-incubation in a time-dependent manner (Figure 3.23). It was shown to be an irreversible inhibitor using the Kitz-Wilson analysis.

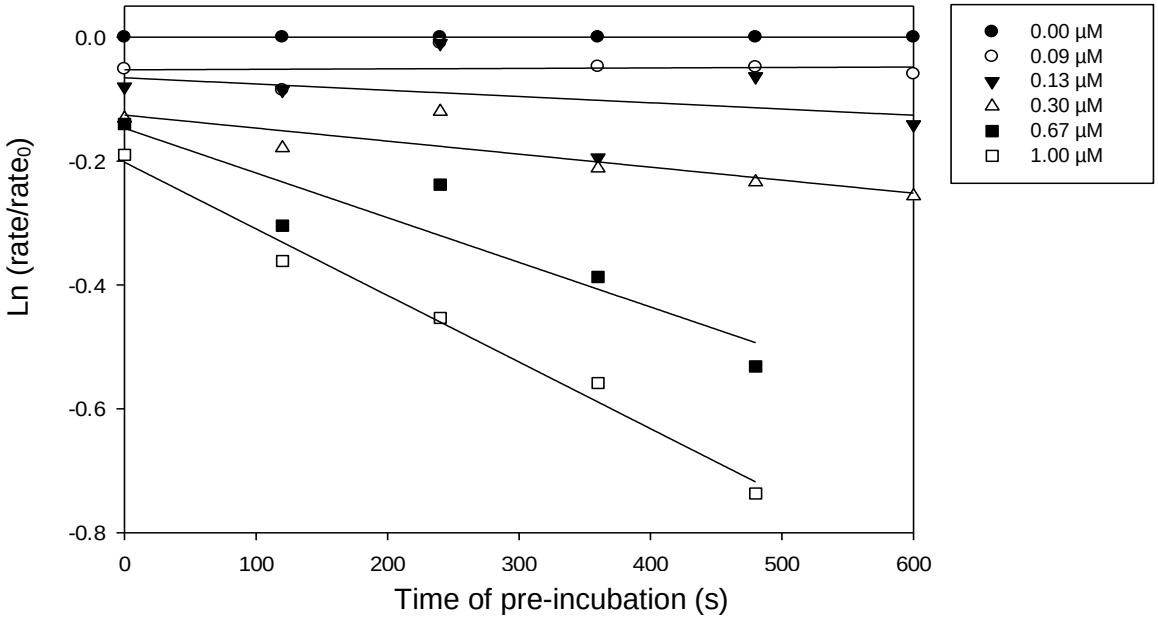

Figure 3.23: Kitz-Wilson analysis on ebselen oxide **35**. Inhibitor concentration and pre-incubation time are inversely correlated with the activity of AMACR.

The data was analysed using the Michalis-Menten model and the kinetic parameters were calculated using the Direct Linear Plot, which gives median values and discards outliers (Figure 3.24).[203, 204] The K_I value was estimated to be 0.975 µM and K_{inact} value was 0.00085 s^{-1}, represented by the intersection of lines. The data given by the Direct Linear Plot was rather inaccurate as the plot showed poor convergence.

An irreversible enzyme inhibitor should show saturation kinetics if it binds to the enzyme active site. The classical Michaelis-Menten model assumes a

single molecule binds to the enzyme and the reaction occurs at first order and then becomes zero order when saturation occurs. When the data were plotted using the Michaelis-Menten model (Figure 3.25), it did not show the classical hyperbola curve (*i.e.*, saturation at high concentration), suggesting that ebselen oxide **35** is a non-specific inactivator that does not saturate. Ther residual plot also showed that the Michaelis-Menten model is inappropriate as the errors are not random scatter (Figure 3.26).[205]

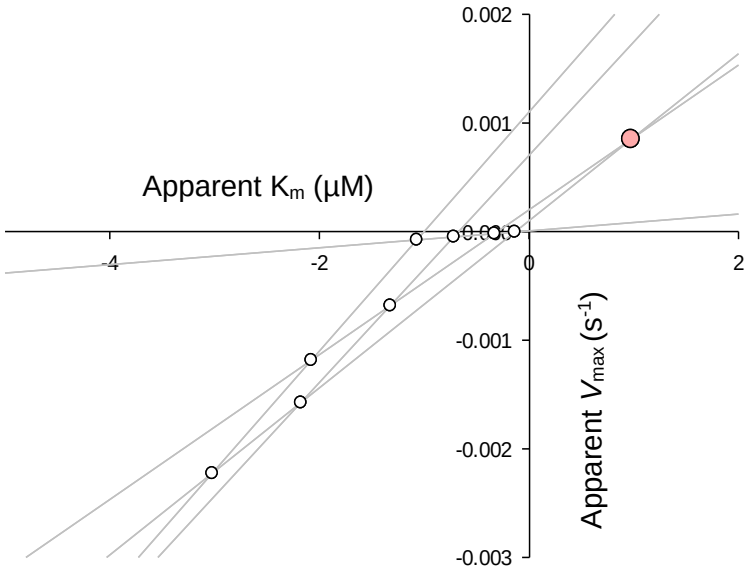

Figure 3.24: Direct Linear Plot of ebselen oxide **35**.

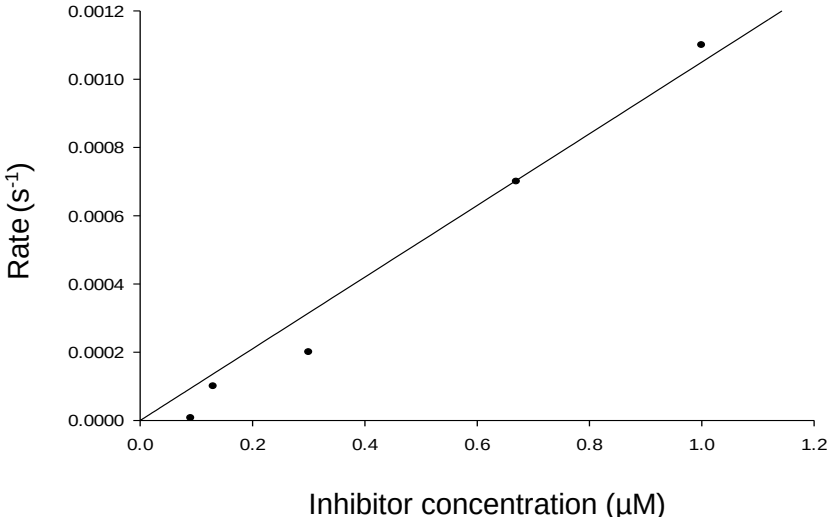

Figure 3.25: Michaelis-Menten Plot of ebselen oxide **35**.

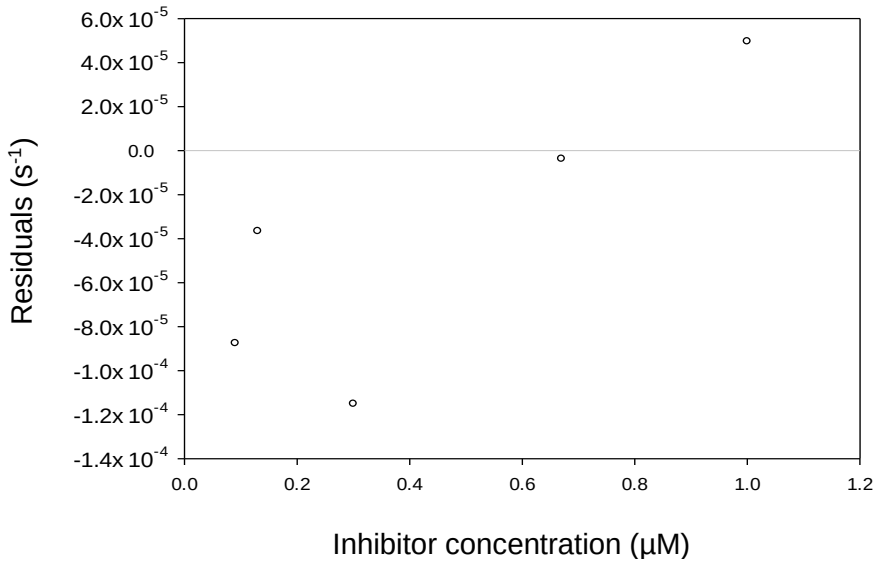

Figure 3.26: Residual plot of ebselen oxide **35**.

However, when the rate constant of ebselen oxide **35** was plotted against the concentration of inhibitor, a straight line was obtained (Figure 3.27). This showed a standard second order reaction, which was dependent on time and the concentration of ebselen oxide **35**. The second order rate constant of ebselen oxide **35** was 1142.6 M^{-1} s^{-1}. The results suggest that ebselen oxide **35** is not a typical irreversible inhibitor that binds to the active-site of AMACR and can reach saturation, instead, its inactivation occurs by non-specific single-step mechanism that is characteristic of non-specific inactivating agents.[190] It is possible that ebselen oxide **35** modifies enzyme residues, possibly histidines, on the outside of the protein.

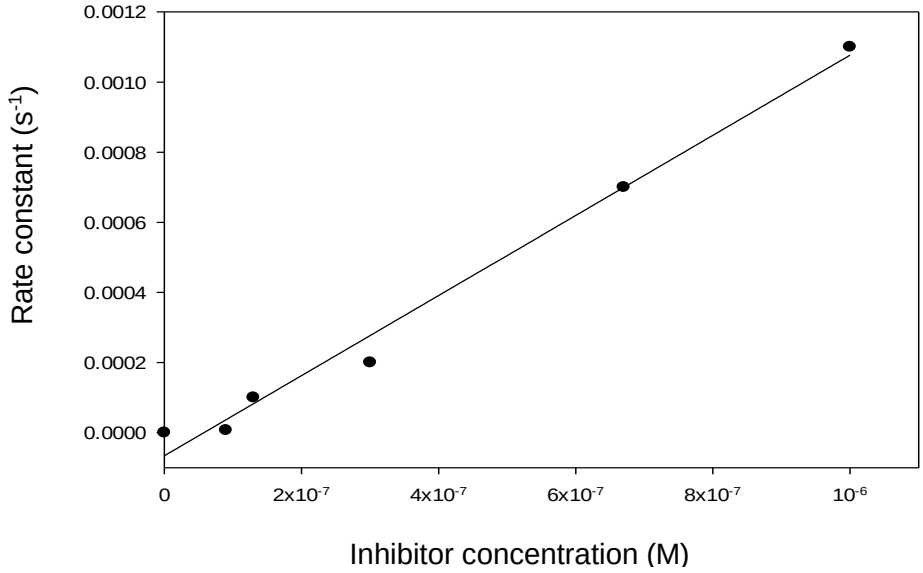

Figure 3.27: The graph showed a linear relationship between the concentration of ebselen oxide **35** and its rate constant.

4 Results and discussion for site-directed mutagenesis study

4.1 Investigation into role of catalytic residues to assist rational drug design

A very powerful approach in drug discovery is to rationally design drugs, which is a strategy used in the design of novel fenoprofenoyl-CoA analogues as AMACR inhibitors (*vide supra*). In order to rationally design drugs to target AMACR, a good understanding of the enzyme structure and its active-site residues is paramount. Rational design is a good strategy for AMACR as all inhibitors produced will be specific in inhibiting the enzyme activity and a targeted therapy can be produced.

There is no X-ray crystal structure of human or a mammalian AMACR reported to date. The identity of the active-site residues have not been conclusively proven and its catalytic mechanism is still incompletely understood. The homologous enzyme of human AMACR that has been widely studied is MCR, from *M. tuberculosis*.[86, 108, 146] This enzyme shares 43% sequence identity with human AMACR (Figure 4.1).[76, 86] There have been a number of studies (X-ray crystallography, quantum chemical modelling and site-directed mutagenesis) that predict the active-site residues and catalytic mechanism of human AMACR based on studies on MCR.[86, 107, 108, 146, 153] These findings have shed some light on the mechanism of human AMACR. However, as these studies were not performed on human AMACR, the predictions are not be absolutely definitive. Studies have shown that homologous enzymes can have different catalytic mechanisms.[206, 207]

```
MCR             MAGPLSGLRVVELAGIGPGPHAAMILGDLGADVVRIDRPSSVDGISRDAMLRNRRIVTAD
AMACR           --MALQGISVVELSGLAPGPFCAMVLADFGARVVRVDRPGSRYDVSR--LGRGKRSLVLD
                   .*.*: ****:*:.***..**:*.*:** ***:***.*  .:**  : *.:* :. *

MCR             LKSDQGLELALKLIAKADVLIEGYRPGVTERLGLGPEECAKVNDRLIYARMTGWGQTGPR
AMACR           LKQPRGAAVLRRLCKRSDVLLEPFRRGVMEKLQLGPEILQRENPRLIYARLSGFGQSGSF
                **. :*  :  :*  ::***:* :* ** *:* ****   : * ******::*:**:*.

MCR             SQQAGHDINYISLNGILHAIGRGDERPVPPLNLVGDFGGGSMFLLVGILAALWERQSSGK
AMACR           CRLAGHDINYLALSGVLSKIGRSGENPYAPLNLLADFAGGGLMCALGIIMALFDRTRTGK
                .: *******::*.*:*  ***..*.* .****:.**.**.::  :**: **::*  :**

MCR             GQVVDAAMVDGSSVLIQMMWAMRATGMWTDTRGANMLDGGAPYYDTYECADGRYVAVGAI
AMACR           GQVIDANMVEGTAYLSSFLWKTQKSSLWEAPRGQNMLDGGAPFYTTYRTADGEFMAVGAI
                ***:** **:*:: * .::*  : :.:*  .** ********:* **. ***.::*****

MCR             EPQFYAAMLAGLGLDAAELPPQNDRARWPELRALLTEAFASHDRDHWGAVFANSDACVTP
AMACR           EPQFYELLIKGLGLKSDELPNQMSMDDWPEMKKKFADVFAKKTKAEWCQIFDGTDACVTP
                *****  :: ****.: *** * .   ***::  :::.**.: : .*  :* .:******

MCR             VLAFGEVHNEPHIIERNTFYEANG---GWQPMPAPRFSRTASSQPRPPAATIDIEAVLTD
AMACR           VLTFEEVVHHDHNKERGSFITSEEQDVSPRPAPLLLNTPAIPSFKRDPFIGEHTEEILEE
                **:* ** :. *  **.:*  ::    . :* *    : : .*  * *    . * :* :

MCR             WDG-----------------------
AMACR           FGFSREEIYQLNSDKIIESNKVKASL
                :.
```

Figure 4.1: Protein sequences of MCR (accession number O06543) and human AMACR 1A (accession number Q9UHK6). The asterisk shows a fully conserved residue, the colon shows amino acids of MCR and AMACR with strongly similar properties, the period shows amino acids of MCR and AMACR with weakly similar properties. The highlighted red residues show those chosen for site-directed mutagenesis in this study (*vide infra*).

The catalytic residues and mechanism of human AMACR was proposed based on the previous data from the site-directed mutagenesis study[86] and X-ray crystal structures of MCR.[107, 146, 153] His-122 and Glu-237 residues in human AMACR correspond to His-126 and Glu-241 residues in MCR (Figure 4.1; *vide supra*), which have been proposed to be working together as a basic dyad for the *S*-substrate.[146] Asp-152 in the human enzyme, which corresponds to Asp-156 in the active site of the MCR, is proposed to work as the catalytic base for the *R*-substrate.[146] This proposed mechanism with two distinct catalytic bases involved in the 'racemisation' of the *R*- and *S*-substrate is known as the two-base mechanism (Scheme 4.1). The two-base mechanism is based on the MCR model[86, 91] and has been observed in other racemases such as the mandelate racemase[208] and proline racemase[209]. The defining feature of a two-base mechanism is that the product of the enzymatic reaction has a configuration which is inverted compared that of the substrate. Moreover,

performing the reaction in $^{2}H_2O$ results in incorporation of ^{2}H into the product, with very little into the substrate. However, the study of Darley *et al.* suggested that human AMACR does not fit in the classical two-base mechanism and may operate with an one-base mechanism.[1] This conclusion was reached because the product is a near 1:1 mixture of epimers at the methyl centre, and deuterium from $^{2}H_2O$ is equally incorporated into both substrate and product. This behaviour is characteristic of 'one-base' racemases.[210]

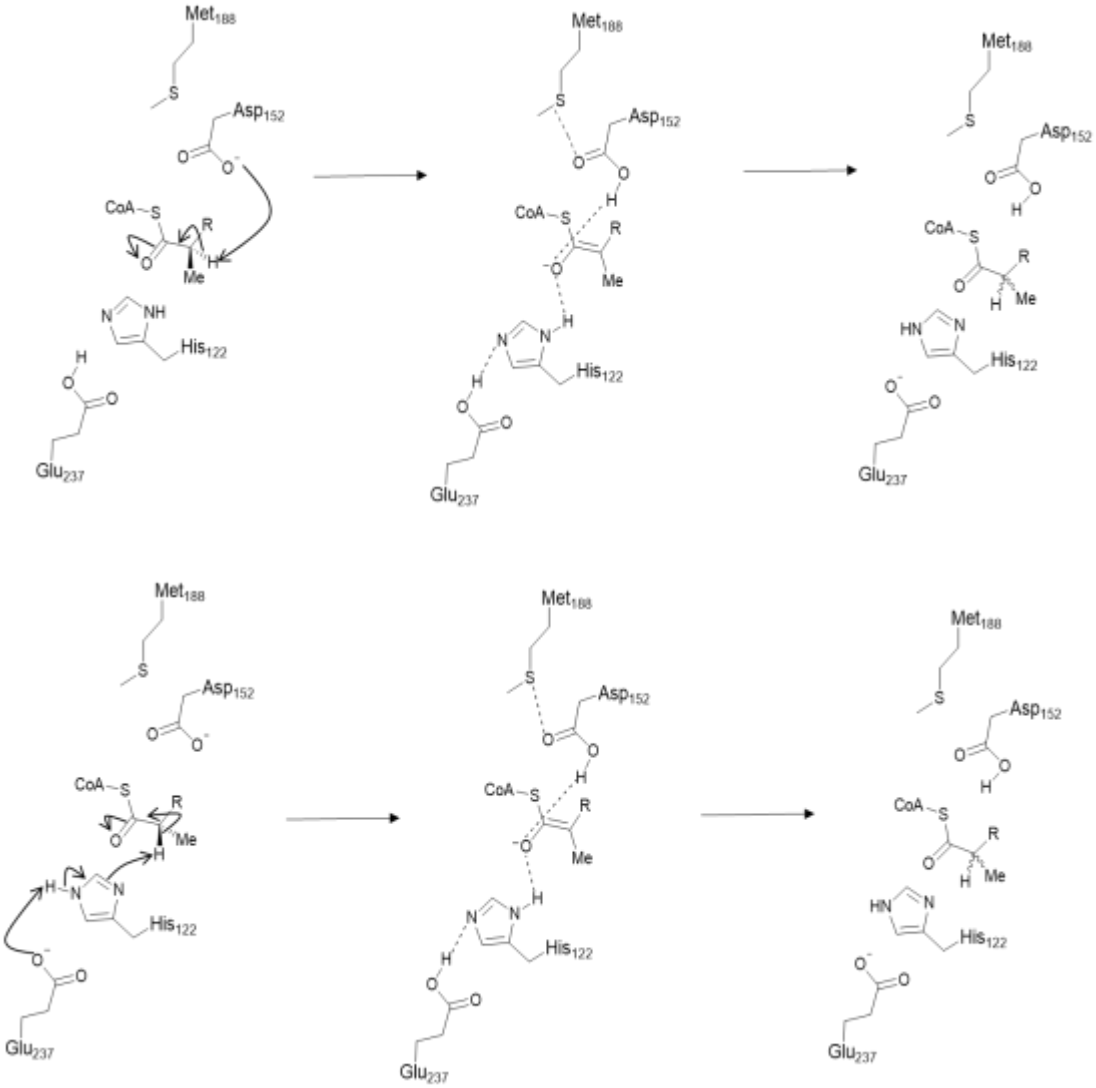

Scheme 4.1: The proposed two-base mechanism of human AMACR where the top panel shows the 'racemisation' of *R*-2-methylacyl-CoA ester and the bottom panel shows the 'racemisation' of *S*-2-methylacyl-CoA ester. The dotted lines show the interactions of the enolate intermediate with the residues in the oxyanion hole.

In order to study the active site and understand the mechanism of human AMACR, a site-directed mutagenesis study on human AMACR 1A was performed. Human AMACR 1A was used instead of other spliced variants as it is known to be an active enzyme and that it is most commonly over-expressed in prostate cancer.[158] The sequence of human AMACR and sequence of MCR were aligned and the chosen residues for site-directed mutagenesis were His-122, Asp-152, Met-184 and Glu-237 (Figure 4.1; *vide supra*). All of these AMACR residues were changed to alanine, which is an amino acid with a methyl side-chain. Alanine is often used in site-directed mutagenesis studies[86, 211] because it possesses a small, non-functional side-chain. Even though glycine is smaller than alanine, it was not considered as it is achiral as it lacks a side-chain and therefore could potentially cause generalised disruption to the structure.[212] Substitution of His-122 with alanine would allow investigation of the mechanism using chemical rescue (Scheme 4.2).

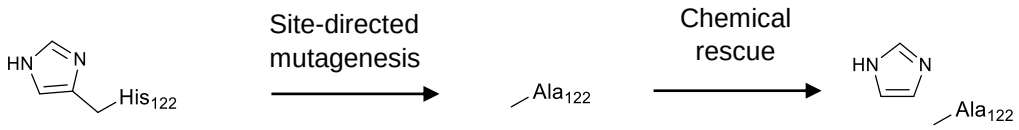

Scheme 4.2: Site-directed mutagenesis of His-122 to Ala-122 (H122A mutant). Chemical rescue could be performed by adding imidazole to the assay which could potentially occupy the empty space left by the missing histidine side-chain.

In addition to alanine residues, mutation of the target residues to other amino acids was also considered. The Asp-152 was mutated to asparagine (D152N) and the Glu-237 was changed to glutamine (E237Q) (Scheme 4.3). A change from an OH group to a NH_2 group introduce the smallest possible structural change, but it was expected to affect the acidity of the side-chain and might affect hydrogen bonding networks.

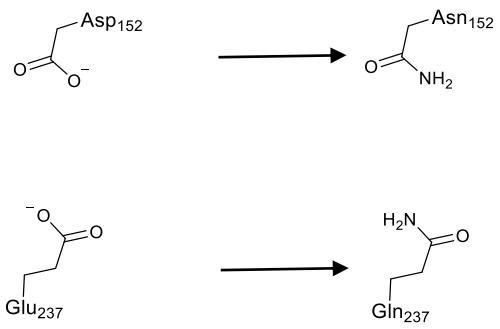

Scheme 4.3: The mutation of Asp-152 and Glu-237 to give the D152N and E237Q mutants.

Met-184 in human AMACR 1A was also chosen for site-directed mutagenesis as previous studies have shown that Met-188 of MCR has an enolate-stabilising role in the oxyanion hole (Figure 1.11; *vide supra*).[146] The Met-188 of the MCR is located in a hydrophobic region of enzyme and is in close proximity to Asp-156 according to the X-ray crystallographic structures of the enzyme. The sulfur atom of Met-188 interacts directly with Asp-156 and modifies its pK_a.[146] This interaction helps stabilise the enolate intermediate.[108] To study whether Met-184 has the same role in human AMACR, this residue was mutated to alanine to give the M184A mutant.

4.2 Production of mutant AMACR 1A plasmids

4.2.1 Q5® site-directed mutagenesis

Initially, site-directed mutagenesis was attempted using Q5® site-directed mutagenesis kit (Figure 4.2) and non-overlapping primers were used. The forward primer had a codon substituted to code for the desired mutation. The reverse primer did not have any substitution as it was in the opposite direction of the forward primer and did not overlap with it.

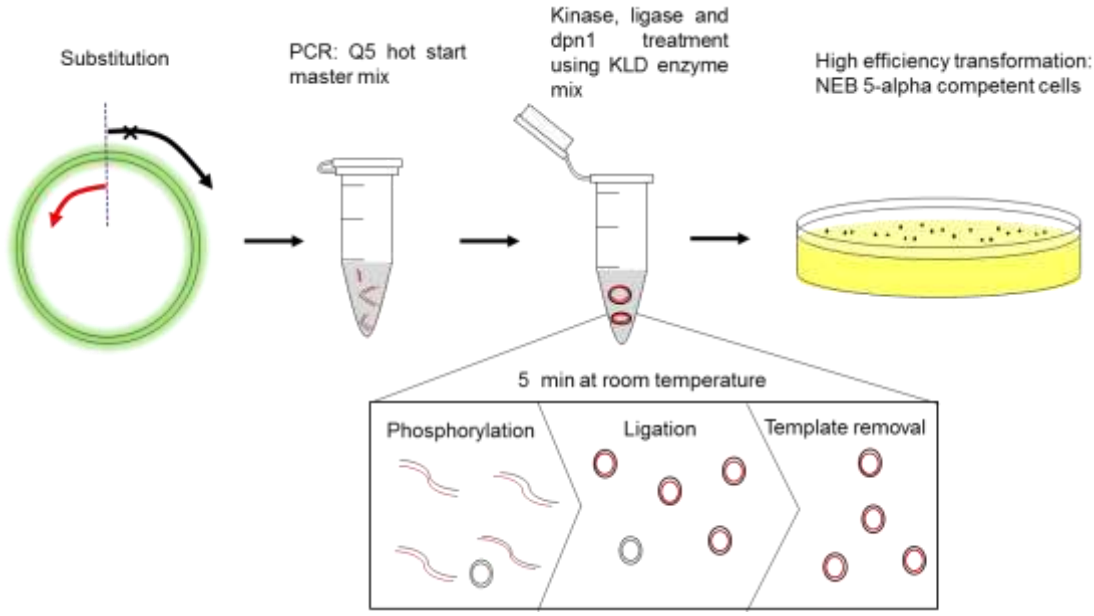

Figure 4.2: Q5® site-directed mutagenesis protocol. The black arrow on the plasmid indicates the forward primer and the cross represents the substitution. The red arrow on the plasmid indicates the reverse primer.

After the DNA was amplified and treated according to the protocol, it was transformed into competent *E.coli* and plated onto agar supplemented with kanamycin sulfate as the selective agent. No colonies were found in any of the LB plates except for the control plate which used the pUC19 vector. This showed that the transformation step had worked but the site-directed mutagenesis experiment had failed to produce viable mutant plasmids. Analysis by agarose gel electrophoresis showed that no DNA band at ~6.6 kb (intact plasmid) or ~1.2 kb (AMACR insert) was observed. A control PCR reaction was also performed with another polymerase, KOD Hot Start polymerase with wild-type plasmid and a DNA fragment of ~1.2 kb was observed (Figure 4.3). The mutagenesis experiment had failed and multiple optimisations of the site-directed mutagenesis did not result in a different outcome. Hence, further experiments were conducted using KOD Hot Start polymerase instead of Q5® polymerase.

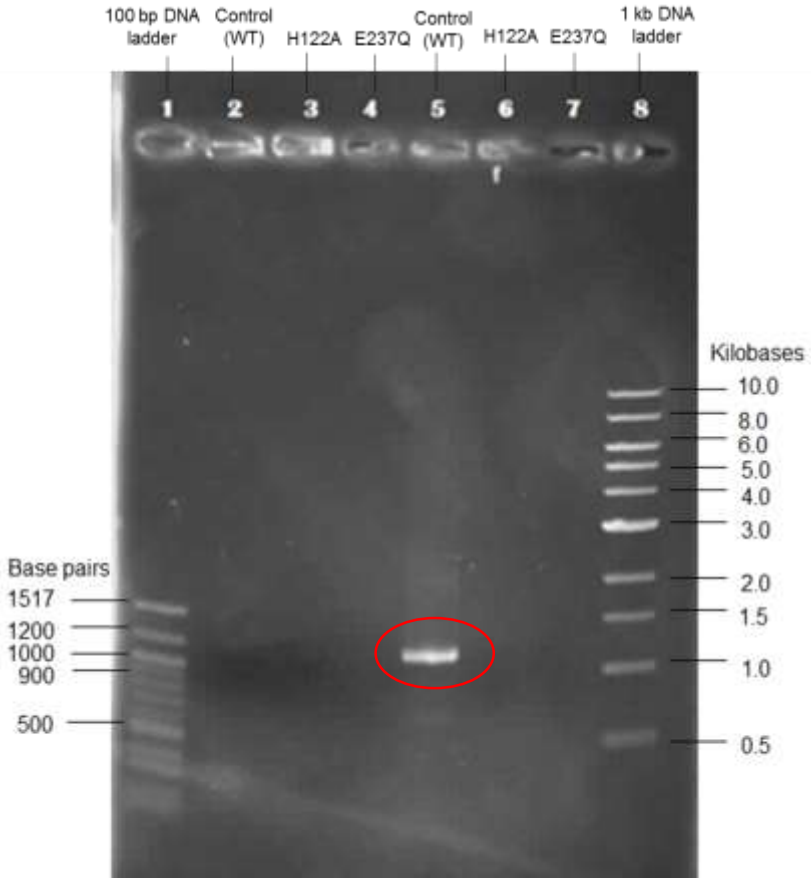

Figure 4.3: PCR products of the site-directed mutagenesis. DNA markers were loaded onto the agarose gel and electrophoresed at 95 volts for 1 h. The gel showed DNA amplifications of some of the mutants performed using Q5® polymerase except for the cDNA control in well 5 (red circle) which was amplified using KOD polymerase.

4.2.2 Optimisations of KOD Hot Start polymerase protocol

The non-overlapping primers designed using NEB website was used for site-directed mutagenesis catalysed by KOD Hot Start polymerase. However, no colonies were observed following transformation and plating onto the LB agar plate containing kanamycin sulfate as the selecting agent. Agarose gel electrophoresis showed that no DNA band of ~6.6 kb (corresponding to intact plasmid containing AMACR cDNA) was observed.

Primers were phosphorylated in an attempt to establish if prior phosphorylation was required for efficient PCR. The DNA was amplified with KOD polymerase, template DNA was digested using *Dpn1* and the product was purified with QIAquick PCR purification kit. The purified DNA was circularised using Quick Ligation™ kit and transformed into competent cells. Bacteria containing the

plasmids for the H122A, M184A and E237Q mutants formed colonies on LB agar plates. Colony PCR was performed on the derived plasmids. No ~1.2 kb DNA band from the mutants was observed (Figure 4.4), although bands of other sizes were observed. Attempts to express these mutants were unsuccessful, which was as expected.

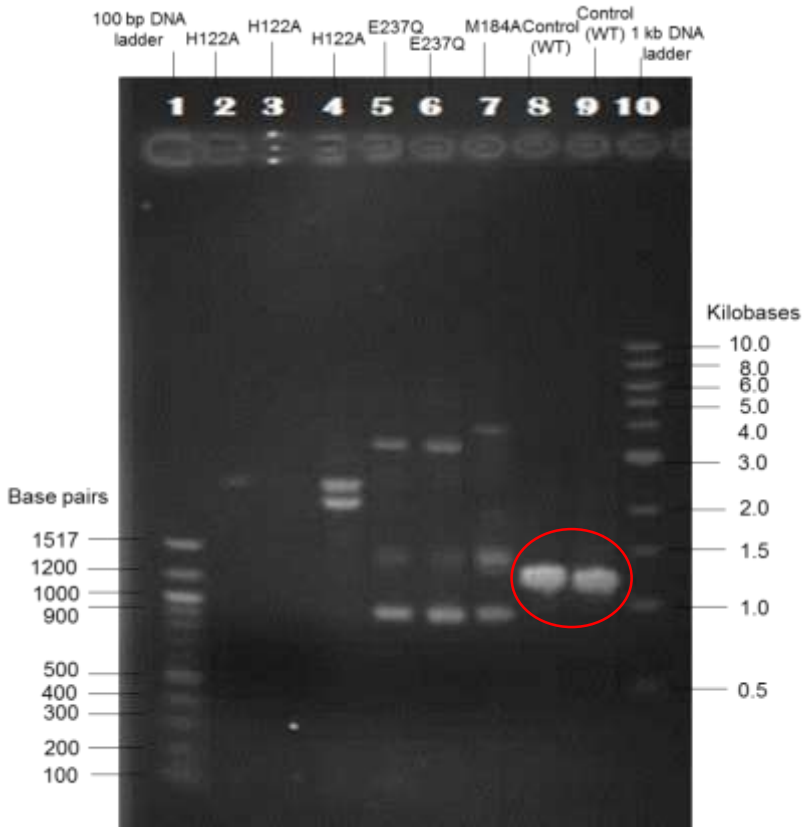

Figure 4.4: Wild-type AMACR forward and reverse primers were used in colony PCR to screen for the AMACR cDNA. *Ca*. 1.2 kb DNA bands were expected for all mutants and wild-type plasmid. Only wild-type controls (red circle) showed the expected ~1.2 kb band but the rest of the mutants either did not show any band or showed bands of incorrect sizes.

4.2.3 Site-directed mutagenesis using optimised KOD Hot Start polymerase protocol

Primers were re-designed manually for use with the 'Stratagene QuickChange Method', where the forward and reverse primers were complementary. Each forward primer was ~32 nucleotides with the mutation site in the middle of the primer and a run of G or C at the termini of either end. If more than one codon

was possible for the amino acid to be substituted, the most common codon in *E. coli* was used.

In addition to the planned substitutions (H122A, M184A, D152A, D152N, E237A and E237Q), the H122F and H122L mutants were also produced. They were added at a later stage, as it was found that H122A plasmid failed to be expressed and produce mutant AMACR (*vide infra*).

PCR was performed using KOD Hot Start polymerase and the PCR products were analysed by agarose gel electrophoresis (Figure 4.5). A band at ~6.6 kb was observed, consistent with the presence of a mutant plasmid.

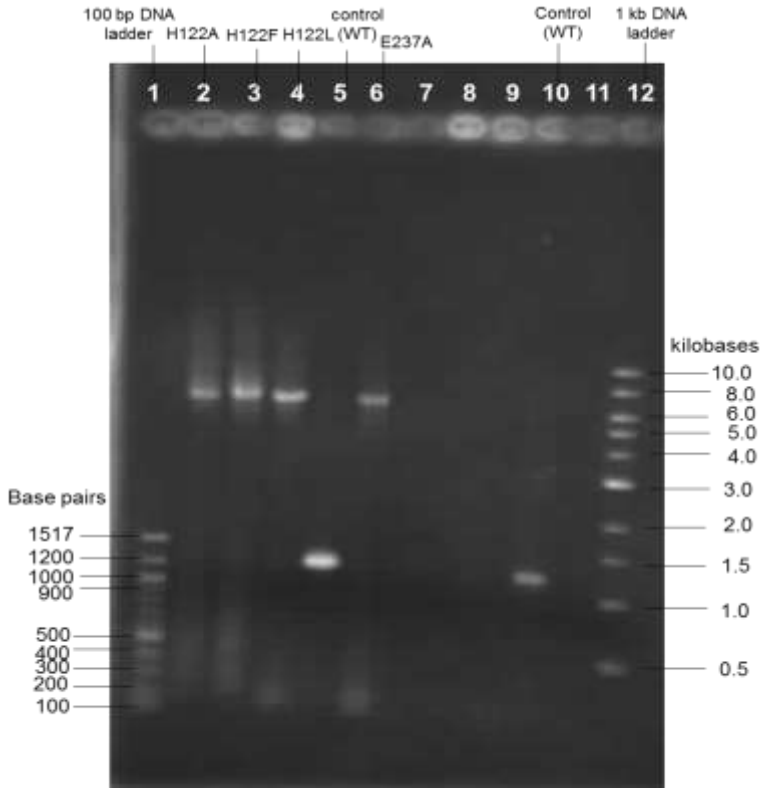

Figure 4.5: One of the examples of PCR products amplified by KOD polymerase and analysed by agarose gel electrophoresis. Plasmids of ~6.6 kb in wells 2, 3, 4 and 6 (the H122A, H122F, H122L and E237A mutants, respectively) were observed. Controls with wild-type AMACR plasmid in wells 5 and 10 showed a ~1.2 kb band.

The PCR products were treated with *Dpn1* to remove wild-type plasmid, purified, and transformed in competent cells. The transformed bacteria with wild-type, H122A, H122F, H122L, D152A, D152N, M184A, E237A or E237Q

plasmids all formed colonies on LB plates supplemented with kanamycin sulfate. Phosphorylation and ligation have been shown to be unnecessary as high-efficiency transformation into cells was achieved following purification of the PCR product. Colony PCR confirmed the presence of the expected ~1.2 kb insert. The presence of the required mutations was confirmed by sequencing the entire cDNA before protein expression experiments were performed, and showed the expected sequences with the required mutations and no other changes.

4.2.4 Double mutations on H122A mutant

As His-122 and Glu-237 are proposed to be working together as a basic dyad in deprotonating its substrate,[76] a double mutation of these two residues was attempted. H122A/E237A and H122A/E237Q mutations were carried in order to investigate the effect of losing these two residues together. E237A or E237Q forward and reverse primers together with H122A plasmid was used for site-directed mutagenesis. H122A/E237A and H122A/E23Q mutants formed colonies on LB plates. Only H122A/E237A but not H122A/E237Q showed ~1.2 kb insert in colony PCR (Figure 4.6). Both H122A/E237A and H122A/E237Q were sent for sequencing but their sequences could not be confirmed, possibly due to the quality of the plasmids. Attempts to re-prepare the plasmids did not result in any improvement of the samples and the samples failed to produce a clear signal for sequencing. Expression of the double mutants was attempted but was unsuccessful.

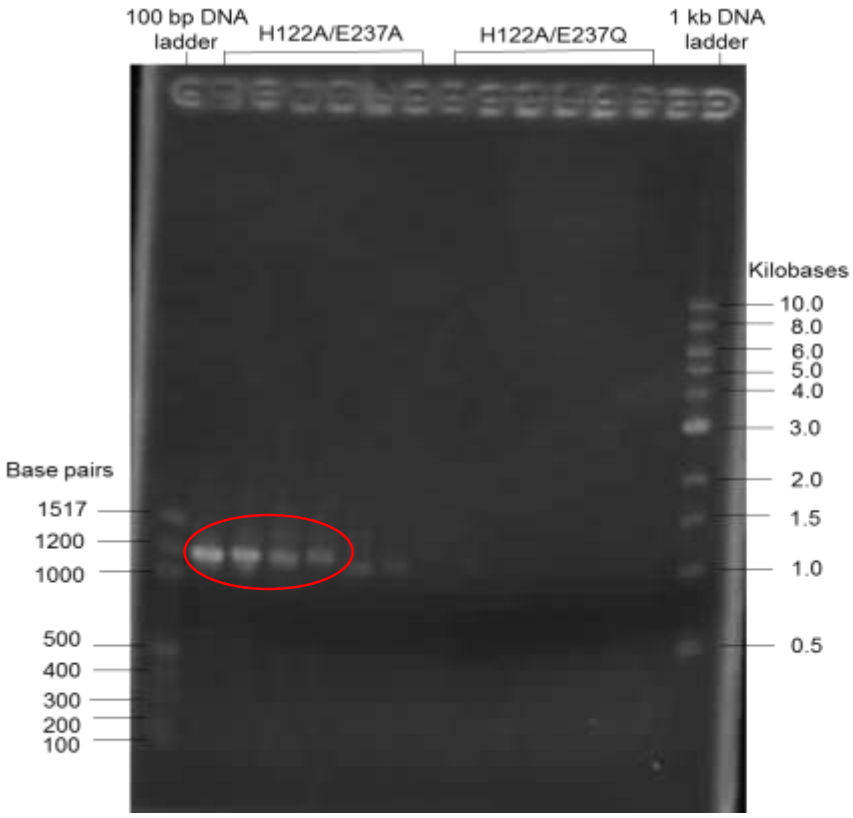

Figure 4.6: Colony PCR for double mutants. H122A/E237A (red circle) showed ~1.2 kb insert but H122A/E237Q did not show ~1.2 kb insert upon analysis by agarose gel electrophoresis.

4.3 Expression and purification of AMACR 1A enzymes

Expression experiments were performed on a small scale to find the most suitable conditions for protein production from each of the mutated pET plasmids. The pET30 Ek/LIC plasmid contains a lac operon where the gene expression is inducible by compounds that binds to and releases the lac repressor protein (LacI).[213] The inducers trialled include the Novagen Overnight express™ autoinduction system 1, IPTG and lactose. The Rosetta2 (DE3) was chosen as the expression strain as this strain has been engineered to provide tRNAs that bind to codons common in eukaryotic species that are rarely found in normal *E. coli*, so the expression of eukaryotic cDNA could be enhanced.[214]

Overnight express™ autoinduction system 1 was the preferred inducer as the monitoring of cell growth was not required. It contains a specific blend of glucose and lactose where the glucose will allow uninduced cell growth and

later, the protein expression would be induced by lactose once the glucose source is used up. Autoinduction system 1 successfully induced the expression of most of the enzymes (wild-type, the M184A, E237A and E237Q mutants) with good yield. The H122A, H122F, H122L, D152A and D152N mutants were not expressed with autoinduction system 1.

Leaky expression was observed for wild-type enzyme at 37 °C so the temperature of the initial growth phase was lowered. Besides preventing leaky expression, a lower temperature could also minimise the formation of inclusion bodies (misfolded and insoluble proteins).[215] The problem of inclusion bodies could arise when the production of recombinant proteins is greater than 50% of the host proteins. This leads to a higher rate of protein aggregation compared to the rate of protein folding.[215] A lower temperature reduces the rate of transcription and translation and hence a lower protein production rate, which will help minimise the formation of inclusion bodies.[215] However, the bacteria culture will be dormant at low temperature, and protein expression can not be induced (if glucose in Autoinduction system is not used up by the dormant culture, lactose will not be used to induce protein expression). Hence, a compromised temperature of 28 °C was chosen to allow sufficient growth of bacteria culture and also to promote correct protein folding.

IPTG (0.25 mM) and lactose (2 mM, 5 mM or 10 mM) were trialled as alternative inducers. Lactose is the natural occurring inducer for the lac operon and has the advantages of being cheap and non-toxic.[216] IPTG is a synthetic form of a lactose metabolite (allolactose) and has been widely used as an inducer of the lac operon.[217, 218] AMACR 1A containing the H122L and D152N mutations were expressed with IPTG whilst the H122A, H122F and D152A mutants failed to express with all three inducers that were trialled. As a result, the planned chemical rescue by adding imidazole to the H122A mutant protein could not be carried out. The expression of double mutants was also not pursued further as their sequences were not confirmed and their expression was not induced by autoinduction system 1, IPTG or lactose.

Once the optimum conditions of expression for each mutant proteins were established, they were expressed on a large scale. A consistent temperature of 28 °C was used in growing and expressing all mutant proteins regardless of the type of inducer used. Attempted mutations and success in the expression of mutant enzymes were summarised in Table 4.1.

Mutations attempted	Success in expressing mutant enzymes
H122A	No
H122F	No
H122L	Yes
D152A	No
D152N	Yes
M184A	Yes
E237A	Yes
E237Q	Yes
H122A/E237A	No
H122A/E237Q	No

Table 4.1: Mutations attempted and success in expressing mutant proteins

The histidine-tagged recombinant proteins were purified using nickel-chelate chromatography. The proteins were eluted with imidazole which displaced the bound proteins from the nickel ions chelated to the column. The eluted fractions containing purified protein (Figure 4.7) were combined and dialysed into 10 mM NaH_2PO_4-NaOH, pH 7.4 buffer. All combined purified enzymes were analysed by SDS-PAGE (Figure 4.8). The concentration of the enzymes were determined using the UV absorbance at 280 nm.

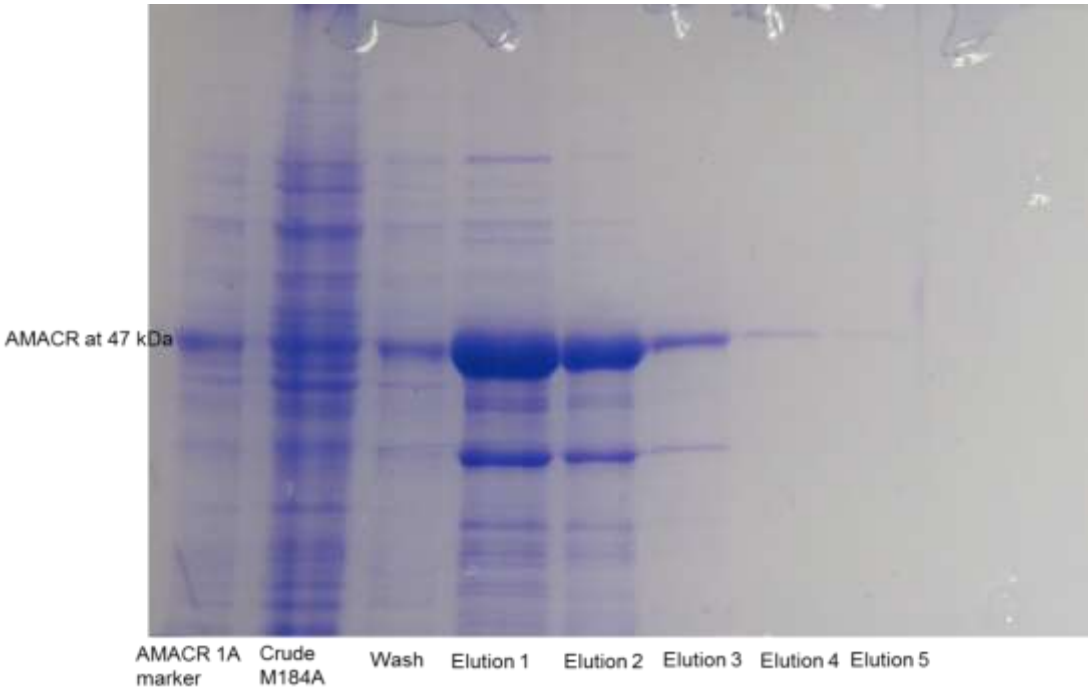

Figure 4.7: SDS-PAGE of different purification fractions of M184A. The standard used was wild-type AMACR 1A, followed by crude M184A, wash fraction and different elution fractions of M184A. Fraction 1 and 2 were combined and dialysed.

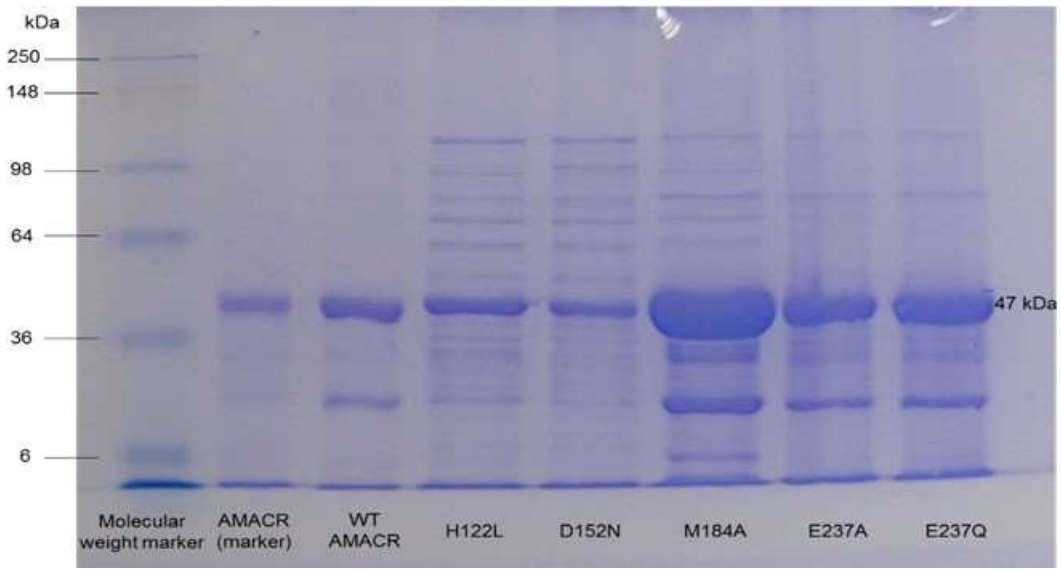

Figure 4.8: SDS-PAGE of purified wild-type, H122L, D152N, M184A, E237A and E237Q, showing a strong band at ~47 kDa. AMACR marker was a purified wild-type AMACR 1A protein obtained from MDL lab.

Wild-type and mutant enzymes were purified to *ca*. 95% purity, as judged by SDS-PAGE analyses. The impurities were consistent across all purified

proteins and could be due to the contamination from bacterial proteins or proteolytic fragments resulting from digestion of the recombinant protein.[219] Additional purifications on the wild-type AMACR 1A have been investigated previously by the MDL lab[1] but this has been proven to be challenging and did not improve the purity of the protein.

SDS-PAGE was repeated on the samples of purified proteins in order to check for protein degradation over time. The result showed that the proteins were stable with no change in purity when stored at -80 °C.

4.4 Protein characterisation

The wild-type AMACR and all of the mutants were characterised using DLS, CD and fluorescent study using ANS in order to check the conformation of the enzymes and whether there was any dissociation of dimeric proteins (*i.e.*, that dimerisation was intact).

4.4.1 Dynamic light scattering (DLS)

DLS, also known as photon correlation spectroscopy can be used to determine the size and size distribution of particles in the nanometer region.[220] The sample is illuminated by laser light and the light is scattered by the Brownian motion of particles.[220] Fluctuations in the intensity of the scattered light are analysed and correlated to the hydrodynamic radii of particles.[221]

The X-ray crystal structure and the site-directed mutagenesis study on MCR have shown that the enzyme is a tight-interlocked dimer with subunits connected *via* their C-termini, and the catalytic centres are at the interface of the dimer.[86, 146] It is assumed that human AMACR 1A has the same or similar catalytic sites, situated at the interface of the dimer. Site-directed mutagenesis of human AMACR catalytic residues might affect the stability of the enzyme. The His-122 residue is thought to be contributed by the large domain and the Glu-237 residue is thought to be contributed by the small domain and they work together as a catalytic dyad. Mutations of these residues could potentially lead to the dissociation of the dimer and hence reduce enzyme catalytic

activity. The integrity of the dimeric state of the protein was therefore investigated using DLS.

The results (Table 4.2) showed that the sizes of the enzyme were greater than an average size of a protein (which are usually in the low nm range).[222] Among the enzymes tested, wild-type AMACR, E237A and E237Q had the largest sized particle, between *ca.* 65 nm and *ca.* 90 nm. These large readings suggested that these proteins had formed aggregates instead of existing freely as a dimer in the solution. The D152N mutant had the smallest size (12.4 nm) and smallest standard deviation, suggesting that it was less likely to form aggregates. Instead of probing the dimeric state of the enzyme, the DLS experiments indicated that the enzymes have a tendency to aggregate.

AMACR	Average size (nm)
Wild-type	89.3 ± 36.4
H122L	21.6 ± 6.9
D152N	12.4 ± 3.8
M184A	21.5 ± 7.7
E237A	65.3 ± 15.0
E237Q	80.0 ± 19.4

Table 4.2: Average sizes (nine replicates) ± standard deviation of wild-type and mutant AMACR estimated by DLS.

4.4.2 Circular dichroism (CD)

To study if the site-directed mutagenesis had affected the stability and hence the folding of the enzyme, CD was used to study the structure of the protein. Polarised light of the CD interacts with the protein to give a CD spectrum that is specific to that particular protein. The pattern and magnitude of the spectrum provides excellent information about the structure of the protein, especially secondary structure.[223] The H122L, D152N, M184A, E237A and E237Q mutants were examined by CD in order to determine if their structures were different from wild-type AMACR.

The CD spectra at the far-UV region (200-240 nm) and near-UV region (250-300 nm) were analysed to examine the protein structure. The far-UV region provides information on the secondary structure of the protein. Theoretically, this region can go below 180 nm, but in practice, it is difficult to obtain accurate readings below 200 nm due to noise from the background.[224] This region shows various secondary structures such as α-helices, β-sheets and β-turns.[224] The CD spectrum of wild-type AMACR expressed at 22 °C[2] was compared with the CD spectrum of the same enzyme expressed at 28 °C (Figure 4.9). Proteins expressed at different temperatures showed slightly different secondary structures. Both enzymes have different K_m and V_{max} values for the same substrate, *S*-2-methyldecanoyl-CoA **38**. Wild-type AMACR expressed at 22 °C gives a K_m value of 277 μM and V_{max} value of 39.3 nmol min^{-1} mg^{-1}.[2] On the other hand, wild-type AMACR expressed at 28 °C (*vide infra*) gives *ca.* 3 times smaller K_m value (95 μM) and *ca.* 3 times larger V_{max} value (108 nmol min^{-1} mg^{-1}), indicating that 28 °C is a better temperature for expressing the protein.

In this study, wild-type and all mutant enzymes were expressed at 28 °C and they did not seem to have a gross structural disruption. None of the enzymes showed a CD spectrum that looked like the denatured protein (Figure 4.9). The results showed that the denatured protein has nearly zero molar ellipticity and did not have any characteristic signals of α-helices or β-sheets. All mutant enzymes except D152N and M184A showed secondary structures similar to wild-type enzyme either expressed at 22 °C or 28 °C (Figure 4.9). The results implied that the activity or inactivity of these mutant enzymes was probably due to the mutation of a single residue, instead of a gross structural disruption of the protein. M184A and D152N mutants seemed to have greater molar ellipticities, suggesting that there might be enhanced α-helicity in their secondary structures. However, it is probable that these molar ellipticities values were affected by different levels of protein aggregation (as shown by differences in DLS readings).

The near-UV region (250-300 nm) provides information about the local environment of aromatic side-chains and tertiary structure of the protein.[224]

Low molar ellipticity readings could be due to high number of aromatic side-chains in a protein (positive and negative readings cancel out each other), close distances between aromatic side-chains and high mobility of aromatic side-chains.[225] Wild-type and mutant AMACR proteins all have near zero molar ellipticity in this region (Figure 4.9), possibly due to the reasons mentioned above. Nevertheless, the near-UV region can act as a fingerprint region of the protein and it showed that mutations on AMACR did not cause any significant change to the tertiary structure.

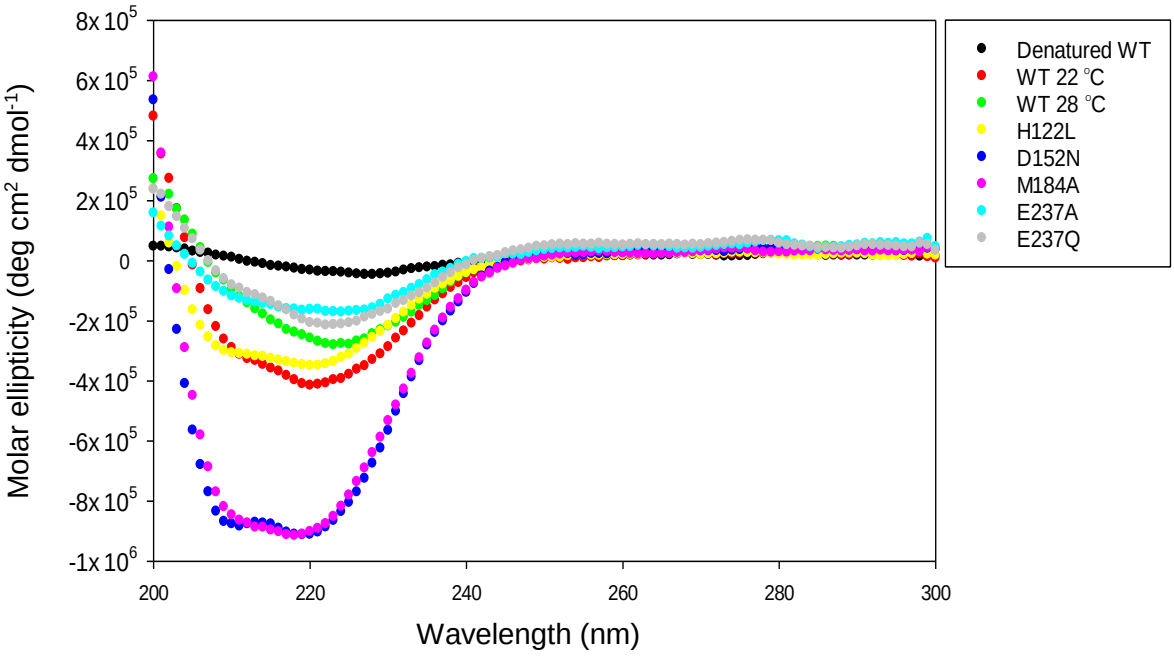

Figure 4.9: CD spectra of wild-type and mutant AMACR.

4.4.3 Fluorescence study using 8-anilino-1-naphthalenesulfonic acid (ANS)

ANS **148** is a fluorescent probe (Figure 4.10) that can be used to study protein folding.[226] The fluorescence intensity of ANS **148** will increase when it binds to hydrophobic surface of protein instead of existing freely in a solution.[227] Hence, it is used to study if the site-directed mutagenesis has disrupted the structure of mutant enzymes and exposed their hydrophobic cores. It could also reveal if the dimerisation is intact as dimers are predominantly held together by hydrophobic interactions. The results of the CD study have shown that D152N and M184A mutants might have changes in their secondary

structures compared with wild-type AMACR. The ANS fluorescence experiment would complement the CD study and reveal if there were indeed any changes in the overall structure of these proteins.

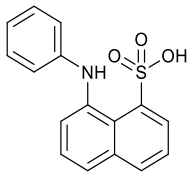

148

Figure 4.10: Structure of 8-anilino-1-naphthalenesulfonic acid (ANS).

The results showed that the fluorescence intensity of ANS **148** was substantially low (almost a flat line) for denatured wild-type AMACR (Figure 4.11). One might expect that a denatured protein would have its hydrophobic core exposed and should bind well with the ANS **148**. To explain this, it is important to understand interactions between the fluorescent probe **148** with a protein. Besides having aromatic rings that could interact with hydrophobic residues of a protein, the ionised form of the fluorescent probe (sulfonate anion) could form ionic interactions with positively charged amino acids.[228] Both ionic interactions and hydrophobic interactions are required in order for the probe to bind stably with a protein to give a strong fluorescence intensity.[229] A fully denatured protein will not form a stable interaction with ANS, so the fluorescence intensity of denatured AMACR is very low.

Wild-type enzymes (both expressed at 22 °C and 28 °C), and mutant enzymes (H122L, D152N, E237A and E237Q) have similar emission spectra (Figure 4.11), suggesting that their hydrophobic surfaces were similar. Even though CD results suggested that the D152N mutant might have a different secondary structure (*vide supra*), it did not seem to have a huge impact to the overall structure of this enzyme. Its ANS emission spectrum was almost identical to the emission spectrum of wild-type AMACR expressed at 28 °C. The only protein with significantly different fluorescent spectra was the M184A mutant (Figure 4.11), with much higher fluorescence intensity. It was obvious that the M184A mutant was not fully denatured because if it has been totally unfolded,

it would have very low fluorescence intensity just like the denatured wild-type AMACR. Assays on the M184A mutant (*vide infra*) have shown that the enzyme was not inactive. On the contrary, it has reasonably good activity, suggesting that the M184A mutant has maintained an intact structure. As ANS **148** does not just bind to hydrophobic surface of a protein, but also interacts with positively charged amino acids, high fluorescence intensity alone does not indicate that the protein is not folded correctly.[230, 231]

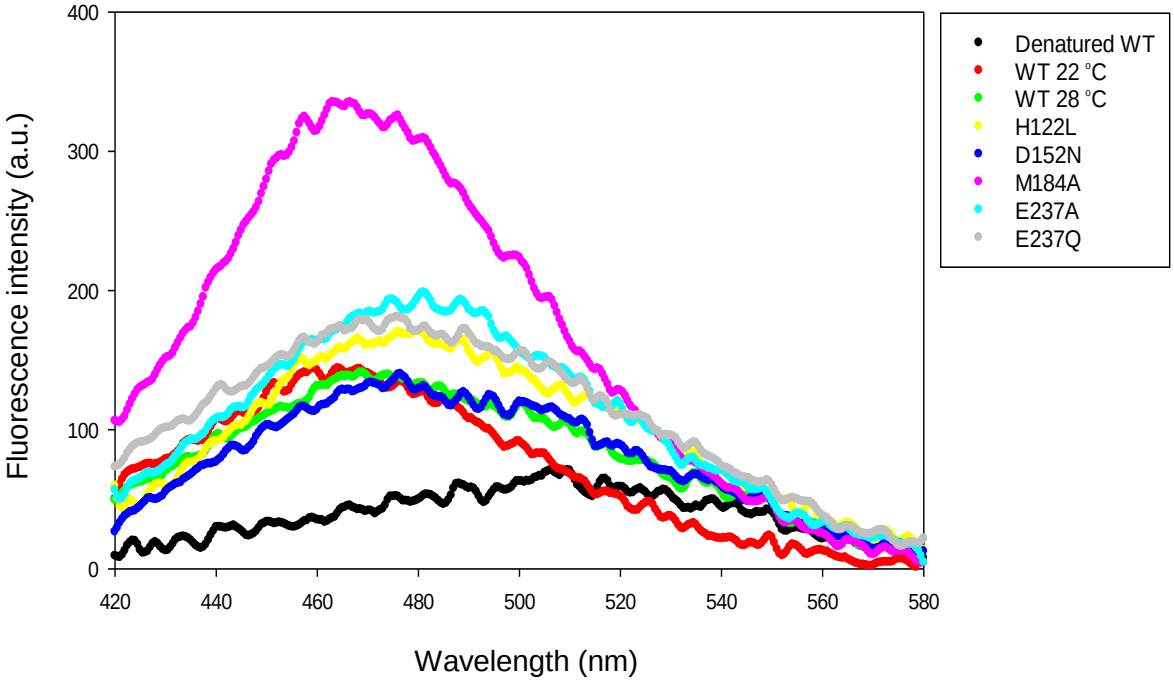

Figure 4.11: The ANS fluorescence emission spectra of denatured wild-type AMACR, wild-type enzymes expressed at 22 °C and 28 °C and mutant enzymes expressed at 28 °C.

4.4 The study of 'racemisation' reaction using the deuterium wash-in assay

The activity of wild-type and mutant enzymes were first tested using the deuterium wash-in assay as previously described.[1, 2] Both the *R*- **44** and *S*- 2-methydecanoyl-CoA **38** were used as substrates in the enzyme assay to determine if the site-directed mutagenesis has any effect on the ability of the wild-type and mutant enzymes to remove the α-proton and exchange it for deuterium from $^{2}H_2O$. As the Asp-152 residue was thought to be involved in the deprotonation of the *R*-substrate and the His-122 and Glu-237 dyad was

thought to be involved in the deprotonation of the *S*-substrate, both *R*- **44** and *S*- **38** substrates were tested with these enzymes to examine their behaviour.

^{1}H NMR was used to analyse the α-proton exchange by quantifying the conversion of the 2-methyl peak from a doublet (at *ca.* 1.00 ppm) to a single peak (at *ca.* 1.00 ppm). The results showed that wild-type AMACR fully exchanged the α-proton to α-deuterium of the *R*- **44** (Figure 4.12) and *S*- 2-methyldecanoyl-CoA **38**. Under identical conditions, the M184A mutant showed 43% conversion of *S*-2-methyldecanoyl-CoA **38** and 40% conversion of *R*-2-methyldecanoyl-CoA **44**. All other mutants did not catalyse significant conversion compared with negative controls containing heat-inactivated enzyme.

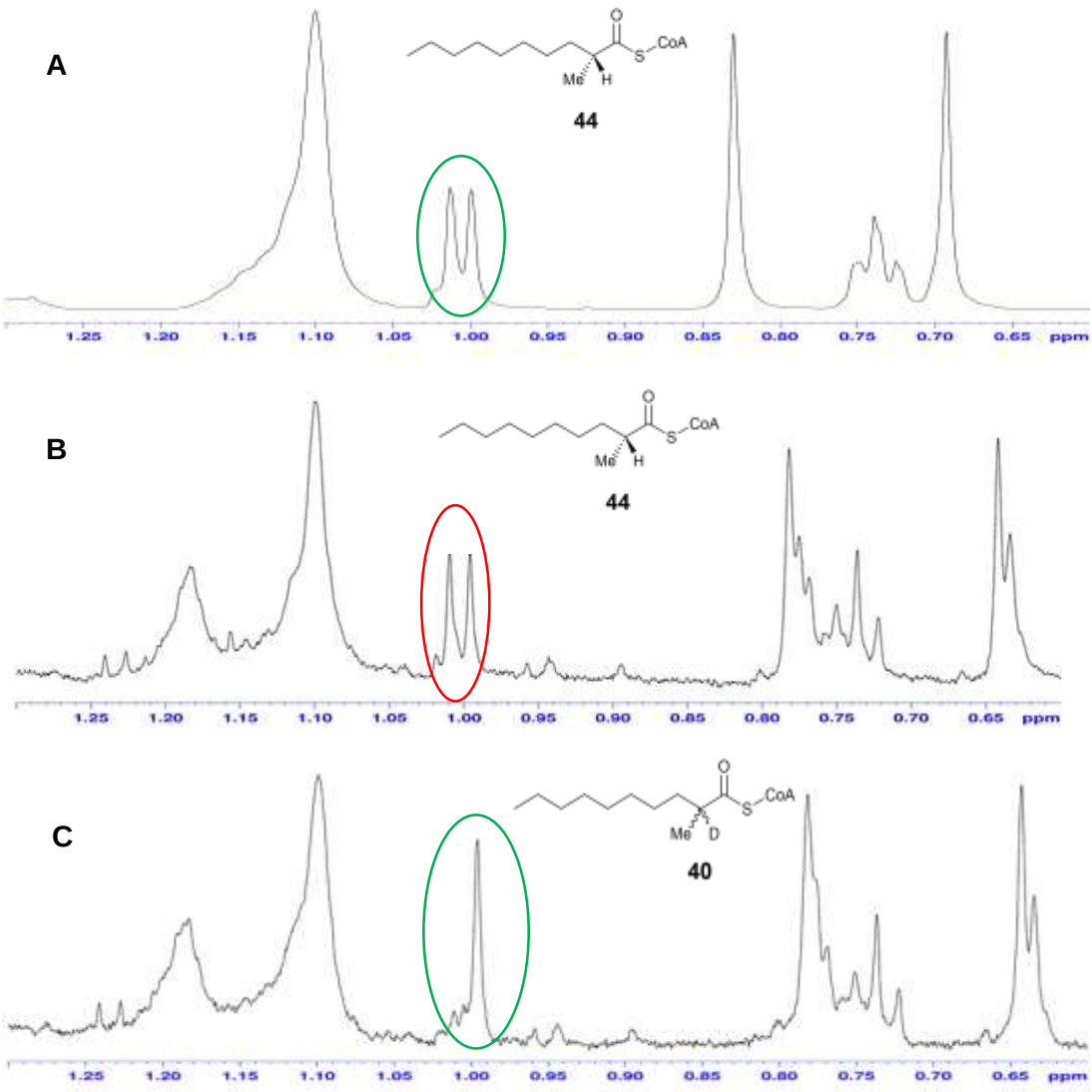

Figure 4.12: ^{1}H NMR of *R*-2-methyldecanoyl-CoA **44** with its 2-methyl peak at 1.00 ppm. A) The substrate was dissolved in $^{2}H_2O$ prior to the enzyme assay; B) The substrate (final assay concentration 100 µM) incubated with heat-inactivated enzyme (final assay concentration 0.12 mg mL^{-1}; 2.55 µM); C) The substrate (final concentration 100 µM) incubated with active wild-type AMACR (final assay concentration 0.12 mg mL^{-1}; 2.55 µM).

As the wild-type AMACR and M184 mutant were active using the deuterium wash-in assay, kinetic analyses were performed on these two enzymes using *R*- **44** and *S*-2-methyldecanoyl-CoA **38**. As expected, these two acyl-CoA esters were shown to be good substrates for wild-type AMACR, results were comparable to previous data.[1, 2] The K_m value for *R*-2-methyldecanoyl-CoA **44** from the Direct Linear Plot was 124 µM and V_{max} value was 107 nmol min^{-1} mg^{-1} (Appendix 2). The calculated k_{cat} value was 0.084 s^{-1} and k_{cat}/K_m value

was 677 M^{-1} s^{-1}. For *S*-2-methyldecanoyl-CoA **38** the K_m value was 95 µM, V_{max} was 108 nmol min^{-1} mg^{-1}, k_{cat} was 0.085 s^{-1} and k_{cat}/K_m was 895 M^{-1} s^{-1} (Appendix 3).

Data from the kinetic assay on M184A mutant with *S*-2-methyldecanoyl-CoA **38** could not be fitted using the Michaelis-Menten kinetic model. Even though the Direct Linear Plot estimated a K_m value of 95 µM and V_{max} value of 0.77 nmol min^{-1} mg^{-1}, the plot was of poor quality and many of the lines did not properly converge (Appendix 4). Multiple preliminary assays were performed on M184A mutant using *R*-2-methyldecanoyl-CoA **44** to establish the appropriate enzyme concentration for the kinetic analysis. However, the results showed a high degree of scatter so kinetic analysis on the M184A mutant with *R*-2-methyldecanoyl-CoA **44** could not be performed. Hence, the effects of the mutation could not be quantified using the deuterium wash-in assay.

4.5 The study of wild-type and mutant enzymes using the fluoride elimination assay

The deuterium wash-in assay suffers from the problem of overlapping doublet and singlet peaks of the 2-methyl group from the substrate and product. If the enzyme has low activity, the ^{1}H NMR peaks that are produced would be very similar to negative controls and the quantification of enzyme activity is difficult. An alternative assay to study the enzyme activity is the fluoride elimination reaction recently described (*vide supra*).[3] The reaction is irreversible, and is more efficient than the 'racemisation' reaction performed by AMACR.[3] The fluorine of the 3-fluoro-2-methylacyl-CoA esters is eliminated to form a corresponding unsaturated product and fluoride anion (Scheme 4.4). The 2-methyl group of the saturated substrate **114** and unsaturated product **117** have very different chemical shifts in the ^{1}H NMR spectrum (Figure 4.13) and hence conversion levels can be determined much more accurately. As the α-proton is removed in the elimination reaction, the effect of site-directed mutagenesis on the deprotonation step can be studied using this assay.

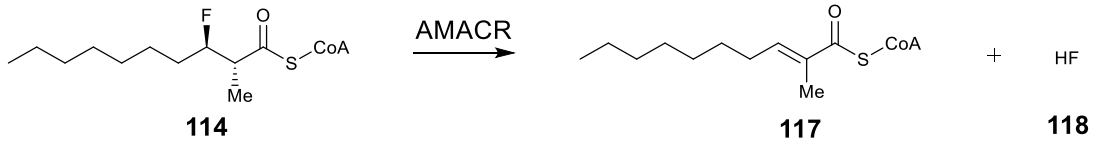

114 **117** **118**

Scheme 4.4: The elimination reaction of (2*R*,3*R*)-3-fluoro-2-methyldecanoyl-CoA **114** to produce a corresponding unsaturated product and fluoride anion.

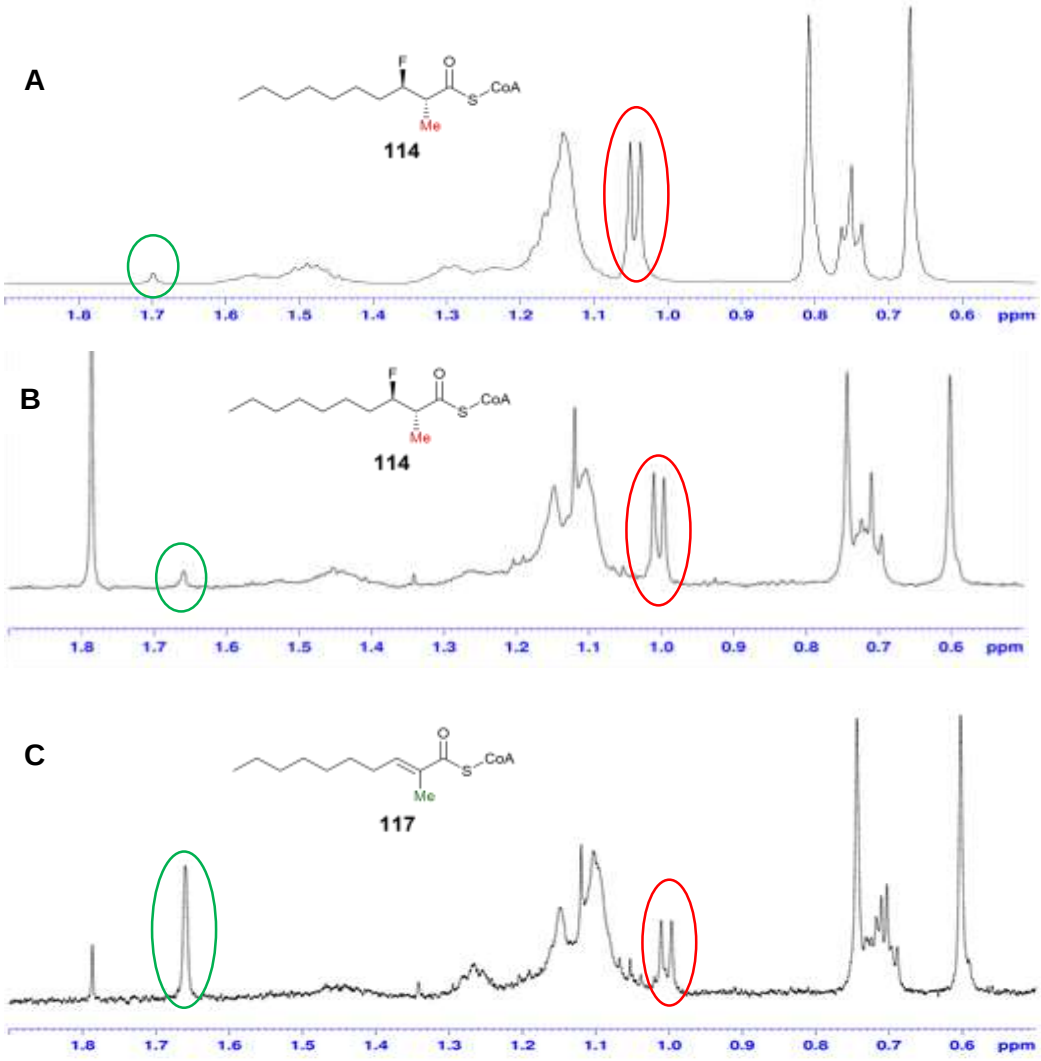

Figure 4.13: ^{1}H NMR of the fluoride elimination assay of (2*R*,3*R*)-3-fluoro-2-methyldecanoyl-CoA substrate **114**. The 2-methyl peak of the substrate **114** is highlighted in red, at *ca.* 1.00 ppm and the 2-methyl peak of the unsaturated product **117** is highlighted in green, at *ca.* 1.65 ppm. A) The substrate was dissolved in $^{2}H_2O$ prior to the enzyme assay; B) The substrate (final assay concentration 100 µM) incubated with heat-inactivated enzyme (final assay concentration 0.12 mg mL^{-1}; 2.55 µM); C) The substrate (final concentration 100 µM) incubated with active wild-type AMACR (final assay concentration 0.12 mg mL^{-1}; 2.55 µM).

(2*R*,3*R*)-3-Fluoro-2-methyldecanoyl-CoA **114** substrate was incubated with wild-type and mutant enzymes. They were initially tested with a single time point assay, where the enzymes were heat-inactivated after one-hour incubation. The ^{1}H NMR analysis (Figure 4.13) showed that wild-type AMACR eliminated 49% of the substrate after 1 h (Figure 4.14). The most active mutant was M184A, which eliminated 8.0% of the substrate, followed by the D152N (6.7%), E237Q (5.5%), H122L (4.1%) and E237A (3.3%) mutants (Figure 4.14). The results were consistent with the deuterium wash-in assay where the most active mutant was M184A.

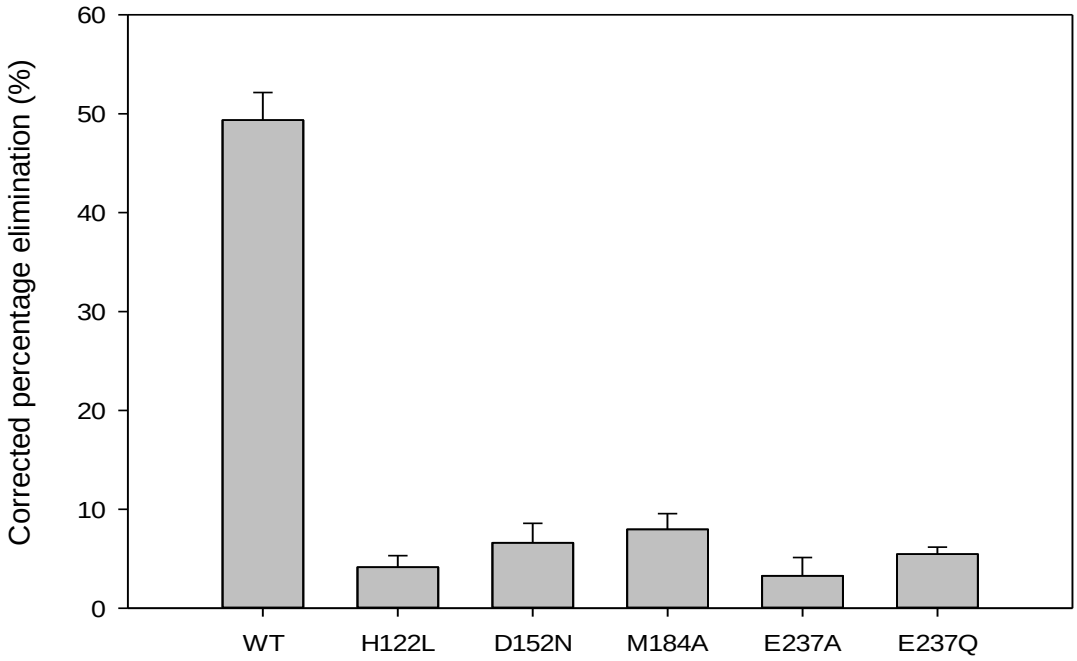

Figure 4.14: Results of single-time-point elimination assay on wild-type and mutant enzymes. Data are mean values (n = 3) ± standard deviation.

As the elimination levels were low for mutant enzymes, it was very difficult to perform kinetic analysis using ^{1}H NMR. Instead, the elimination of (2*R*,3*R*)-3-fluoro-2-methyldecanoyl-CoA **114** was further investigated by following the reaction at 30 °C using the ^{1}H NMR spectrometer over ~16 h (Figure 4.15). After 4 h, the elimination reaction by wild-type AMACR was almost near to completion but the reactions were relatively slow for all mutants. The results were consistent with the single time point assay, where M184A was the most active mutant in catalysing the elimination of (2*R*,3*R*)-3-fluoro-2-

methyldecanoyl-CoA **114**, achieving 39% conversion after 15.5 h. This was followed by D152N mutant, with 23% conversion after 15.5 h. The E237A and H122L mutants were almost inactive, with conversion levels of *ca.* 4% and these did not seem to change much with time. The result did not support the hypothesis that Asp-152 deprotonates the α-proton of a 2*R*-substrate and Met-184 is involved in stabilising the enolate intermediate (*vide supra*).[86, 108, 146] The observation that the D152N and M184A mutants were the two most active mutants completely opposes this hypothesis.

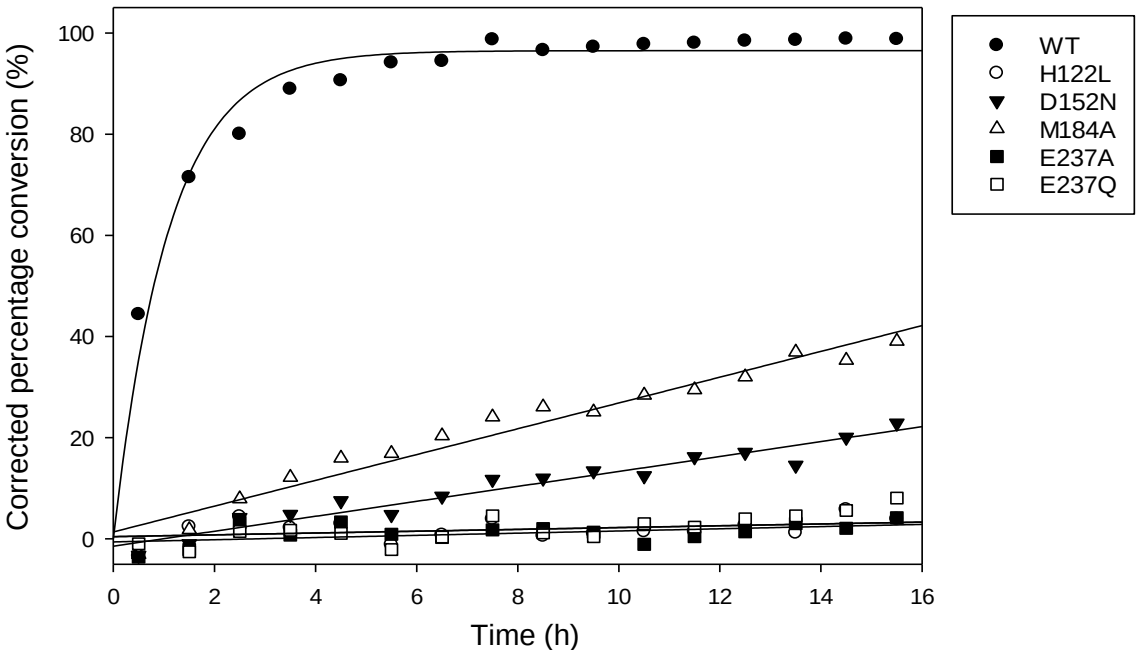

Figure 4.15: ^{1}H NMR time course of wild-type and mutants enzymes (final assay concentration 0.12 mg mL^{-1}; 2.55 µM) with (2*R*,3*R*)-3-fluoro-2-methyldecanoyl-CoA **114** (final assay concentration 100 µM) as substrate**.** The conversion at 30 °C was measured every hour.

To further investigate the proposed hypothesis, the (2*S*,3*S*)-3-fluoro-2-methyldecanoyl-CoA **147** was synthesised using an analogous protocol to that previously described.[3] The results showed that it was still the D152N and M184A mutants that were active in eliminating the 2*S*-substrate **147**, whilst H122L, E237A, E237Q mutants were almost completely dead (Figure 4.16). The only difference compared to the 2*R*-substrate **114** was that D152N mutant was more active in eliminating the 2*S*-substrate **147** than the M184A mutant (59% *vs*. 16% after 15.5 h). The results are inconsistent with the 'two-base'

mechanism where Asp-152 deprotonates the *R*-substrate and His-122 and Glu-237 dyad from another face deprotonates the *S*-substrate (Figure 4.17).[86, 108, 146] In both experiments, the M184A and D152N mutants were active, suggesting that human AMACR works by a 'one-base' mechanism.

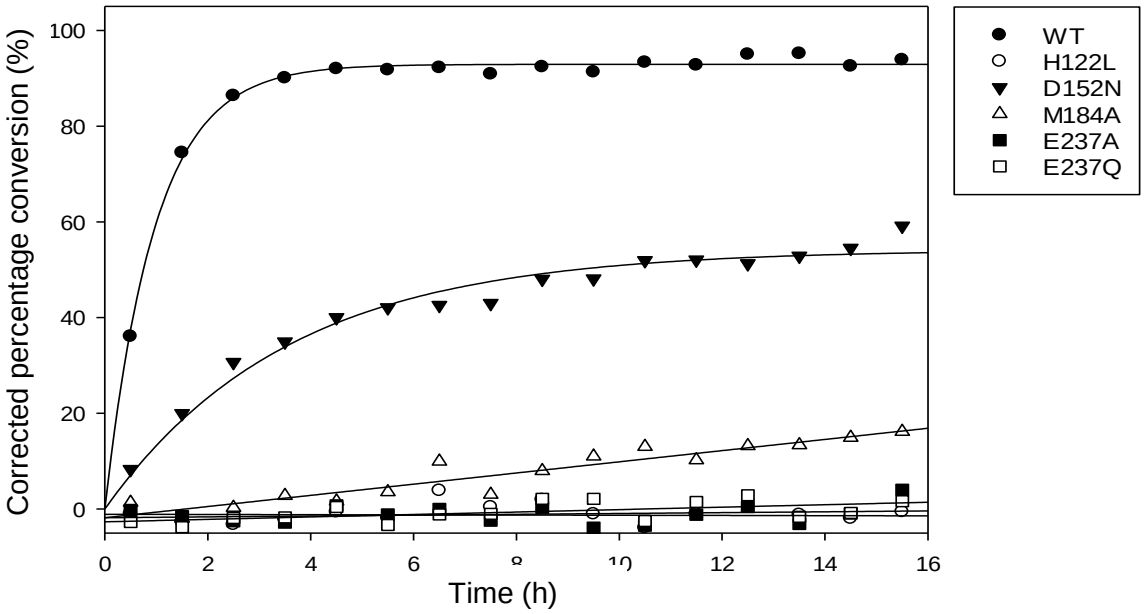

Figure 4.16: ^{1}H NMR time course of wild-type and mutants enzymes (final assay concentration 0.12 mg mL^{-1}; 2.55 µM) with (2*S*,3*S*)-3-fluoro-2-methyldecanoyl-CoA **147** (final assay concentration 100 µM) as substrate**.** The conversion at 30 °C was measured every hour.

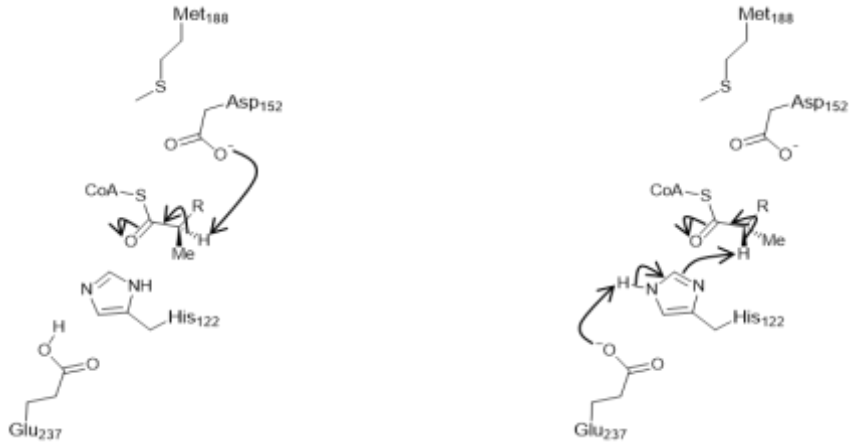

Figure 4.17: The proposed 'two-base' mechanism of human AMACR. The Asp-152 residue stabilised by Met-184 residue deprotonates the *R*-2-methylacyl-CoA ester as shown on the left panel, whilst the His-122/Glu-237 dyad deprotonates the *S*-2-methylacyl-CoA ester as shown on the right panel.

In order to ensure that the results were reproducible, experiments on wild-type AMACR, D152N and M184A mutants were repeated. The experiments using (2*R*,3*R*)-3-fluoro-2-methyldecanoyl-CoA **114** and (2*S*,3*S*)-3-fluoro-2-methyldecanoyl-CoA **147** were run in parallel in order to allow direct comparison of reaction rates. As the acquisition with ^{1}H NMR was alternating between the *R*- and *S*- substrate, the temperature was set at 20 °C for the reaction to occur at a constant temperature within and outside the NMR spectrometer (room temperature was *ca*. 20 °C). At 20 °C, wild-type AMACR took much longer (10 h instead of 4 h) for substrate conversion to go to near completion. Even though the overall rates were much lower for both wild-type and mutant enzymes at 20 °C, a consistent trend of conversion was observed (Figure 4.18). The M184A mutant was more active (24% conversion) than D152N mutant (3% conversion) when the *R*-substrate **114** was used. D152N mutant was more active (35% conversion) than the M184A mutant (4% conversion) when the *S*-substrate **147** was used. These results were consistent with the above observations and showed that human AMACR is unlikely to work by a ‘two-base’ mechanism. The results also showed that these two mutant enzymes did not have a gross structural disruption as they were active and showed opposite levels of conversion for substrates with different stereochemical configurations.

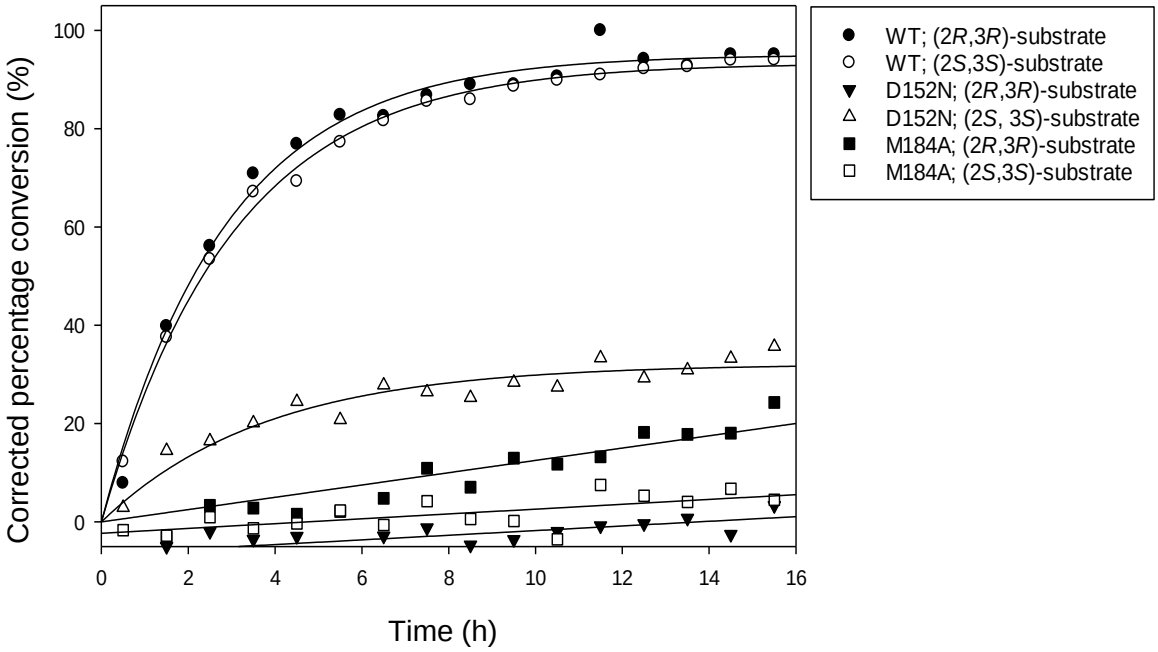

Figure 4.18: ^{1}H NMR time course of wild-type AMACR, D152N and M184A mutants (final assay concentration 0.12 mg mL^{-1}; 2.55 µM) with (2*R*,3*R*)-3-fluoro-2-methyldecanoyl-CoA **114** or (2*S*,3*S*)-3-fluoro-2-methyldecanoyl-CoA **147** as substrate (final assay concentration 100 µM)**.** The temperature was set at 20 °C and the acquisition by ^{1}H NMR was alternated between the *R*- and *S*- substrate for each mutant.

A subset of racemases catalyse their substrates by the deprotonation/reprotonation reaction and they usually operate *via* a 'two-base' or 'one-base' mechanism. For a 'two-base' mechanism, the proton is removed by a catalytic base and the intermediate is reprotonated by a catalytic residue from the opposite face, resulting in a product with the opposite stereochemical configuration from the substrate. Examples of 'two-base' racemases include alanine racemase,[232] glutamate racemase,[152, 233] mandelate racemase[208, 234] and proline racemase.[209, 235] As there are two catalytic bases involved in the racemisation reaction, the mutation of one of these two residues will inactivate the enzyme as a racemase. For example, Tanner *et al.* showed that mutation of the Cys-73 or Cys-184 residues of the glutamate racemase results in mutants with no detectable racemase activity.[152] These mutants were further tested to determine if they could perform an elimination reaction, where only one of the two catalytic bases is require for the elimination of HCl from the 3-

chloroglutamate substrate.[152] Each mutant was shown to be active against one of the two diasteromers of the substrate, indicating that each of the mutants have a specific requirement for a particular stereochemical configuration of substrate.[152] Their inability to racemise glutamate is because two catalytic bases are required for the racemisation reaction, a behaviour that fits a 'two-base' mechanism.[152] The results from our study are not consistent with a 'two-base' mechanism. The His-122 and Glu-237 mutants were not active when eliminating either the *R*- **114** or *S*-fluoro-methyldecanoyl-CoA **147** substrates, whilst the D152N mutant was active in eliminating both the *R*- and *S*- substrates.

For a 'two-base' mechanism, a separate catalytic base is responsible in reprotonating the deprotonated intermediate. If the reaction occurs in heavy water such as in $^{2}H_2O$, the deuterium will be incorporated into the product but little will be incorporated into the substrate. The chiral inversion will occur at the same time as the exchange of deuterium. This is not what happened in the 'racemisation' reaction performed by human AMACR. Darley *et al*. showed that the product of human AMACR is in nearly 1:1 racemic mixture and that deuterium is incorporated in both substrate and product, consistent with a 'one-base' mechanism.[1] The 'one-base' mechanism, as the name suggests, involves only a single catalytic base in deprotonating substrate and reprotonating the intermediate, and results in a product that is a near racemic mixture. Enzymes operating with a 'one-base' mechanism are relatively rare, examples include α-amino-ε-caprolactam racemase[210] and possibly acyl-CoA dehydrogenase.[236]

The observation by Darley *et al.*[1] supports the results from our site-directed mutagenesis study where mutants showed similar activities (or inactivity) towards both the *R*- and *S*-substrate. In the 'racemisation' assay, the D152N, H122L, E237A and E237Q mutants were all inactive towards both the 2*R*- and 2*S*- substrate. This is probably because after the first cycle of reaction, the catalytic bases are in an inappropriate protonation state. In the elimination assay, the mutants do not discriminate between *R*- or *S*- substrates. Their catalytic activities were significantly reduced but all showed ability in

eliminating both *R*- and *S*-substrates, suggesting that deprotonation can occur when the α-proton is either on the same side or opposite side of the catalytic residue. The ability to deprotonate the substrate with both configurations is consistent with a 'one-base' mechanism.

Even though the crystal structures of MCR, the homologous enzyme of human AMACR, have suggested that the enzyme works by a 'two-base' mechanism,[86, 108, 146] our study using site-directed mutagenesis showed that human AMACR is more likely to work by a 'one-base' mechanism. Human AMACR appears to be atypical, as it does have two catalytic bases, one on each side of the substrate, which is usually consistent with the mechanism of a 'two-base' enzyme. This observation may have contributed to the false assumption that human AMACR works by a 'two-base' mechanism. The phenomenon where AMACR has two catalytic bases but work as a 'one-base' mechanism can be explained by the existence of water molecules in the active site. Instead of the catalytic bases directly deprotonate the substrate and reprotonate the intermediate, water molecules act as the intermediaries, which are the actual bases to the substrate. It is a 'one-base' mechanism because the water molecule is the only base that deprotonates the substrate and reprotonates the enolate intermediate. The presence of a hydrogen-bonding network including water molecules allows deprotonation and reprotonation from opposite sides by one base.

The crystal structure of MCR has shown that there are two conserved water molecules in the active site which form a hydrogen-bonding network with multiple residues including side-chain of Asp127 and main chain of Leu-151, Leu-153, Val-154 and Gly-155 (Figure 4.19).[146] They may have a role in acting as the intermediaries in deprotonating and reprotonating the substrate, but this is unlikely as they are anchored to the enzyme residues (*via* hydrogen bonds) and are situated quite far from the substrate (Figure 4.19).[146] An other possible source of water molecules could be disordered waters from outside of the active site, *i.e*., the bulk solvent.[108] These water molecules may also form hydrogen bonds with the main-chain and side-chains of active-site residues,

been protonated and deprotonated by the catalytic bases and in turn reacting with the substrate from both faces.

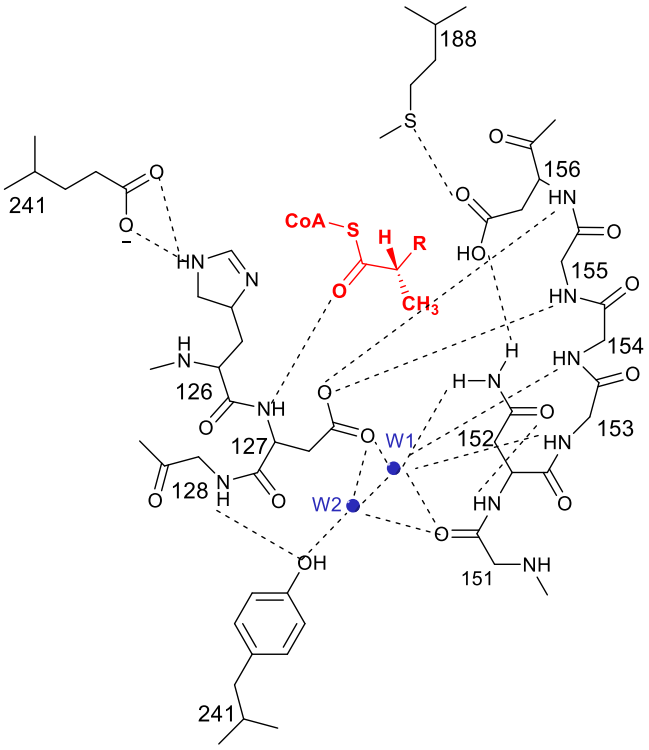

Figure 4.19: The active site of MCR according to the X-ray crystal structure.[146] The *S*-2-methylacyl-CoA substrate is highlighted in red and the two conserved water molecules (W1 and W2) are in blue. Hydrogen bonds are shown as dotted lines.

The site-directed mutagenesis on human AMACR changed the side-chains of the catalytic residues and hence affected electrostatic charges and hydrogen bonds between the residues and water molecules, which might disrupt the whole hydrogen-bonding network. This in turn affects proton transfer between catalytic residues and water molecules, and reduces the ability of water molecules to deprotonate the substrate and reprotonate the enolate intermediate. Similar observations have also been reported in other enzymes, catalysing proton transfer reactions, such as carbonic anhydrase II.[237-239] When His-64 residue is mutated to alanine in carbonic anhydrase II, the hydrogen-bonding network is disrupted and the proton transfer is affected, hence the enzymes loses much of its catalytic function.[237, 238]

4.6 The study of wild-type and mutant enzymes using the multi-well colorimetric assay

The kinetic study using the fluoride elimination assay was not conducted as the levels of enzyme activity of mutants were low. ^{1}H NMR would not be very sensitive in detecting activity at low substrate concentrations and it would be too laborious to measure enzyme activity at a range of substrate concentrations for each mutant. Hence, the multi-well colorimetric assay (*vide supra*) using 3-(2,4-dinitrophenoxy)-2-methylpropanoyl-CoA **135** as the substrate was used to measure the kinetic parameters of mutant enzymes as it is more sensitive and allows continuous monitoring of the reaction.

In order to study the ability of mutant enzymes in eliminating the substrate, and to confirm that AMACR works by a 'one-base' mechanism, substrates ideally have to be tested in *R*- and *S*- configurations instead of a racemic mixture. The substrate, 3-(2,4-dinitrophenoxy)-2-methylpropanoyl-CoA **135**, synthesised by Dr Maksims Yevglevskis is a 1:1 mixture of 2-methyl epimers.[197] Chiral resolutions were attempted in order to resolve the substrate **135** for use in the enzyme assay.

4.6.1 Attempts to resolve 3-(2,4-dinitrophenoxy)-2-methylpropanoyl-CoA

The racemic substrate **135** was first synthesised by Dr Maksims Yevglevskis using the route described in Scheme 4.5.[197] The reaction between 1-fluoro-2,4-dinitrobenzene **149** and a diol produced alcohol **150**. The alcohol **150** was oxidised to the corresponding carboxylic acid **151** using Jones oxidation.[240] The acid **151** was activated using carbonyldiimidazole **71** and coupled with CoA-Li_3 to form the racemic acyl-CoA ester **135**.

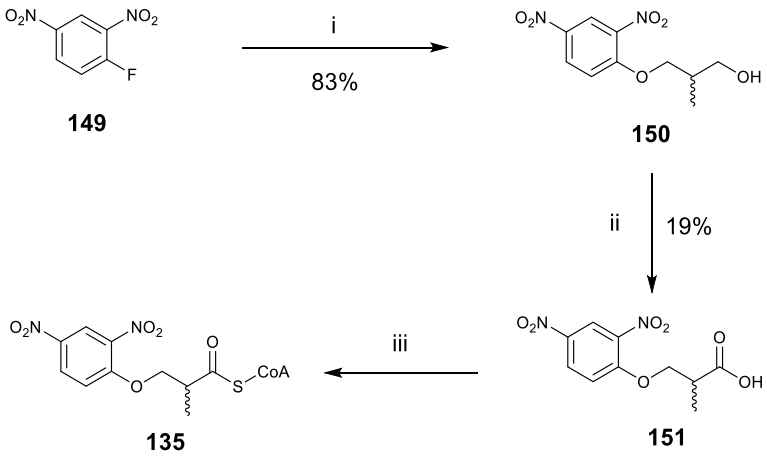

Scheme 4.5: Synthesis of the racemic substrate **135** as described by Dr Maksims Yevglevskis.[197] Reagents and conditions: i) Na metal, 2-methyl-1,3-propanediol, rt, 6 h; 80 °C, 2 h; then rt overnight; ii) H_2O, H_2SO_4, CrO_3, acetone, 0 °C, overnight; iii) DCM, CDI, rt, 1 h, then THF, 0.1 M $NaHCO_{3\ aq.}$, CoA-Li_3, rt, 18 h.

To obtain a single enantiomer, a chiral reagent was investigated to resolve the alcohol **150**. The same route using 1-fluoro-2,4-dinitrobenzene **149** and 2-methyl-1,3-propanediol was used to synthesise the alcohol **150** (Scheme 4.5). The alcohol **150** was reacted with a chiral acid, *S*-2-acetoxy-2-phenylacetic acid **152** to produce diastereomers (**153** and **154**) which could potentially be separated (Scheme 4.6). This commercially available chiral auxillary **152** has previously been used in the esterification of racemic alcohols to produce diastereomers that could be separated by chromatography.[241, 242] Unfortunately, in our case, the diastereomers produced failed to separate using traditional column chromatography, automated chromatography (Teledyne Isco CombiFlash Rf) and HPLC (possibly due to the use of an unsuitable type of HPLC column).

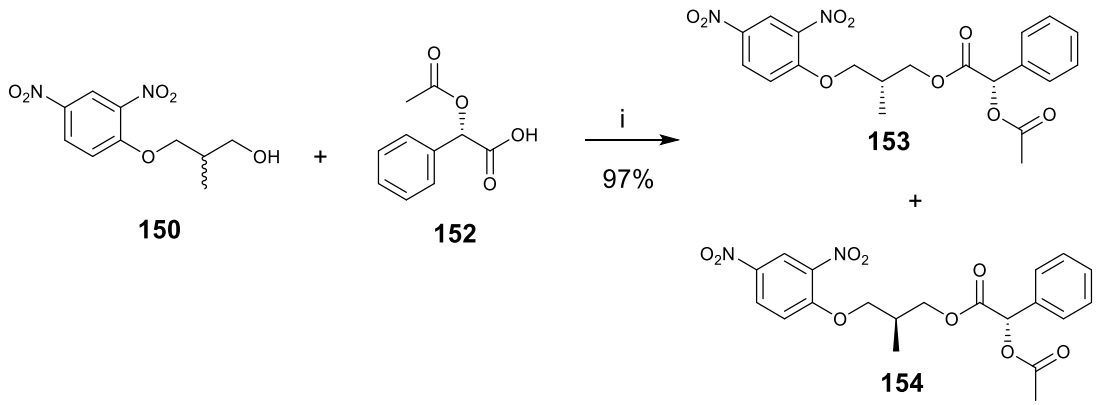

Scheme 4.6: Attempted resolution of alcohol **150** using a chiral acid **152**. Reagents and conditions: i) DCC, DMAP, DCM, rt, 18 h.

Another chiral resolving agent, (1*S*)-10-camphorsulfonyl chloride **155** was therefore coupled to the racemic alcohol **150** to produce diastereomers (Scheme 4.7). It encountered the same problem as the chiral acid **152**, the diastereomeric products could not be separated.

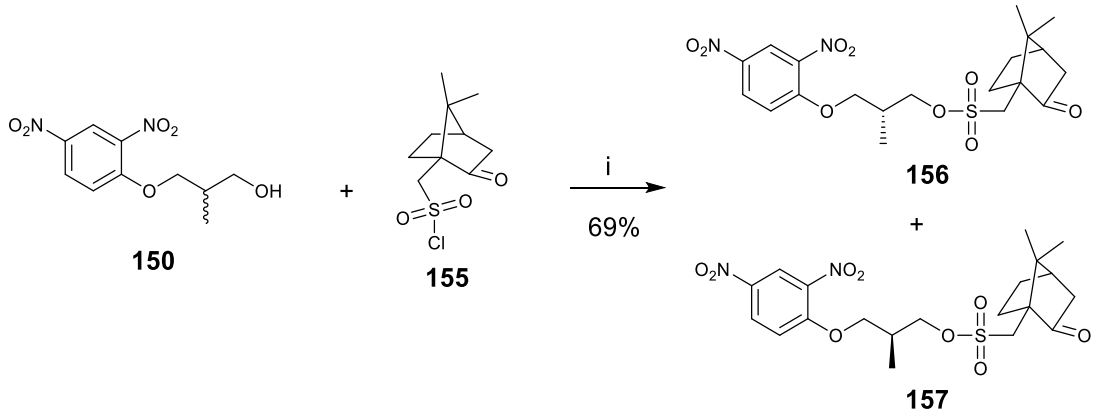

Scheme 4.7: Attempted resolution of alcohol **150** using (1*S*)-10-camphorsulfonyl chloride **155**. Reagents and conditions: i) pyridine, -5 °C then 0 °C, 2 h.

The third chiral resolving agent to be investigated was an Evans' chiral auxillary **158**. The alcohol **150** was first substituted with bromine to give a brominated product **159** before it was coupled with the Evans' auxillary **158** (Scheme 4.8). However, the coupling failed and no desired products (**160** and **161**) were formed.

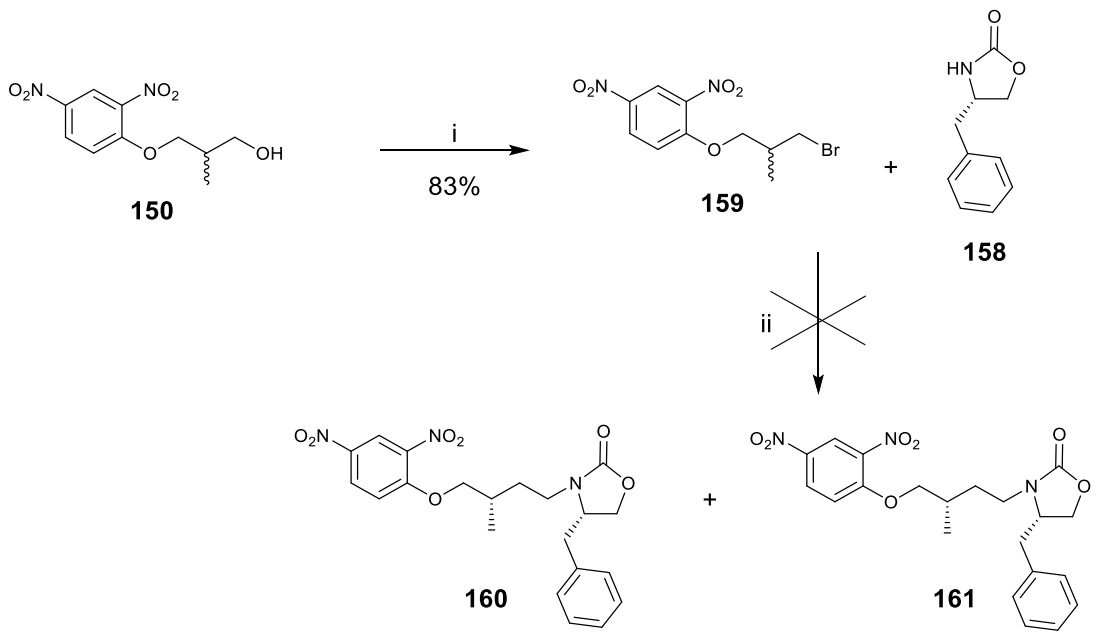

Scheme 4.8: Attempted resolution of alcohol **150** using an Evans' chiral auxillary **158**. Reagents and conditions: i) CBr_4, PPh_3, DCM, 1.5 h; ii) NaH, DMF, rt, 18 h.

Attempts to resolve the racemic substrate **135** were therefore unsuccessful either due to the failure to produce the required diastereomers or failure to separate them. Instead of resolving the compound, an enantioselective synthesis was attempted using an enantiomerically pure starting material.

4.6.2 Attempted enantioselective synthesis

A chiral alcohol **162** was chosen as the starting material for the enantioselective synthesis (Scheme 4.9). The OH group of methyl *S*-3-hydroxy-2-methylpropanoate **162** was protected with a *tert*-butyldiphenylsilyl-group. The methyl ester **163** was reduced to alcohol **164**. The reduction was first attempted with $LiAlH_4$, but the reducing agent was too strong and removed the silyl protecting group. DIBAL was then used as the reducing agent to produce a reduced OH group with an intact silyl-protecting group at its opposite end **164**. Sequential protection and deprotection of the OH groups at two ends of the molecule should allow the chirality of the methyl group to be maintained. The reduced alcohol **164** was reacted with 1-chloro-2,4-dinitrobenzene to introduce a dinitrophenol group into the compound **165**. The silyl-protected alcohol at the opposite end was then deprotected. The deprotected alcohol **166** was oxidised to the carboxylic acid **167** which could

be coupled with CoA-Li_3 to form the *S*-acyl-CoA ester **168**. Unfortunately, the chirality was unexpectedly lost during the synthesis. Compounds were optically active until the deprotected alcohol **166** was produced, which had zero optical rotation. The removal of silyl-protecting group is unlikely to remove the chirality of the compound. It is unknown if the chirality had been lost in earlier steps. The measured optical rotations have been low for compounds from earlier steps, where protected alcohol **164** has $[\alpha]_D^{20}$ value of +8.7 (*c* 1.50 in $CHCl_3$) [lit. $[\alpha]_D^{20}$ +6.1 (*c* 0.93 in $CHCl_3$)][243] and the dinitrophenol compound **165** has $[\alpha]_D^{21}$ value of +11.9 (*c* 1.09 in $CHCl_3$). Such low optical rotation values are susceptible to experimental errors. These compounds might have lost their chirality but were unnoticed until later steps.

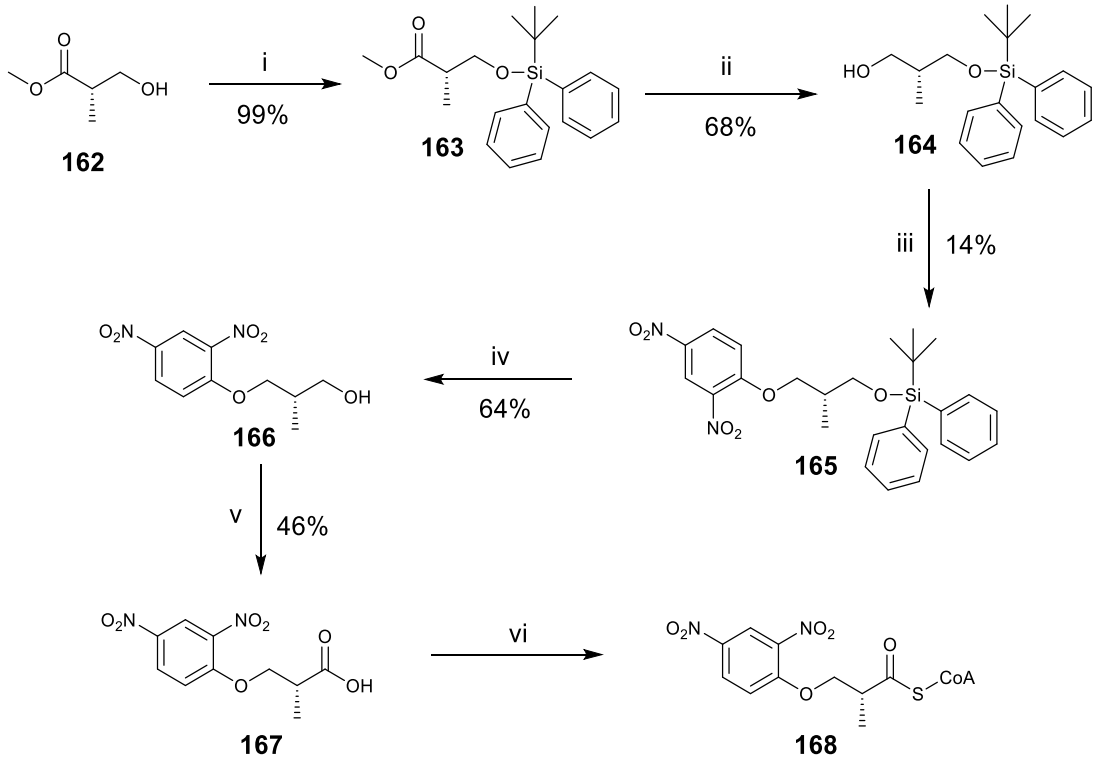

Scheme 4.9: Attempted enantioselective synthesis of *S*-acyl-CoA ester **168**. Reagents and conditions: i) TBDPSCl, imidazole, DCM, 0 °C then 20 °C, 2.5 h; ii) DIBAL, DCM, 0 °C, 3 h, then Rochelle's salt, rt, 18 h; iii) NaH, 1-chloro-2,4-dinitrobenzene, DMF, 60 °C, 2 days; iv) TBAF, THF, rt, 18 h; v) CrO_3, H_2SO_4, acetone, 0 °C, 1.5 h, then rt, 2 h.

The same synthetic route was used to produce the *R*-acyl-CoA ester **169**, starting from *R*-3-hydroxy-2-methylpropanoate **170** (Scheme 4.10). The same problem of losing chirality was encountered. This time, the dinitrophenol

compound **173** was shown to be optically inactive, confirming the possibility that chirality could have been lost during the earlier steps in the synthesis.

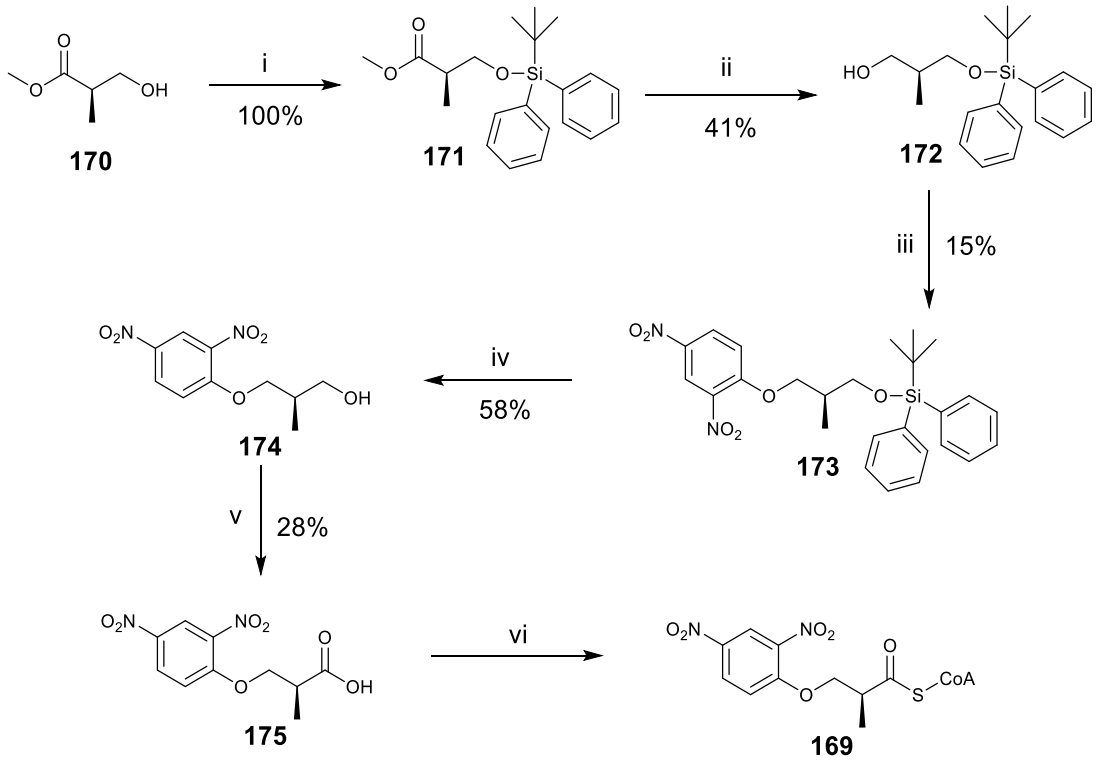

Scheme 4.10: Attempted enantioselective synthesis of *R*-acyl-CoA ester **169**. Reagents and conditions: i) TBDPSCl, imidazole, DCM, 0 °C then 20 °C, 2.5 h; ii) DIBAL, DCM, 0 °C, 4 h, then Rochelle's salt, rt, 18 h; iii) NaH, 1-chloro-2,4-dinitrobenzene, DMF, 60 °C, 1 day, then 50 °C, 2 days; iv) TBAF, THF, rt, 18 h; v) CrO_3, H_2SO_4, acetone, 0 °C, 1.5 h, then rt, 2 h.

To confirm that the acids (**167** and **175**) were indeed racemic mixture, they were derivatised with a chiral amine. The derivatisation method was reported by Darley *et al.* who coupled the *R*- **176** and *S*- 2-methyldecanoic acid **177** with *S*-1-phenylethylamine **178** to form diastereomers (Scheme 4.11) and their chemical shifts were analysed with the ^{1}H NMR.[1] The 2-methyl peak of the *R*-derivative **179** has chemical shift of 1.11 ppm and the 2-methyl peak of *S*-derivative **180** has a chemical shift of 1.13 ppm.[1] The work was repeated and the (1*S*,2*R*)- **179** and (1*S*,2*S*)- **180** diastereomers were shown to have consistently different chemical shifts on ^{1}H NMR (Figure 4.20). The derivatisation of an acid using a chiral amine is a useful method to distinguish

whether the acid is a single enantiomer and its enantiomeric excess or whether it is a racemic mixture.

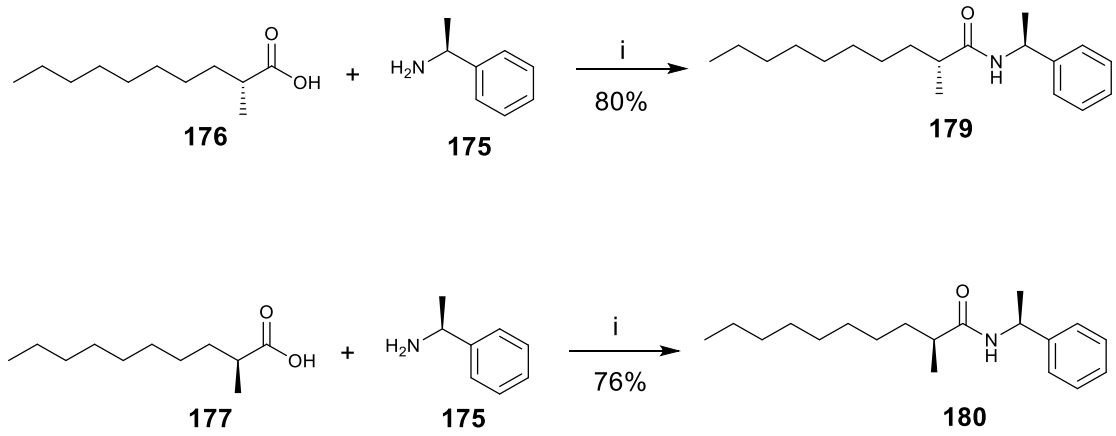

Scheme 4.11: Derivatisation of *R*- **176** and *S*- 2-methyldecanoic acid **177** with a chiral amine. Reagents and conditions: i) oxalyl chloride, DCM, DMF, rt, 45 min.

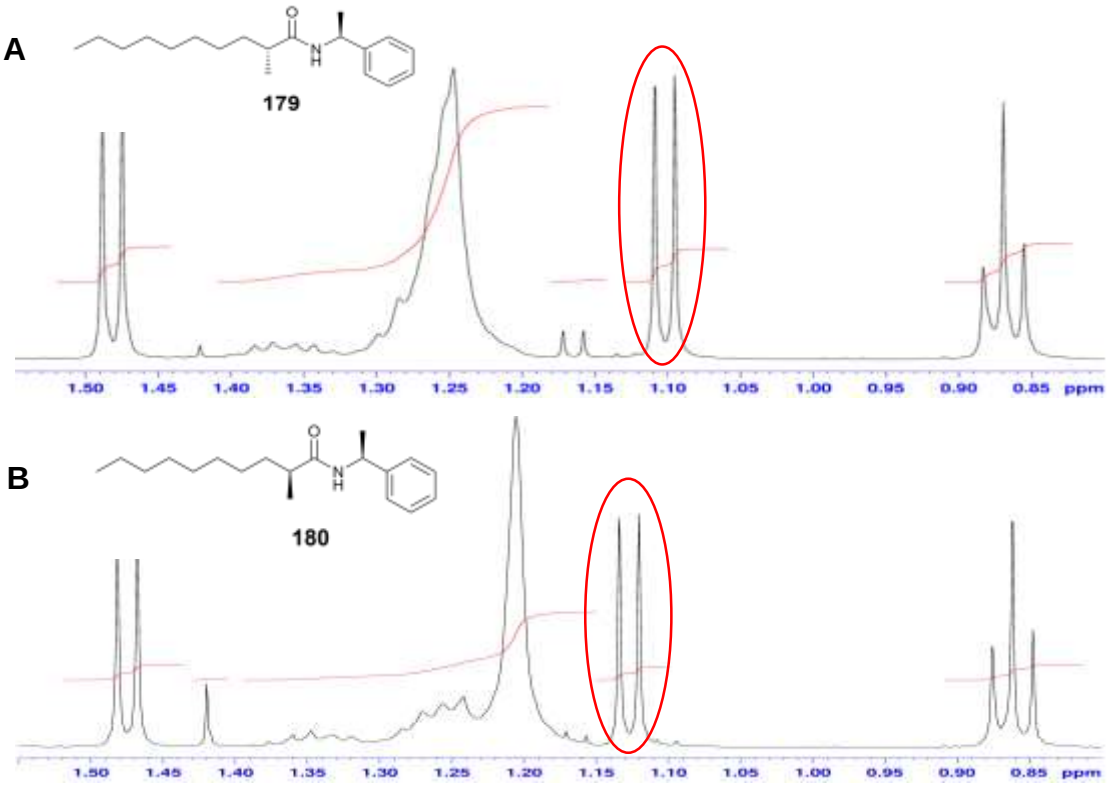

Figure 4.20: ^{1}H NMR of (2*R*)-2-methyl-*N*-[(1*S*)-1-phenylethyl]decanamide **179** (Panel A) and (2*S*)-2-methyl-*N*-[(1*S*)-1-phenylethyl]decanamide **180** (Panel B) resulted from the derivatisation with a chiral amine. The 2-methyl peaks (highlighted in red) show different chemical shifts, where the (1*S*,2*R*)-product **179** is at 1.10 ppm and (1*S*,2*S*)-product **180** is at 1.13 ppm.

Acids (**167** and **175**) resulted from the enantioselective synthesis (*vide supra*) were derivatised with chiral amine **178** using the same procedure described by Darley *et al*.[1] (Scheme 4.12). Both acid derivatives showed the same chemical shifts on ^{1}H NMR (Figure 4.21). This confirmed that both acids have indeed been racemised during the synthesis.

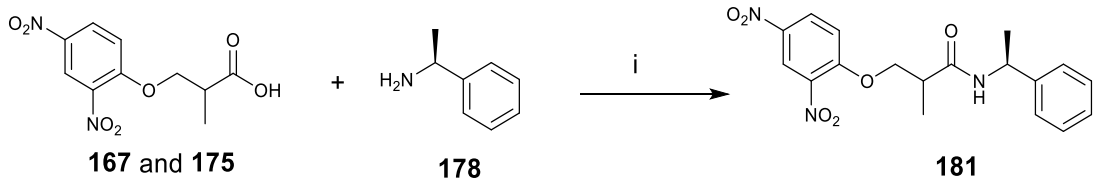

167 and **175** **178** **181**

Scheme 4.12: Derivatisation of acids (with an unknown stereochemical configuration) with a chiral amine. Reagents and conditions: i) oxalyl chloride, DCM, DMF, rt, 45 min.

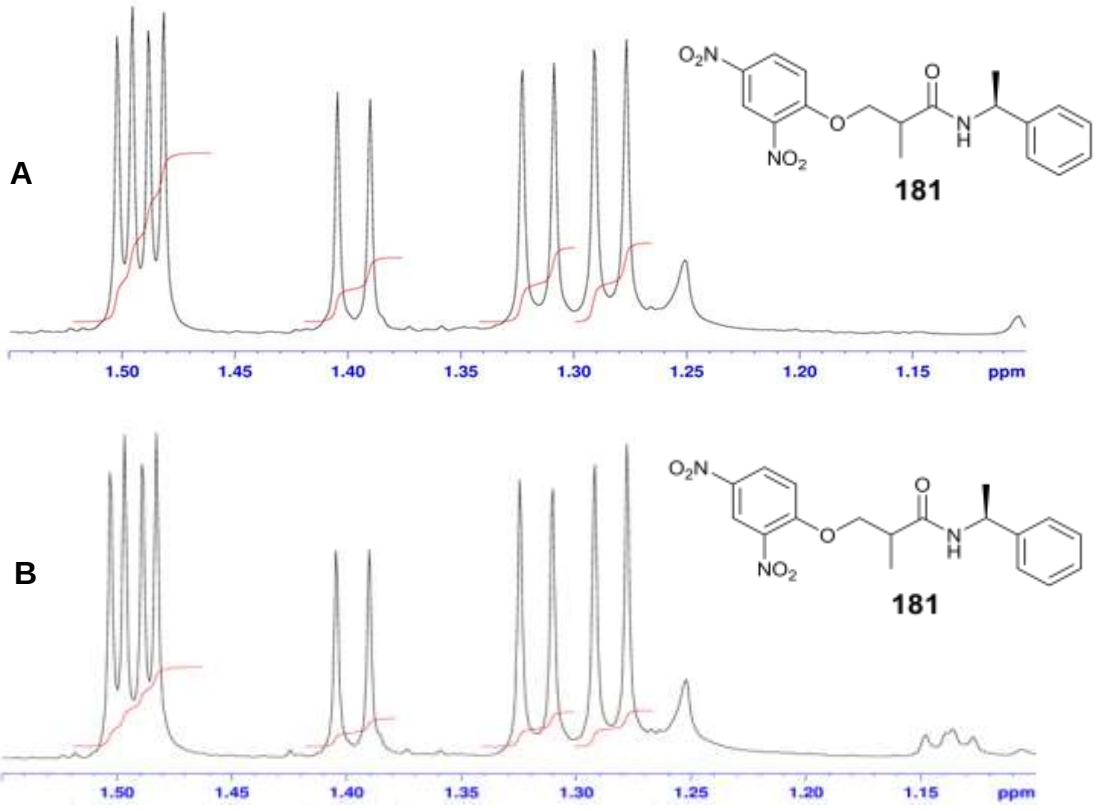

Figure 4.21: ^{1}H NMR of 3-(2,4-dinitrophenoxy)-2-methyl-*N*-[(1*S*)-1-phenylethyl]propanamide **181**, the derivative of acids **167** (Panel A) and **175** (Panel B). The products have same chemical shifts, confirming that both of the acids are racemic mixture.

4.6.3 Assay using racemic 3-(2,4-dinitrophenoxy)-2-methylpropanoyl-CoA as substrate

Due to the failure to produce the *R*- and *S*- enantiomers, racemic 3-(2,4-dinitrophenoxy)-2-methylpropanoyl-CoA **135** substrate was used to assay the activity of wild-type and mutant AMACR enzymes. The enzymes were tested with a time-course assay over 10 h in order to understand their activities in eliminating the 2,4-dinitrophenolate **137** from 3-(2,4-dinitrophenoxy)-2-methylpropanoyl-CoA **135** substrate (Figure 4.22). As expected, the wild-type enzyme was the most active of all enzymes. Surprisingly, the E237Q mutant showed high activity, achieving half of the absorbance of wild-type AMACR after 10 h of reaction time. Previous assays based on deuterium wash-in and fluoride elimination showed that E237Q mutant was almost inactive, showing barely any activity. This result showed that the mutants were not dead, but that they have different activities with different substrates. On the other hand, the M184A mutant showed very low activity in this assay, which is very different from its behaviour in deuterium wash-in assay and fluoride elimination assay where the M184A mutant had much higher activity compared to most of the other mutants.

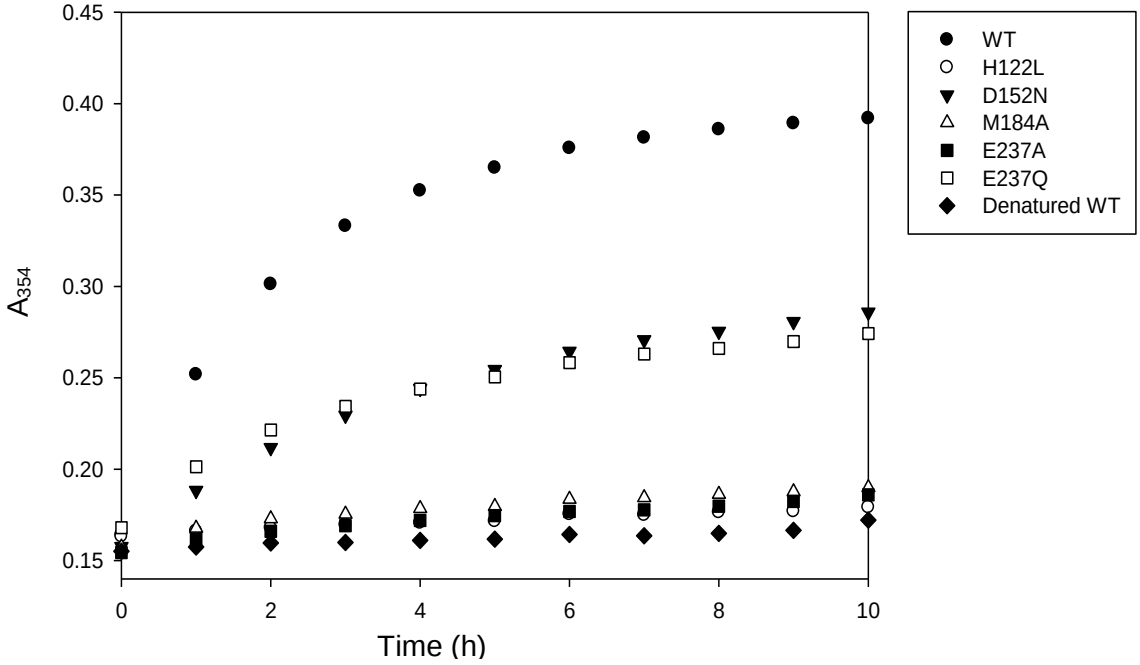

Figure 4.22: Time-course multi-well colorimetric assays of wild-type and mutant enzymes over 10 h.

4.6.4 Kinetic studies on wild-type and mutants enzymes using multi-well colorimetric assay

As the eliminated product of 3-(2,4-dinitrophenoxy)-2-methylpropanoyl-CoA **135** substrate absorbs in the UV range, its absorbance can be measured using a multi-well format. This convenient, high-throughput assay allows the kinetic parameters of wild-type and mutant enzymes to be easily measured. Wild-type and mutant enzymes were titrated to determine the appropriate concentrations to use in order to measure their initial reaction rate. Once the final concentrations of the enzyme were determined, the substrate **135** at a range of concentrations were used to determine the K_m, V_{max} and k_{cat} values (Table 4.3). However, the Direct Linear Plots of mutant enzymes do not converge and the data fits poorly to the Michaelis-Menten model (Appendix 6-10). Hence, it is rather difficult to interpret the data accurately and to draw a conclusion based on the kinetic parameters obtained.

Enzyme	K_m (μM)	V_{max} (nmol min^{-1} mg^{-1})	k_{cat} (s^{-1})	k_{cat}/K_m (M^{-1} s^{-1})
Wild-type	27	274	0.2150	7963
H122L	1.3	1.5	0.0012	923
D152N	6.8	1.9	0.0015	221
M184A	1.3	0.3	0.0002	154
E237A	0.2	1.8	0.0014	7000
E237Q	2.0	2.7	0.0021	1050

Table 4.3: The kinetic parameters of wild-type and mutant AMACR enzymes obtained from Direct Linear Plots.

The 3-(2,4-dinitrophenoxy)-2-methylpropanoyl-CoA **135** substrate used in the kinetic analysis was racemic and this might be the reason for the poor fitting of data in the Michaelis-Menten model. Since the substrate was racemic, the result obtained could not be used to deduce if AMACR operates with a 'one-base' or 'two-base' mechanism. Nevertheless, the result was rather interesting as it showed that the same mutant enzyme has very different levels of activity with two different substrates even though wild-type AMACR has been shown to be able to eliminate both of them with similar efficiencies. The K_m values of wild-type AMACR with (2*R*,3*R*)-3-fluoro-2-methyldecanoyl-CoA **114** and 3-

(2,4-dinitrophenoxy)-2-methylpropanoyl-CoA **135** were similar, 21 μM[3] and 58 μM, respectively. The V_{max} values were not very different either, 96.5 nmol min^{-1} mg^{-1} for (2*R*,3*R*)-3-fluoro-2-methyldecanoyl-CoA **114**[3] and 274 nmol min^{-1} mg^{-1} for 3-(2,4-dinitrophenoxy)-2-methylpropanoyl-CoA **135**. On the other hand, the trends were different for mutant enzymes. The fluoride elimination assay has shown that D152N and M184A mutants were the most active mutant enzymes compared to the H122L, E237A and E237Q mutants, which were almost inactive (*vide supra*). However, the multi-well colorimetric assay based on the elimination of 3-(2,4-dinitrophenoxy)-2-methylpropanoyl-CoA **135** showed that the D152N and E237Q mutants were the most active mutant enzymes whilst the activity for the M184A mutant was very low (Figure 4.22). The results suggest that the low activity of the mutant enzymes is not due to them been denatured. Their lack of activity in some of the assays was due to the mutation of a specific residue. The difference in the activity of mutants might be explained by the size of the leaving group of the substrates. 3-Fluoro-2-methyldecanoyl-CoA is a substrate with long alkyl chain and a fluorine leaving group whilst 3-(2,4-dinitrophenoxy)-2-methylpropanoyl-CoA **135** does not have a long alkyl chain but has an aromatic dinitrophenol leaving group. The dinitrophenol group is a much larger group than fluorine, and the side-chains might bind in different conformations to different mutants as their catalytic residues have been mutated. As Met-184 residue is important in stabilising the enolate intermediate in the oxyanion pocket, different types of leaving group could have a profound effect in the ability of the M184A mutant enzyme to stabilise the enolate intermediate. M184A mutant might still stabilise the intermediate of (2*R*,3*R*)-3-fluoro-2-methyldecanoyl-CoA **114** to a greater extent whilst the intermediate produced from 3-(2,4-dinitrophenoxy)-2-methylpropanoyl-CoA **135** is stabilised to a lesser extent.

5 Conclusions and future work

A range of novel compounds have been designed based on the structure of fenoprofenoyl-CoA **13**. Transition-state mimics (structures with an electron-withdrawing group at the β-position) and substrate mimics (structures with an electron-donating group at the β-position) were produced. There is no statistically difference in the potency of inhibition of the transition-state mimics and substrate mimics. The IC_{50} and K_i values are not hugely different when the structures have an electron-donating oxygen group or an electron-withdrawing sulfide (or sulfone) group next to the 2-methyl group. The same trend occurs in side-chains with *meta*- and *para*- substituents, no statistically difference in their potency is observed. However, aromatic side-chains tend to have lower IC_{50} and K_i values compared to alkyl side-chains, possibly due to π-interactions from aromatic rings. The 2-methyl group was designed to have a *R*- or *S*- stereochemical configuration and the results showed that they act as competitive inhibitors with similar potency.

The results showed that the methionine-rich hydrophobic surface of AMACR can accept a wide spectrum of side-chains. Minimal changes on the side-chains (such as changing the orientation of the substituents or the substitution of a single group) do not bring in a huge difference in the potency of a compound when inhibiting AMACR. The results also showed that the 2-methyl group and the acyl-CoA moiety are important for the binding with AMACR. Compounds designed by Professor Paul Groundwater do not have these two moieties and they were shown to be very poor AMACR inhibitors (almost no inhibition was observed). This research confirmed that to be a good AMACR inhibitor, the compound needs to have a 2-methyl group, an acyl-CoA moiety and a hydrophobic side-chain, ideally aromatic groups. As the enzyme can tolerate a huge change in the side-chain of the compound, future designs need to be less conservative in order to bring a large change in IC_{50} and K_i values. This research acts as a starting point for the SAR study of side-chains of AMACR inhibitors but a larger range of compounds will be need to be designed and evaluated in the future in order to fully explore the SAR. A potent AMACR

inhibitor will act as a lead for producing a drug that can inhibit AMACR which is an important treatment strategy for castrate-resistant prostate cancer.

It has been difficult to produce a convenient assay to measure the potency of AMACR inhibitors due to the fact that the enzyme is a racemase. The fluoride elimination reaction has been shown as a viable method for measuring the potency of AMACR inhibitors. The potency of an inhibitor corresponds to the reduction in the conversion of (2*R*,3*R*)-3-fluoro-2-methyldecanoyl-CoA **114** substrate to an unsaturated product **117** and fluoride anion **118**, measured using ^{1}H and ^{19}F NMR. However, it has been difficult to turn the fluoride elimination assay into a high-throughput method. Several fluoride sensors have been trialled to detect the fluoride anion in order to develop the assay so that product can be quantified fluorescently. The *tert*-butyldimethylsilyl-protected fluorescein **128** and the boronate-based fluorescent sensor **131** were attempted to react with fluoride anions to produce a fluorescent read-out. However, these attempts resulted in readings that were poorly reproducible, possibly due to the contamination of fluoride from external sources or the high levels of hydration experienced by fluoride in an aqueous environment. Nevertheless, the fluoride elimination assay based on ^{1}H and ^{19}F NMR is a proof of concept that the reaction can be used to measure the potency of AMACR inhibitors. A different type of sensor may be needed to turn the reaction into a high-throughput assay.

On the other hand, the multi-well colorimetric assay using the 3-(2,4-dinitrophenoxy)-2-methylpropanoyl-CoA **135** was a success. This is the very first high-throughput AMACR assay that does not require complicated sample preparation. It allows the screening of multiple inhibitors in a plate. The assay takes much less than half an hour to perform and this includes the time needed for pre-incubation of inhibitors with enzyme. Compared to the laborious ^{1}H NMR study that scans a single sample at a time and manages to investigate just a few samples in a day, this assay potentially allows the screening of hundreds of compounds in a day. With this assay, a large compound library could be screened in order to look for potent AMACR inhibitors that could be used as treatment for castrate-resistant prostate cancer. Following this research, the MDL group has started the screening of libraries of small, drug-

like molecules obtained from the MRC Technology and several hits have been found. The assay can also be used to screen in-house libraries of pharmaceutical companies and our research group can collaborate with these companies to turn hits into drugs targeting AMACR. Further research should be able to turn the multi-well colorimetric assay into a fluorescent assay, which is more sensitive and will be useful to screen drugs with much higher potency.

The site-directed mutagenesis study is the first extensive study on human AMACR which investigates the role of various residues reported to-date. There have been several studies on MCR, the homologous enzyme of human AMACR, including the X-ray crystal structure[108, 153] and site-directed mutagenesis studies.[86] However, there have been a limited number of studies on human AMACR, possibly due to the inherent difficulties in producing and handling the enzyme. In this research, a lot of protocol optimisations have been carried out in order to mutate and express the mutant human AMACR enzymes. This study has established optimal protocols for the production of mutant AMACR enzymes and these protocols will be useful when mutating other residues of human AMACR in the future.

This research showed that His-122, Asp-152, Met-184 and Glu-237 are important residues for the catalytic function of human AMACR. By mutating these residues, the activity of the enzyme decreased in both terms of 'racemisation' and elimination of its substrate. This study also showed that human AMACR is unlikely to work by a 'two-base' mechanism. This discovery is very significant as it had always been assumed that as the enzyme has two catalytic bases at two different sites it works by a 'two-base' mechanism. However, human AMACR has been shown to be an atypical enzyme that has catalytic centres at two sides of the substrate but operates with a 'one-base' mechanism (Scheme 5.1). It is likely that water molecules, possibly the disordered water molecules found within the active site, act as intermediaries in transferring protons within hydrogen-bonding networks. Besides providing insight into the mechanism of human AMACR, the results also inform the importance of these hydrogen-bonding networks. The knowledge obtained from this research is useful in the future design of AMACR inhibitors to be used

as drugs. Designing compounds that can interfere with hydrogen-bonding networks within the active site may be a new approach in inhibiting this enzyme.

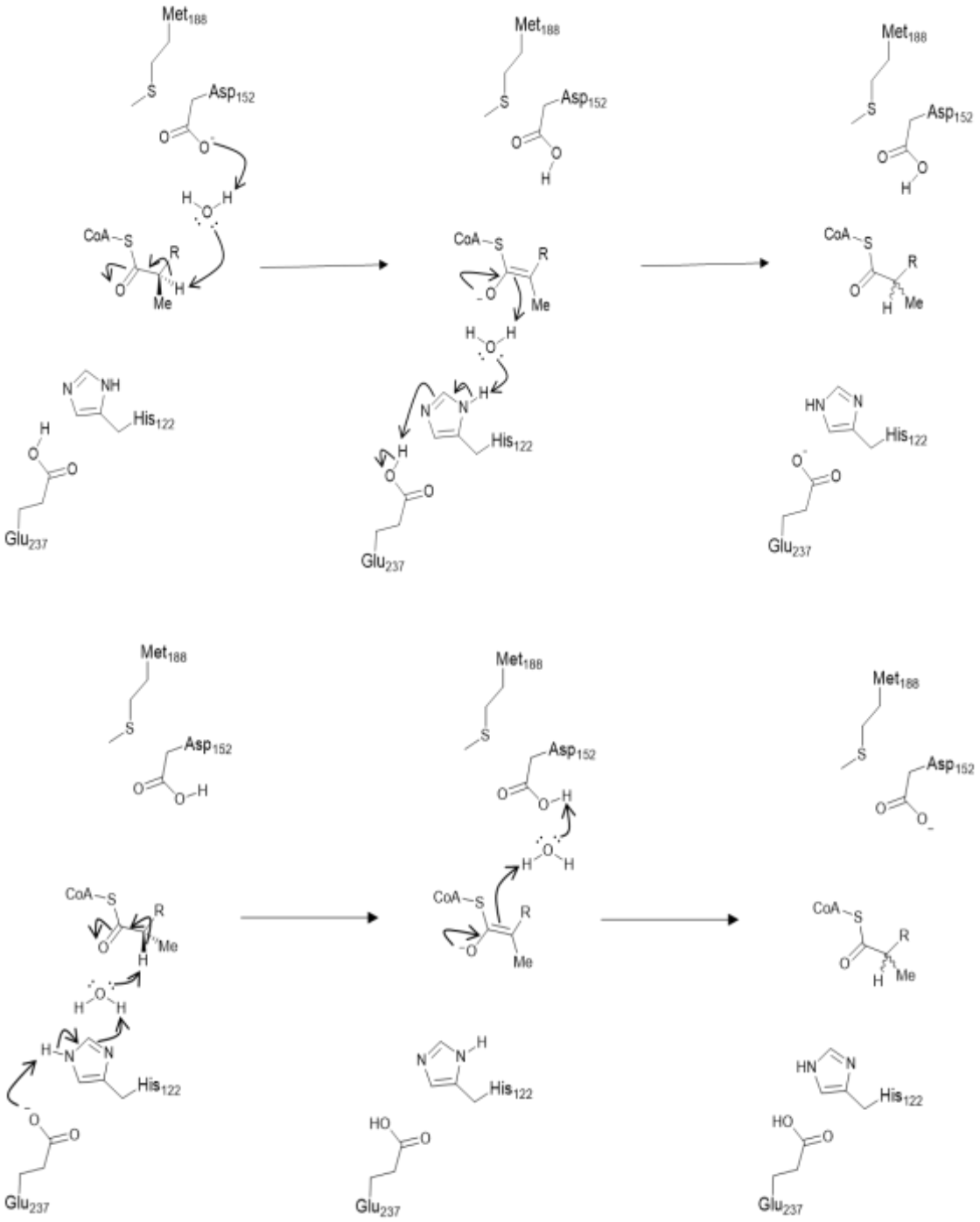

Scheme 5.1: The 'one-base' mechanism of human AMACR where water molecules act as intermediaries in transferring protons within the active site. The top panel shows the 'racemisation' of *R*-2-methylacyl-CoA ester and the bottom panel shows the 'racemisation' of S-2-methylacyl-CoA ester.

The next step will involve the use of molecular modelling to visualise water molecules and hydrogen-bonding networks, which will supplement the data from this research. In addition, there should be further attempts to synthesise enantiomerically pure *R*- and S- 3-(2,4-dinitrophenoxy)-2-methylpropanoyl-CoA substrate in order to better characterise mutant AMACR enzymes and to understand the role of each of the catalytic residues in the mechanism of the reaction.

6 Experimental

6.1 General (inhibitor syntheses and assays)

Chemicals were sourced from the Sigma-Aldrich Chemical Co. or Fisher Scientific Ltd. and were used without further purification unless otherwise stated. Coenzyme A, trilithium salt was purchased from Calbiochem, oxazolidinone chiral auxiliaries were purchased from Fluorochem and deuterated solvents were obtained from Goss Scientific. (2*S*,3*R*)-3-Fluoro-2-methyldecanoic acid,[3, 183] fluorescent ligand **134**, racemic 3-(2,4-dinitrophenoxy)-2-methylpropanoyl-CoA **135** were provided by Dr Maksims Yevglevskis from the MDL lab. 3-(Hexylsulfanyl)-2-methylpropanoic acid **107** and 3-(hexylsulfonyl)-2-methylpropanoic acid **108** were obtained from Dr Daniel Darley from the MDL lab. The boronate-based fluorescence sensor **131** was obtained from Dr Xiaolong Sun from the group of Professor Tony James, Department of Chemistry, University of Bath.[192] Small molecules identified by structure-based design were sent by Professor Paul Groundwater from the Faculty of Pharmacy, University of Sydney, Australia. Argon gas was used for reactions requiring anhydrous conditions. Organic solvents were removed using a Stuart RE300 rotary evaporator at 40 °C [except for acyl-CoA esters where a water bath at ambient room temperature (*ca*. 20 °C) was used]. All IR spectra were obtained on a Perkin-Elmer Spectrum RXI FT-IR spectrometer using KBr or NaCl discs and are reported in cm^{-1}. All mass spectra were obtained on a Bruker micrOTOF™ ESI-TOF mass spectrometer (Bruker Daltonics, Bremen). All NMR spectra were obtained on Bruker Avance III spectrometers. Chemical shifts are reported in parts per million (ppm) referenced to residual solvent ($CDCl_3$, ^2H_2O or DMSO-d_6). Assignments of spectra were confirmed using COSY, NOESY, HSQC and HMBC data. Coupling constants (*J*) are reported in Hertz (Hz) to a single decimal place. Multiplicities are abbreviated as: s (singlet), br s (broad singlet), d (doublet), dd (doublet of doublets), dt (doublet of triplets), t (triplet), td (triplet of doublets), tt (triplet of triplets), q (quartet), qd (quartet of doublets) and m (multiplet). Optical rotations were obtained using an Optical Activity Ltd. AA-10 polarimeter with a 5 mL cell of 1 dm path length. Values of $[\alpha]_D$ are given in 10^{-1} deg cm^2 g^{-1} and concentrations are reported in 0.01 g cm^{-3}. Melting points

(uncorrected) were determined using a Reichert-Jung heated-stage microscope. Thin-layer chromatography was performed on Merck aluminium-backed silica plates (silica gel 60 F_{254}) and visualised using UV light (λ = 254 nm), phosphomolybdic acid, iodine or potassium permanganate. Column chromatography was carried out on Fisher silica gel (35-70 µm) unless otherwise stated. Fluorescent spectra were obtained using a Perkin-Elmer Luminescence LS 50B Spectrometer. Fluorescence intensity and absorbance detections were performed using a FLUOstar Omega plate reader (BMG Labtech). Purification of acyl-CoA esters was carried out using solid-phase extraction cartridges (Oasis HLB, 6cc, Water Corporation). The acyl-CoA esters were eluted from the cartridges with water, and 10%, 20%, 40% and 50% (v/v) acetonitrile in water. For enzyme assays, all acyl-CoA ester stock solutions were vortex-mixed for 5 min before being diluted to their desired concentrations. The diluted solutions have to vortex-mixed for 2 min before being added to the enzyme. Solutions for enzyme assays were prepared using water from a Nanopure Diamond system and was of 18.2 Mega-$\Omega.cm^{-1}$ quality. The pH of buffers was adjusted using 5.0 M $NaOH_{aq.}$ or concentrated $HCl_{aq.}$ as appropriate and measured using a Corning pH meter 240 at room temperature, calibrated with standard commercial buffers at pH 7.0 and pH 4.0 or pH 10.0.

6.2 Synthesis of novel AMACR inhibitors

6.2.1 Synthesis of 3-sulfide inhibitors

_O_-4-Phenoxyphenyl-_N_,_N_-dimethylthiocarbamate (68)

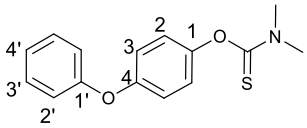

NaH [60% (w/w) dispersion in mineral oil, 1.20 g, 30.0 mmol] was added slowly to a solution of 4-phenoxyphenol **67** (5.59 g, 30.0 mmol) in DMF (27 mL) at 10 °C. *N*,*N*-dimethylthiocarbamoyl chloride (5.78 g, 46.8 mmol) was added to the stirred solution once hydrogen gas formation had ceased. The reaction mixture was stirred at 70 °C for 21 h, and then cooled to ambient temperature. Water (100 mL) was added and the mixture was extracted with chloroform (3 x 50 mL). The organic layers were combined, washed with $KOH_{aq.}$ (50 mL, 0.89

M), brine (50 mL), dried over $MgSO_4$ and evaporated *in vacuo* to give a yellow oil. The crude product was purified by column chromatography [silica, 5:1 (v/v) PE:EtOAc] to afford a white solid (7.12 g, 86.8%). R_f = 0.50 [5:1 (v/v) PE:EtOAc]. ^1H and ^{13}C spectra and mass of the product were consistent with previously reported data.[174] δ_H (400.04 MHz; $CDCl_3$) 7.37-7.30 (2 H, m, Ar 3'-*H*), 7.11 (1 H, t, *J* = 7.4 Hz, Ar 4'-*H*), 7.04 (2 H, d, *J* = 7.7 Hz, Ar 2'-*H*), 7.02-6.97 (4 H, m, Ar 2-*H* and Ar 3-*H*), 3.46 (3 H, s, NCH_3) and 3.34 (3 H, s, NCH_3); δ_C (100.59 MHz; $CDCl_3$) 187.89 (*C*=S), 156.95 (Ar 1'-*C*), 154.88 (Ar 1-*C* or Ar 4-*C*), 149.31 (Ar 1-*C* or Ar 4-*C*), 129.75 (Ar 3'-*C*), 123.80 (Ar 2-*C* or Ar 3-*C*), 123.42 (Ar 4'-*C*), 119.03 (Ar 2-*C* or Ar 3-*C*), 119.02 (Ar 2'-*C*), 43.29 (N*C*H_3) and 38.67 (N*C*H_3); ESI-MS m/z calcd. for $[M+Na]^+$ $C_{15}H_{15}NO_2SNa$: 296.0721, found 296.0716.

S-4-Phenoxyphenyl-*N*,*N*-dimethylcarbamothioate (69)

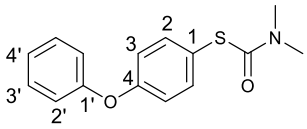

O-4-Phenoxyphenyl-*N*,*N*-dimethylthiocarbamate **68** (7.10 g, 25.9 mmol) was heated at 280 °C under an argon atmosphere for 1 h 40 min. The crude dark yellow oil was purified by column chromatography [silica, gradient elution with 19:1, 9:1, 5:1, 3:1 (v/v) PE:EtOAc] to give a pale yellow solid (2.59 g, 36.4%) that eluted in 3:1 (v/v) PE:EtOAc. R_f = 0.30 [5:1 (v/v) PE:EtOAc]. ^1H and ^{13}C NMR spectra and mass of the product were consistent with previously reported data.[174] δ_H (400.04 MHz; $CDCl_3$) 7.42-7.50 (2 H, m, Ar 2-*H*), 7.38-7.30 (2 H, m, Ar 3'-*H*), 7.16-7.11(1 H, m, Ar 4'-*H*), 7.10-7.04 (2 H, m, Ar 2'-*H*), 7.03-6.98 (2 H, m, Ar 3-*H*) and 3.03 (6 H, br s, N(CH_3)$_2$); δ_C (100.59 MHz; $CDCl_3$) 166.77 (*C*=O), 158.33 (Ar 4-*C*), 156.06 (Ar 1'-*C*), 137.14 (Ar 2-*C*), 129.59 (Ar 3'-*C*), 123.63 (Ar 4'-*C*), 122.03 (Ar 1-*C*), 119.32 (Ar 2'-*C*), 118.42 (Ar 3-*C*) and 36.55 (N*C*H_3); ESI-MS m/z calcd. for $[M+H]^+$ $C_{15}H_{16}NO_2S$: 274.0902, found 274.0903.

4-Phenoxybenzenethiol (58)

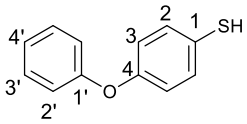

NaOH $_{aq.}$ (4.0 mL, 2.50 M, 10.0 mmol) was added to a solution of *S*-4-phenoxyphenyl-*N*,*N*-dimethylcarbamothioate **69** (957 mg, 3.5 mmol) in methanol (9 mL), and the reaction mixture was heated at reflux for 4 h. The reaction mixture was cooled to ambient temperature, acidified to pH 1 by addition of 1.0 M HCl $_{aq.}$ and the aqueous layer was extracted with chloroform (3 x 50 mL). The organic layers were combined, washed with brine (50 mL), dried over $MgSO_4$ and evaporated *in vacuo* to afford a yellow oil. The crude product was purified by column chromatography [silica, 10:1 (v/v) PE:EtOAc] to give a pale yellow oil (618 mg, 87.2%). The product was estimated to be 90% pure (by ^{1}H NMR) and used without further purification. R_f = 0.78 [5:1 (v/v) PE:EtOAc]. ^{1}H and ^{13}C NMR spectra and mass of the product were consistent with previously reported data.[174] δ_H (400.04 MHz; $CDCl_3$) 7.45-7.36 (2 H, m, Ar 3'-*H*), 7.35-7.29 (2 H, m, Ar 2-*H*), 7.21-7.15 (1 H, m, Ar 4'-*H*), 7.12-7.05 (2 H, m, Ar 2'-*H*), 7.00-6.95 (2 H, m, Ar 3-*H*) and 3.50 (1 H, s, S*H*); δ_C (100.59 MHz; $CDCl_3$) 156.89 (Ar 1'-*C*), 155.61 (Ar 4-*C*), 131.64 (Ar 2-*C*), 129.66 (Ar 3'-*C*), 123.72 (Ar 1-*C*), 123.24 (Ar 4'-*C*), 119.51 (Ar 3-*C*) and 118.62 (Ar 2'-*C*); ESI-MS m/z calcd. for $[M-H]^-$ $C_{12}H_9OS$: 201.0374 found 201.0379.

Ethyl 2-[(4-phenoxyphenyl)thio]propanoate (59)

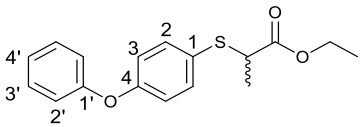

Anhydrous potassium carbonate (367 mg, 2.65 mmol) was added to a solution of 4-phenoxybenzenethiol **58** (534 mg, 2.64 mmol) in anhydrous acetonitrile (4.9 mL) at -45 °C and the resulting mixture was stirred for 15 min. Acetonitrile (1.8 mL) was added to the mixture, followed by a solution of ethyl 2-bromopropionate (0.35 mL, 2.64 mmol) in acetonitrile (1.2 mL). The reaction mixture was warmed to ambient temperature and stirred for 20 h. The mixture was filtered through celite and concentrated *in vacuo* to give a pale yellow oil. The crude product was purified by column chromatography [silica, 30:1 (v/v)

PE:EtOAc] to afford a colourless oil (630 mg, 78.9%). R_f = 0.51 [10:1 (v/v) PE:EtOAc]; IR ν_{max}/cm^{-1} 1731 (C=O); δ_H (400.04 MHz; $CDCl_3$) 7.46-7.41 (2 H, m, Ar 2-*H*), 7.37-7.31 (2 H, m, Ar 3'-*H*), 7.13 (1 H, tt, *J* = 7.4, 1.1 Hz, Ar 4'-*H*), 7.04-6.98 (2 H, m, Ar 2'-*H*), 6.95-6.90 (2 H, m, Ar 3-*H*), 4.15-4.07 (2 H, m, O*CH*$_2$), 3.68 (1 H, q, *J* = 7.1 Hz, C*H*), 1.45 (3 H, d, *J* = 7.1 Hz, CHC*H*$_3$) and 1.20 (3 H, t, *J* = 7.1 Hz, CH_2CH_3); δ_C (100.59 MHz and $CDCl_3$) 172.54 (*C*=O), 158.04 (Ar 4-*C*), 156.37 (Ar 1'-*C*), 135.99 (Ar 2-*C*), 129.84 (Ar 3'-*C*), 126.16 (Ar 1-*C*), 123.82 (Ar 4'-*C*), 119.38 (Ar 2'-*C*), 118.68 (Ar 3-*C*), 61.05 (O*C*H$_2$), 45.76 (*C*H), 12.20 (CH*C*H$_3$) and 14.07 (CH_2CH_3); ESI-MS m/z calcd. for $[M+Na]^+$ $C_{17}H_{18}O_3SNa$: 325.0869, found 325.0991.

2-[(4-Phenoxyphenyl)thio]propanoic acid (60)

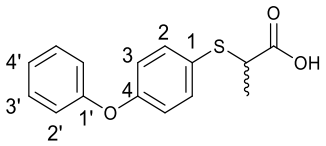

NaOH $_{aq.}$ [1.5 mL, 2.50 M, 3.75 mmol] was added to a solution of ethyl 2-[(4-phenoxyphenyl)thio]propanoate **59** (387 mg, 1.28 mmol) in methanol (4.0 mL), and the resulting mixture was stirred at ambient temperature for 1.5 h. The volatiles were evaporated and the remaining solution was acidified to pH 1 by addition of 1.0 M HCl $_{aq}$. Water (100 mL) was added and the mixture was extracted with chloroform (3 x 50 mL). The combined organic extracts were washed with brine (100 mL), dried over $MgSO_4$ and evaporated *in vacuo* to afford a colourless oil (339 mg, 96.5%) which was found to be *ca.* 99% pure (by ^{1}H NMR) and used in the next step without further purification. R_f = 0.49 [10% (v/v) methanol in DCM]; IR ν_{max}/cm^{-1} 3038 (OH), 1705 (C=O); δ_H (400.04 MHz; $CDCl_3$) 11.89 (1 H, br s, O*H*), 7.47 (2 H, d, *J* = 8.8 Hz, Ar 2-*H*), 7.36 (2 H, t, *J* = 7.9 Hz, Ar 3'-*H*), 7.15 (1 H, t, *J* = 7.4 Hz, Ar 4'-*H*), 7.03 (2 H, d, *J* = 7.6 Hz, Ar 2'-*H*), 6.94 (2 H, d, *J* = 8.8 Hz, Ar 3-*H*), 3.69 (1 H, q, *J* = 7.2 Hz, C*H*) and 1.48 (3 H, d, *J* = 7.2 Hz, C*H*$_3$); δ_C (100.59 MHz; $CDCl_3$) 179.17 (*C*=O), 158.33 (Ar 4-*C*), 156.25 (Ar 1'-*C*), 136.09 (Ar 2-*C*), 129.88 (Ar 3'-*C*), 125.56 (Ar 1-*C*), 123.93 (Ar 4'-*C*), 119.52 (Ar 2'-*C*), 118.76 (Ar 3-*C*), 45.73 (*C*H) and 17.04 (*C*H$_3$); ESI-MS m/z calcd. for $[M-H]^-$ $C_{15}H_{13}O_3S$: 273.0585, found 273.0580.

2-[(4-Phenoxyphenyl)thio]propanoyl-CoA (49)

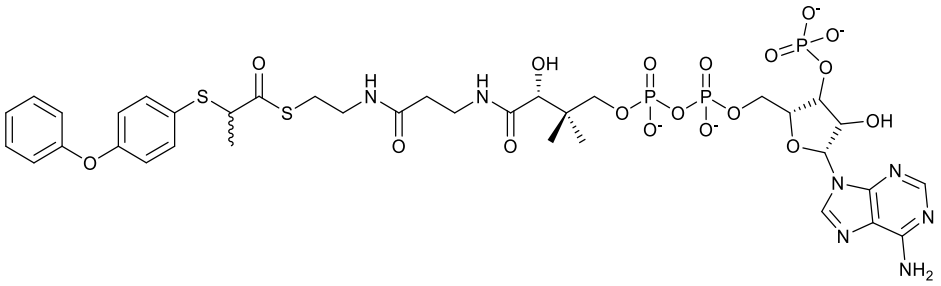

CDI (36 mg, 0.22 mmol) was added in one portion to a solution of 2-[(4-phenoxyphenyl)thio]propanoic acid **60** (30 mg, 0.11 mmol) in anhydrous DCM (2 mL), and the resulting mixture was stirred at ambient temperature for 1 h. DCM (3 mL) was added to the reaction mixture which was then washed with water (5×2 mL), brine (2 mL), dried over $MgSO_4$ and evaporated *in vacuo* to afford the crude intermediate. $NaHCO_{3\ aq.}$ (1 mL, 0.10 M), followed by CoA-Li_3 (17 mg, 0.02 mmol) was added to the solution of crude intermediate in THF (1 mL), and the resulting mixture was stirred at ambient temperature under an argon atmosphere for 18 h. The volatile organics were evaporated *in vacuo* and the remaining solution was acidified to *ca.* pH 3 by addition of 1.0 M HCl_{aq}. The mixture was diluted with water (2 mL) and extracted with EtOAc (5×3 mL). The crude aqueous product was freeze-dried and purified by solid phase extraction to afford a white solid (5.8 mg). δ_H (500.13 MHz, ^2H_2O) 8.60 (1 H, s, adenosine C*H*), 8.32 (1 H, s, adenosine C*H*), 7.39-7.30 (4 H, m, Ar-*H*), 7.14 (1 H, t, *J* = 6.5 Hz, Ar-*H*), 7.00-6.94 (2 H, m, Ar-*H*), 6.91-6.85 (2 H, m, Ar-*H*), 6.12 (1 H, d, *J* = 5.0 Hz, adenosine C*H*), 4.82-4.75 (1 H, m, adenosine C*H*), 4.52 (1 H, br s, adenosine C*H*), 4.18 (2 H, br s, adenosine CH_2), 4.04-3.97 (1 H, m, C*H*), 3.96 (1 H, s, adenosine C*H*), 3.83-3.74 (1 H, m, CoA(OCH_a)), 3.55-3.46 (1 H, m, CoA(OCH_b)), 3.41-3.30 (2 H, m, CoA(CH_2)), 3.24-3.11 (2 H, m, CoA(CH_2)), 2.96-2.80 (2 H, m, CoA(SCH_2)), 2.33 (2 H, t, *J* = 6.5 Hz, CoA(CH_2)), 1.36 (3 H, d, *J* = 7.0 Hz, CH_3), 0.85 (3 H, d, *J* = 4.0 Hz, CoA(CH_3)) and 0.70 (3 H, s, CoA(CH_3)); ESI-MS m/z calcd. for $[M-H]^-$ $C_{36}H_{47}N_7O_{18}P_3S_2$: 1022.1626, found 1022.1656.

O-(3-Phenoxyphenyl) dimethylthiocarbamate (74)

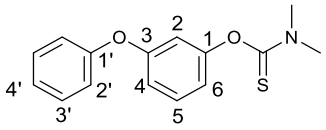

Compound **74** was prepared from 3-phenoxyphenol **73** (1.86 g, 10.0 mmol) using the same procedure as for compound **68**. The crude product was purified by column chromatography [silica, 5:1 (v/v) PE:EtOAc] to afford a colourless oil (1.86 g, 68.1%). R_f = 0.68 [2:1 (v/v) PE:EtOAc]; IR ν_{max}/cm^{-1} 1139 (C=S); δ_H (400.04 MHz; $CDCl_3$) 7.38-7.30 (3 H, m, Ar 5-*H* and Ar 3'-*H*), 7.15-7.05 (3 H, m, Ar 2'-*H* and Ar 4'-*H*), 6.95-6.90 (1 H, m, Ar 4-*H* or Ar 6-*H*), 6.87-6.82 (1 H, m, Ar 4-*H* or Ar 6-*H*), 6.78 (1 H, t, *J* = 2.0 Hz, Ar 2-*H*), 3.40 (3 H, s, NCH_3) and 3.26 (3 H, s, NCH_3); δ_C (100.59 MHz; $CDCl_3$) 187.26 (*C*=S), 157.90 (Ar 1-*C* or Ar 3-*C*), 156.59 (Ar 1'-*C*), 154.98 (Ar 1-*C* or Ar 3-*C*), 129.92 (Ar 3'-*C*), 129.80 (Ar 5-*C*), 123.74 (Ar 4'-*C*), 119.24 (Ar 2'-*C*), 117.56 (Ar 4-*C* or Ar 6-*C*), 116.01 (Ar 4-*C* or Ar 6-*C*), 113.64 (Ar 2-*C*), 43.24 (N*C*H$_3$), 38.75 (N*C*H$_3$); ESI-MS m/z calcd. for $[M+H]^+$ $C_{15}H_{16}NO_2S$: 274.0902, found 274.0900.

S-3-Phenoxyphenyl-*N*,*N*-dimethylcarbamothioate (75)

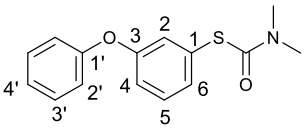

Compound **75** was prepared from *O*-3-Phenoxyphenyl-*N*,*N*-dimethylthiocarbamate **74** (1.76 g, 6.43 mmol) using the same procedure as for compound **69** to give a brown oil (664 mg, 37.8%). R_f = 0.61 [2:1 (v/v) PE:EtOAc]; IR ν_{max}/cm^{-1} 1671 (C=O); δ_H (400.04 MHz; $CDCl_3$) 7.39-7.30 (3 H, m, Ar 5-*H* and Ar 3'-*H*), 7.29-7.24 (1 H, m, Ar 4-*H*), 7.20 (1 H, t, *J* = 2.2 Hz, Ar 2-*H*), 7.12 (1 H, tt, *J* = 7.4, 1.0 Hz, Ar 4'-*H*), 7.09-7.01 (3 H, m, Ar 2'-*H* and Ar 6-*H*) and 3.02 (6 H, br s, N(CH_3)$_2$); δ_C (100.59 MHz; $CDCl_3$) 166.01 (*C*=O), 157.09 (Ar 3-*C*), 156.46 (Ar 1'-*C*), 130.10 (Ar 4-*C*), 129.98 (Ar 1-*C*), 129.63 (Ar 5-*C*), 129.59 (Ar 3'-*C*), 125.37 (Ar 2-*C*), 123.32 (Ar 4'-*C*), 119.14 (Ar 6-*C*), 118.91 (Ar 2'-*C*) and 36.60 (N*C*H$_3$); ESI-MS m/z calcd. for $[M+H]^+$ $C_{15}H_{16}NO_2S$: 274.0902, found 274.0879.

3-Phenoxybenzenethiol (76)[171]

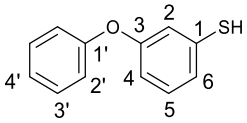

Compound **76** was prepared from *S*-(3-phenoxyphenyl)-*N*,*N*-dimethylcarbamothioate **75** (254 mg, 0.93 mmol) using the same procedure as for compound **58**. The crude brown oil was purified by column chromatography [silica, 40:1 (v/v) PE:EtOAc] to give a colourless oil (98 mg, 52.1%). R_f = 0.43 [30:1 (v/v) PE:EtOAc]. The product was estimated to be *ca.* 85% pure (by ^{1}H NMR) and used without further purification. δ_H (400.04 MHz; $CDCl_3$) 7.40-7.30 (2 H, m, Ar 3'-*H*), 7.21-7.10 (2 H, m, Ar 5-*H* and Ar 4'-*H*), 7.05-6.96 (3 H, m, Ar 6-*H* and Ar 2'-*H*), 6.92 (1 H, t, *J* = 2.1 Hz, Ar 2-*H*), 6.83-6.76 (1 H, m, Ar 4-*H*) and 3.47 (1 H, s, S*H*); δ_C (100.59 MHz; $CDCl_3$) 157.76 (Ar 3-*C*), 156.55 (Ar 1'-*C*), 132.51 (Ar 1-*C*), 130.16 (Ar 5-*C*), 129.80 (Ar 3'-*C*), 123.75 (Ar 6-*C*), 123.63 (Ar 4'-*C*), 119.20 (Ar 2'-*C*), 119.08 (Ar 2-*C*) and 115.83 (Ar 4-*C*); ESI-MS m/z calcd. for $[M-H]^-$ $C_{12}H_9OS$: 201.0374 found 201.0376.

Ethyl 2-[(3-phenoxyphenyl)thio]propanoate (77)

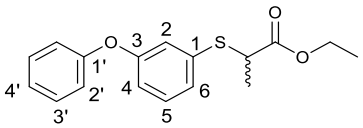

Compound **77** was prepared from 3-phenoxybenzenethiol **76** (94 mg, 0.47 mmol) using the procedure as for compound **59** to afford a colourless oil (94 mg, 66.8%). R_f = 0.51 [10:1 (v/v) PE:EtOAc]; IR ν_{max}/cm^{-1} 1732 (C=O); δ_H (400.04 MHz; $CDCl_3$) 7.38-7.30 (2 H, m, Ar 3'-*H*), 7.25 (1 H, t, *J* = 8.0 Hz, Ar 5-*H*), 7.20-7.07 (3 H, m, Ar 2-*H*, 6-*H* and Ar 4'-*H*), 7.04-6.97 (2 H, m, Ar 2'-*H*), 6.94-6.89 (1 H, m, Ar 4-*H*), 4.10 (2 H, q, *J* = 7.2 Hz, OCH_2), 3.78 (1 H, q, *J* = 7.2 Hz, C*H*), 1.48 (3 H, d, *J* = 7.2 Hz, CHCH_3) and 1.17 (3 H, t, *J* = 7.2 Hz, CH_2CH_3); δ_C (100.59 MHz; $CDCl_3$) 172.43 (*C*=O), 157.49 (Ar 3-*C*), 156.65 (Ar 1'-*C*), 135.08 (Ar 1-*C*), 129.94 (Ar 5-*C*), 129.81 (Ar 3'-*C*), 127.00 (Ar 6-*C*), 123.59 (Ar 4'-*C*), 122.29 (Ar 2-*C*), 119.06 (Ar 2'-*C*), 118.09 (Ar 4-*C*), 61.22 (O*C*H_2), 44.99 (*C*H), 17.34 (CH*C*H_3) and 14.02 (CH_2*C*H_3); ESI-MS m/z calcd. for $[M+Na]^+$ $C_{17}H_{18}O_3SNa$: 325.0874, found 325.0868.

2-[(3-Phenoxyphenyl)thio]propanoic acid (78)

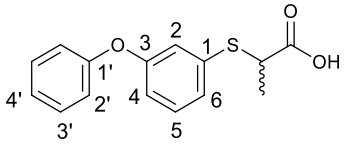

Compound **78** was prepared from ethyl 2-[(3-phenoxyphenyl)thio]propanoate **77** (87 mg, 0.29 mmol) using the same procedure as for compound **60** to give a colourless oil (79 mg, 98.9%). R_f = 0.23 [5% (v/v) methanol in DCM]; IR ν_{max}/cm^{-1} 3064 (O-H), 1707 (C=O); δ_H (400.04 MHz; $CDCl_3$) 11.24 (1 H, br s, O*H*), 7.38-7.31 (2 H, m, Ar 3'-*H*), 7.26 (1 H, t, *J* = 7.9 Hz, Ar 5-*H*), 7.18 (1 H, dt, *J* = 7.9, 1.4 Hz, Ar 6-*H*), 7.15-7.09 (2 H, m, Ar 2-*H* and Ar 4'-*H*), 7.04-6.97 (2 H, m, Ar 2'-*H*), 6.95-6.90 (1 H, m, Ar 4-*H*), 3.79 (1 H, q, *J* = 7.2 Hz, C*H*) and 1.50 (3 H, d, *J* = 7.2 Hz, CH_3); δ_C (100.59 MHz; $CDCl_3$) 178.78 (*C*=O), 157.61 (Ar 3-*C*), 156.52 (Ar 1'-*C*), 134.57 (Ar 1-*C*), 130.10 (Ar 5-*C*), 129.83 (Ar 3'-*C*), 126.85 (Ar 6-*C*), 123.66 (Ar 4'-*C*), 122.18 (Ar 2-*C*), 119.12 (Ar 2'-*C*), 118.25 (Ar 4-*C*), 44.81 (*C*H) and 17.17 (*C*H_3); ESI-MS m/z calcd. for $[M-H]^-$ $C_{15}H_{13}O_3S$: 273.0585, found 273.0587.

2-[(3-Phenoxyphenyl)thio]propanoyl-CoA (50)

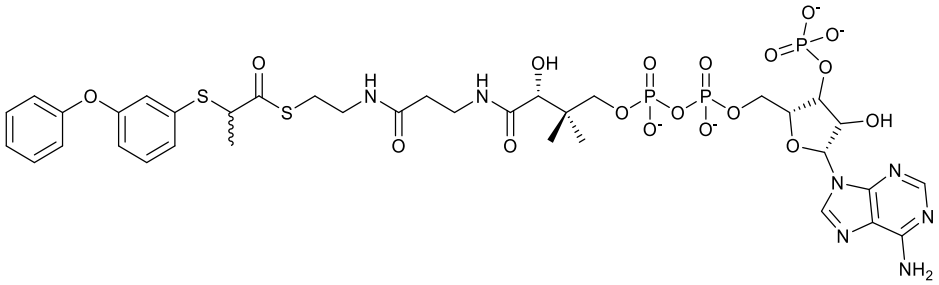

Compound **50** was prepared from 2-[(3-phenoxyphenyl)thio]propanoic acid **78** (30 mg, 0.11 mmol) using the same procedure as for compound **49** to give a white solid (14 mg). δ_H (500.13 MHz; ^2H_2O) 8.55 (1 H, s, adenosine C*H*), 8.24 (1 H, s, adenosine C*H*), 7.36-7.25 (2 H, m, Ar-*H*), 7.20 (1 H, t, *J* = 8.0 Hz, Ar-*H*), 7.10-7.01 (2 H, m, Ar-*H*), 7.00-6.79 (4 H, m, Ar-*H*), 6.06 (1 H, d, *J* = 5.5 Hz, adenosine C*H*), 4.70 (1 H, s, adenosine C*H*), 4.47 (1 H, br s, adenosine C*H*), 4.13 (2 H, br s, adenosine CH_2), 4.03-3.95 (1 H, m, C*H*), 3.91 (1 H, s, adenosine C*H*), 3.83-3.68 (1 H, m, CoA(OCH_a)), 3.50-3.42 (1 H, m, CoA(OCH_b)), 3.29 (2 H, t, *J* = 6.5 Hz, CoA(CH_2)), 3.14-3.00 (2 H, m, CoA(CH_2)), 2.83-2.70 (2 H, m, CoA(SCH_2)), 2.24 (2 H, t, *J* = 6.5 Hz,

CoA(CH_2)), 1.29 (3 H, d, J = 6.3 Hz, CH_3), 0.80 (3 H, s, CoA(CH_3)) and 0.65 (3 H, s, CoA(CH_3)); ESI-MS m/z calcd. for $[M-H]^-$ $C_{36}H_{47}N_7O_{18}P_3S_2$: 1022.1626, found 1022.1616.

6.2.2 Synthesis of 3-sulfone inhibitors

Ethyl 2-[(4-phenoxyphenyl)sulfonyl]propanoate (79)[42]

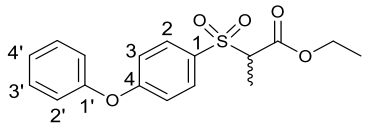

A solution of OXONE® (470 mg, 1.53 mmol) in water (4.7 mL) was added to a solution of ethyl 2-[(4-phenoxyphenyl)thio]propanote **59** (143 mg. 0.47 mmol) in 1:1 methanol/THF (4.7 mL), and the resulting mixture was stirred at ambient temperature for 4 h. The reaction mixture was filtered through celite and the volatiles were evaporated *in vacuo*. Water (100 mL) was added and mixture was extracted with EtOAc (3×50 mL). The organic layers were combined, dried over $MgSO_4$ and evaporated *in vacuo*. The crude product was purified by column chromatography [silica, gradient elution with 20:1, 7:1, 5:1, 3:1 (v/v) PE:EtOAc] to give a colourless oil (129 mg, 81.8%) that eluted in 3:1 (v/v) PE:EtOAc. R_f = 0.59 [2:1 (v/v) PE:EtOAc]; IR ν_{max}/cm^{-1} 1738 (C=O), 1324 and 1144 (S=O); δ_H (400.04 MHz; $CDCl_3$) 7.82-7.77 (2 H, m, Ar 2-*H*), 7.45-7.37 (2 H, m, Ar 3'-*H*), 7.23 (1 H, tt, J = 7.4, 1.1 Hz, Ar 4'-*H*), 7.10-7.02 (4 H, m, Ar 3-*H* and Ar 2'-*H*), 4.13 (2 H, q, J = 7.2 Hz, OCH_2), 4.02 (1 H, q, J = 7.1 Hz, C*H*), 1.55 (3 H, d, J = 7.1 Hz, CHCH_3) and 1.20 (3 H, t, J = 7.2 Hz, CH_2CH_3); δ_C (100.59 MHz; $CDCl_3$) 166.36 (*C*=O), 162.97 (Ar 4-*C*), 154.65 (Ar 1'-*C*), 131.69 (Ar 2-*C*), 130.22 (Ar 3'-*C*), 130.04 (Ar 1-*C*), 125.24 (Ar 4'-*C*), 120.48 (Ar 2'-*C*), 117.15 (Ar 3-*C*), 65.47 (*C*H), 62.16 (O*C*H_2), 13.85 (CH_2CH_3) and 11.93 (CH*C*H_3); ESI-MS m/z calcd. for $[M-H]^-$ $C_{17}H_{17}O_5S$: 333.0797, found 333.0807.

2-[(4-Phenoxyphenyl)sulfonyl]propanoic acid (81)

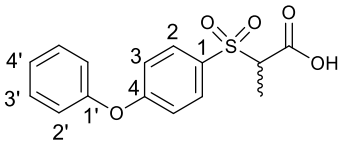

Compound **81** was prepared from ethyl 2-[(4-phenoxyphenylsulfonyl]propanoate **79** (105 mg, 0.31 mmol) using the

same procedure as for compound **60** to afford a waxy white solid (95 mg, 99.5%) which was found to be *ca.* 99 % pure (by ^{1}H NMR). R_f = 0.28 [5% (v/v) methanol in DCM]; melting point 119-120 °C; IR ν_{max}/cm^{-1} 3251 (O-H), 1741 (C=O), 1306 and 1125 (S=O); δ_H (400.04 MHz; $CDCl_3$) 7.86-7.79 (2 H, m, Ar 2-*H*), 7.64 (1 H, br s, O*H*), 7.46-7.38 (2 H, m, Ar 3'-*H*), 7.28-7.21 (1 H, m, Ar 4'-*H*), 7.12-7.02 (4 H, m, Ar 3-*H* and Ar 2'-*H*), 4.06 (1 H, q, *J* = 7.2 Hz, C*H*) and 1.57 (3 H, d, *J* = 7.2 Hz, CH_3); δ_C (100.59 MHz; $CDCl_3$) 170.34 (C=O), 163.25 (Ar 4-*C*), 154.52 (Ar 1'-*C*), 131.73 (Ar 2-*C*), 130.25 (Ar 3'-*C*), 129.42 (Ar 1-*C*), 125.34 (Ar 4'-*C*), 120.56 (Ar 2'-*C*), 117.28 (Ar 3-*C*), 65.19 (*C*H) and 12.03 (*C*H_3); ESI-MS m/z calcd. for [M-H]$^-$ $C_{15}H_{13}O_5S$: 305.0484, found 305.0494.

2-[(4-Phenoxyphenyl)sulfonyl]propanoyl-CoA (51)

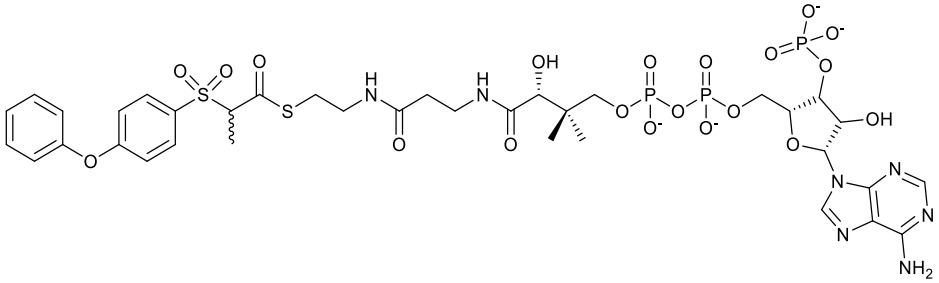

Compound **51** was prepared from 2-[(4-phenoxyphenyl)sulfonyl]propanoic acid **81** (30 mg, 0.10 mmol) using the same procedure as for compound **49** to give a white solid (6.1 mg). δ_H (500.13 MHz; $^{2}H_2O$) 8.61 (1 H, s, adenosine C*H*), 8.33 (1 H, s, adenosine C*H*), 7.72 (2 H, d, *J* = 8.5 Hz, Ar-*H*), 7.40 (2 H, t, *J* = 7.0 Hz, Ar-*H*), 7.23 (1 H, t, *J* = 6.5 Hz, Ar-*H*), 7.14-7.02 (4 H, m, Ar-*H*), 6.12 (1 H, d, *J* = 4.5 Hz, adenosine C*H*), 4.79 (1 H, s, adenosine C*H*), 4.52 (1 H, br s, adenosine C*H*), 4.18 (2 H, br s, adenosine CH_2), 3.96 (1 H, s, adenosine C*H*), 3.84-3.74 (1 H, m, CoA(OCH_a)), 3.53-3.47 (1 H, m, CoA(OCH_b)), 3.43-3.33 (2 H, m, CoA(CH_2)), 3.23-3.08 (2 H, m, CoA(CH_2)), 2.98-2.83 (2 H, m, CoA(SCH_2)), 2.36 (2 H, t, *J* = 6.5 Hz, CoA(CH_2)), 1.47 (3 H, s, CH_3), 0.85 (3 H, d, *J* = 4.0 Hz, CoA(CH_3)) and 0.71 (3 H, s, CoA(CH_3)); ESI-MS m/z calcd. for [M-H]$^-$ $C_{36}H_{48}N_7O_{20}P_3S_2Na$: 1078.1501, found 1078.1478.

Ethyl 2-[(3-phenoxyphenyl)sulfonyl]propanoate (80)

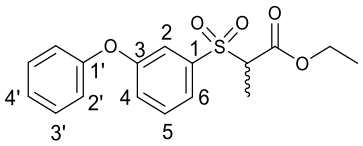

Compound **80** was synthesised from ethyl 2-[(3-phenoxyphenylthio]propanoate **77** (115 mg, 0.38 mmol) using the same procedure as for compound **79**. The reaction mixture was stirred for 21 h to give a colourless oil (123 mg, 96.9%) which was found to be >95% pure (by ^{1}H NMR) and used in the next step without further purification. R_f = 0.40 [5:1 (v/v) PE:EtOAc]; IR ν_{max}/cm^{-1} 1738 (C=O), 1326 and 1139 (S=O); δ_H (500.13 MHz; $CDCl_3$) 7.58 (1 H, d, *J* = 7.5 Hz, Ar 6-*H*), 7.50 (1 H, t, *J* = 8.0 Hz, Ar 5-*H*), 7.46 (1 H, t, *J* = 2.0 Hz, Ar 2-*H*), 7.38 (2 H, t, *J* = 7.5 Hz, Ar 3'-*H*), 7.31-7.26 (1 H, m, Ar 4-*H*), 7.18 (1 H, t, *J* = 7.5 Hz, Ar 4'-*H*), 7.03 (2 H, d, *J* = 8.0 Hz, Ar 2'-*H*), 4.10 (2 H, q, *J* = 7.3 Hz, OC*H*$_2$), 4.02 (1 H, q, *J* = 7.3 Hz, C*H*), 1.55 (3 H, d, *J* = 7.3 Hz, CHC*H*$_3$) and 1.17 (3 H, t, *J* = 7.3 Hz, CH$_2$C*H*$_3$); δ_C (126 MHz; $CDCl_3$) 165.96 (*C*=O), 158.04 (Ar 3-*C*), 155.65 (Ar 1'-*C*), 138.37 (Ar 1-*C*), 130.34 (Ar 5-*C*), 130.10 (Ar 3'-*C*), 124.52 (Ar 4'-*C*), 123.86 (Ar 4-*C*), 123.42 (Ar 6-*C*), 119.48 (Ar 2'-*C*), 118.53 (Ar 2-*C*), 65.31 (*C*H), 62.21 (O*C*H$_2$), 13.78 (CH$_2$*C*H$_3$) and 11.63 (CH*C*H$_3$); ESI-MS m/z calcd. for [M-H]$^-$ $C_{17}H_{17}O_5S$: 333.0797, found 333.0799.

2-[(3-Phenoxyphenyl)sulfonyl]propanoic acid (82)

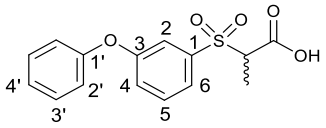

NaOH $_{aq.}$ [2.2 mL, 2.50 M, 5.50 mmol] was added to a solution of ethyl 2-[(3-phenoxyphenyl)sulfonyl]propanoate **80** (638 mg, 1.91 mmol) in methanol (6 mL), and the resulting mixture was stirred at ambient temperature for 2.5 h. The volatile organics were evaporated *in vacuo* and the remaining solution was acidified to pH 1 by addition of 1.0 M HCl_{aq}. Water (100 mL) was added and the mixture was extracted with chloroform (3 x 50 mL). The combined organic extracts were washed with brine (100 mL), dried over $MgSO_4$ and evaporated *in vacuo* to afford a colourless oil (585 mg, 100%) which was found

to be *ca.* 99% pure (by ^{1}H NMR) and used in the next step without further purification. R_f = 0.29 [5% (v/v) methanol in DCM]; IR ν_{max}/cm^{-1} 3073 (OH), 1742 (C=O); δ_H (400.04 MHz; $CDCl_3$) 10.92 (1 H, br s, O*H*), 7.64-7.58 (1 H, m, Ar 6-*H*), 7.55-7.48 (2 H, m, Ar 5-*H* and Ar 2-*H*), 7.41-7.34 (2 H, m, Ar 3'-*H*), 7.31-7.27 (1 H, m, Ar 4-*H*), 7.21-7.15 (1 H, m, 4'-*H*), 7.05-7.00 (2 H, m, Ar 2'-*H*), 4.08 (1 H, q, *J* = 7.2 Hz, C*H*) and 1.57 (3 H, d, *J* = 7.2 Hz, CH_3); δ_C (100.59 MHz, $CDCl_3$) 171.07 (*C*=O), 158.15 (Ar 3-*C*), 155.54 (Ar 1'-*C*), 137.88 (Ar 1-*C*), 130.59 (Ar 5-*C*), 130.15 (Ar 3'-*C*), 124.60 (Ar 4'-*C*), 124.13 (Ar 4-*C*), 123.44 (Ar 6-*C*), 119.46 (Ar 2'-*C*), 118.48 (Ar 2-*C*), 65.11 (*C*H) and 11.79 (*C*H_3); ESI-MS *m/z* calcd. for [M-H]$^-$ $C_{15}H_{13}O_5S$: 305.0484, found 305.0489.

6.2.3 Synthesis of phenoxyphenol side-chain inhibitors

Methyl (2*R*)-2-(4-phenoxyphenoxy)propanoate (87)

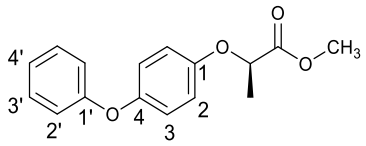

A solution of DEAD (0.88 mL, 5.6 mmol) in THF (1.3 mL) was added dropwise to 4-phenoxyphenol (1.00 g, 5.4 mmol), triphenylphosphine (1.42 g, 5.4 mmol) and methyl *S*-lactate **89** (0.52 mL, 5.4 mmol) in THF (7 mL) over 30 min at ambient temperature. The resulting mixture was stirred at ambient temperature for 24 h. The volatile organics were evaporated *in vacuo* and 1:1 PE/Et_2O (200 mL) was added to the residue. The mixture was filtered through silica gel-celite and washed with 1:1 PE/Et_2O. The filtrate was evaporated *in vacuo*, and the crude product was purified by column chromatography [silica, gradient elution with 30:1, 20:1 (v/v) PE:EtOAc] to give a white solid (0.95 g, 64.4%) that eluted in 20:1 (v/v) PE:EtOAc. R_f = 0.27 [10:1 (v/v) PE:EtOAc]; melting point 35-38 °C; $[\alpha]_D^{21}$ +33.3 (*c* 0.51 in $CHCl_3$); IR ν_{max}/cm^{-1} 1750 (C=O); δ_H (400.04 MHz, $CDCl_3$) 7.34-7.27 (2 H, m, Ar 3'-*H*), 7.05 (1 H, tt, *J* = 7.6, 0.8 Hz, Ar 4'-*H*), 6.99-6.93 (4 H, m, Ar 2'-*H* and Ar 3-*H*), 6.90-6.84 (2 H, m, Ar 2-*H*), 4.73 (1 H, q, *J* = 6.8 Hz, C*H*), 3.77 (3 H, s, OCH_3) and 1.63 (3 H, d, *J* = 6.8 Hz, CH_3); δ_C (100.59 MHz, $CDCl_3$) 172.52 (*C*=O), 157.99 (Ar 1'-*C*), 153.58 (Ar 1-*C*), 150.95 (Ar 4-*C*), 129.52 (Ar 3'-*C*), 122.55 (Ar 4'-*C*), 120.46 (Ar 3-*C*),

117.78 (Ar 2'-*C*), 116.25 (Ar 2-*C*), 73.08 (*C*H), 52.18 (O*C*H_3) and 18.50 (*C*H_3); ESI-MS m/z calcd. for $[M-H]^-$ $C_{16}H_{16}NaO_4$: 295.0946 found 295.0944.

(2*R*)-2-(4-phenoxyphenoxy)propanoic acid (88)

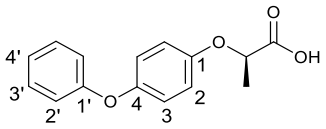

Compound **88** was prepared from methyl (2*R*)-2-(4-phenoxyphenoxy)propanoate **87** (597 mg, 2.19 mmol) using the same procedure as for compound **60** to afford a white solid (500 mg, 88.4%) which was found to be *ca.* 99% pure (by ^{1}H NMR) and used in the next step without further purification. R_f = 0.23 [10:1 (v/v) DCM:methanol]; melting point 69-70 °C; $[\alpha]_D^{21}$ +16.3 (*c* 0.52 in $CHCl_3$); IR ν_{max}/cm^{-1} 3050 (OH), 1709 (C=O); δ_H (400.04 MHz; $CDCl_3$) 7.34-7.27 (2 H, m, Ar 3'-*H*), 7.06 (1 H, tt, *J* = 7.6, 0.8 Hz, Ar 4'-*H*), 7.00-6.93 (4 H, m, Ar 2'-*H* and Ar 3-*H*), 6.92-6.85 (2 H, m, Ar 2-*H*), 6.75 (1 H, br s, O*H*), 4.75 (1 H, q, *J* = 7.0 Hz, C*H*) and 1.67 (3 H, d, *J* = 7.0 Hz, CH_3); δ_C (100.59 MHz, $CDCl_3$) 177.40 (C=O), 157.96 (Ar 1'-*C*), 153.29 (Ar 1-*C*), 151.35 (Ar 4-*C*), 129.64 (Ar 3'-*C*), 122.75 (Ar 4'-*C*), 120.57 (Ar 3-*C*), 117.97 (Ar 2'-*C*), 116.49 (Ar 2-*C*), 72.79 (*C*H) and 18.45 (*C*H_3); ESI-MS m/z calcd. for $[M-H]^-$ $C_{15}H_{13}O_4$: 257.0814 found 257.0820.

(2*R*)-2-(4-phenoxyphenoxy)propanoyl-CoA (53)

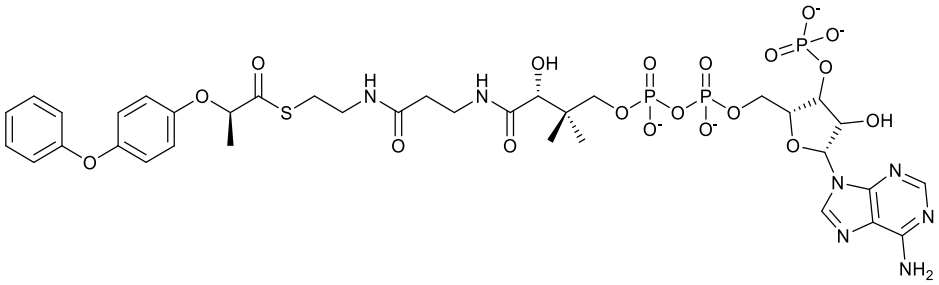

Compound **53** was prepared from (2*R*)-2-(4-phenoxyphenoxy)propanoic acid **88** (30 mg, 0.12 mmol) using the same procedure as for compound **49** to give a white solid (20 mg). δ_H (500.13 MHz, ^2H_2O) 8.57 (1 H, s, adenosine C*H*), 8.31 (1 H, s, adenosine C*H*), 7.34-7.25 (2 H, m, Ar-*H*), 7.11-7.02 (1 H, m, Ar-*H*), 6.95-6.85 (6 H, m, Ar-*H*), 6.12 (1 H, s, adenosine C*H*), 5.00-4.90 (1 H, m, C*H*), 4.52 (1 H, br s, adenosine C*H*), 4.18 (2 H, br s, adenosine CH_2), 3.95 (1

H, s, adenosine C*H*), 3.83-3.75 (1 H, m, CoA(OCH_a)), 3.55-3.45 (1 H, m, CoA(OCH_b)), 3.35-3.20 (4 H, m, 2×CoA(CH_2)), 3.05-2.93 (2 H, m, CoA(SCH_2)), 2.33-2.21 (2 H, m, CoA(CH_2)), 1.50 (3 H, d, *J* = 5.5 Hz, CHCH_3), 0.85 (3 H, s, CoA(CH_3)) and 0.71 (3 H, s, CoA(CH_3)); ESI-MS m/z calcd. for $[M+Na]^+$ $C_{36}H_{48}N_7NaO_{19}P_3S$: 1030.1836, found 1030.1889.

Methyl (2*S*)-2-(4-phenoxyphenoxy)propanoate (91)

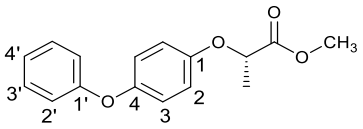

Compound **91** was prepared from 4-phenoxyphenol (1.00 g, 5.4 mmol) and methyl *R*-lactate **90** (0.52 mL, 5.4 mmol) using the same procedure as for compound **87** to give a white solid (1.04 g, 70.7%). $[\alpha]_D^{21}$ -33.6 (*c* 0.68 in $CHCl_3$); ^1H and ^{13}C NMR spectra of the compound were consistent with its enantiomer **87** (*vide supra*). δ_H (400.04 MHz, $CDCl_3$) 7.33-7.24 (2 H, m, Ar 3'-*H*), 7.03 (1 H, tt, *J* = 6.8, 1.2 Hz, Ar 4'-*H*), 6.98-6.93 (4 H, m, Ar 2'-*H* and Ar 3-*H*), 6.90-6.84 (2 H, m, Ar 2-*H*), 4.73 (1 H, q, *J* = 6.8 Hz, C*H*), 3.76 (3 H, s, OCH_3) and 1.62 (3 H, d, *J* = 6.8 Hz, CH_3); δ_C (100.59 MHz, $CDCl_3$) 172.44 (*C*=O), 157.95 (Ar 1'-*C*), 153.54 (Ar 1-*C*), 150.90 (Ar 4-*C*), 129.48 (Ar 3'-*C*), 122.50 (Ar 4'-*C*), 120.41 (Ar 3-*C*), 117.73 (Ar 2'-*C*), 116.20 (Ar 2-*C*), 73.00 (*C*H), 52.10 (O*C*H_3) and 18.44 (*C*H_3).

(2*S*)-2-(4-phenoxyphenoxy)propanoic acid (92)

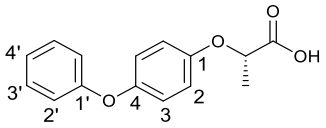

Compound **92** was prepared from methyl (2*S*)-2-(4-phenoxyphenoxy)propanoate **91** (588 mg, 2.16 mmol) using the same procedure as for compound **60** to afford a white solid (556 mg, 99.6%) which was found to be *ca.* 99% pure (by ^1H NMR) and used in the next step without further purification. $[\alpha]_D^{21}$ -17.7 (*c* 0.56 in $CHCl_3$); ^1H and ^{13}C NMR spectra of the compound were consistent with its enantiomer **88** (*vide supra*). δ_H (400.04 MHz; $CDCl_3$) 12.00 (1 H, br s, O*H*), 7.36-7.29 (2 H, m, Ar 3'-*H*), 7.08 (1 H, tt, *J* = 7.2, 1.2 Hz, Ar 4'-*H*), 7.02-6.96 (4 H, m, Ar 2'-*H* and Ar 3-*H*), 6.95-6.88 (2

H, m, Ar 2-*H*), 4.78 (1 H, q, *J* = 6.8 Hz, C*H*) and 1.70 (3 H, d, *J* = 6.8 Hz, CH_3); δ_C (100.59 MHz, $CDCl_3$) 178.46 (C=O), 157.91 (Ar 1'-*C*), 153.27 (Ar 1-*C*), 151.30 (Ar 4-*C*), 129.60 (Ar 3'-*C*), 122.71 (Ar 4'-*C*), 120.52 (Ar 3-*C*), 117.93 (Ar 2'-*C*), 116.43 (Ar 2-*C*), 72.67 (*C*H) and 18.41 (*C*H_3).

(2*S*)-2-(4-phenoxyphenoxy)propanoyl-CoA (55)

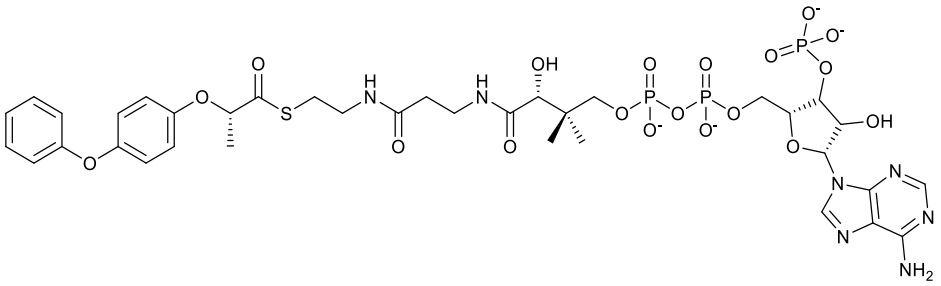

Compound **55** was prepared from (2*S*)-2-(4-phenoxyphenoxy)propanoic acid **92** (90 mg, 0.35 mmol) using the same procedure as for compound **49** to give a white solid (46 mg). δ_H (500.13 MHz, ^2H_2O) 8.52 (1 H, s, adenosine C*H*), 8.21 (1 H, s, adenosine C*H*), 7.28 (2 H, t, *J* = 8.0 Hz, Ar-*H*), 7.05 (1 H, t, *J* = 7.5 Hz, Ar-*H*), 6.95-6.84 (6 H, m, Ar-*H*), 6.08 (1 H, d, *J* = 6.0 Hz, adenosine C*H*), 4.18 (2 H, br s, adenosine CH_2), 3.94 (1 H, s, adenosine C*H*), 3.83-3.73 (1 H, m, CoA(OCH_a)), 3.53-3.45 (1 H, m, CoA(OCH_b)), 3.35-3.20 (4 H, m, 2×CoA(CH_2)), 2.97 (2 H, t, *J* = 6.0 Hz, CoA(SCH_2)), 2.26 (2 H, t, *J* = 6.0 Hz, CoA(CH_2)), 1.49 (3 H, d, *J* = 7.0 Hz, CHCH_3), 0.82 (3 H, s, CoA(CH_3)) and 0.68 (3 H, s, CoA(CH_3)); ESI-MS m/z calcd. for $[M-H]^-$ $C_{36}H_{47}N_7O_{19}P_3S$: 1006.1860, found 1006.1882.

Methyl (2*R*)-2-(3-phenoxyphenoxy)propanoate (93)

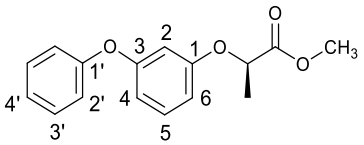

Compound **93** was prepared from 3-phenoxyphenol (0.86 mL, 5.4 mmol) and methyl *S*-lactate **89** (0.52 mL, 5.4 mmol) using the same procedure as for compound **87** to give a colourless oil (1.17 g, 79.9%). R_f = 0.30 [10:1 (v/v) PE:EtOAc]; $[\alpha]_D^{21}$ +19.4 (*c* 0.52 in $CHCl_3$); IR ν_{max}/cm^{-1} 1747 (C=O); δ_H (400.04 MHz; $CDCl_3$) 7.39-7.29 (2 H, m, Ar 3'-*H*), 7.21 (1 H, t, *J* = 8.0 Hz, Ar 5-*H*), 7.12 (1 H, tt, *J* = 7.6, 0.8 Hz, Ar 4'-*H*), 7.05-7.00 (2 H, m, Ar 2'-*H*), 6.67-6.59 (2 H,

m, Ar 4-*H* and Ar 6-*H*), 6.56 (1 H, t, *J* = 2.0 Hz, Ar 2-*H*), 4.74 (1 H, q, *J* = 6.8 Hz, C*H*), 3.74 (3 H, s, OCH_3) and 1.61 (3 H, d, *J* = 6.8 Hz, CH_3); δ_C (100.59 MHz, $CDCl_3$) 172.29 (*C*=O), 158.69 (Ar 1-*C* or Ar 3-*C*), 158.56 (Ar 1-*C* or Ar 3-*C*), 156.57 (Ar 1'-*C*), 130.17 (Ar 5-*C*), 129.65 (Ar 3'-*C*), 123.46 (Ar 4'-*C*), 119.20 (Ar 2'-*C*), 111.60 (Ar 4-*C* or Ar 6-*C*), 109.32 (Ar 4-*C* or Ar 6-*C*), 105.71 (Ar 2-*C*), 72.39 (*C*H), 52.20 (O*C*H_3) and 18.38 (*C*H_3); ESI-MS m/z calcd. for $[M+H]^+$ $C_{16}H_{17}O_4$: 273.1127, found 273.1150.

(2*R*)-2-(3-phenoxyphenoxy)propanoic acid (94)

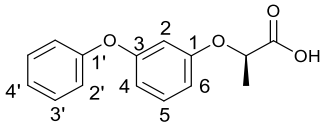

Compound **94** was prepared from methyl (2*R*)-2-(3-phenoxyphenoxy)propanoate **93** (566 mg, 2.08 mmol) using the same procedure as for compound **60** to afford a white solid (536 mg, 99.8%) which was found to be *ca.* 99% pure (by ^{1}H NMR) and used in the next step without further purification. R_f = 0.23 [10:1 (v/v) DCM:methanol]; melting point 51-52 °C; $[\alpha]_D^{21}$ -7.46 (*c* 0.54 in $CHCl_3$); IR ν_{max}/cm^{-1} 3064 (OH), 1710 (C=O); δ_H (400.04 MHz; $CDCl_3$) 11.93 (1 H, br s, OH), 7.39-7.30 (2 H, m, Ar 3'-*H*), 7.24 (1 H, t, *J* = 6.0 Hz, Ar 5-*H*), 7.13 (1 H, tt, *J* = 7.2, 1.2 Hz, Ar 4'-*H*), 7.07-7.01 (2 H, m, Ar 2'-*H*), 6.70-6.62 (2 H, m, Ar 4-*H* and Ar 6-*H*), 6.60 (1 H, t, *J* = 2.0 Hz, Ar 2-*H*), 4.78 (1 H, q, *J* = 6.8 Hz, C*H*) and 1.67 (3 H, d, *J* = 6.8 Hz, CH_3); δ_C (100.59 MHz, $CDCl_3$) 178.31 (*C*=O), 158.70 (Ar 3-*C*), 158.42 (Ar 1-*C*), 156.46 (Ar 1'-*C*), 130.30 (Ar 5-*C*), 129.72 (Ar 3'-*C*), 123.60 (Ar 4'-*C*), 119.30 (Ar 2'-*C*), 111.84 (Ar 4-*C* or Ar 6-*C*), 109.23 (Ar 4-*C* or Ar 6-*C*), 105.80 (Ar 2-*C*), 71.89 (*C*H) and 18.28 (*C*H_3); ESI-MS m/z calcd. for $[M+Na]^+$ $C_{15}H_{14}NaO_4$: 281.0790, found 281.0801.

(2*R*)-2-(3-phenoxyphenoxy)propanoyl-CoA (54)

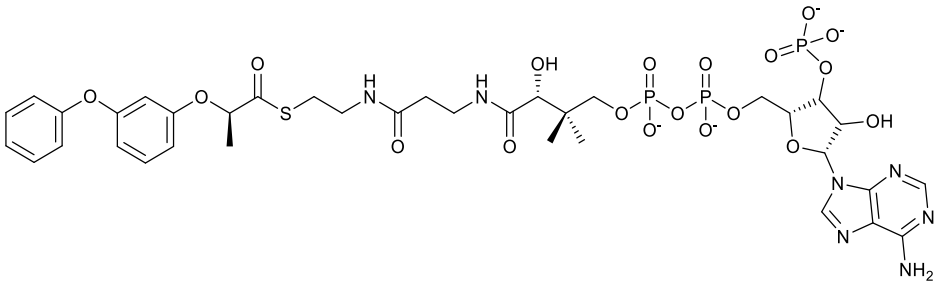

Compound **54** was prepared from (2*R*)-2-(3-phenoxyphenoxy)propanoic acid **94** (90 mg, 0.35 mmol) using the same procedure as for compound **49** to give a white solid (43 mg). δ_H (500.13 MHz, ^2H_2O) 8.59 (1 H, s, adenosine C*H*), 8.31 (1 H, s, adenosine C*H*), 7.31 (2 H, t, *J* = 8.0 Hz, Ar-*H*), 7.21 (1 H, t, *J* = 8.0 Hz, Ar-*H*), 7.11 (1 H, t, *J* = 8.0 Hz, Ar-*H*), 6.92 (2 H, d, *J* = 8.0 Hz, Ar-*H*), 6.69-6.57 (2 H, m, Ar-*H*), 6.48-6.39 (1 H, m, Ar-*H*), 6.11 (1 H, d, *J* = 5.0 Hz, adenosine C*H*), 4.19 (2 H, br s, adenosine CH_2), 3.95 (1 H, s, adenosine C*H*), 3.85-3.75 (1 H, m, CoA(OCH_a)), 3.58-3.47 (1 H, m, CoA(OCH_b)), 3.30 (2 H, t, *J* = 6.5 Hz, CoA(CH_2)), 3.25-3.15 (2 H, m, CoA(CH_2)), 2.93 (2 H, t, *J* = 6.5 Hz, CoA(SCH_2)), 2.27 (2 H, t, *J* = 5.0 Hz, CoA(CH_2)), 1.46 (3 H, d, *J* = 6.5 Hz, CCH_3), 0.85 (3 H, s, CoA(CH_3)) and 0.71 (3 H, s, CoA(CH_3)); ESI-MS m/z calcd. for $[M+Na]^+$ $C_{36}H_{48}N_7NaO_{19}P_3S$: 1030.7779, found 1030.7315.

Methyl (2*S*)-2-(3-phenoxyphenoxy)propanoate (95)

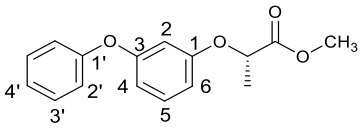

Compound **95** was prepared from 3-phenoxyphenol (0.86 mL, 5.4 mmol) and methyl *R*-lactate **90** (0.52 mL, 5.4 mmol) using the same procedure as for compound **87** to give a colourless oil (1.02 g, 69.1%). $[\alpha]_D^{21}$ -21.6 (*c* 0.56 in $CHCl_3$); ^1H and ^{13}C NMR spectra of the compound were consistent with its enantiomer **93** (*vide supra*). δ_H (400.04 MHz; $CDCl_3$) 7.38-7.30 (2 H, m, Ar 3'-*H*), 7.21 (1 H, t, *J* = 8.4 Hz, Ar 5-*H*), 7.12 (1 H, tt, *J* = 7.2, 1.2 Hz, Ar 4'-*H*), 7.06-7.01 (2 H, m, Ar 2'-*H*), 6.66-6.60 (2 H, m, Ar 4-*H* and Ar 6-*H*), 6.57 (1 H, t, *J* = 2.0 Hz, Ar 2-*H*), 4.74 (1 H, q, *J* = 6.8 Hz, C*H*), 3.73 (3 H, s, OCH_3) and 1.61 (3 H, d, *J* = 6.8 Hz, CH_3); δ_C (100.59 MHz, $CDCl_3$) 172.15 (*C*=O), 158.63 (Ar 1-*C* or Ar 3-*C*), 158.47 (Ar 1-*C* or Ar 3-*C*), 156.50 (Ar 1'-*C*), 130.09 (Ar 5-

C), 129.57 (Ar 3'-*C*), 123.37 (Ar 4'-*C*), 119.11 (Ar 2'-*C*), 111.50 (Ar 4-*C* or Ar 6-*C*), 109.24 (Ar 4-*C* or Ar 6-*C*), 105.62 (Ar 2-*C*), 72.28 (*C*H), 52.06 (O*C*H_3) and 18.27 (*C*H_3).

(2*S*)-2-(3-phenoxyphenoxy)propanoic acid (96)

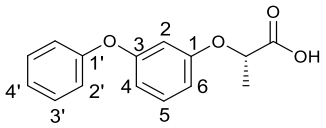

Compound **96** was prepared from methyl (2*S*)-2-(3-phenoxyphenoxy)propanoate **95** (566 mg, 2.08 mmol) using the same procedure as for compound **60** affording a white solid (536 mg, 99.8%) which was found to be *ca.* 99% pure (by ^{1}H NMR) and used in the next step without further purification. $[\alpha]_D^{21}$ +5.38 (*c* 0.56 in $CHCl_3$); ^{1}H and ^{13}C NMR spectra of the compound were consistent with its enantiomer **94** (*vide supra*). δ_H (400.04 MHz; $CDCl_3$) 11.44 (1 H, br s, OH), 7.38-7.30 (2 H, m, Ar 3'-*H*), 7.23 (1 H, t, *J* = 8.0 Hz, Ar 5-*H*), 7.12 (1 H, tt, *J* = 7.2, 1.2 Hz, Ar 4'-*H*), 7.06-7.00 (2 H, m, Ar 2'-*H*), 6.68-6.60 (2 H, m, Ar 4-*H* and Ar 6-*H*), 6.58 (1 H, t, *J* = 2.0 Hz, Ar 2-*H*), 4.77 (1 H, q, *J* = 7.0 Hz, C*H*) and 1.66 (3 H, d, *J* = 7.0 Hz, CH_3); δ_C (100.59 MHz, $CDCl_3$) 178.15 (*C*=O), 158.75 (Ar 3-*C*), 158.44 (Ar 1-*C*), 156.51 (Ar 1'-*C*), 130.34 (Ar 5-*C*), 129.76 (Ar 3'-*C*), 123.64 (Ar 4'-*C*), 119.35 (Ar 2'-*C*), 111.90 (Ar 4-*C* or Ar 6-*C*), 109.28 (Ar 4-*C* or Ar 6-*C*), 105.85 (Ar 2-*C*), 71.96 (*C*H) and 18.33 (*C*H_3).

(2*S*)-2-(3-phenoxyphenoxy)propanoyl-CoA (56)

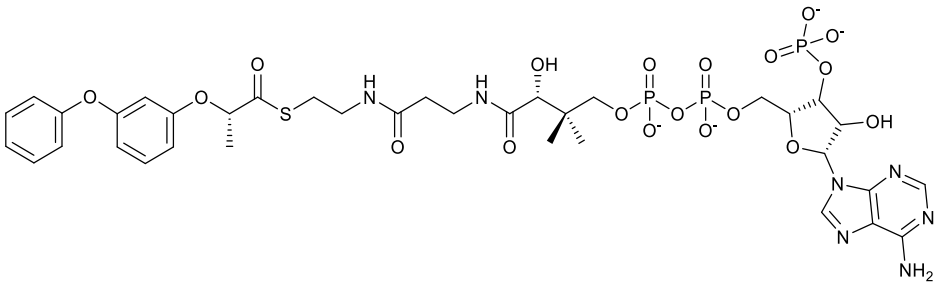

Compound **56** was prepared from (2*S*)-2-(3-phenoxyphenoxy)propanoic acid **96** (90 mg, 0.35 mmol) using the same procedure as for compound **49** to give a white solid (51 mg). δ_H (500.13 MHz, ^2H_2O) 8.55 (1 H, s, adenosine C*H*), 8.25 (1 H, s, adenosine C*H*), 7.31 (2 H, t, *J* = 7.5 Hz, Ar-*H*), 7.21 (1 H, t, *J* =

8.5 Hz, Ar-*H*), 7.11 (1 H, t, *J* = 7.5 Hz, Ar-*H*), 6.93 (2 H, d, *J* = 8.5 Hz, Ar-*H*), 6.68-6.56 (2 H, m, Ar-*H*), 6.46-6.39 (1 H, m, Ar-*H*), 6.09 (1 H, d, *J* = 5.0 Hz, adenosine C*H*), 4.88 (1 H, q, *J* = 7.0 Hz, C*H*), 4.82-4.75 (1 H, m, adenosine C*H*), 4.51 (1 H, br s, adenosine C*H*), 4.18 (2 H, br s, adenosine CH_2), 3.96 (1 H, s, adenosine C*H*), 3.85-3.72 (1 H, m, CoA(OCH_a)), 3.55-3.45 (1 H, m, CoA(OCH_b)), 3.30 (2 H, t, *J* = 6.0 Hz, CoA(CH_2)), 3.23 (2 H, t, *J* = 6.0 Hz, CoA(CH_2)), 3.00-2.85 (2 H, m, CoA(SCH_2)), 2.27 (2 H, t, *J* = 6.5 Hz, CoA(CH_2)), 1.46 (3 H, d, *J* = 6.5 Hz, CCH_3), 0.84 (3 H, s, CoA(CH_3)) and 0.69 (3 H, s, CoA(CH_3)); ESI-MS m/z calcd. for $[M-H]^-$ $C_{36}H_{47}N_7O_{19}P_3S$: 1006.1860, found 1006.1879.

6.2.4 Synthesis of long-chain inhibitors

3-(Hexylsulfanyl)-2-methylpropanoyl-CoA (109)

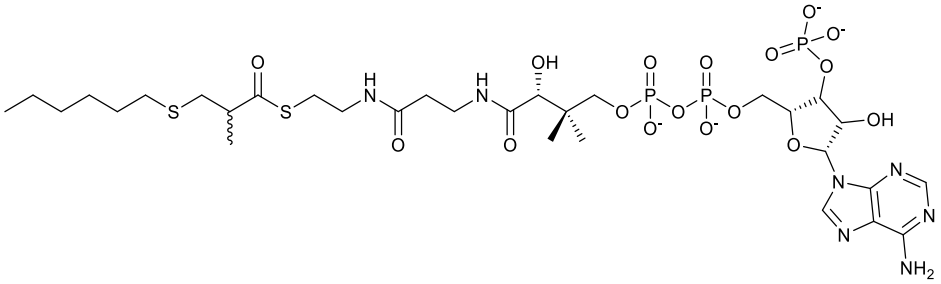

Compound **109** was prepared from 3-(hexylsulfanyl)-2-methylpropanoic acid **107** (90 mg, 0.44 mmol) using the same procedure as for compound **49** to give a white solid (48 mg). δ_H (500.13 MHz, ^2H_2O) 8.61 (1 H, s, adenosine C*H*), 8.30 (1 H, s, adenosine C*H*), 6.14 (1 H, d, *J* = 6.0 Hz, adenosine C*H*), 4.18 (2 H, br s, adenosine CH_2), 3.97 (1 H, s, adenosine C*H*), 3.83-3.72 (1 H, m, CoA(OCH_a)), 3.57-3.45 (1 H, m, CoA(OCH_b)), 3.39 (2 H, t, *J* = 6.5 Hz, CoA(CH_2)), 3.26 (2 H, t, *J* = 6.0 Hz, CoA(CH_2)), 3.02-2.85 (3 H, m, CoA(SCH_2) and C*H*CH_3), 2.75-2.66 (1 H, m, SCH_a), 2.64-2.55 (1 H, m, SCH_b), 2.46 (2 H, t, *J* = 7.5 Hz, SCH_2), 2.37 (2 H, t, *J* = 6.5 Hz, CoA(CH_2)), 1.50-1.39 (2 H, m, CH_2), 1.30-1.07 (9 H, m, 3×CH_2 and CHCH_3), 0.85 (3 H, s, CoA(CH_3)), 0.75 (3 H, t, *J* = 7.0 Hz, CH_2CH_3) and 0.72 (3 H, s, CoA(CH_3)); ESI-MS m/z calcd. for $[M+Na-2H]^-$ $C_{31}H_{52}N_7NaO_{17}P_3S_2$: 974.1971, found 974.1987.

3-(Hexylsulfonyl)-2-methylpropanoyl-CoA (110)

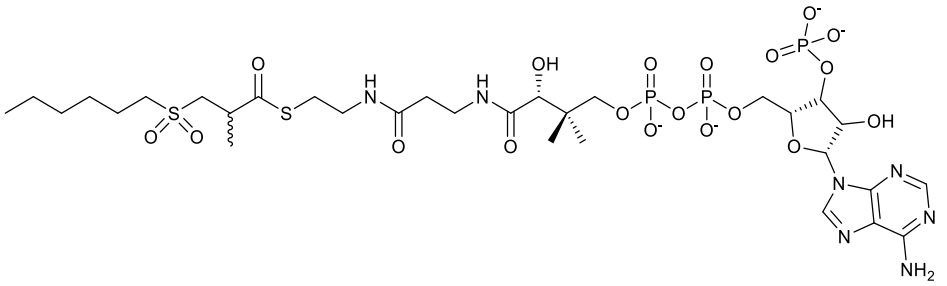

Compound **110** was prepared from 3-(hexylsulfonyl)-2-methylpropanoic acid **108** (53 mg, 0.23 mmol) using the same procedure as for compound **49** to give a white solid (10 mg). δ_H (500.13 MHz, ^2H_2O) 8.62 (1 H, s, adenosine C*H*), 8.37 (1 H, s, adenosine C*H*), 6.16 (1 H, d, *J* = 5.5 Hz, adenosine C*H*), 4.25-4.12 (2 H, m, adenosine CH_2), 3.97 (1 H, s, adenosine C*H*), 3.85-3.75 (1 H, m, CoA(OCH_a)), 3.72-3.60 (1 H, m, C*H*CH$_3$), 3.57-3.48 (1 H, m, CoA(OCH_b)), 3.38 (2 H, t, *J* = 6.5 Hz, CoA(CH_2)), 3.36-3.20 (4 H, m, CoA(CH_2) and CoA(SCH_2)), 3.07-2.90 (2 H, m, CHCH_a and CHCH_b), 3.13 (2 H, t, *J* = 8.0 Hz, OSOCH_2), 2.37 (2 H, t, *J* = 6.5 Hz, CoA(CH_2)), 1.75-1.62 (2 H, m, CH_2), 1.40-1.10 (9 H, m, 3×CH_2 and CHCH_3), 0.87 (3 H, s, CoA(CH_3)), 0.78 (3 H, t, *J* = 7.0 Hz, CH$_2$CH_3) and 0.74 (3 H, s, CoA(CH_3)); ESI-MS m/z calcd. for $[M-H]^-$ $C_{31}H_{53}N_7O_{19}P_3S_2$: 984.2050, found 984.2070.

6.3 Synthesis of known AMACR ligands

6.3.1 Synthesis of (2*R*)-2-methydecanoyl-CoA

(4*R*)-4-benzyl-3-decanoyl-1,3-oxazolidin-2-one (182)

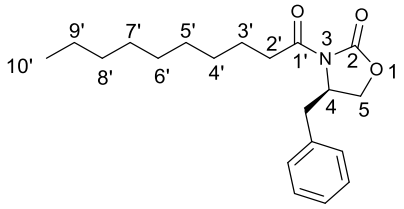

The oxazolidinone **182** was synthesised using the protocol previously described.[1] n-Butyl lithium (2.5 M in hexanes, 5.8 mL, 14.4 mmol) was added dropwise to *R*-4-benzyloxazolidin-2-one (2.50 g, 14.1 mmol) in THF (25 mL) at -78 °C over 15 min. Decanoyl chloride (3.3 mL, 15.6 mmol) was then added and the mixture was stirred at -78 °C for 1 h. It was allowed to reach ambient room temperature and stirred for further 2 h. Saturated $NH_4Cl_{aq.}$ (25 mL) was added to quench the reaction. The mixture was extracted with DCM (3×20

mL). The organic layers were combined, washed with 1.0 M $K_2CO_{3\ aq.}$ (100 mL) and brine (100 mL), dried over $MgSO_4$ and evaporated *in vacuo* to give a colourless oil. The oil crystallised on standing to give a colourless solid (4.66 g, 99.8%) which was found to be >90 % pure (by ^{1}H NMR) and used in the next step without further purification. R_f = 0.41 [10:1 (v/v) PE:EtOAc]. ^{1}H and ^{13}C NMR spectra of the product were consistent with previously reported data.[1] δ_H (400.04 MHz; $CDCl_3$) 7.36-7.14 (5 H, m, Ar-*H*), 4.70-4.60 (1 H, m, 4-*H*), 4.20-4.10 (2 H, m, 5-*H*), 3.27 (1 H dd, *J* = 13.4, 3.2 Hz, ArCH_a), 3.01-2.82 (2 H, m, 2'-H), 2.76 (1 H, dd, *J* = 13.4, 9.6, ArCH_b), 1.73-1.58 (2 H, m, 3'-*H*), 1.42-1.17 (12 H, m, 6×CH_2) and 0.87 (3 H, t, *J* = 6.8 Hz, 10'-*H*); δ_C (100.59 MHz, $CDCl_3$) 173.26 (1'-*C*), 153.32 (2-*C*), 135.25 (Ar-*C*), 129.30 (Ar-*C*), 128.79 (Ar-*C*), 127.17 (Ar-*C*), 66.00 (5-*C*), 55.00 (4-*C*), 37.78 (Ar*C*H_aH_b), 35.41 (2'-C), 31.75 (*C*H_2), 29.33 (*C*H_2), 29.29 (*C*H_2), 29.16 (*C*H_2), 29.02 (*C*H_2), 24.15 (3'-*C*), 22.55 (*C*H_2) and 13.99 (10'-*C*); ESI-MS *m/z* calcd. for $[M+H]^+$ $C_{20}H_{30}NO_3$: 332.2226, found 332.2227.

(4*R*)-4-benzyl-3-[(2*R*)-2-methyldecanoyl]-1,3-oxazolidin-2-one (183)

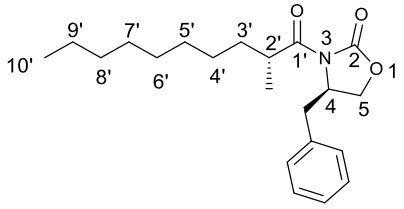

The oxazolidinone **183** was synthesised using the protocol previously described.[1] A solution of (4*R*)-4-benzyl-3-decanoyl-1,3-oxazolidin-2-one **182** (1.60 g, 4.85 mmol) in THF (20 mL) at 0 °C was added dropwise to sodium bis(trimethylsilyl)amide (1.0 M in THF, 5.4 mL, 5.34 mmol) at -78 °C. After stirring the mixture at -78 °C for 1 h, iodomethane (1.5 mL, 24.25 mmol) in THF (0.8 mL) at -78 °C was added. The mixture was stirred for 1 h at -78 °C and allowed to reach ambient temperature. It was further stirred for 30 min at room temperature before being quenched with saturated $NH_4Cl_{\ aq.}$ (20 mL). The mixture was extracted with DCM (3×20 mL). The organic layers were combined, washed with 1.0 M $Na_2SO_{3\ aq.}$, dried over $MgSO_4$ and evaporated *in vacuo* to give a light yellow oil. The crude product was purified by column chromatography [silica, 10:1 (v/v) PE: EtOAc] to afford a colourless oil (1.09

g, 59.0%). R_f = 0.45 [10:1 (v/v) PE:EtOAc]. ^{1}H and ^{13}C NMR spectra of the product were consistent with previously reported data.[1] δ_H (400.04 MHz; $CDCl_3$) 7.35-7.15 (5 H, m, Ar-*H*), 4.70-4.60 (1 H, m, 4-*H*), 4.20-4.09 (2 H, m, 5-*H*), 3.74-3.64 (1 H, m, 2'-H), 3.24 (1 H, dd, *J* = 13.2, 3.2 Hz, ArCH_a), 2.76 (1 H, dd, *J* = 13.2, 9.2, ArCH_b), 1.80-1.65 (1 H, m, 3'-H_a), 1.45-1.35 (1 H, m, 3'-H_b), 1.34-1.18 (15 H, m, 6×CH_2 and CH_3CH) and 0.86 (3 H, t, *J* = 6.8 Hz, 10'-*H*); δ_C (100.59 MHz, $CDCl_3$) 177.17 (1'-*C*), 152.90 (2-*C*), 135.24 (Ar-*C*), 129.31 (Ar-*C*), 128.74 (Ar-*C*), 127.14 (Ar-*C*), 65.84 (5-*C*), 55.18 (4-*C*), 37.72 (Ar*C*H_aH_b), 37.56 (2'-C), 33.28 (3'-C), 31.71 (*C*H_2), 29.52 (*C*H_2), 29.32 (*C*H_2), 29.11 (*C*H_2), 27.12, (*C*H_2), 22.51 (*C*H_2), 17.22 (*C*H_3CH) and 13.97 (10'-*C*); ESI-MS *m/z* calcd. for $[M+H]^+$ $C_{21}H_{32}NO_3$: 346.2382, found 346.2381.

(2*R*)-2-methyldecanoic acid (184)

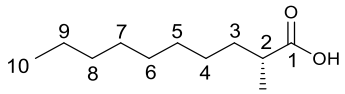

The acid **184** was synthesised using the protocol previously described.[1] $H_2O_{2\ aq.}$ [30% (w/w), 0.94 mL, 8.3 mmol] and lithium hydroxide monohydrate (110 mg, 2.54 mmol) were added to (4*R*)-4-benzyl-3-[(2*R*)-2-methyldecanoyl]-1,3-oxazolidin-2-one **183** (439 mg, 1.27 mmol) in THF (18 mL) and water (6 mL). The mixture was stirred at 0 °C for 3 h. $Na_2SO_{3\ aq.}$ (1.5 M, 10 mL, 15.0 mmol) was added to the reaction mixture, which was then acidified with $HCl_{aq.}$ (1.0 M) to pH 1. The mixture was extracted with DCM (3×20 mL). The organic layers were combined, dried over $MgSO_4$ and evaporated *in vacuo* to afford a mixture of colourless oil and white solid. The crude product was purified by column chromatography [silica, 1:2 (v/v) PE: EtOAc] to afford a colourless oil (160 mg, 67.4%). R_f = 0.84 [2:1 (v/v) PE:EtOAc]. $[\alpha]_D^{20}$ -15.5 (*c* 1.32 in methanol); lit. $[\alpha]_D^{20}$ -16.3 (*c* 1.00 in methanol);[1] ^{1}H and ^{13}C NMR spectra of the product were consistent with previously reported data.[1] δ_H (400.04 MHz; $CDCl_3$) 12.05 (1 H, s, O*H*), 2.50-2.38 (1 H, m, 2-*H*), 1.74-1.60 (1 H, m, 3-H_a), 1.50-1.37 (1 H, m, 3-H_b), 1.37-1.20 (12 H, m, 6×CH_2), 1.16 (3 H, d, *J* = 6.8 Hz, 2-CH_3), and 0.87 (3 H, t, *J* = 6.4 Hz, 10-*H*); δ_C (100.59 MHz, $CDCl_3$) 183.82 (*C*=O), 39.42 (2-*C*), 33.51 (3-*C*), 31.84 (*C*H_2), 29.49(*C*H_2), 29.41 (*C*H_2), 29.24 (*C*H_2), 27.12 (*C*H_2), 22.64 (*C*H_2), 16.77 (2-*C*H_3), and 14.05 (10-*C*); ESI-MS *m/z* calcd. for $[M-H]^-$ $C_{11}H_{21}O_2$: 185.1542, found 185.1560.

(2*R*)-2-methyldecanoyl-CoA (44)

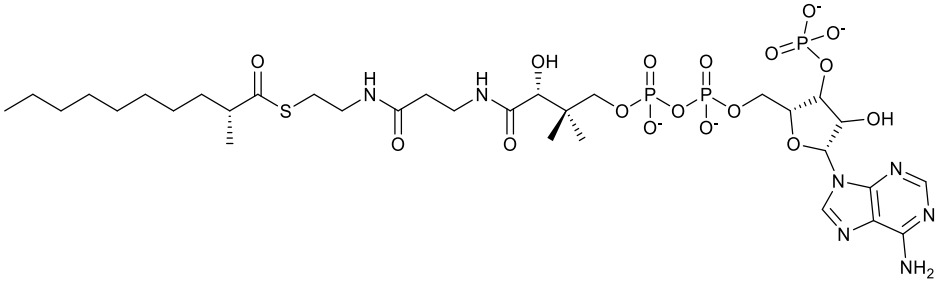

Compound **44** was prepared from (2*R*)-2-methyldecanoic acid **184** (90 mg, 0.48 mmol) using the same procedure as for compound **49** to give a white solid (31 mg). The ^{1}H NMR spectrum of the product was consistent with previously reported data.[1] δ_H (500.13 MHz, $^{2}H_2O$) 8.60 (1 H, s, adenosine C*H*), 8.22 (1 H, s, adenosine C*H*), 6.10 (1 H, d, *J* = 6.0 Hz, adenosine C*H*), 4.52 (1 H, br s, adenosine C*H*), 4.17 (2 H, br s, adenosine CH_2), 3.95 (1 H, s, adenosine C*H*), 3.84-3.70 (1 H, m, CoA(OCH_a)), 3.55-3.45 (1 H, m, CoA(OCH_b)), 3.36 (2 H, t, *J* = 7.0 Hz, CoA(CH_2)), 3.25 (2 H, t, *J* = 6.0 Hz, CoA(CH_2)), 3.00-2.84 (2 H, m, CoA(SCH_2)), 2.70-2.55 (1 H, m, C*H*CH$_3$), 2.34 (2 H, t, *J* = 7.0 Hz, CoA(CH_2)), 1.54-1.41 (1 H, m, CHCH_a), 1.36-1.23 (1 H, m, CHCH_b), 1.20-1.05 (12 H, m, 6×CH_2), 1.01 (3 H, d, *J* = 6.5 Hz, CHCH_3), 0.82 (3 H, s, CoA(CH_3)), 0.74 (3 H, t, *J* = 5.0 Hz, CH$_2$CH_3) and 0.69 (3 H, s, CoA(CH_3)); ESI-MS m/z calcd. for [M+Na-2H]$^-$ $C_{32}H_{54}N_7NaO_{17}P_3S$: 956.2407, found 956.2378.

6.3.2 Synthesis of (2*S*)-2-methydecanoyl-CoA

(4*S*)-4-benzyl-3-decanoyl-1,3-oxazolidin-2-one (185)

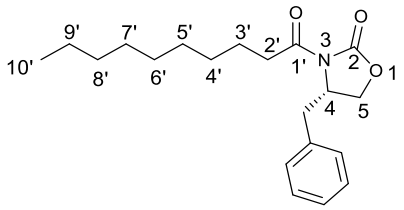

Compound **185** was prepared from *S*-4-benzyloxazolidin-2-one (5.00 g, 28.2 mmol) using the same procedure[1] as compound **182** to give a colourless oil that crystallised on standing to give a colourless solid (9.24 g, 98.8%). The crude product was taken forward to the next step without purification. ^{1}H and ^{13}C NMR spectra of the product were consistent with previously reported data.[1] δ_H (400.04 MHz; $CDCl_3$) 7.34-7.15 (5 H, m, Ar-*H*), 4.69-4.59 (1 H, m, 4-*H*), 4.20-4.09 (2 H, m, 5-*H*), 3.26 (1 H dd, *J* = 13.4, 3.2 Hz, ArCH_a), 3.01-2.81 (2

H, m, 2'-*H*), 2.75 (1 H, dd, *J* = 13.4, 9.6, ArC*H*$_b$), 1.73-1.58 (2 H, m, 3'-*H*), 1.43-1.17 (12 H, m, 6×C*H*$_2$) and 0.87 (3 H, t, *J* = 6.8 Hz, 10'-*H*); δ_C (100.59 MHz, $CDCl_3$) 173.18 (1'-*C*), 153.26 (2-*C*), 135.22 (Ar-*C*), 129.25 (Ar-*C*), 128.73 (Ar-*C*), 127.11 (Ar-*C*), 65.95 (5-*C*), 54.93 (4-*C*), 37.71 (Ar*C*H$_a$H$_b$), 35.35 (2'-C), 31.71 (*C*H$_2$), 29.29 (*C*H$_2$), 29.24 (*C*H$_2$), 29.11 (*C*H$_2$), 28.98 (*C*H$_2$), 24.11 (3'-*C*), 22.50 (*C*H$_2$) and 13.94 (10'-*C*); ESI-MS *m/z* calcd. for $[M+Na]^+$ $C_{20}H_{29}NNaO_3$: 354.2045, found 354.2096.

(4*S*)-4-benzyl-3-[(2*S*)-2-methyldecanoyl]-1,3-oxazolidin-2-one (186)

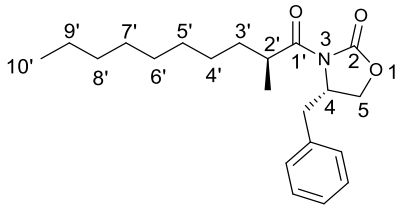

Compound **186** was prepared from (4*S*)-4-benzyl-3-decanoyl-1,3-oxazolidin-2-one **185** (3.65 g, 11.0 mmol) using the same procedure[1] as compound **183**. The crude product was purified by column chromatography [silica, 10:1 (v/v) PE: EtOAc] to afford a colourless oil (2.60 g, 68.4%). ^{1}H and ^{13}C NMR spectra of the product were consistent with previously reported data.[1] δ_H (400.04 MHz; $CDCl_3$) 7.34-7.16 (5 H, m, Ar-*H*), 4.70-4.60 (1 H, m, 4-*H*), 4.20-4.10 (2 H, m, 5-*H*), 3.75-3.62 (1 H, m, 2'-*H*), 3.24 (1 H, dd, *J* = 13.2, 3.2 Hz, ArC*H*$_a$), 2.76 (1 H, dd, *J* = 13.2, 9.6, ArC*H*$_b$), 1.80-1.65 (1 H, m, 3'-*H*$_a$), 1.45-1.35 (1 H, m, 3'-*H*$_b$), 1.34-1.17 (15 H, m, 6×C*H*$_2$ and C*H*$_3$CH) and 0.86 (3 H, t, *J* = 6.8 Hz, 10'-*H*); δ_C (100.59 MHz, $CDCl_3$) 177.16 (1'-*C*), 152.90 (2-*C*), 135.23 (Ar-*C*), 129.30 (Ar-*C*), 128.74 (Ar-*C*), 127.14 (Ar-*C*), 65.84 (5-*C*), 55.17 (4-*C*), 37.72 (Ar*C*H$_a$H$_b$), 37.55 (2'-C), 33.28 (3'-C), 31.71 (*C*H$_2$), 29.52 (*C*H$_2$), 29.32 (*C*H$_2$), 29.11 (*C*H$_2$), 27.12, (*C*H$_2$), 22.51 (*C*H$_2$), 17.21 (*C*H$_3$CH) and 13.96 (10'-*C*); ESI-MS *m/z* calcd. for $[M+H]^+$ $C_{21}H_{32}NO_3$: 346.2382, found 346.2398.

(2*S*)-2-methyldecanoic acid (187)

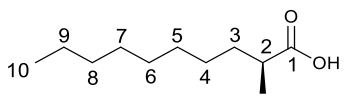

Compound **187** was prepared from (4*S*)-4-benzyl-3-[(2*S*)-2-methyldecanoyl]-1,3-oxazolidin-2-one **186** (1.36 g, 3.94 mmol) using the same procedure[1] as

compound **184**. The crude product was purified by column chromatography [silica, 1:2 (v/v) PE: EtOAc] to afford a colourless oil (665 mg, 90.6%). R_f = 0.84 [2:1 (v/v) PE:EtOAc]. $[\alpha]_D^{20}$ +14.9 (*c* 1.28 in methanol); lit. $[\alpha]_D^{20}$ +15.8 (*c* 1.00 in methanol).[1] ^{1}H and ^{13}C NMR spectra of the product were consistent with previously reported data.[1] δ_H (400.04 MHz; $CDCl_3$) 12.24 (1 H, s, O*H*), 2.50-2.35 (1 H, m, 2-*H*), 1.73-1.58 (1 H, m, 3-H_a), 1.50-1.36 (1 H, m, 3-H_b), 1.36-1.18 (12 H, m, 6×CH_2), 1.16 (3 H, d, *J* = 6.8 Hz, 10'-H, 2-CH_3), and 0.87 (3 H, t, *J* = 6.4 Hz, 10-*H*); δ_C (100.59 MHz, $CDCl_3$) 183.89 (*C*=O), 39.44 (2-*C*), 33.52 (3-*C*), 31.86 (*C*H_2), 29.51(*C*H_2), 29.43 (*C*H_2), 29.26 (*C*H_2), 27.14 (*C*H_2), 22.65 (*C*H_2), 16.74 (2-*C*H_3), and 14.03 (10-*C*); ESI-MS *m/z* calcd. for $[M-H]^-$ $C_{11}H_{21}O_2$: 185.1542, found 185.1553.

(2*S*)-2-methyldecanoyl-CoA (38)

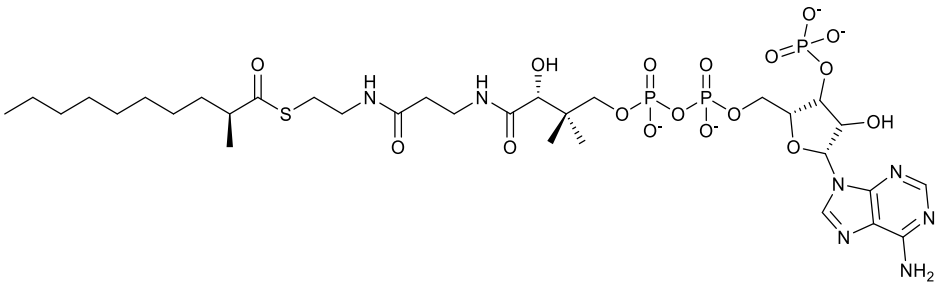

Compound **38** was prepared from (2*S*)-2-methyldecanoic acid **187** (90 mg, 0.48 mmol) using the same procedure as for compound **49** to give a white solid (14 mg). The ^{1}H NMR spectrum of the product was consistent with previously reported data.[1] δ_H (500.13 MHz, ^2H_2O) 8.61 (1 H, s, adenosine C*H*), 8.23 (1 H, s, adenosine C*H*), 6.10 (1 H, d, *J* = 6.5 Hz, adenosine C*H*), 4.52 (1 H, br s, adenosine C*H*), 4.16 (2 H, br s, adenosine CH_2), 3.96 (1 H, s, adenosine C*H*), 3.84-3.70 (1 H, m, CoA(OCH_a)), 3.53-3.44 (1 H, m, CoA(OCH_b)), 3.37 (2 H, t, *J* = 7.0 Hz, CoA(CH_2)), 3.26 (2 H, t, *J* = 5.5 Hz, CoA(CH_2)), 3.00-2.82 (2 H, m, CoA(SCH_2)), 2.70-2.56 (1 H, m, C*H*CH_3), 2.34 (2 H, t, *J* = 7.0 Hz, CoA(CH_2)), 1.53-1.42 (1 H, m, CHCH_a), 1.36-1.25 (1 H, m, CHCH_b), 1.20-1.05 (12 H, m, 6×CH_2), 1.01 (3 H, d, *J* = 6.5 Hz, CHCH_3), 0.82 (3 H, s, CoA(CH_3)), 0.75 (3 H, t, *J* = 6.5 Hz, CH_2CH_3) and 0.69 (3 H, s, CoA(CH_3)); ESI-MS m/z calcd. for $[M+2Na-3H]^-$ $C_{32}H_{53}N_7Na_2O_{17}P_3S$: 978.2227, found 978.2243.

6.3.3 Synthesis of *N*-dodecyl-*N*-methylcarbamoyl-CoA

_N_-dodecyl-_N_-methyl-1_H_-imidazole-1-carboxamide (188)

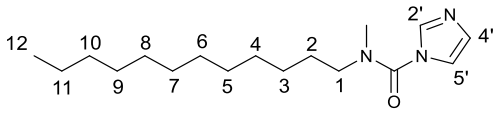

N-Methyldodecylamine (2.00 g, 10.0 mmol) was added dropwise over 15 min to CDI (1.78 g, 11.0 mmol) in DCM (16 mL) at 0 °C. The mixture was allowed to reach room temperature and was then stirred for 24 h. Water (25 mL) was added and the mixture was extracted with DCM (3 x 25 mL). The combined organic extracts were dried over $MgSO_4$ and evaporated *in vacuo* to afford a pale yellow oil. The crude product was purified by column chromatography [silica, 10:1 (v/v) DCM:methanol] to afford a colourless oil (2.33 g, 79.5%). R_f = 0.77 [10:1 (v/v) DCM:methanol]. ^1H and ^{13}C NMR spectra of the product were consistent with previously reported data.[145] δ_H (400.04 MHz; $CDCl_3$) 7.78 (1 H, s, 2'-*H*), 7.12 (1 H, t, *J* = 1.6 Hz, 5'-*H*), 6.99-6.94 (1 H, m, 4'-*H*), 3.30 (2 H, t, *J* = 7.6 Hz, 1-*H*), 2.96 (3 H, s, NC*H*$_3$), 1.60-1.48 (2 H, m, 2-*H*), 1.25-1.17 (18 H, m, 3-*H* to 11-*H*) and 0.77 (3 H, t, *J* = 6.8 Hz, 12-*H*); δ_C (100.59 MHz, $CDCl_3$) 151.33 (*C*=O), 136.55 (2'-*C*), 129.15 (4'-*C*), 117.65 (5'-*C*), 50.33 (1-*C*), 35.93 (N*C*H$_3$), 31.60 (10-*C*), 29.40-28.80 (4-*C* to 9-*C*), 26.96 (2-*C*), 26.27 (3-*C*), 22.38 (11-*C*) and 13.82 (12-*C*); ESI-MS m/z calcd. for $[M+H]^+$ $C_{17}H_{32}N_3O$: 294.2545, found 294.2719.

1-[Dodecyl(methyl)carbamoyl]-3-methyl-1*H*-imidazol-3-ium iodide (189)

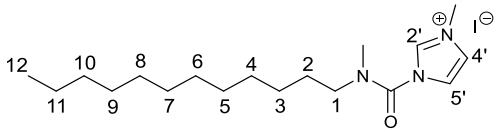

Methyl iodide (1.7 mL, 26.66 mmol) was added to *N*-dodecyl-*N*-methyl-1*H*-imidazole-1-carboxamide **188** (978 mg, 3.33 mmol) in acetonitrile (15 mL), and the resulting mixture was stirred at room temperature overnight. The mixture was filtered and filtrate was evaporated *in vacuo*. The crude gummy yellow solid was purified *via* trituration from petroleum ether to give a gummy dark-yellow solid (972 mg, 67.0%). R_f = 0.53 [10:1 (v/v) DCM:methanol]. ^1H and ^{13}C NMR spectra of the product were consistent with previously reported data.[145]

δ_H (400.04 MHz; $CDCl_3$) 10.18 (1 H, s, 2'-*H*), 7.71 (2 H, s, 4'-*H* and 5'-*H*), 4.25 (3 H, s, N^+CH_3), 3.45 (2 H, t, *J* = 9.0 Hz, 1-*H*), 3.26 (3 H, s, NCH_3), 1.71-1.58 (2 H, m, 2-*H*), 1.35-1.10 (18 H, m, 3-*H* to 11-*H*) and 0.84 (3 H, t, *J* = 6.5 Hz, 12-*H*); δ_C (100.59 MHz, $CDCl_3$) 146.74 (*C*=O), 136.77 (2'-*C*), 124.02 (4'-*C*), 121.02 (5'-*C*), 51.50 (1-*C*), 38.04 (NCH_3 and N^+CH_3), 31.75-22.53 (*C*-2 to *C*-11) and 13.98 (12-*C*); ESI-MS m/z calcd. for $[M]^+$ $C_{18}H_{34}N_3O$: 308.2702, found 308.2778; ESI-MS m/z calcd. for $[M]^-$ I: 126.9045, found 126.9054.

N-Dodecyl-*N*-methylcarbamoyl-CoA (30)

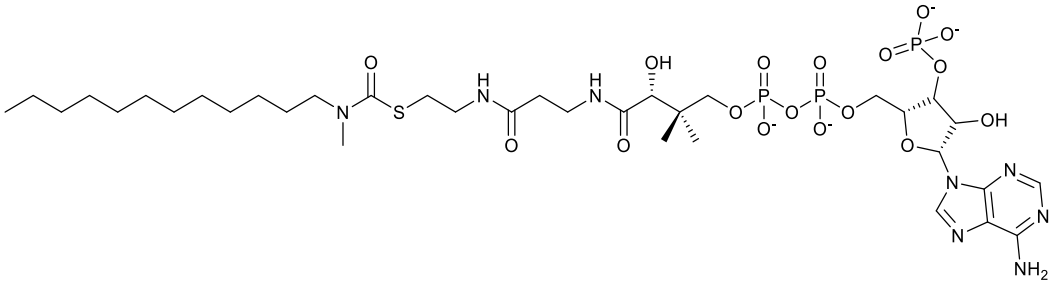

1-[Dodecyl(methyl)carbamoyl]-3-methyl-1*H*-imidazol-3-ium iodide **189** (40 mg, 0.09 mmol) was dissolved in THF (1 mL) at room temperature. $NaHCO_{3\,aq.}$ (1 mL, 0.10 M), followed by CoA-Li_3 (17 mg, 0.02 mmol) was added to the solution. The resulting mixture was stirred at ambient temperature under an argon atmosphere for 18 h. The volatile organics were evaporated *in vacuo* and the remaining solution was acidified to *ca.* pH 3 by addition of 1.0 M HCl_{aq}. The mixture was diluted with water (2 mL) and extracted with EtOAc (5×3 mL). The crude aqueous product was freeze-dried and purified by solid phase extraction to afford a white solid (7 mg). δ_H (500.13 MHz, ^2H_2O) 8.62 (1 H, s, adenosine C*H*), 8.35 (1 H, s, adenosine C*H*), 6.15 (1 H, d, *J* = 6.0 Hz, adenosine C*H*), 4.53 (1 H, br s, adenosine C*H*), 4.18 (2 H, br s, adenosine CH_2), 3.97 (1 H, s, adenosine C*H*), 3.84 (3 H, s,NCH_3), 3.81-3.76 (1 H, m, CoA(OCH_a)), 3.53-3.47 (1 H, m, CoA(OCH_b)), 3.39 (2 H, t, *J* = 6.5 Hz, NCH_2), 3.35-3.22 (3 H, m, CoA(C*H*OH)) and CoA(CH_2)), 2.95-2.82 (4 H, m, CoA(CH_2) and CoA(SCH_2)), 2.38 (2 H, t , *J* = 6.5 Hz, CoA(CH_2)), 1.55-1.35 (2 H, m, CH_2), 1.25-1.05 (18 H, m, 9×CH_2), 0.87 (3 H, s, CoA(CH_3)), 0.76 (3 H, t, *J* = 7.0 Hz, CH_2CH_3) and 0.72 (3 H, s, CoA(CH_3)); ESI-MS m/z calcd. for $[M+2Na-3H]^-$ $C_{35}H_{60}N_8Na_2O_{17}P_3S$: 1035.2805, found 1035.3050.

6.3.4 Synthesis of acyl-CoA esters of 2-APA

Fenoprofenoyl-CoA (13)

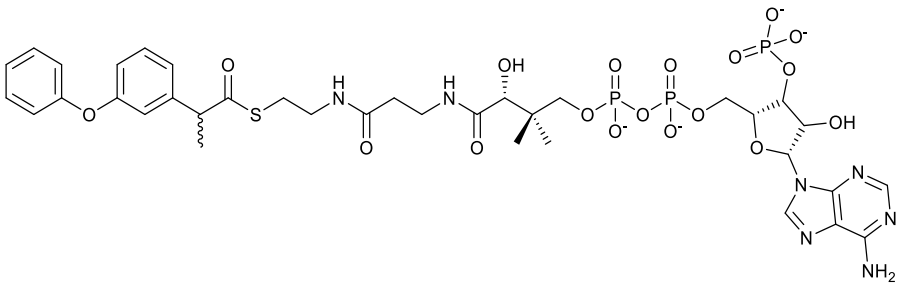

Fenoprofen calcium salt hydrate (1.00 g, 1.91 mmol) was treated with excess 1.0 M HCl $_{aq.}$ and was extracted with chloroform to obtain fenoprofen (acid). Compound **13** was prepared from fenoprofen (acid) (93 mg, 0.38 mmol) using the same procedure as for compound **49** to give a white solid (48 mg). The ^{1}H NMR spectrum of the product was consistent with previously reported data.[2] δ_H (500.13 MHz, $^{2}H_2O$) 8.57 (1 H, s, adenosine C*H*), 8.28 (1 H, s, adenosine C*H*), 7.32-7.18 (3 H, m, Ar-*H*), 7.05 (1 H, t, *J* = 7.5 Hz, Ar-*H*), 7.00 (1 H, d, *J* = 7.5 Hz, Ar-*H*), 6.94-6.78 (4 H, m, Ar-*H*), 6.09 (1 H, d, *J* = 5.0 Hz, adenosine C*H*), 4.49 (1 H, br s, adenosine C*H*), 4.15 (2 H, br s, adenosine CH_2), 4.00-3.85 (2 H, m, C*H*CH$_3$ and CoA(OCH_a)), 3.81-3.71 (1 H, m, CoA(OCH_b)), 3.52-3.42 (1 H, m, CoA(OHC*H*)), 3.30-3.10 (4 H, m, 2×CoA(CH_2)), 2.95-2.89 (1 H, m, CoA(SC*H*)), 2.87-2.78 (1 H, m, CoA(SC*H*)), 2.26-2.07 (2 H, m, CoA(CH_2)), 1.33 (3 H, d, *J* = 6.5 Hz, CHCH_3), 0.82 (3 H, s, CoA(CH_3)) and 0.66 (3 H, s, CoA(CH_3)); ESI-MS m/z calcd. for $[M+4Na-3H]^+$ $C_{36}H_{45}N_7Na_4O_{18}P_3S$: 1080.1345, found 1080.1340.

Ibuprofenoyl-CoA (119)

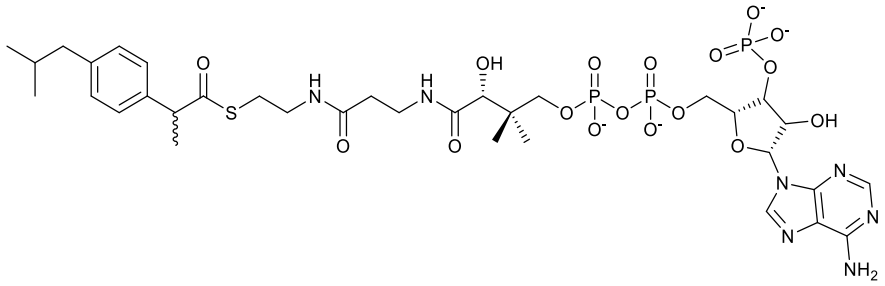

Compound **119** was prepared from ibuprofen (90 mg, 0.43 mmol) using the same procedure as for compound **49** to give a white solid (49 mg). The ^{1}H NMR spectrum of the product was consistent with previously reported data.[2] δ_H (500.13 MHz, $^{2}H_2O$) 8.58 (1 H, s, adenosine C*H*), 8.31 (1 H, s, adenosine C*H*), 7.13 (2 H, d, *J* = 7.8 Hz, Ar-*H*), 7.06 (2 H, d, *J* = 7.8 Hz, Ar-*H*), 6.11 (1 H, d, *J* = 5.5 Hz, adenosine C*H*), 4.50 (1 H, br s, adenosine C*H*), 4.16 (2 H, br s, adenosine CH_2), 3.95-3.85 (2 H, m, C*H*CH_3 and CoA(OCH_a)), 3.82-3.71 (1 H, m, CoA(OCH_b)), 3.53-3.43 (1 H, m, CoA(OHC*H*)), 3.28-3.13 (4 H, m, 2×CoA(CH_2)), 2.99-2.88 (1 H, m, CoA(SC*H*)), 2.87-2.78 (1 H, m, CoA(SC*H*)), 2.32 (1 H, d, *J* = 6.7 Hz, CH_2CH(CH_3)$_2$), 2.20-2.08 (2 H, m, CoA(CH_2)), 1.66 (1 H, nonet, *J* = 6.7 Hz, CH_2C*H*(CH_3)$_2$), 1.35 (3 H, d, *J* = 7.0 Hz, CHCH_3), 0.83 (3 H, s, CoA(CH_3)), 0.72 (6 H, d, *J* = 6.7 Hz, CH_2CH(CH_3)$_2$) and 0.69 (3 H, s, CoA(CH_3)); ESI-MS m/z calcd. for $[M+Na-2H]^-$ $C_{34}H_{50}N_7NaO_{17}P_3S$: 976.2094, found 976.2569.

Ketoprofenoyl-CoA (120)

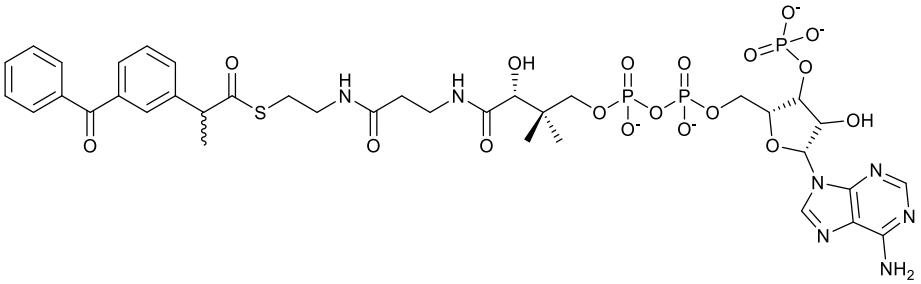

Compound **120** was prepared from ketoprofen (90 mg, 0.35 mmol) using the same procedure as for compound **49** to give a white solid (37 mg). The ^{1}H NMR spectrum of the product was consistent with previously reported data.[2] δ_H (500.13 MHz, $^{2}H_2O$) 8.57 (1 H, s, adenosine C*H*), 8.30 (1 H, d, *J* = 2.0 Hz, adenosine C*H*), 7.75-7.55 (6 H, m, Ar-*H*), 7.52-7.38 (3 H, m, Ar-*H*), 6.09 (1 H, d, *J* = 5.5 Hz, adenosine C*H*), 4.17 (1 H, br s, adenosine C*H*), 4.11-4.02 (1 H,

m, C*H*CH_3), 3.94 (1 H, s, adenosine C*H*), 3.82-3.74 (1 H, m, CoA(OCH_a)), 3.55-3.45 (1 H, m, CoA(OCH_b)), 3.23 (4 H, t, *J* = 6.0 Hz, 2×CoA(CH_2)), 3.03-2.94 (1 H, m, CoA(SC*H*)), 2.93-2.84 (1 H, m, CoA(SC*H*)), 2.25-2.11 (2 H, m, CoA(CH_2)), 1.46-1.40 (3 H, 2×d overlapping, *J* = 7.0 Hz, CHCH_3), 0.84 (3 H, s, CoA(CH_3)) and 0.69 (3 H, s, CoA(CH_3)); ESI-MS m/z calcd. for $[M+Na-2H]^-$ $C_{37}H_{46}N_7NaO_{18}P_3S$: 1024.1731, found 1024.1831.

Naproxenoyl-CoA (121)

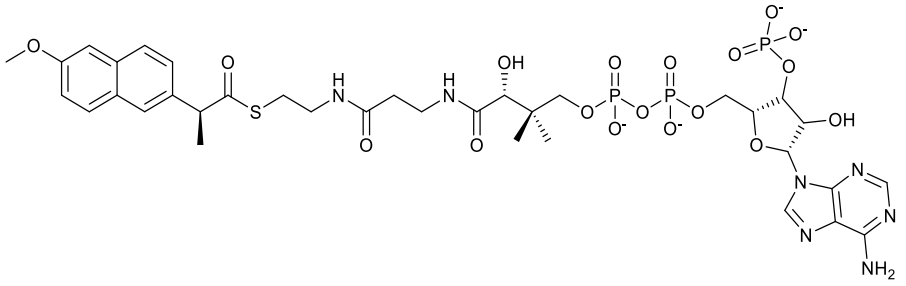

Compound **121** was prepared from naproxen (90 mg, 0.39 mmol) using the same procedure as for compound **49** to give a white solid (17 mg). δ_H (500.13 MHz, ^2H_2O) 8.43 (1 H, s, adenosine C*H*), 8.00 (1 H, s, adenosine C*H*), 7.62-7.52 (2 H, m, Ar-*H*), 7.36 (1 H, s, Ar-*H*), 7.28 (1 H, d, *J* = 8.5 Hz, Ar-*H*), 7.05 (1 H, s, Ar-*H*), 6.98 (1 H, d, *J* = 9.0 Hz, Ar-*H*), 5.95 (1 H, d, *J* = 5.0 Hz, adenosine C*H*), 4.50 (1 H, br s, adenosine C*H*), 4.17 (2 H, br s, adenosine CH_2), 4.08 (1 H, q, *J* = 7.0 Hz, C*H*CH_3), 3.88 (1 H, s, adenosine C*H*), 3.80 (3 H, s, OCH_3), 3.77-3.69 (1 H, m, CoA(OCH_a)), 3.48-3.39 (1 H, m, CoA(OCH_b)), 3.27-3.16 (2 H, m, CoA(CH_2)), 3.12-3.01 (2 H, m, CoA(CH_2)), 3.01-2.93 (1 H, m, CoA(SC*H*)), 2.89-2.79 (1 H, m, CoA(SC*H*)), 2.10-1.95 (2 H, m, CoA(CH_2)), 1.48 (3 H, d, *J* = 7.0 Hz, CHCH_3), 0.77 (3 H, s, CoA(CH_3)) and 0.63 (3 H, s, CoA(CH_3)); ESI-MS m/z calcd. for $[M+2Na-3H]^-$ $C_{35}H_{45}N_7Na_2O_{18}P_3S$: 1022.1550, found 1022.1699.

Flurbiprofenoyl-CoA (122)

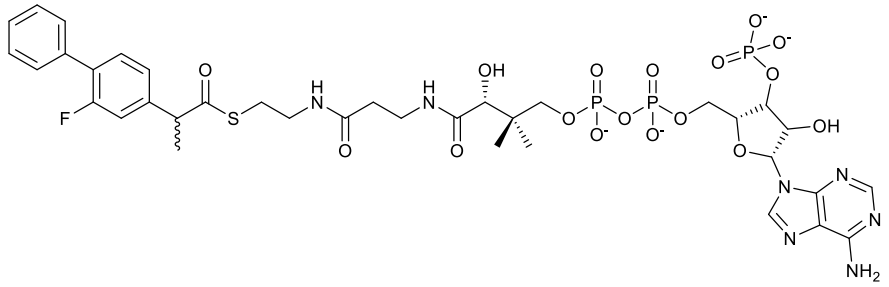

Compound **122** was prepared from flurbiprofen (90 mg, 0.37 mmol) using the same procedure as for compound **49** to give a white solid (13 mg). The ^{1}H NMR spectrum of the product was consistent with previously reported data.[2] δ_H (500.13 MHz, $^{2}H_2O$) 8.61 (1 H, s, adenosine C*H*), 8.55 (1 H, s, adenosine C*H*), 7.51-7.29 (6 H, m, Ar-*H*), 7.22-7.10 (2 H, m, Ar-*H*), 6.11-6.04 (1 H, m, adenosine C*H*), 4.17 (2 H, br s, adenosine CH_2), 4.10-4.01 (1 H, m, C*H*CH$_3$), 3.92 (1 H, d, *J* = 5.5 Hz, adenosine C*H*), 3.81-3.75 (1 H, m, CoA(OCH_a)), 3.53-3.45 (1 H, m, CoA(OCH_b)), 3.32-3.16 (4 H, m, 2×CoA(CH_2)), 3.08-2.98 (1 H, m, CoA(SC*H*)), 2.95-2.85 (1 H, m, CoA(SC*H*)), 2.24-2.12 (2 H, m, CoA(CH_2)), 1.46 (3 H, d, *J* = 7.0 Hz, CHCH_3), 0.82 (3 H, s, CoA(CH_3)) and 0.67 (3 H, s, CoA(CH_3)); ESI-MS m/z calcd. for [M+2Na-3H]$^-$ $C_{36}H_{41}FN_7Na_2O_{17}P_3S$: 1036.1507, found 1036.1673.

6.24 Synthesis of (2S,3*S*)-3-fluoro-2-methyldecanoyl-CoA (4*S*)-4-benzyl-3-[(2*S*,3*R*)-3-hydroxy-2-methyldecanoyl]-1,3-oxazolidin-2-one (190)

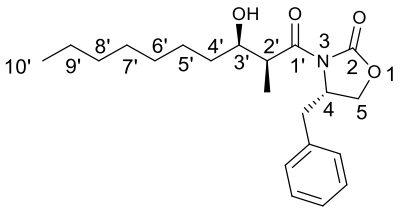

The oxazolidinone **190** was synthesised using the protocol previously described.[3, 143] (*S*)-(+)-4-benzyl-3-propionyl-2-oxazolidinone (3.00 g, 12.9 mmol) in DCM (30 mL) was cooled to -78°C. Dibutylboron triflate in DCM (1.00 M, 13.0 mL, 12.9 mmol) and diisopropylethylamine (2.3 mL, 13.2 mmol) were added to the solution, and the resulting mixture was stirred for 30 min. Octanal (1.4 mL, 9.2 mmol) was dissolved in DCM (9 mL) and the solution was added dropwise to the reaction mixture at -78 °C. It was stirred for 30 min at -78 °C,

allowed to reach room temperature and further stirred for 2 h. 0.1 M NaH_2PO_4-NaOH, pH 7.0 (100 mL) was slowly added to the mixture to quench the reaction. The organic layer was washed with $HCl_{aq.}$ (1.0 M, 100 mL), saturated $NaHCO_{3\ aq.}$ (100 mL) and brine (100 mL), dried over $MgSO_4$ and evaporated *in vacuo*. The crude product was purified by column chromatography [silica, gradient elution with 10:1, 6:1 (v/v) PE:EtOAc] to give a colourless oil (2.53 g, 76.2%) that eluted in 6:1 (v/v) PE:EtOAc. R_f=0.25 [1:1 (v/v) PE:Et_2O]; $[\alpha]_D^{21}$ +51.4 (*c* 0.74 in $CHCl_3$); IR ν_{max}/cm^{-1} 3517 (OH), 1780 (C=O) and 1692 (C=O); δ_H (500.13 MHz; $CDCl_3$) 7.26-7.07 (5 H, m, Ar-*H*), 4.65-4.55 (1 H, m, 4-*H*), 4.16-4.05 (2 H, m, 5-*H*), 3.89-3.80 (1 H, m, 3'-*H*), 3.68 (1 H, qd *J* = 7.0, 3.0 Hz, 2'-*H*), 3.14 (1 H, dd, *J* = 13.0, 3.0 Hz, ArCH_a), 2.92 (1 H, s, O*H*), 2.70 (1 H, dd, *J* = 13.0, 9.0 Hz, ArCH_b), 1.50-1.10 (15 H, m, 6×CH_2 and CH_3CH) and 0.79 (3 H, t, *J* = 6.5 Hz, 10'-*H*); δ_C (125.76 MHz, $CDCl_3$) 177.23 (1'-*C*), 152.87 (2-*C*), 134.92 (Ar-*C*), 129.24 (Ar-*C*), 128.73 (Ar-*C*), 127.18 (Ar-*C*), 71.35 (3'-*C*), 65.96 (5-*C*), 54.91 (4-*C*), 42.02 (2'-*C*), 37.53 (Ar*C*H_aH_b), 33.77 (*C*H_2), 31.62 (*C*H_2), 29.35 (*C*H_2), 29.05 (*C*H_2), 25.84 (*C*H_2), 22.45 (*C*H_2), 13.90 (*C*H_3CH) and 10.31 (10'-*C*); ESI-MS *m/z* calcd. for $[M+Na]^+$ $C_{21}H_{31}NNaO_4$: 384.2151, found 384.2134.

(4*S*)-4-benzyl-3-[(2*R*,3*S*)-3-fluoro-2-methyldecanoyl]-1,3-oxazolidin-2-one (191)

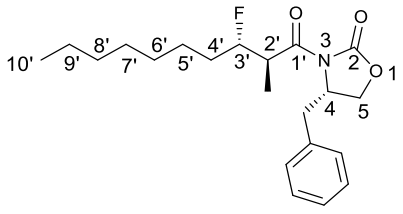

The oxazolidinone **191** was synthesised using the protocol previously described.[3, 143] DAST (0.5 mL, 3.87 mmol) in DCM (10 mL) was added dropwise to (4*S*)-4-benzyl-3-[(2*S*,3*R*)-3-hydroxy-2-methyldecanoyl]-1,3-oxazolidin-2-one **190** (1.40 g, 3.87 mmol) in DCM (20 mL) at -78°C. The mixture was stirred at -78 °C for 2 h, then allowed to reach room temperature and stirred for a further 2 h. Water (50 mL) was added slowly to the reaction mixture and it was extracted with DCM (50 mL). The organic layer was washed with saturated $NaHCO_{3\ aq.}$ (100 mL), brine (100 mL), dried over $MgSO_4$ and

evaporated *in vacuo* to afford a colourless oil. The crude product was purified by column chromatography [silica, 30:1 (v/v) PE:EtOAc] to give a colourless oil (490 mg, 35.0%). R_f = 0.63 [5:1 (v/v) PE:EtOAc]; $[\alpha]_D^{21}$ +49.2 (*c* 0.63 in $CHCl_3$); IR ν_{max}/cm^{-1} 1782 (C=O) and 1700 (C=O); δ_H (500.13 MHz; $CDCl_3$) 7.27-7.06 (5 H, m, Ar-*H*), 4.76-4.57 (2 H, m, 4-*H* and 3'-*H*), 4.15-3.96 (3 H, m, 5-*H* and 2'-*H*), 3.17 (1 H, dd, *J* = 13.5, 3.5 Hz, ArCH_a), 2.72 (1 H, dd, *J* = 13.5, 9.5 Hz, ArCH_b), 1.70-1.14 (12 H, m, 6×CH_2), 1.10 (3 H, d, *J* = 7.0 Hz, CH_3CH) and 0.80 (3 H, t, *J* = 6.5 Hz, 10'-*H*); δ_C (125.76 MHz, $CDCl_3$) 174.37 (d, *J* = 2.8 Hz, 1'-*C*), 153.12 (2-*C*), 135.25 (Ar-*C*), 129.47 (Ar-*C*), 128.93 (Ar-*C*), 127.37 (Ar-*C*), 94.89 (d, *J* = 169.8 Hz, 3'-*C*), 66.19 (5-*C*), 55.38 (4-*C*), 42.03 (d, *J* = 20.9 Hz, 2'-*C*), 37.85 (ArCH_aH_b), 32.04 (d, *J* = 20.9 Hz, CH_2), 31.79 (CH_2), 29.37 (CH_2), 29.16 (CH_2), 24.57 (d, *J* = 2.8 Hz, CH_2), 22.64 (CH_2), 14.10 (10'-*C*) and 13.62 (d, *J* = 8.5 Hz, 2'-CH_3); δ_F (470.59 MHz, $CDCl_3$) -179.67; ESI-MS m/z calcd. for $[M+Na]^+$ $C_{21}H_{30}FNNaO_3$: 386.2107, found 386.2126.

(2*R*,3*S*)-3-Fluoro-2-methyldecanoic acid (192)

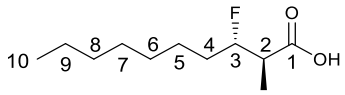

The acid **192** was synthesised using the protocol previously described.[3, 143] $H_2O_{2\ aq.}$ [30% (w/w), 0.7 mL, 6.2 mmol] and LiOH (62 mg, 2.60 mmol) were added to (4*S*)-4-benzyl-3-[(2*R*,3*S*)-3-fluoro-2-methyldecanoyl]-1,3-oxazolidin-2-one **191** (472 mg, 1.3 mmol) in THF (14 mL) at 0 °C. The mixture was stirred for 20 h and saturated $Na_2SO_{3\ aq.}$ (14 mL) was added to quench the reaction. THF was evaporated and the mixture was acidified with 1.0 M $HCl_{aq.}$ to pH 1 and extracted with DCM (100 mL). The organic layer was washed with water (75 mL) and brine (75 mL), dried over $MgSO_4$ and evaporated *in vacuo* to afford a colourless oil. The crude product was purified by column chromatography [silica, 5:1 (v/v) PE: EtOAc] to afford a white solid (245 mg, 92.4%). R_f = 0.40 [5:1 (v/v) PE:EtOAc]; melting point 64-65 °C; $[\alpha]_D^{21}$ -7.8 (*c* 0.51 in $CHCl_3$); IR ν_{max}/cm^{-1} 2925 (OH) and 1693 (C=O); δ_H (400.04 MHz; $CDCl_3$) 10.89 (1 H, br s, O*H*), 4.58-4.50 (1 H, m, 3-*H*), 2.58-2.52 (1 H, m, 2-*H*), 1.75-1.23 (12 H, m, 6×CH_2), 1.20 (3 H, d, *J* = 7.2 Hz, CH_3CH) and 0.88 (3 H, t, *J* = 6.8 Hz, 10-*H*); δ_C (100.59 MHz, $CDCl_3$) 180.02 (d, *J* = 5.6 Hz, *C*=O), 94.28

(d, *J* = 172.2 Hz, 3-*C*), 44.37 (d, *J* = 22.0 Hz, 2-*C*), 31.74 (d, *J* = 21.1 Hz, *C*H_2), 31.74 (*C*H_2), 29.30 (*C*H_2), 29.12 (*C*H_2), 24.82 (d, *J* = 3.0 Hz, *C*H_2), 22.61 (*C*H_2), 14.05 (10-*C*) and 12.56 (d, *J* = 6.6 Hz, 2-*C*H_3); δ_F (470.59 MHz, $CDCl_3$) -181.94; ESI-MS m/z calcd. for $[M-H]^-$ $C_{11}H_{20}FO_2$: 203.1447, found 203.1449.

(2S,3*S*)-3-Fluoro-2-methyldecanoyl-CoA (147)

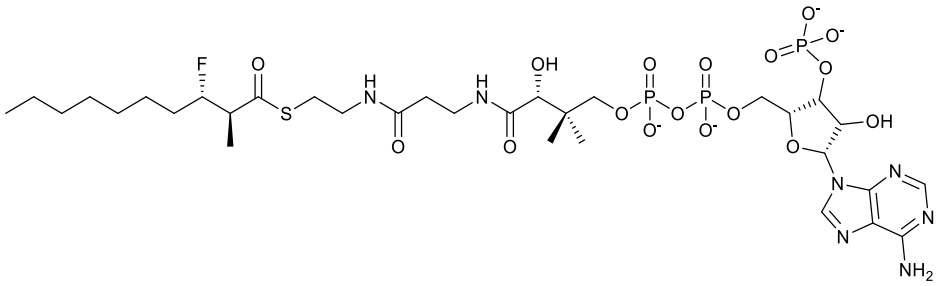

Compound **147** was prepared from (2*R*,3*S*)-3-fluoro-2-methyldecanoic acid **192** (30 mg, 0.15 mmol) using the same procedure as for compound **49** to give a white solid (14 mg). δ_H (500.13 MHz, ^2H_2O) 8.63 (1 H, s, adenosine C*H*), 8.38 (1 H, s, adenosine C*H*), 6.16 (1 H, d, *J* = 6.0 Hz, adenosine C*H*), 4.30-4.10 (2 H, br s, adenosine C*H*$_2$), 3.97 (1 H, s, adenosine C*H*), 3.85-3.72 (1 H, m, CoA(OC*H*$_a$)), 3.58-3.47 (1 H, m, CoA(OC*H*$_b$)), 3.39 (2 H, t, *J* = 6.5 Hz, CoA(C*H*$_2$)), 3.29 (2 H, t, *J* = 6.0 Hz, CoA(C*H*$_2$)), 3.08-2.90 (3 H, m, CoA(SC*H*$_2$) and C*H*CH_3), 2.36 (2 H, t, *J* = 6.5 Hz, CoA(C*H*$_2$)), 1.68-1.44 (2 H, m, C*H*$_a$ and C*H*$_b$), 1.39-1.12 (10 H, m, 5×C*H*$_2$), 1.07 (3 H, d, *J* = 7.0 Hz, CHC*H*$_3$), 0.87 (3 H, s, CoA(C*H*$_3$)) and 0.81-0.70 (6 H, m, CH_2C*H*$_3$ and CoA(C*H*$_3$)); δ_F (470.59 MHz, ^2H_2O) -181.11; ESI-MS m/z calcd. for $[M-2H]^{2-}$ $C_{32}H_{53}FN_7O_{17}P_3S$: 475.6208, found 475.6220.

6.5 Synthesis of substrate for fluoride elimination assay to evaluate potential AMACR inhibitors

(2*R*,3*R*)-3-Fluoro-2-methyldecanoyl-CoA (114)

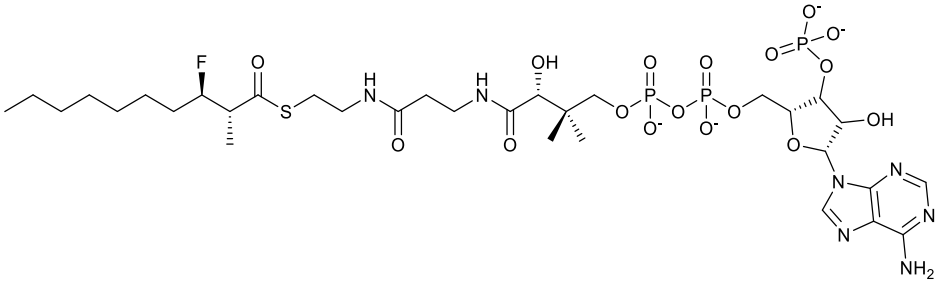

Compound **114** was prepared from (2*S*,3*R*)-3-fluoro-2-methyldecanoic acid (30 mg, 0.15 mmol) using the same procedure as for compound **49** to give a white solid (18 mg). δ_H (500.13 MHz, ^2H_2O) 8.43 (1 H, s, adenosine C*H*), 8.13 (1 H, s, adenosine C*H*), 6.04 (1 H, d, *J* = 6.5 Hz, adenosine C*H*), 4.55-4.51 (1 H, m, C*H*F), 4.49 (1 H, br s, adenosine C*H*), 4.11 (2 H, br s, adenosine CH_2), 3.90 (1 H, s, adenosine C*H*), 3.77-3.67 (1 H, m, CoA(OCH_a)), 3.47-3.38 (1 H, m, CoA(OCH_b)), 3.32 (2 H, t, *J* = 6.5 Hz, CoA(CH_2)), 3.22 (2 H, t, *J* = 5.0 Hz, CoA(CH_2)), 2.98-2.80 (3 H, m, CoA(SCH_2) and C*H*CH_3), 2.29 (2 H, t, *J* = 6.5 Hz, CoA(CH_2)), 1.58-1.35 (2 H, m, CH_a and CH_b), 1.30-1.04 (10 H, m, 5×CH_2), 1.00 (3 H, d, *J* = 7.0 Hz, CHCH_3), 0.77 (3 H, s, CoA(CH_3)), 0.71 (3 H, t, *J* = 6.5 Hz, CH_2CH_3) and 0.63 (3 H, s, CoA(CH_3)); δ_F (470.59 MHz, ^2H_2O) -181.15; ESI-MS m/z calcd. for $[M-H]^-$ $C_{32}H_{54}FN_7O_{17}P_3S$: 952.2494, found 952.2528.

6.6 Synthesis of the fluoride sensor

3',6'-Bis((*tert*-butyldimethylsilyl)oxy)-3*H*-spiro[2-benzofuran-1,9'-xanthen]-3-one (128)

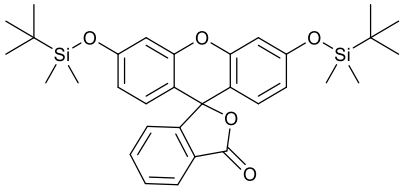

2,6-Dimethylpyridine (2.2 mL, 18.8 mmol) was added to a solution of fluorescein (2.50 g, 7.52 mmol) in DCM (40 ml). *tert*-Butyldimethylsilyl triflate (4.6 ml, 20.0 mmol) was added dropwise and the mixture was stirred for 4.5 h at room temperature. Water (100 mL) was added and the mixture was extracted with DCM (3 x 50 mL). The combined organic extracts were washed

with brine (100 mL), dried over $MgSO_4$ and evaporated *in vacuo* to afford a dark brown oil. The crude product was purified by column chromatography [silica, 30:1 (v/v) PE: EtOAc] to afford a white solid (2.79 g, 66.2%). R_f = 0.82 [4:1 (v/v) PE:EtOAc]. ^1H and ^{13}C NMR spectra were consistent with previously reported data.[191] δ_H (400.04 MHz; $CDCl_3$) 8.01 (1 H, d, *J* = 7.6 Hz, Ar-*H*), 7.66 (1 H, td, *J* = 7.6, 1.2 Hz, Ar-*H*), 7.60 (1 H, td, *J* = 7.6, 1.2 Hz, Ar-*H*), 7.18 (1 H, d, *J* = 7.6 Hz, Ar-*H*), 6.73 (2 H, d, *J* = 2.4 Hz, Ar-*H*), 6.64 (2 H, d, *J* = 8.8 Hz, Ar-*H*), 6.52 (2 H, dd, *J* = 8.8, 2.4 Hz, Ar-*H*), 0.98 (18 H, s, 2×(C*H*$_3$)$_3$), 0.23 (6 H, s, 2×Si-C*H*$_3$) and 0.22 (6 H, s, 2×Si-C*H*$_3$); δ_c (100.59 MHz; $CDCl_3$) 169.4 (*C*=O), 157.5 (Ar-*C*), 153.1 (Ar-*C*), 152.3 (Ar-*C*), 134.9 (Ar-*C*), 129.6 (Ar-*C*), 128.9 (Ar-*C*), 126.8 (Ar-*C*), 124.9 (Ar-*C*), 123.9 (Ar-*C*), 116.5(Ar-*C*), 112.0 (Ar-*C*), 107.6 (Ar-*C*), 83.2 (*C*OC), 25.6 (C*C*H$_3$), 18.1 (Si*C*) and -4.5 (Si-*C*H$_3$); ESI-MS *m/z* calcd. for $[M+H]^+$ $C_{32}H_{41}O_5Si_2$: 561.2493, found 561.2594.

6.7 Deuterium wash-in assay to measure exchange of potential AMACR inhibitors

The deuterium wash-in assay was performed using the protocol previously described.[1, 2, 184] Acyl-CoA esters were dissolved in ^2H_2O and their concentrations were determined by ^1H NMR.[2] The vortex-mixed acyl-CoA ester (100 µM final concentration in the assay) was incubated with human recombinant AMACR (0.18 mg mL^{-1}; 3.82 µM) in 50 mM NaH_2PO_4-NaOH, pH 7.4 and ^2H_2O in a final volume of 550 µL. There was *ca.* 85% (v/v) ^2H_2O in the reaction mixture. The assay mixture was incubated at 30°C for 1 h before the enzyme was heat-inactivated at 60 °C for 30 min. *R*-2-methyldecanoyl-CoA was used as a positive control and heat-inactivated AMACR was used as a negative control. ^1H NMR (^2H_2O, 500.13 MHz) was used to analyse α-proton exchange by quantifying the conversion of the 2-methyl peak from a doublet (at *ca.* 1.34 ppm) to an unresolved single peak (at *ca.* 1.33 ppm).

6.8 Fluoride elimination

6.8.1 Fluoride elimination assay (trial/initial protocol)

The vortex-mixed (2*R*,3*R*)-3-fluoro-2-methyldecanoyl-CoA **114** in ^2H_2O (100 µM final concentration) and the potential AMACR inhibitor in ^2H_2O (100 µM

final concentration) were incubated with human recombinant AMACR (0.12 mg mL^{-1}; 2.55 µM) in 50 mM NaH_2PO_4-NaOH, pH 7.4 and ^2H_2O in a final volume of 550 µL. The reaction mixture contained *ca.* 87% (v/v) ^2H_2O. The mixture was incubated at 30°C for 1 h before the enzyme was inactivated by heating at 60 °C for 30 min. The positive control lacked an inhibitor whilst the negative control contained heat-inactivated AMACR. Each inhibitor was tested in duplicate. ^1H NMR (^2H_2O, 500.13 MHz) was used to analyse the elimination of substrate by quantifying the conversion from the saturated 2-methyl group (a doublet at *ca.* 1.10 ppm) to an unsaturated product (a singlet at *ca.* 1.75 ppm).

6.8.2 Fluoride elimination assay (optimised protocol for the evaluation of AMACR inhibitors)

Potential AMACR inhibitors were dissolved in ^2H_2O or deuterated dimethyl sulfoxide (DMSO) if they were not water soluble. A potential AMACR inhibitor (200 µM in the incubation phase) was incubated with human recombinant AMACR (0.24 mg mL^{-1}; 5.10 µM in the incubation phase) in NaH_2PO_4-NaOH, pH 7.4 and ^2H_2O in a volume of 275 µL. The mixture was incubated for 10 min at room temperature. An equal volume (275 µL) of (2*R*,3*R*)-3-fluoro-2-methyldecanoyl-CoA **114** substrate in the same buffer and ^2H_2O was added to the pre-incubated mixture to a make a final 1× concentration of substrate (100 µM), inhibitor (100 µM) and enzyme (0.12 mg mL^{-1}; 2.55 µM). The final mixture also contained 50 mM NaH_2PO_4-NaOH, pH 7.4 and *ca.* 87% (v/v) ^2H_2O. It was incubated at 30 °C for 1 h before the enzyme was inactivated by heating at 60 °C for 30 min. The positive control lacked an inhibitor while the negative control contained heat-inactivated AMACR. Each inhibitor was tested in duplicate. ^1H NMR (^2H_2O, 500.13 MHz) was used to analyse the elimination of substrate by quantifying the conversion from the saturated 2-methyl group (a doublet at *ca.* 1.10 ppm) to an unsaturated product (a singlet at *ca.* 1.75 ppm).

For potential inhibitors **123**, **124**, **125**, **126** and **127** designed by Professor Paul Groundwater, the same protocol as above applied but the final concentration of (2*R*,3*R*)-3-fluoro-2-methyldecanoyl-CoA **114** substrate was 20 µM and the enzyme was 0.01 mg mL^{-1} (0.21 µM). As the potential inhibitors were not water

soluble, they were dissolved in deuterated DMSO [2% (v/v) final concentration in the assay]. AMACR was shown not to be inhibited by 2% (v/v) DMSO.

6.8.3 Calibration of fluorescence intensity against fluoride concentration using protected fluorescein

The calibration was carried out using the protocol as described by Rydzik *et al.*[191] with some modifications of the concentrations. *tert*-Butyldimethylsilyl-protected fluorescein was dissolved in DMSO and its concentration was determined using ^{1}H NMR. The protected fluorescein (80 µL, final concentration 256 µM) was added to solutions of fluoride anion (NaF solution; 20 µL; final concentrations 0, 2.5, 5, 10, 20, 40, 80, 160, 320, and 640 µM) in 50 mM Tris-HCl, pH 7.5. The buffer was prepared using highly purified water. The mixture was incubated in a solid black 96-well plate at room temperature in the dark for 1 h. 50 mM HEPES-NaOH buffer, pH 7.0 (50 µL) was added to the mixture after 1 h and the samples were further incubated for 2 min. The fluorescence was measured using FLUOstar Omega plate reader (BMG Labtech) with an excitation wavelength of 480 nm and an emission wavelength of 520 nm. Quadruplicate reactions were performed in a 96-well plate. Triplicate readings of each reaction were taken and the readings were corrected by subtracting the baseline signal (control with 0 µM fluoride). The readings were averaged and the standard deviation of the sample was calculated using Microsoft Excel.

6.8.4 Calibration of fluorescence intensity against fluoride concentration using boronate-based fluorescent sensor

The boronate-based fluorescence sensor **131** was dissolved in deuterated methanol and its concentration was determined by ^{1}H NMR. The sensor was diluted in acetonitrile and the solution (160 µL, final concentration 2 µM) was added to NaF (40 µL, final concentrations 0, 9.375, 18.75, 37.5, 75, 150 and 300 µM) in 50 mM NaH_2PO_4-NaOH, pH 7.4. The buffer was prepared using highly purified water. The final concentration of acetonitrile was ~80% (v/v).

For experiment that used 100% (v/v) acetonitrile, TBAF instead of NaF was used, and the final concentrations of the sensor and fluoride anion were the

same as above. For experiment with final concentration of ~95% (v/v) acetonitrile, the sensor (190 µL, final concentration 2 µM) and NaF solution (10 µL, final concentrations 0, 6.25, 12.5, 25, 50, 100, 200 µM) were in the assay.

The 200 µL solution was mixed in a solid black 96-well plate at room temperature for 3 min. The 96-well plate was measured with FLUOstar Omega plate reader (BMG Labtech) with an excitation wavelength of 350 nm and an emission wavelength of 520 nm. Duplicate reactions were performed in a 96-well plate and triplicate readings were taken. The readings were averaged and the standard deviation of the sample was calculated using Microsoft Excel.

6.9 Fluorescence-based competitive binding assay

The fluorescent ligand, 2-methyl-3-(3-(2-(6-morpholino-1,3-dioxo-1*H*-benzo[de]isoquinolin-2(3H)-yl)ethoxy)phenyl)-3-oxopropanoyl-CoA **134** (5 µM) was incubated with human recombinant AMACR (0.049 mg mL^{-1}; 1.04 µM) in 50 mM NaH_2PO_4-NaOH, pH 7.4. Water was added to a final volume of 1000 µL. The mixture was incubated at room temperature for 10 min. Potential inhibitor at various concentrations (0, 0.1, 1, 5, 10, 50 and 100 µM, except potential inhibitors **49** and **50** where the final concentrations were 0, 0.1, 1, 10 and 100 µM) was added and incubated for another 10 min. The fluorescence intensity was measured using a Perkin-Elmer Luminescence LS 50B Spectrometer, with an excitation wavelength of 400 nm and an emission wavelength between 450 and 650 nm (Excitation slit: 10 nm; Emission slit: 10 nm). IC_{50} values were calculated with SigmaPlot 12.3, using the four parameter logistic equation. K_i values were calculated using the K_i calculator (website: http://sw16.im.med.umich.edu/software/calc_ki/).[195, 196]

In order to test for slow-binding of inhibitors, the order of addition of the fluorescent ligand and potential AMACR inhibitor was reversed. The potential inhibitor was pre-incubated with human recombinant AMACR at room temperature for 10 min. The fluorescent ligand was added and incubated for another 10 min before the fluorescence intensity was measured. The final

concentrations of reactants remained the same. Readings were obtained and data was analysed as above.

6.10 Multi-well colorimetric assay

The potential inhibitor (150 µL; final assay concentrations 100.00, 33.33, 11.11, 3.70, 1.23, 0.41, 0.14, 0.05 µM; except for *N*-dodecyl-*N*-methylcarbamoyl-CoA **30** which had final assay concentrations of 411.5, 137.2, 45.7, 15.2, 5.1, 1.7, 0.6, 0.2 nM) in 50 mM NaH_2PO_4-NaOH, pH 7.4, supplemented with 8% (v/v) DMSO was incubated with human recombinant AMACR (150 µL; final assay concentration 0.035 mg mL^{-1}, 0.74 µM) in a 96-well plate at room temperature for 10 min. The 300 µL mixture was split into three (100 µL each) and the substrate 3-(2,4-dinitrophenoxy)-2-methylpropanoyl-CoA **135** (100 µL, final assay concentration 40 µM) was added after 10 min. The reaction was measured immediately using FLUOstar Omega plate reader (BMG Labtech) at 30 °C. The absorbance was measured at 354 nm and 390 nm every 5 min for 15 min. The positive control lacked an inhibitor while the negative control lacked active enzyme (buffer as the substitute). Each assay was performed in triplicate. The absorbance readings at 10 min were averaged and plotted against inhibitor concentration. IC_{50} values were calculated with SigmaPlot 12.3, using four parameter logistic equation. K_i values were calculated from IC_{50} values using the Cheng-Prusoff equation for competitive inhibition.[200]

6.10.1 Multi-well colorimetric assay (mode of binding: experiment 1)

The potential inhibitor (150 µL; pre-incubation phase 20× IC_{50}) in 50 mM NaH_2PO_4-NaOH, pH 7.4, supplemented with 8% (v/v) DMSO was pre-incubated with human recombinant AMACR (150 µL; pre-incubation concentration 0.07 mg mL^{-1}, 1.48 µM) in a 96-well plate at room temperature for 10 min. The 300 µL mixture was split into three (100 µL in each well). The 3-(2,4-dinitrophenoxy)-2-methylpropanoyl-CoA **135** substrate (100 µL, final assay concentration 40 µM) was added to the potential inhibitor (final assay concentration 10× IC_{50}) and the enzyme (final assay concentration 0.035 mg

mL^{-1}, 0.74 µM) mixture. The reaction was measured immediately using FLUOstar Omega plate reader (BMG Labtech) at 30 °C.

Each assay was performed in triplicate. The absorbance was measured at 354 nm and 390 nm every min for 60 min. The positive control lacked an inhibitor while the negative control lacked active AMACR. The absorbance readings at 354 nm were averaged and plotted against time. If an inhibitor absorbed at 354 nm, then absorbance at 390 nm was plotted.

6.10.2 Multi-well colorimetric assay (mode of binding: experiment 2)

The potential inhibitor (6 µL; pre-incubation concentration 20× IC_{50}) in 50 mM NaH_2PO_4-NaOH, pH 7.4, supplemented with 8% (v/v) DMSO was pre-incubated with human recombinant AMACR (6 µL; pre-incubation concentration 1.75 mg mL^{-1}, 37 µM) in a 96-well plate at room temperature for 10 min. The 12 µL mixture was split into three (4 µL in each well). The 3-(2,4-dinitrophenoxy)-2-methylpropanoyl-CoA **135** substrate (196 µL, final assay concentration 40 µM) was added to the potential inhibitor (final assay concentration 0.4× IC_{50}) and enzyme (final assay concentration 0.035 mg mL^{-1}, 0.74 µM) mixture. The reaction was measured immediately in a plate reader using the condition as experiment 1 (*vide supra*).[85] Each assay was performed in triplicate.

6.10.3 Multi-well colorimetric assay (mode of binding: experiment 3)

The potential inhibitor (50 µL; 4× stock, final assay concentration 10× IC_{50}) in 50 mM NaH_2PO_4-NaOH, pH 7.4, supplemented with 8% (v/v) DMSO was incubated with substrate 3-(2,4-dinitrophenoxy)-2-methylpropanoyl-CoA **135** (100 µL, 2× stock, final assay concentration 40 µM) at room temperature for 10 min. Human recombinant AMACR (50 µL; 4× stock, final assay concentration 0.035 mg mL^{-1}, 0.74 µM) was added. The reaction was measured immediately in a plate reader using the condition as experiment 1 (*vide supra*). Each assay was performed in triplicate.

6.10.4 Kitz-Wilson analysis

The procedure was carried out as described by Kitz and Wilson.[85, 202] Ebselen oxide **35** (10 µL; final concentration 0.00, 0.09, 0.13, 0.30, 0.67 and 1.00 µM) in 50 mM NaH_2PO_4-NaOH, pH 7.4, supplemented with 8% (v/v) DMSO was pre-incubated with human recombinant AMACR (10 µL; final assay concentration 0.105 mg mL^{-1}, 2.23 µM) in a 96-well plate at room temperature for 0, 2, 4, 6, 8 and 10 min. The substrate 3-(2,4-dinitrophenoxy)-2-methylpropanoyl-CoA **135** (180 µL, final assay concentration 40 µM) was added and the reaction was measured using FLUOstar Omega plate reader (BMG Labtech) at 30 °C. The absorbance was measured at 354 nm every min for 15 min. The initial reaction rate was calculated from the slope of the straight line of absorbance against time. A graph showing the remaining activity (y-axis) against the time of pre-incubation was plotted. The y-axis was obtained by calculating the natural log of the ratio of initial rate with inhibitor and initial rate without inhibitor [ln ($rate/rate_0$)].

6.11 General (site-directed mutagenesis)

Reagents for biological experiments were obtained from the Sigma-Aldrich Chemical Co. or Fisher Scientific Ltd. unless otherwise stated and were of analytical or molecular biology grade. KOD Hot Start DNA polymerase, Overnight Express™ Autoinduction System 1, NovaBlue GigaSingles™ competent cells, the Rosetta2 (DE3) expression strain and benzonase were purchased from Novagen (Merck Millipore). QIAquick PCR purification kit was obtained from Qiagen Ltd. SeeBlue® Plus2 pre-stained protein standard and primers were sourced from Invitrogen. Q5® site-directed mutagenesis kit, 100 bp and 1 kb DNA ladders, *Dpn*I, DNA sample loading buffer (6×), Quick Ligation™ kit, dATP solution and T4 polynucleotide kinase were purchased from New England Biolabs. Metal-chelate chromatography columns (HisTrap FF) were obtained from GE Healthcare. Ebselen and ebselen oxide were purchased from Cayman Chemical. The pET30 Ek/LIC vector containing wild-type AMACR was obtained from the MDL lab[1] and was used as the template DNA for site-directed mutagenesis. Solutions were prepared using water from a Nanopure Diamond system and was of 18.2 Mega-Ω.cm^{-1} quality. The pH of buffers was adjusted using 5.0 M NaOH $_{aq.}$ or concentrated HCl $_{aq.}$ as appropriate and measured using a Corning pH meter 240 at room temperature, calibrated with standard commercial buffers at pH 7.0 and pH 4.0 or pH 10.0. Plasmids were quantified using GeneQuant II RNA/DNA calculator (GE Healthcare). The incubation of bacterial culture was performed in a shaking incubator (Thermo Scientific MaxQ 4000). Circular dichroism was performed using a Chirascan™ CD Spectrometer (Applied Photophysics). Dynamic light scattering was measured using the Zetasizer nano series instrument (Malvern). Thermo-cycling was performed using a Techne Flexigene or Techne Techgene PCR machine. Centrifugation was carried out either with an Eppendorf Mini-spin micro-centrifuge (at 13 400 r.p.m. and ambient room temperature unless otherwise stated) or a Beckman J2-MC centrifuge.

6.12 Microbiological techniques

All microbiological experiments were conducted under flame using standard aseptic technique. Sterilisation of reagents was performed by autoclaving at

121 °C, 103 kPa for 15 min or filtering through a 0.2 µm filter for heat-labile reagents. Plastic-ware were acquired pre-sterilised or sterilised by autoclaving under the conditions above.

LB (Lennox) media was used throughout the experiments for the cultivation of *E. coli*. LB agar was prepared by supplementing the media with 1% (w/v) agar. LB media was supplemented with antibiotics as appropriate (Table 6.1).

Media	**Purpose**	**Antibiotics supplemented**	**Final concentration of antibiotics (µg mL^{-1})**
LB broth	Rosetta2 (DE3) culture	Chloramphenicol	32
	Rosetta2 (DE3) transformed with AMACR cDNA plasmid	Chloramphenicol	32
		Kanamycin sulfate	30
LB agar	Control with pUC19 vector	Ampicillin	100
	Cells transformed with pET30 Ek/LIC vector	Kanamycin sulfate	30
	Rosetta2 (DE3) transformed with AMACR cDNA plasmid	Chloramphenicol	32
		Kanamycin sulfate	30

Table 6.1: LB broth and agar were supplemented with different antibiotics as needed.

6.13 Glycerol stocks

The glycerol stock was made by adding the overnight bacterial culture (1.0 mL) to sterile glycerol [0.2 mL, 80% (w/v)] and stored in a sterile cryogenic vial at -80 °C.

6.14 Site-directed mutagenesis using Q5® mutagenesis kit

The sequences of AMACR 1A (http://www.uniprot.org/uniprot/, accession number Q9UHK6) and sequence of MCR (http://www.uniprot.org/uniprot/, accession number O06543) were aligned using Clusterw

(http://www.ch.embnet.org/software/ClustalW.html). Potential active site residues were chosen for site-directed mutagenesis based on this alignment and the known active site residues of MCR.[86]

The pET30 Ek/LIC vector containing wild-type human AMACR 1A was obtained from the MDL lab[1] and was used as a template. The Q5® site-directed mutagenesis used the non-overlapping primers and the E0554 protocol was followed. The circularisation of the PCR product and digestion of the template DNA was catalysed by the KLD enzyme mixture (contained kinase, ligase, and *DpnI*). As the template came from bacteria and therefore was methylated, it would be digested by *DpnI*. The mutant plasmid was made by PCR and was not methylated, so it would survive the *DpnI* digestion. The treated PCR product was transformed into NEB 5-alpha competent *E. coli* cells. The cells were selected using LB agar plate supplemented with kanamycin sulfate as the pET30 Ek/LIC vector contains a kanamycin-resistant gene.

Non-overlapping primers for Q5® mutagenesis (Table 6.2) were designed using the New England Biolabs' website: http://nebasechanger.neb.com/.

Primer	Sequence
H122A forward	5'-GTTAGCTGGC**GCG**GATATCAACTATTTGGCTTTGTC-3'
H122A reverse	5'-CGGCAGAAGCTTCCTGAC-3'
D152A forward	5'-TCTCCTGGCT**GCG**TTTGCTGGTGGTGG-3'
D152N forward	5'-TCTCCTGGCT**AAC**TTTGCTGGTG-3'
D152A and D152N reverse	5'-TTCAGCGGGGCATACGGA-3'
M184A forward	5'-TGATGCAAAT**GCG**GTGGAAGGAACAG-3'
M184A reverse	5'-ATGACCTGACCCTTGCCA-3'
E237A forward	5'-TGGAGCAATA**GCG**CCCCAGTTCTAC-3'
E237Q forward	5'-TGGAGCAATA**CAG**CCCCAGTTCTAC-3'
E237A and E237Q reverse	5'-ACAGCCATGAATTCCCCATC-3'
Control forward	5'-GGTATTGAGGGTCGCATGGCACTGCAGGGCATCTC-3'
Control reverse	5'-AGAGGAGAGTTAGAGCCTTAGAGACTAGCTTTTACCTTATTACTTTCAATG-3'

Table 6.2: Primers of the pET30Ek/LIC plasmid for Q5® site-directed mutagenesis experiments. Mutated codons are shown as bold letters.

Optimal annealing temperatures for each primers given by the NEBaseChanger™ webite were used in PCR reactions. Sterile water instead of primers was used as a negative control.

6.15 Primer phosphorylation

Primers were phosphorylated by mixing the following: primer (3 µL, 100 pmol/µL), dATP (5 µL, 10 mM), T4 polynucleotide kinase reaction buffer (5 µL, 10×), T4 polynucleotide kinase (1 µL, 10 U μL^{-1}) and water (36 µL). The mixture was incubated at 37 °C for 30 min. Heat-inactivated was performed at

65 °C for 20 min. Phosphorylation of primer was attempted but subsequently was not used in mutagenesis as it was shown that *in vitro* phosphorylation was not required.

6.16 DNA ligation

DNA ligation was performed by mixing the following: purified DNA (50 ng), Quick ligation reaction buffer (10 µL, 2×), Quick T4 DNA ligase (1 µL, 400,000 units mL^{-1}) and water (to 21 µL). The mixture was incubated at 25 °C for 5 min. Heat inactivation was not required. The purified DNA was initially ligated *in vitro* before it was transformed into competent cells. The DNA ligation step was subsequently abandoned. It was shown that the *in vitro* ligation was unnecessary and in fact, could jeopardise the success of transformation.

6.17 Site-directed mutagenesis using KOD Hot Start polymerase

The primers for site-directed mutagenesis with KOD Hot Start polymerase were designed manually. The forward and reverse primers were overlapping and complementary (Table 6.3).

Primer	***Sequence***
H122A forward	5'-GCCGGTTAGCTGGC**GCG**GATATCAACTATTTGGC-3'
H122A reverse	5'-GCCAAATAGTTGATATC**CGC**GCCAGCTAACCGGC-3'
H122F forward	5'-GCCGGTTAGCTGGC**TTT**GATATCAACTATTTGGC-3'
H122F reverse	5'-GCCAAATAGTTGATATC**AAA**GCCAGCTAACCGGC-3'
H122L forward	5'-GCCGGTTAGCTGGC**CTG**GATATCAACTATTTGGC-3'
H122L reverse	5'-GCCAAATAGTTGATATC**CAG**GCCAGCTAACCGGC-3'
D152A forward	5'-CTGAATCTCCTGGCT**GCG**TTTGCTGGTGGTGGC-3'
D152A reverse	5'-GCCACCACCAGCAAA**CGC**AGCCAGGAGATTCAG-3'
D152N forward	5'-CTGAATCTCCTGGCT**AAC**TTTGCTGGTGGTGGC-3'
D152N reverse	5'-GCCACCACCAGCAAA**GTT**AGCCAGGAGATTCAG-3'
M184A forward	5'-CAGGTCATTGATGCAAAT**GCG**GTGGAAGGAACAGC-3'
M184A reverse	5'-GCTGTTCCTTCCAC**CGC**ATTTGCATCAATGACCTG-3'
E237A forward	5'-GGCTGTTGGAGCAATA**GCG**CCCCAGTTCTACGAGC-3'
E237A reverse	5'-GCTCGTAGAACTGGGG**CGC**TATTGCTCCAACAGCC-3'
E237Q forward	5'-GGCTGTTGGAGCAATA**CAG**CCCCAGTTCTACGAGC-3'
E237Q reverse	5'-GCTCGTAGAACTGGGG**CTG**TATTGCTCCAACAGCC-3'
Colony screening forward	5'-GGTATTGAGGGTCGCATGGCACTGCAGGGCATCTC-3'
Colony screening reverse	5'-TTAGAGACTAGCTTTTACCTTATTACTTTCAATG-3'

Table 6.3: Primers of the pET30Ek/LIC plasmid for site-directed mutagenesis catalysed by KOD Hot Start polymerase. Mutated codons are shown as bold letters.

The PCR reaction was carried out by mixing the following on ice: Buffer (5 µL, 10×); dNTPs (5 µL, 2 mM each); $MgSO_4$ (2 µL, 25 mM); pET30 Ek/LIC plasmid

containing AMACR (100 ng); KOD Hot Start polymerase (1 µL, 1 U μL^{-1}); forward primer (3.75 µL, 4 µM); reverse primer (3.75 µL, 4 µM) and sterile water (to 50.0 µL). The mixture was transferred to a PCR machine and PCR amplification was carried out using the following conditions: Initial denaturation at 95 °C for 2 min; 25 cycles of: 95 °C, 20 s; 55 °C, 30 s; 68 °C, 8 min 20 s; and final extension at 68 °C for 5 min. Control reactions used primers that amplified the 1.2 kb wild-type AMACR 1A insert. The presence of the required DNA was confirmed by agarose gel electrophoresis.

6.18 Agarose gel electrophoresis

50× TAE buffer: EDTA (10.0 mL, 0.5 M, pH 8.0), glacial acetic acid (5.71 mL), Tris base (24.2 g) and water to 100 mL, pH 8.5

Agarose powder [0.8% (w/v) for DNA ≥1.5 kb or 1.0% (w/v) for DNA ≤1.5 kb] was suspended in 1× TAE buffer. The suspension was heated in a microwave until fully dissolved into a clear solution. The mixture was poured evenly into the casting tray. The comb was inserted and the gel was left to solidify at room temperature. The solidified gel was transferred to an electrophoresis cell (Bio-Rad) and submerged in 1× TAE buffer. All samples [DNA (5 µL) with 6× DNA sample loading buffer (2 µL)] were loaded to the gel wells. DNA ladders (100 bp and 1 kb in 1× DNA sample loading buffer; 0.5 µg each) were added as standard markers. The gel was run at 95 volts for 1 h before transfer into ethidium bromide solution (~3 µg mL^{-1} in 1× TAE buffer). They was stained for 10 min and visualised with a GeneGenius bio-imaging system (Syngene) under UV light (λ = 312 nm).

6.19 Manipulation of PCR products and transformation

The PCR product was treated with *DpnI* (2 µL; 40 units) at 37 °C for 2 h to remove the template plasmid. The treated product was purified using the QIAquick PCR purification kit using the manufacturers' procedure and eluted into sterile 10 mM Tris-HCl buffer, pH 8.0 (30 µL). The purified DNA (5 µL) was transformed into NovaBlue GigaSingles^{TM} competent cells. The DNA was mixed with the cells by flicking gently and incubated on ice for 5 min. The

mixture was heat shocked at 42 °C for 30 s and incubated on ice for a further 2 min. SOC media (250 µL) was added to the mixture and the sample was incubated at 37 °C and 220 r.p.m. for 1 h. The bacterial culture (100 µL) was placed onto a LB agar plate pre-warmed at 37 °C and supplemented with kanamycin sulfate. The plate was incubated at 37 °C overnight. A LB agar plate supplemented with ampicillin was used as a positive control with the pUC19 plasmid transformed into competent cells. A single colony from the agar plate was inoculated into LB broth (6 mL) supplemented with kanamycin sulfate. It was incubated at 37 °C and 220 r.p.m. overnight. Plasmid mini-preparation was performed from 5 mL bacterial culture (Section 6.20) and the remainder was stored as glycerol stock (Section 6.13).

6.20 Plasmid mini-prep procedures

Overnight bacterial culture was harvested by centrifugation at 13 400 r.p.m. for 60 s. Solution I (250 µL; 10 mM EDTA, 50 mM Tris-HCl, pH 8.0 with 50 mM glucose and 100 µg mL^{-1} RNase A) was used to suspend the harvested cells. To the suspension, solution II [250 µL; 200 mM NaOH, 1% (w/v) SDS] was subsequently added. The mixture was gently inverted five times to give a clearer mixture and was left at room temperature for 5 min. Solution III (250 µL; 2.55 M KOAc-HOAc, pH 5.4) was added and inverted 5 times to mix before incubation on ice for 15 min. The mixture was centrifuged at 13 400 r.p.m. for 30 min and the supernatant was transferred to a sterile Eppendorf tube. Isopropanol (525 µL) was added, and the mixture was gently inverted 5 times and incubated at room temperature for 5 min. Centrifugation at 13 400 r.p.m. for 30 min was carried out and the supernatant was discarded. The precipitated DNA pellet was washed with cold ethanol [100 µL, 70% (v/v)] twice. The pellet was dried on bench for at least 1 h to get rid of any residual ethanol. Sterile water (40 µL) was used to suspend the DNA pellet and the mixture was stored at -20 °C until ready to be used.

6.21 Colony PCR

Colony PCR was performed in order to confirm that the required insert of the correct size for AMACR 1A was present. Each PCR reaction contained the following: Buffer (2 µL, 10×); dNTPs (2 µL, 2 mM each); $MgSO_4$ (0.8 µL, 25

mM); template DNA containing the mutated insert (1 µL); KOD Hot Start polymerase (0.4 µL, 1 U μL^{-1}); forward primer (1.5 µL, 4 µM); reverse primer (1.5 µL, 4 µM) and sterile water (to 20.0 µL). The mixture was transferred to a PCR machine and PCR amplification was carried out using the following conditions: Initial denaturation at 95 °C for 2 min; 35 cycles of: 95 °C, 20 s; 52 °C, 10 s; 70 °C, 24 s; and final extension at 70 °C for 5 min. Agarose gel electrophoresis was performed and the gel was stained with ethidium bromide (Section 6.18). Once the insert of the correct size was confirmed, the plasmid was sent for sequencing to Source BioScience, U.K. in order to confirm that the desired mutation was present with no other changes to the sequence.

6.22 Protein expression

6.22.1 Preparation of competent cell for protein expression

A thawed glycerol stock of Rosetta2 (DE3) (200 µL) was inoculated into 1 mL SOC media supplemented with chloramphenicol in a 50 mL Falcon tube at 37 °C and 220 r.p.m. for 90 min. LB media supplemented with chloramphenicol (10 mL) was added to the bacterial culture and incubated at 37 °C and 220 r.p.m. until turbid (usually 3 h). Cells were harvested by centrifugation (JA-14 rotor, 10 000 r.p.m., 15 300 *g*, 10 min). The harvested cells were gently suspended in sterile, ice-cold 50 mM $CaCl_{2\ aq.}$ (1 mL). The suspension was centrifuged again and the supernatant was discarded. The pellet was re-suspended in sterile, ice-cold 50 mM $CaCl_{2\ aq.}$ (0.5 mL). The suspended cells were left on ice in the cold room for 30 min or until ready to be used.

6.22.2 Transformation of competent cell for protein expression

Mini-prep plasmid (2 µL) was cooled on ice and mixed with the freshly prepared competent Rosetta2 (DE3) (100 µL) by flicking gently. Cells were incubated on ice for 5 min before being spread onto an agar plate that was pre-warmed at 37 °C and supplemented with chloramphenicol and kanamycin sulfate. Plates were incubated at 37 °C overnight.

6.22.3 Small scale protein expression using IPTG or lactose

A single colony from the transformation plate (Section 6.22.2) was inoculated into 5 mL LB media supplemented with chloramphenicol and kanamycin

sulfate. The culture was incubated at 37 °C and 220 r.p.m. until OD_{600} reached ~1.5. The culture temperature was lowered to 16 °C for 1 h before IPTG (0.25 mM) or lactose (2 mM, 5 mM or 10 mM) was added. The induced culture was incubated at 16 °C and 220 r.p.m. overnight.

6.22.4 Small scale protein expression using overnight express™ autoinduction system 1

1× autoinduction system 1 (100 µL OnEx™ Solution 1, 250 µL OnEx Solution 2 and 5 µL OnEx Solution 3) was added to 5 mL LB media supplemented with kanamycin sulfate and chloramphenicol. A single colony was inoculated into the mixture and incubated at 37 °C and 220 r.p.m. overnight.

6.22.5 Small scale protein sample preparation

The cells were harvested by centrifugation at 13 400 r.p.m. to give ~30 mg cell pellet. Lysozyme (1 mg mL^{-1}) in 20 mM Tris-HCl and 150 mM NaCl, pH 8.0 buffer (150 µL) was used to re-suspend the centrifuged cell pellet (~30 mg). The suspension was incubated at room temperature for 20 min. Triton™ X-100 solution [10 µL, 10% (v/v)] was added to the mixture which was incubated at room temperature for 30 min. To 30 µL of the lysed cells, was added $TCA_{aq.}$ [final concentration 10% (w/v)]. The sample was centrifuged at 13 400 r.p.m. for 10 min. The supernatant was removed and 30 µL of 1× SDS-PAGE sample loading buffer (Section 6.24) was added to the protein pellet. The protein sample was heated at 90 °C for 10 min with periodic vortex mixing.

6.22.6 Large scale protein expression

A single transformed Rosetta2 (DE3) colony (Section 6.22.2) was inoculated into 5 mL LB media supplemented with chloramphenicol and kanamycin sulfate. The culture was incubated at 28 °C and 220 r.p.m. for 6 h. Fresh LB media (12 mL) supplemented with the same antibiotics was added after 6 h and the incubation was continued under the same conditions overnight.

The expression of wild-type, M184A, E237A and E237Q were induced using the overnight express™ autoinduction system 1. The starter culture produced above (15 mL) was inoculated into 500 mL of LB media supplemented with

chloramphenicol, kanamycin sulfate and was induced with 1× autoinduction system 1 (10 mL OnEx™ Solution 1, 25 mL OnEx Solution 2 and 0.5 mL OnEx Solution 3). The induced culture was incubated overnight at 28 °C and 220 r.p.m. Cells were harvested by centrifugation (JA-10 rotor, 9000 r.p.m., 14 300 *g*, 30 min) and stored at -80 °C.

IPTG was used to induce the expression of the H122L and D152N mutants. The starter culture (15 mL) was inoculated into 500 mL of LB media supplemented with chloramphenicol and kanamycin sulfate and was incubated at 28 °C and 220 r.p.m. until OD_{600} reached ~1.0 (~6 h). IPTG (0.25 mM) was added and the culture was further incubated under the same conditions overnight. Cells were harvested by centrifugation (JA-10 rotor, 9000 r.p.m., 14 300*g*, 30 min) and stored at -80 °C.

6.23 Large scale purification of AMACR

Cell pellet was re-suspended in start buffer (30 mL; 20 mM NaH_2PO_4-NaOH, 300 mM NaCl, 10 mM imidazole, pH 7.2) supplemented with 1 mM benzamidine-HCl, 1 mM PMSF and 250 U benzonase. The suspension was stirred gently at 4 °C until a homogenous mixture was produced. Cells were lysed with an One Shot cell disruption system (Constant System Ltd.). The lysate was centrifuged (JA-14 rotor, 5000 r.p.m., 3800 *g*, 5 min) to remove excessive bubbles. *N*-Lauroylsarcosine was added to the lysate dropwise to a final concentration of 1.5% (w/v) and stirred gently at 4 °C for 1 h. The treated mixture was centrifuged (JA-14 rotor, 10 000 r.p.m., 15 300 *g*, 10 min). The supernatant was passed through a 0.8 µm filter. The filtrate was loaded onto a metal-chelate chromatography column (HisTrap FF) which has been equilibrated with start buffer supplemented with 0.2 mM PMSF and 0.2 mM benzamidine-HCl. The protein was eluted with elution buffer (300 mM imidazole in start buffer, pH 7.2) supplemented with 0.2 mM PMSF and 0.2 mM benzamidine-HCl. Each eluted fractions were analysed by SDS-PAGE (Section 6.24). Fractions containing the purified protein were pooled and dialysed into 10 mM NaH_2PO_4-NaOH, pH 7.4 (3× 600 mL). The dialysed enzyme was quantified (Section 6.25) and stored at -80 °C until ready to be used.

6.24 Sodium dodecyl sulfate-polyacrylamide gel electrophoresis (SDS-PAGE)

SDS-PAGE was carried out by the method of Laemmli.[244] A 3% stacking gel and 10% running gel (to resolve 40 kDa protein) was transferred to a Mini Protean III™ apparatus (Bio-Rad) and 1× running buffer was added.

Crude protein samples should be prepared by TCA precipitation (Section 6.22.5) before they were analysed by SDS-PAGE. TCA precipitation was not required for purified protein samples eluted from a metal-chelate chromatography column. Protein sample loading buffer (5 µL, 5×) was added to the purified sample (20 µL) and was heated at 90 °C for 10 min with periodic vortex mixing.

All protein samples with a final concentration of 1×sample loading buffer were loaded onto the SDS-PAGE gel. SeeBlue® Plus2 molecular weight markers were used as standard. The gel was electrophoresed at 170 volts for ~5 min to stack and run at 220 volts afterwards. The gel was removed from electrophoresis, washed with water and stained with 0.25% (w/v) Coomassie Brilliant Blue R-250 in 50% (v/v) ethanol and 10% (v/v) acetic acid for 10 min. The stained gel was washed with water and destained with 10% (v/v) ethanol and 5% (v/v) acetic acid. The de-staining with ethanol and acetic acid was repeated at least twice to observe protein bands.

Stacking gel (3%): Tris-HCl (400 µL, 1.0 M, pH 6.8), ammonium persulfate [160 µL, 1% (w/v)], SDS [32 µL, 10% (w/v)], acrylamide/bis-acrylamide solution [37.5:1, 240 µL, 40% (w/v)], tetramethylethylenediamine (TEMED) (5 µL) and H_2O (2.4 mL).

Running gel (10%): Tris-HCl (4.5 mL, 0.75 M, pH 8.8), ammonium persulfate [450 µL, 1% (w/v)], SDS [90 µL, 10% (w/v)], acrylamide/bis-acrylamide solution [37.5:1, 2.25 mL, 40% (w/v)], TEMED (10 µL) and H_2O (1.8 mL).
10× Running buffer: 250 mM Tris-HCl, 1.92 M glycine, 1% (w/v) SDS, pH 8.3

5× Protein sample loading buffer: Tris-HCl (2.5 mL, 0.625 M, pH 6.8), 10% (v/v) β-mercaptoethanol, 0.01% (w/v) bromophenol blue, 10% (w/v) SDS, 50% (w/v) glycerol and H_2O.

SeeBlue® Plus2 pre-stained standards: A ready-to use molecular weight marker consisting of 10 polypeptides that have been pre-stained (8 blue and 2 coloured) in the range of 4-250 kDa.: myosin (250 kDa), phosphorylase (148 kDa, orange), BSA (98 kDa); glutamic dehydrogenase (64 kDa), alcohol dehydrogenase (50 kDa), carbonic anhydrase (36 kDa), myoglobin red (22 kDa, pink), lysozyme (16 kDa), aprotinin (6 kDa) and B-chain insulin (4 kDa).

6.25 Enzyme quantification

Protein concentrations were quantified using an UV-visible spectrophotometer (Helios γ, Unicam) at 280 nm. The concentrations were calculated from the extinction coefficients obtained from Protparam (http://web.expasy.org/protparam/), which was 35785 M^{-1} cm^{-1} for each His-tag proteins. Proteins in molar concentration was converted to mg mL^{-1} using the molecular weights obtained from Protparam (http://web.expasy.org/protparam/): wild-type (47074.8 Da); H122L (47050.8 Da); D152N (47073.8 Da); M184A (47014.6 Da); E237A (4716.7 Da) and E237Q (47073.8 Da). The concentration of wild-type AMACR was 3.48 mg mL^{-1} (73.72 µM), H122L was 1.08 mg mL^{-1} (22.96 µM), D152N was 0.98 mg mL^{-1} (20.66 µM), M184A was 2.59 mg mL^{-1} (55.13 µM), E237A was 5.06 mg mL^{-1} (107.56 µM) and E237Q was 3.64 mg mL^{-1} (77.36 µM).

6.26 Protein characterisation

6.26.1 Protein characterisation using dynamic light scattering (DLS)

AMACR (final concentration 1 mg mL^{-1}) in 10 mM NaH_2PO_4-NaOH buffer, pH 7.4 was filtered through a 0.2 µm filter. Its size was measured using a DLS instrument (Zetasizer nano series instrument, Malvern) at 25 °C. Nine measurements were taken to determine the average size of the protein, given in number distribution. The readings were averaged and the standard deviation of the sample was calculated using Microsoft Excel.

6.26.2 Protein characterisation using circular dichroism (CD)

The CD spectrum of the enzyme was obtained using a Chirascan™ CD Spectrometer (Applied Photophysics). The protein (~0.1 mg mL^{-1}) in 10 mM NaH_2PO_4-NaOH buffer, pH 7.4 was placed in a quartz cuvette with a path length of 1 cm. The solution was scanned 10 times, and the ellipticity readings from 200 to 300 nm at 20 °C were recorded. The spectra were averaged and buffer-corrected. The molar ellipticity was calculated using the formula: $[\theta] = 100x\theta/(Cxl)$; where θ is the observed ellipticity (degree); C is the concentration of the enzyme (M), and l is the path length (cm).[245] A denatured wild-type enzyme (10-min heating at 95 °C with periodic vortex mixing) was used as a negative control.

6.26.3 Protein characterisation with 8-anilino-1-naphthalenesulfonic acid (ANS) as a fluorescent probe

The protein (0.1 mg mL^{-1}) in 50 mM NaH_2PO_4-NaOH buffer, pH 7.4 was incubated with ANS **148** (0.2 mM) in the dark for 20 min. The fluorescent spectra were recorded using a Perkin-Elmer Luminescence LS 50B Spectrometer with an excitation wavelength of 385 nm and a bandwidth of 5 nm. The emission spectra were recorded between 420 and 580 nm, with a bandwidth of 10 nm. The spectra were corrected by subtracting the baseline (ANS **148** in buffer without protein). A denatured wild-type enzyme (10-min heating at 95 °C with periodic vortex mixing) was used as a negative control.

6.27 The study of the 'racemisation' reaction on wild-type and mutant enzymes

6.27.1 The deuterium wash-in assay

R- **44** or *S*- 2-methyldecanoyl-CoA **38** was dissolved in ^2H_2O and used as a substrate for the assay. The vortex-mixed substrate (final concentration 100 µM) was incubated with wild-type or mutant enzymes (final concentration 0.12 mg mL^{-1}, 2.55 µM) in 50 mM NaH_2PO_4-NaOH, pH 7.4 and ^2H_2O [77% (v/v)] in a final volume of 550 µL. The assay mixture was incubated at 30°C for 1 h before the enzyme was heat-inactivated at 60 °C for 30 min. *R*-2-Methyldecanoyl-CoA was used as a positive control and heat-inactivated AMACR was used as a negative control. ^1H NMR (^2H_2O, 500.13 MHz) was

used to analyse α-proton exchange by quantifying the conversion of the 2-methyl peak from a doublet to an unresolved single peak at *ca.* 1.00 ppm.

6.27.2 Kinetic studies using the deuterium wash-in assay

The *R*- **44** or *S*- 2-methyldecanoyl-CoA **38** substrate (50, 100, 200, 300, 400 and 600 µM) was incubated with wild-type AMACR (5.0 µg mL^{-1}, 0.11 µM for *R*-substrate and 2.5 µg mL^{-1}, 0.05 µM for *S*-substrate) in 50 mM NaH_2PO_4-NaOH, pH 7.4 and ^2H_2O [77% (v/v)] in a final volume of 550 µL. For M184A mutant, substrate concentrations were 30, 50, 75, 100, 200 and 250 µM and an enzyme concentration of 0.40 mg mL^{-1} (8.51 µM) was used. Each substrate concentration was measured in duplicate. The assay mixture was incubated at 30°C for 1 h before the enzyme was heat-inactivated at 60 °C for 30 min. ^1H NMR (^2H_2O, 500.13 MHz) was used to analyse α-proton exchange by quantifying the conversion of the 2-methyl peak from a doublet to an unresolved single peak at *ca.* 1.00 ppm. Rates were corrected for non-enzymatic exchange using data from heat-inactivated enzymes. Data was analysed with SigmaPlot 12.3 software, using the Direct Linear Plot,[203, 204] Michaelis-Menten Plot,[246, 247] Lineweaver-Burk Plot[248] and Residual Plot.[205]

6.25 Fluoride elimination assay on wild-type and mutant enzymes

6.28.1 Fluoride elimination assay using a single time point

(2*R*,3*R*)-3-Fluoro-2-methyldecanoyl-CoA **114** substrate (final concentration 100 µM) was incubated with wild-type or mutant enzymes (final concentration 0.12 mg mL^{-1}; 2.55 µM) in 50 mM NaH_2PO_4-NaOH, pH 7.4 and ^2H_2O [77% (v/v)] in a final volume of 550 µL. The mixture was incubated at 30 °C for 1 h before the enzyme was inactivated by heating at 60 °C for 30 min. Three replicates for each enzyme were performed. Rates were corrected for non-enzymatic elimination using negative controls containing heat-inactivated enzyme. ^1H NMR (^2H_2O, 500.13 MHz) was used to analyse the elimination of substrate by quantifying the conversion from the saturated 2-methyl group (a doublet at *ca.* 1.00 ppm) to an unsaturated product (a singlet at *ca.* 1.65 ppm).

6.28.2 Time course of fluoride elimination over 16 h using ^{1}H NMR

(2*R*,3*R*)-3-Fluoro-2-methyldecanoyl-CoA **114** or (2*S*,3*S*)-3-fluoro-2-methyldecanoyl-CoA **147** (final concentration 100 µM) was incubated with wild-type or mutant enzymes (final concentration 0.12 mg mL^{-1}; 2.55 µM) in 50 mM NaH_2PO_4-NaOH, pH 7.4 and $^{2}H_2O$ [77% (v/v)] in a final volume of 715 µL. The experiment was performed using a 500.13 MHz ^{1}H NMR spectrometer at 30 °C (or 20 °C for simultaneous measurements) and the reaction was followed for 15.5 h with a one-hour intervals. Rates were corrected for non-enzymatic elimination using negative controls containing heat-inactivated enzyme.

6.29 Multi-well colorimetric assay on wild-type and mutant enzymes

6.29.1 Time-course multi-well colorimetric assay

The 3-(2,4-dinitrophenoxy)-2-methylpropanoyl-CoA **135** substrate (100 µL; final concentration 40 µM) was incubated with the wild-type or mutant enzymes (50 µL; final concentration 0.035 mg mL^{-1}, ~0.74 µM) in 50 mM NaH_2PO_4-NaOH, pH 7.4 in a 96-well plate. The reactions were performed in triplicate. Heat-inactivated wild-type AMACR was used as a negative control. The absorbance of the 200 µL reaction mixture was measured using FLUOstar Omega plate reader (BMG Labtech) at 30 °C. The absorbance was measured at 354 nm and 390 nm every 1 h for 10 h. The absorbance readings were averaged (using Microsoft Excel) and plotted against time.

6.29.2 The kinetic study using multi-well colorimetric assay

Wild-type and mutant enzymes were titrated to an appropriate concentration in order to determine their activity at the initial reaction rate (linear part of the curve). The final concentrations chosen were: wild-type (0.035 mg mL^{-1}, 0.74 µM); H122L (0.540 mg mL^{-1}, 11.48 µM); D152N (0.326 mg mL^{-1}, 6.93 µM); M184A (1.295 mg mL^{-1}, 27.54 µM); E237A (2.528 mg mL^{-1}, 53.77 µM) and E237Q (0.450 mg mL^{-1}, 9.56 µM). The 3-(2,4-dinitrophenoxy)-2-methylpropanoyl-CoA **135** substrate (50 µL; final concentrations 200, 100, 50, 25, 12.5, 6.25, 3.125, 1.563 µM) was incubated with each enzyme (50 µL, concentration as above) in 50 mM NaH_2PO_4-NaOH, pH 7.4. The 100 µL

reaction mixture was run in a Greiner 96 half area plate and measured using FLUOstar Omega plate reader (BMG Labtech) at 30 °C. The absorbance was measured at 354 nm and 390 nm every 1 min for 8 min. Rates were determined by plotting absorbance against time in SigmaPlot 12.3. Rates in absorbance unit min^{-1} were converted to nmol min^{-1} mg^{-1} unit using path length of 0.509 cm (determined by the plate-reader) and an extinction coefficient of 15.3 mM^{-1} cm^{-1}.[199] Data was analysed with SigmaPlot 12.3 software, using the Direct Linear Plot,[203, 204] Michaelis-Menten Plot,[246, 247] Lineweaver-Burk Plot[248] and Residual Plot.[205]

6.30 Attempts to chirally resolve 3-(2,4-dinitrophenoxy)-2-methylpropanoyl-CoA substrate

(2*R*,*S*)3-(2,4-dinitrophenoxy)-2-methylpropan-1-ol (150)

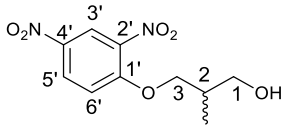

Sodium (1.50 g, 65 mmol) was stirred with 2-methyl-1,3-propanediol (34.00 g, 377 mmol) for 3 h at room temperature before 1-fluoro-2,4-dinitrobenzene (8.4 mL, 67 mmol) was added to the mixture. The mixture was stirred at 80 °C for 2 h and left stirring at room temperature for 18 h. The mixture was filtered and the filtrate was washed with cold water, dried over $MgSO_4$ and evaporated *in vacuo* to afford a dark brown oil. The crude product was purified by column chromatography [silica, gradient elution with 5:1, 3:1, 2:1 (v/v) PE:EtOAc] to give a yellow solid (3.60 g, 21.6%) that eluted in 2:1 (v/v) PE:EtOAc. R_f = 0.27 [1:1 (v/v) PE:EtOAc]; melting point 46-48 °C; IR ν_{max}/cm^{-1} 3583 (OH), 1528 (N-O) and 1343 (N-O); δ_H (400.04 MHz; $CDCl_3$) 8.74 (1 H, d, *J* = 2.8 Hz, Ar 3'-*H*), 8.41 (1 H, dd, *J* = 9.2, 2.8 Hz, Ar 5'-*H*), 7.26 (1 H, d, *J* = 9.2 Hz, Ar 6'-*H*), 4.29-4.18 (2 H, m, 3-CH_2), 3.74 (1 H, dd, *J* = 10.8, 4.8 Hz, 1-CH_a), 3.68 (1 H, dd, *J* = 10.8, 6.8 Hz, 1-CH_b), 2.35-2.19 (2 H, m, 2-C*H* and O*H*) and 1.07 (3 H, d, *J* = 6.8 Hz, 2-CH_3); δ_C (100.59 MHz, $CDCl_3$) 156.91 (Ar 1'-*C*), 139.83 (Ar 4'-*C*), 138.36 (Ar 2'-*C*), 129.30 (Ar 5'-*C*), 121.97 (Ar 3'-*C*), 114.38 (Ar 6'-*C*), 72.82 (3-*C*H_2), 64.40 (1-*C*H_2), 35.34 (2-*C*H) and 13.28 (2-*C*H_3); ESI-MS m/z calcd. for $[M-H]^-$ $C_{10}H_{11}N_2O_6$: 255.0617, found 255.0612.

(2*R*,*S*)-3-(2,4-dinitrophenoxy)-2-methylpropyl (2*S*)-2-acetoxy-2-phenyl-acetate (racemic mixture of 153 and 154)

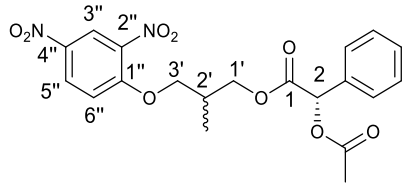

(2*R*,*S*)-3-(2,4-dinitrophenoxy)-2-methylpropan-1-ol **150** (243 mg, 0.94 mmol) was dissolved in DCM (5 mL). DCC (1.0 M in DCM) (1.08 mL, 1.08 mmol) and DMAP (11 mg, 0.094 mmol) were added, and the resulting mixture was stirred until fully dissolved. (*S*)-2-Acetoxy-2-phenylacetic acid (202 mg, 1.04 mmol) was added to the solution and stirred overnight. The mixture was filtered through celite and the filtrate was concentrated *in vacuo*. The crude product was purified by column chromatography [silica, 4:1 (v/v) PE:EtOAc] to afford a yellow oil (392 mg, 96.7%) as a mixture of diastereomers. Attempts to separate the diastereomers were unsuccessful. R_f = 0.69 [1:1 (v/v) PE:EtOAc]; IR ν_{max}/cm^{-1} 1747 (C=O), 1530 (N-O) and 1343 (N-O); δ_H (400.04 MHz; $CDCl_3$) 8.71 (1 H, d, *J* = 2.8 Hz, Ar 3''-*H*), 8.36, 8.35 (1 H, 2×dd overlapping , *J* = 9.2, 2.8 Hz, Ar 5''-*H*)*, 7.45-7.38 (2 H, m, Ar-*H*), 7.35-7.28 (3 H, m, Ar-*H*), 7.05, 7.01 (1 H, 2×d, *J* = 9.2 Hz, Ar 6''-*H*)*, 5.85, 5.84 (1 H, 2×s, 2-C*H*)*, 4.33-4.10 (2 H, m, 1'-CH_2), 4.40-3.87 (2 H, m, 3'-CH_2), 2.43-2.28 (1 H, m, 2'-C*H*), 2.16, 2.15 (3 H, 2×s, COCH_3)* and 1.06, 1.03 (3 H, 2×d, *J* = 7.2 Hz, 2'-CH_3)*; δ_C (100.59 MHz, $CDCl_3$) 170.39, 170.35 (CH_3*C*=O)*, 168.54, 168.51 (1-*C*=O)*, 156.55, 156.351 (Ar 1''-*C*)*, 139.88 (Ar 4''-*C*), 138.43 (Ar 2''-*C*), 133.52-121.83 (Ar-*C* and Ar 5''-*C*)*, 121.83, 121.82 (Ar 3''-*C*)*, 114.33, 114.32 (Ar 6''-*C*)*, 74.40, 74.34 (2-*C*H)*, 71.21, 71.17 (3'-*C*H_2)*, 65.70 (1'-*C*H_2), 32.82, 32.74 (2'-*C*H)*, 20.55 (COCH_3) and 13.30, 13.24 (2'-*C*H_3)*; ESI-MS m/z calcd. for $[M+Na]^+$ $C_{20}H_{20}N_2NaO_9$: 455.1067, found 455.1074.*overlapping peaks or duplicated peaks arising due to inseparable diastereomers.

(2*R*,*S*)3-(2,4-dinitrophenoxy)-2-methylpropyl (7,7-dimethylbicyclo[2.2.1] hept-1-yl)methanesulfonate (racemic mixture of 156 and 157)

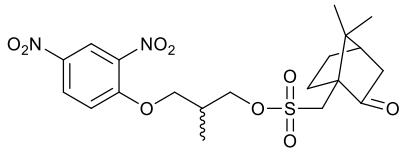

(1*S*)-10-camphorsulfonyl chloride (201 mg, 0.80 mmol) was added to a solution of (2*R*,*S*)-3-(2,4-dinitrophenoxy)-2-methylpropan-1-ol **150** (205 mg, 0.80 mmol) in pyridine (2.0 mL) at -5°C and then stirred at 0 °C for 2 h. Water (50 mL) was added to quench the reaction and the mixture was extracted with DCM (3 x 30 mL). The organic layers were combined, dried over $MgSO_4$ and evaporated *in vacuo* to afford a brown oil. The crude product was purified by column chromatography [silica, gradient elution with 4:1, 3:1, 2.5:1 (v/v) PE:EtOAc] to give a yellow solid (250 mg, 68.5%) that eluted in 2.5:1 (v/v) PE:EtOAc as a mixture of diastereomers. Attempts to separate the diastereomers were unsuccessful. R_f = 0.63 [1:1 (v/v) PE:EtOAc]; IR ν_{max}/cm^{-1} 1745 (C=O), 1530 (N-O) and 1344 (N-O); δ_H (400.04 MHz; $CDCl_3$) 8.77 (1 H, d, *J* = 2.8 Hz, Ar-*H*), 8.43 (1 H, dd, *J* = 9.2, 2.8 Hz, Ar-*H*), 7.24 (1 H, d, *J* = 9.2 Hz, Ar-*H*), 4.50-4.10 (4 H, m, 2×OC*H*$_2$), 3.55 (1 H, d, *J* = 15.2 Hz, OSOC*H*$_a$), 2.97 (1 H, dd, *J* = 15.2, 0.8 Hz, OSOC*H*$_b$), 2.56-2.25 (3 H, m, C*H* and 2×bicyclic C*H*), 2.10 (1 H, t, *J* = 4.4 Hz, bicyclic C*H*), 2.07-1.95 (1 H, m, bicyclic C*H*), 1.86 (1 H, dd, *J* = 18.4, 2.8 Hz, bicyclic C*H*), 1.65-1.58 (1 H, m, bicyclic C*H*), 1.46-1.36 (1 H, m, bicyclic C*H*), 1.18, 1.17 (3 H, 2×d, *J* = 6.8 Hz, C*H*$_3$)*, 1.06 (3 H, s, bicyclic C*H*$_3$) and 0.84 (3 H, s, bicyclic C*H*$_3$); δ_C (100.59 MHz, $CDCl_3$) 214.37. 214.32 (C=O)*, 156.57 (Ar-*C*), 140.11 (Ar-*C*), 138.52 (Ar-*C*), 129.27 (Ar-*C*H), 122.03 (Ar-*C*H), 114.48 (Ar-*C*H), 70.82 (O*C*H$_2$), 70.61 (O*C*H$_2$), 57.83 (bicyclic *C*), 48.01, 48.00 (bicyclic *C*)*, 46.73 (OSO*C*H$_2$), 42.62 (bicyclic *C*H), 42.40 (bicyclic *C*H), 33.39, 33.36 (*C*H)*, 26.78 (bicyclic *C*H), 24.84 (bicyclic *C*H), 19.58 (bicyclic *C*H$_3$), 19.54 (bicyclic *C*H$_3$) and 13.15 (*C*H$_3$); ESI-MS m/z calcd. for $[M+Na]^+$ $C_{20}H_{26}N_2NaO_9S$: 493.1257, found 493.1256.*Overlapping peaks or duplicated peaks arised due to inseparable diastereomers.

(2*R*,*S*)-1-(3-bromo-2-methylpropoxy)-2,4-dinitrobenzene (159)

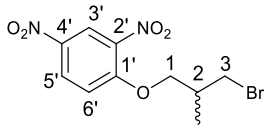

Tetrabromomethane (470 mg, 1.41 mmol) was added to a solution of (2*R*,*S*)-3-(2,4-dinitrophenoxy)-2-methylpropan-1-ol **150** (295 mg, 1.15 mmol) in DCM (3 mL). The mixture was stirred at room temperature for 5 min before dropwise addition of triphenylphosphine (333 mg, 1.27 mmol) in DCM (1 mL). The reaction mixture was stirred at room temperature for 1.5 h before it was quenched with saturated $NaHCO_{3\ aq.}$ The mixture was extracted with DCM (3×30 mL) and the combined organic extracts were dried over $MgSO_4$ and evaporated *in vacuo* to afford a brown oil. The crude product was purified by column chromatography [silica, 4:1 (v/v) PE:EtOAc] to afford an orange oil (303 mg, 82.6%). R_f = 0.65 [2:1 (v/v) PE:EtOAc]; IR ν_{max}/cm^{-1} 1529 (N-O) and 1344 (N-O); δ_H (400.04 MHz; $CDCl_3$) 8.73 (1 H, d, *J* = 2.8 Hz, Ar 3'-*H*), 8.42 (1 H, dd, *J* = 9.2, 2.8 Hz, Ar 5'-*H*), 7.26 (1 H, d, *J* = 9.2 Hz, Ar 6'-*H*), 4.29-4.12 (2 H, m, 1-CH_2), 3.64 (1 H, dd, *J* = 10.0, 4.4 Hz, 3-CH_a), 3.53 (1 H, dd, *J* = 10.0, 6.4 Hz, 3-CH_b), 2.50-2.33 (1 H, m, 2-C*H*) and 1.18 (3 H, d, *J* = 6.8 Hz, 2-CH_3); δ_C (100.59 MHz, $CDCl_3$) 156.52 (Ar 1'-*C*), 139.96 (Ar 4'-*C*), 138.37 (Ar 2'-*C*), 129.23 (Ar 5'-*C*), 121.88 (Ar 3'-*C*), 114.42 (Ar 6'-*C*), 72.24 (1-*C*H_2), 36.26 (3-*C*H_2), 34.71 (2-*C*H) and 15.44 (2-*C*H_3).

6.31 Attempts of enantioselective synthesis of 3-(2,4-dinitrophenoxy)-2-methylpropanoyl-CoA

Methyl (*S*)-3-((*tert*-butyldiphenylsilyl)oxy)-2-methylpropanoate (163)

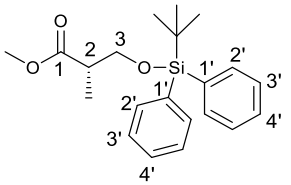

Methyl (*S*)-3-hydroxy-2-methylpropionate (5.10 g, 43.17 mmol) was dissolved in DCM (40 mL) at 0° C. Imidazole (6.47 g, 95.04 mmol) and *tert*-butyl(chloro)diphenylsilane (12.4 mL, 47.66 mmol) was added. The mixture was stirred at room temperature for 2.5 h before it was quenched with saturated $NaHCO_{3\ aq.}$ (100 mL). It was extracted with DCM (3×100 mL) and

the organic extracts were combined, dried over $MgSO_4$ and evaporated *in vacuo* to afford a colourless oil (15.21 g, 98.8%). The oil was found to be >95% pure (by ^{1}H NMR) and was used in next step without purification. R_f = 0.58 [10:1 (v/v) PE:EtOAc]; $[\alpha]_D^{20}$ +20.5 (*c* 0.59 in $CHCl_3$); lit. $[\alpha]_D^{20}$ +16.9 (*c* 1.11 in $CHCl_3$);[249] IR ν_{max}/cm^{-1} 1744 (C=O); ^{1}H and ^{13}C NMR spectra of the product were consistent with previously reported data.[249] δ_H (400.04 MHz; $CDCl_3$) 7.78-7.73 (4 H, m, Ar 2'-*H*), 7.52-7.38 (6 H, m, Ar 3'-*H* and Ar 4'-*H*), 3.93 (1 H, dd, *J* = 10.0, 7.2 Hz, 3-C*H*$_a$), 3.83 (1 H, dd, *J* = 10.0, 6.0 Hz, 3-C*H*$_b$), 3.74 (3 H, s, OC*H*$_3$), 2.87-2.76 (1 H, m, 2-C*H*), 1.24 (3 H, d, *J* = 7.2 Hz, 2-C*H*$_3$) and 1.14 (9 H, s, (C*H*$_3$)$_3$); δ_C (100.59 MHz, $CDCl_3$) 175.24 (*C*=O), 135.42 (Ar 2'-*C*), 133.31 (Ar 1'-*C*), 133.25 (Ar 1'-*C*), 129.56 (Ar 4'-*C*), 127.56 (Ar 3'-*C*), 65.78 (3-*C*H$_2$), 51.38 (O*C*H$_3$), 42.24 (2-*C*H), 26.58 (C(*C*H$_3$)$_3$), 19.09 (Si*C*) and 13.31 (2-*C*H$_3$); ESI-MS m/z calcd. for $[M+H]^+$ $C_{21}H_{29}O_3Si$: 357.1886, found 357.1895.

(*R*)-3-((*tert*-Butyldiphenylsilyl)oxy)-2-methylpropan-1-ol (164)

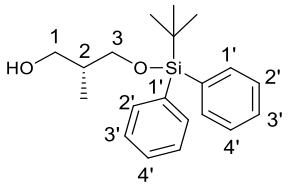

Methyl (*S*)-3-((*tert*-butyldiphenylsilyl)oxy)-2-methylpropanoate **163** (5.14 g, 14.42 mmol) was dissolved in DCM (70 mL) at 0 °C. DIBAL (1.0 M in DCM, 32 mL, 32.0 mmol) was added dropwise to the solution, and the resulting mixture was stirred at 0 °C for 4 h. Saturated aqueous Rochelle's salt (58 mL) was added slowly at 0 °C and stirred at room temperature overnight until a bilayer formed. The layers were separated, and the aqueous layer was extracted with EtOAc (3×50 mL). The organic layers were combined, dried over $MgSO_4$ and evaporated *in vacuo* to afford a colourless oil. The crude product was purified by column chromatography [silica, 12:1 (v/v) PE:EtOAc] to afford a colourless oil (3.23 g, 68.1%). R_f = 0.24 [10:1 (v/v) PE:EtOAc]; $[\alpha]_D^{20}$ +8.7 (*c* 1.50 in $CHCl_3$); lit. $[\alpha]_D^{20}$ +6.1 (*c* 0.93 in $CHCl_3$);[243] ^{1}H and ^{13}C NMR spectra and mass of the product were consistent with previously reported data.[243] δ_H (400.04 MHz; $CDCl_3$) 7.76-7.68 (4 H, m, Ar 2'-*H*), 7.50-7.38 (6 H, m, Ar 3'-*H* and Ar 4'-*H*), 3.76 (1 H, dd, *J* = 10.0, 4.4 Hz, 3-C*H*$_a$), 3.73-3.68 (2 H, m, 1-C*H*$_2$), 3.64 (1 H, dd, *J* = 10.0, 7.6 Hz, 3-C*H*$_b$), 2.70 (1 H, br s, O*H*), 2.10-1.97 (1 H, m, 2-C*H*),

1.11 (9 H, s, (C*H*$_3$)$_3$) and 0.88 (3 H, d, *J* = 6.8 Hz, 2-C*H*$_3$); δ_C (100.59 MHz, $CDCl_3$) 135.52 (Ar 2'-*C*), 135.50 (Ar 2'-*C*), 133.15 (Ar 1'-*C*), 129.71 (Ar 4'-*C*), 127.69 (Ar 3'-*C*), 68.45 (3-*C*H$_2$), 67.33 (1-*C*H$_2$), 37.32 (2-*C*H), 26.79 ((*C*H$_3$)$_3$), 19.09 (Si*C*) and 13.14 (2-*C*H$_3$); ESI-MS m/z calcd. for $[M+H]^+$ $C_{20}H_{29}O_2Si$: 329.1937, found 329.1957.

(2*R*)-*tert*-Butyl(3-(2,4-dinitrophenoxy)-2-methylpropoxy)diphenylsilane (165)

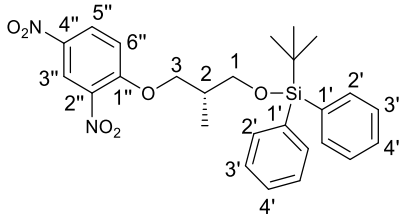

A solution of (*R*)-3-((*tert*-butyldiphenylsilyl)oxy)-2-methylpropan-1-ol **164** (2.63 g, 8.0 mmol) in DMF (40 mL) and a solution of 1-chloro-2,4-dinitrobenzene (3.24 g, 16.0 mmol) in DMF (18 mL) were added to NaH [60% (w/w) dispersion in mineral oil, 0.64 g, 16.0 mmol] in DMF (20 mL). The mixture was stirred at 60 °C for 2 days and was then filtered. The crude product was purified by column chromatography [Teledyne Isco CombiFlash Rf, RediSep prepacked columns, linear gradient of 0-15% (v/v) EtOAC in PE] to afford a yellow oil (545 mg, 13.8%). R_f = 0.50 [5:1 (v/v) PE:EtOAc]; $[\alpha]_D^{20}$ +11.9 (*c* 1.09 in $CHCl_3$); IR ν_{max}/cm^{-1} 1538 (N-O) and 1344 (N-O); δ_H (400.04 MHz; $CDCl_3$) 8.77 (1 H, d, *J* = 2.8 Hz, Ar 3''-*H*), 8.41 (1 H, dd, *J* = 9.2, 2.8 Hz, Ar 5''-*H*), 7.67-7.60 (4 H, m, Ar 2'-*H*), 7.45-7.31 (6 H, m, Ar 3'-*H* and Ar 4'-*H*), 7.19 (1 H, d, *J* = 9.2 Hz, Ar 6''-*H*), 4.28 (1 H, dd, *J* = 8.8, 5.6 Hz, 3-C*H*$_a$), 4.20 (1 H, dd, *J* = 8.8, 5.2 Hz, 3-C*H*$_b$), 3.83 (1 H, dd, *J* = 10.4, 4.4 Hz, 1-C*H*$_a$), 3.73 (1 H, dd, *J* = 10.4, 7.2 Hz, 1-C*H*$_b$), 2.35-2.23 (1 H, m, 2-C*H*), 1.10 (3 H, d, *J* = 7.2 Hz, 2-C*H*$_3$) and 1.07 (9 H, s, (C*H*$_3$)$_3$); δ_C (100.59 MHz, $CDCl_3$) 157.01 (Ar 1''-*C*), 139.75 (Ar 4''-*C*), 138.52 (Ar 2''-*C*), 135.44 (Ar 2'-*C*), 135.41 (Ar 2'-*C*), 133.34 (Ar 1'-*C*), 133.30 (Ar 1'-*C*), 129.67 (Ar 4'-*C*), 129.04 (Ar 5''-*C*), 127.62 (Ar 3'-*C*), 121.89 (Ar 3''-*C*), 114.24 (Ar 6''-*C*), 71.98 (3-*C*H$_2$), 64.53 (1-*C*H$_2$), 35.66 (2-*C*H), 26.83 ((*C*H$_3$)$_3$), 19.24 (Si*C*) and 13.36 (2-*C*H$_3$); ESI-MS m/z calcd. for $[M+Na]^+$ $C_{26}H_{30}N_2NaO_6Si$: 517.1771, found 517.1965.

Attempted synthesis of (2*S*)-3-(2,4-dinitrophenoxy)-2-methylpropan-1-ol (166)

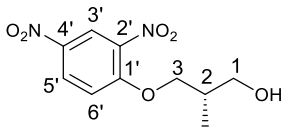

TBAF (1.0 M in THF, 2.0 mL, 2.00 mmol) was added to (*R*)-*tert*-butyl(3-(2,4-dinitrophenoxy)-2-methylpropoxy)diphenylsilane **165** (482 mg, 0.98 mmol) in THF (10 mL) and was stirred at room temperature for 18 h. Brine (20 mL) was added to the reaction mixture and was extracted with chloroform (3×20 mL). The organic layers were combined, dried over $MgSO_4$ and evaporated *in vacuo* to afford a brown oil. The crude product was purified by column chromatography [Teledyne Isco CombiFlash Rf, RediSep prepacked columns, linear gradient of 0-94% (v/v) EtOAC in PE] to give a yellow solid (145 mg, 58.0%). R_f = 0.30 [1:1 (v/v) PE:EtOAc]; $[\alpha]_D^{20}$ 0.0 (*c* 2.71 in $CHCl_3$); melting point 47-49 °C; IR ν_{max}/cm^{-1} 3404 (OH), 1526 (N-O) and 1352 (N-O); δ_H (400.04 MHz; $CDCl_3$) 8.71 (1 H, d, *J* = 2.8 Hz, Ar 3'-*H*), 8.40 (1 H, dd, *J* = 9.2, 2.8 Hz, Ar 5'-*H*), 7.25 (1 H, d, *J* = 9.2 Hz, Ar 6'-*H*), 4.27-4.17 (2 H, m, 3-C*H*$_2$), 3.72 (1 H, dd, *J* = 10.8, 4.8 Hz, 1-C*H*$_a$), 3.65 (1 H, dd, *J* = 10.8, 7.2 Hz, 1-C*H*$_b$), 2.35-2.17 (2 H, m, 2-C*H* and O*H*) and 1.05 (3 H, d, *J* = 6.8 Hz, 2-C*H*$_3$); δ_C (100.59 MHz, $CDCl_3$) 156.93 (Ar 1'-*C*), 139.86 (Ar 4'-*C*), 138.43 (Ar 2'-*C*), 129.26 (Ar 5'-*C*), 121.92 (Ar 3'-*C*), 114.42 (Ar 6'-*C*), 72.82 (3-*C*H$_2$), 64.34 (1-*C*H$_2$), 35.39 (2-*C*H) and 13.28 (2-*C*H$_3$); ESI-MS m/z calcd. for $[M+Na]^+C_{10}H_{12}N_2NaO_6$: 279.0593, found 279.0573.

Attempted synthesis of (2*R*)-3-(2,4-dinitrophenoxy)-2-methylpropanoic acid (167)

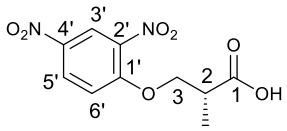

3-(2,4-Dinitrophenoxy)-2-methylpropan-1-ol **166** (130 mg, 0.51 mmol) in acetone (2.6 mL) was added over 1.5 h to CrO_3 (2.7 M in H_2SO_4 $_{aq}$, 0.36 mL, 0.97 mmol) at 0 °C, and the resulting mixture was stirred at room temperature for 2 h. *iso*-Propanol (0.10 mL) was added to the mixture and stirred for 10 min to quench the reaction. The mixture was filtered through celite and washed

with DCM. The DCM layer was washed with water (3×20 mL), dried over $MgSO_4$ and evaporated *in vacuo* to afford a pale yellow oil. The crude product was purified by column chromatography [silica, gradient elution with 2:1, 1.5:1 (v/v) PE:EtOAc, 20:1 (v/v) DCM:MeOH] to give a white solid (39 mg, 28.3%) that eluted in 20:1 (v/v) DCM:MeOH. R_f = 0.19 [1:2 (v/v) PE:EtOAc]; $[\alpha]_D^{20}$ 0.0 (*c* 0.78 in $CHCl_3$); melting point 134-137 °C; IR ν_{max}/cm^{-1} 3085 (OH), 1698 (C=O), 1526 (N-O) and 1354 (N-O); δ_H (500.13 MHz; $CDCl_3$) 8.74 (1 H, d, *J* = 3.0 Hz, Ar 3'-*H*), 8.43 (1 H, dd, *J* = 9.0, 3.0 Hz, Ar 5'-*H*), 7.23 (1 H, d, *J* = 9.0 Hz, Ar 6'-*H*), 6.58 (1 H, br s, O*H*), 4.43 (1 H, dd, *J* = 9.0, 6.5 Hz, 3-CH_a), 4.31 (1 H, dd, *J* = 9.0, 6.0 Hz, 3-CH_b), 3.14-3.04 (1 H, m, 2-C*H*) and 1.40 (3 H, d, *J* = 7.0 Hz, 2-CH_3); δ_C (125.76 MHz, $CDCl_3$) 178.39 (*C*=O), 156.27 (Ar 1'-*C*), 140.38 (Ar 4'-*C*), 138.85 (Ar 2'-*C*), 129.13 (Ar 5'-*C*), 121.95 (Ar 3'-*C*), 114.53 (Ar 6'-*C*), 71.44 (3-CH_2), 39.21 (2-*C*H) and 13.59 (2-CH_3); ESI-MS m/z calcd. for $[M-H]^-C_{10}H_9N_2O_7$: 269.0410, found 269.0398.

Methyl (*R*)-3-((*tert*-butyldiphenylsilyl)oxy)-2-methylpropanoate (171)

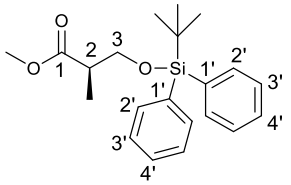

Compound **171** was prepared from (*R*)-3-hydroxy-2-methylpropionate (5.10 g, 43.17 mmol) using the same procedure as for compound **163** to give a colourless oil (15.39 g, 100.0%). The oil was found to be >95% pure (by ^{1}H NMR) and was used in next step without purification. R_f = 0.60 [10:1 (v/v) PE:EtOAc]; $[\alpha]_D^{20}$ -17.0 (*c* 1.00 in $CHCl_3$); lit. $[\alpha]_D^{20}$ -17.8 (*c* 1.16 in $CHCl_3$);[250] ^{1}H and ^{13}C NMR spectra of the product were consistent with previously reported data.[250] δ_H (400.04 MHz; $CDCl_3$) 7.74-7.66 (4 H, m, Ar 2'-*H*), 7.50-7.36 (6 H, m, Ar 3'-*H* and Ar 4'-*H*), 3.88 (1 H, dd, *J* = 10.0, 6.8 Hz, 3-CH_a), 3.78 (1 H, dd, *J* = 10.0, 6.0 Hz, 3-CH_b), 3.71 (3 H, s, OCH_3), 2.81-2.71 (1 H, m, 2-C*H*), 1.20 (3 H, d, *J* = 7.2 Hz, 2-CH_3) and 1.08 (9 H, s, (CH_3)$_3$); δ_C (100.59 MHz, $CDCl_3$) 175.33 (*C*=O), 135.51 (Ar 2'-*C*), 133.47 (Ar 1'-*C*), 133.41 (Ar 1'-*C*), 129.62 (Ar 4'-*C*), 127.62 (Ar 3'-*C*), 65.87 (3-CH_2), 51.47 (OCH_3), 42.34 (2-*C*H), 26.67 (C(*C*H_3)$_3$), 19.18 (Si*C*) and 13.41 (2-CH_3); ESI-MS m/z calcd. for $[M+H]^+$ $C_{21}H_{29}O_3Si$: 357.1886, found 357.1878.

(S)-3-((*tert*-Butyldiphenylsilyl)oxy)-2-methylpropan-1-ol (172)

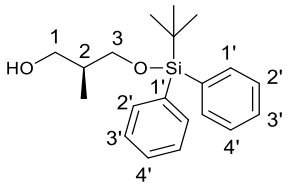

Compound **172** was prepared from methyl (*R*)-3-((*tert*-butyldiphenylsilyl)oxy)-2-methylpropanoate **171** (10.28 g, 28.83 mmol) using the same procedure as for compound **164** to give a colourless oil (3.90 g, 41.2%). R_f = 0.24 [10:1 (v/v) PE:EtOAc]; $[\alpha]_D^{20}$ -5.1 (*c* 0.99 in $CHCl_3$); lit. $[\alpha]_D^{20}$ -4.3 (*c* 1.15 in $CHCl_3$);[251] ^1H and ^{13}C NMR spectra of the product were consistent with previously reported data.[251] δ_H (400.04 MHz; $CDCl_3$) 7.76-7.70 (4 H, m, Ar 2'-*H*), 7.50-7.40 (6 H, m, Ar 3'-*H* and Ar 4'-*H*), 3.77 (1 H, dd, *J* = 10.0, 4.4 Hz, 3-CH_a), 3.74-3.67 (2 H, m, 1-CH_2), 3.65 (1 H, dd, *J* = 10.0, 7.6 Hz, 3-CH_b), 2.75 (1 H, br s, O*H*), 2.10-1.97 (1 H, m, 2-C*H*), 1.12 (9 H, s, (CH_3)$_3$) and 0.88 (3 H, d, *J* = 6.8 Hz, 2-CH_3); δ_C (100.59 MHz, $CDCl_3$) 135.51 (Ar 2'-*C*), 135.50 (Ar 2'-*C*), 133.15 (Ar 1'-*C*), 129.70 (Ar 4'-*C*), 127.68 (Ar 3'-*C*), 68.39 (3-*C*H_2), 67.25 (1-*C*H_2), 37.33 (2-*C*H), 26.78 ((*C*H_3)$_3$), 19.08 (Si*C*) and 13.14 (2-*C*H_3); ESI-MS m/z calcd. for $[M+H]^+$ $C_{20}H_{29}O_2Si$: 329.1937, found 329.1918.

Attempted synthesis of (2*S*)-*tert*-butyl(3-(2,4-dinitrophenoxy)-2-methylpropoxy)diphenylsilane (173)

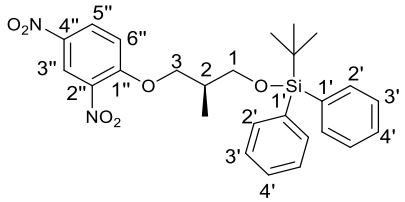

Compound **173** was prepared from (*S*)-3-((*tert*-butyldiphenylsilyl)oxy)-2-methylpropan-1-ol **172** (10.28 g, 28.83 mmol) using the same procedure as for compound **165** to give a yellow oil (816 mg, 14.9%). R_f = 0.53 [5:1 (v/v) PE:EtOAc]; $[\alpha]_D^{20}$ 0.0 (*c* 1.10 in $CHCl_3$); IR ν_{max}/cm^{-1} 1539 (N-O) and 1344 (N-O); δ_H (400.04 MHz; $CDCl_3$) 8.76 (1 H, d, *J* = 2.8 Hz, Ar 3''-*H*), 8.40 (1 H, dd, *J* = 9.2, 2.8 Hz, Ar 5''-*H*), 7.67-7.60 (4 H, m, Ar 2'-*H*), 7.45-7.31 (6 H, m, Ar 3'-*H* and Ar 4'-*H*), 7.19 (1 H, d, *J* = 9.2 Hz, Ar 6''-*H*), 4.28 (1 H, dd, *J* = 8.8, 5.6 Hz, 3-CH_a), 4.21 (1 H, dd, *J* = 8.8, 5.6 Hz, 3-CH_b), 3.84 (1 H, dd, *J* = 10.0, 4.4 Hz, 1-CH_a), 3.73 (1 H, dd, *J* = 10.4, 6.8 Hz, 1-CH_b), 2.35-2.24 (1 H, m, 2-C*H*),

1.11 (3 H, d, *J* = 7.2 Hz, 2-C*H*$_3$) and 1.07 (9 H, s, (C*H*$_3$)$_3$); δ_C (100.59 MHz, $CDCl_3$) 157.00 (Ar 1''-*C*), 139.70 (Ar 4''-*C*), 138.46 (Ar 2''-*C*), 135.40 (Ar 2'-*C*), 135.38 (Ar 2'-*C*), 133.31 (Ar 1'-*C*), 133.27 (Ar 1'-*C*), 129.63 (Ar 4'-*C*), 129.02 (Ar 5''-*C*), 127.59 (Ar 3'-*C*), 121.84 (Ar 3''-*C*), 114.25 (Ar 6''-*C*), 71.95 (3-*C*H$_2$), 64.50 (1-*C*H$_2$), 35.63 (2-*C*H), 26.79 ((*C*H$_3$)$_3$), 19.20 (Si*C*) and 13.33 (2-*C*H$_3$); ESI-MS m/z calcd. for $[M+Na]^+$ $C_{26}H_{30}N_2NaO_6Si$: 517.1771, found 517.1756.

Attempted synthesis of (2*R*)-3-(2,4-dinitrophenoxy)-2-methylpropan-1-ol (174)

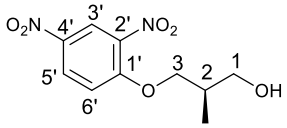

Compound **174** was prepared from *tert*-butyl(3-(2,4-dinitrophenoxy)-2-methylpropoxy)diphenylsilane **173** (800 mg, 1.62 mmol) using the same procedure as for compound **166** to give a yellow solid (267 mg, 64.3%). R_f = 0.32 [1:1 (v/v) PE:EtOAc]; $[\alpha]_D^{20}$ 0.0 (*c* 0.48 in $CHCl_3$); melting point 47-49 °C; IR ν_{max}/cm^{-1} 3282 (OH), 1524 (N-O) and 1356 (N-O); δ_H (400.04 MHz; $CDCl_3$) 8.73 (1 H, d, *J* = 2.8 Hz, Ar 3'-*H*), 8.40 (1 H, dd, *J* = 9.2, 2.8 Hz, Ar 5'-*H*), 7.25 (1 H, d, *J* = 9.2 Hz, Ar 6'-*H*), 4.27-4.18 (2 H, m, 3-C*H*$_2$), 3.74 (1 H, dd, *J* = 10.8, 4.8 Hz, 1-C*H*$_a$), 3.66 (1 H, dd, *J* = 10.8, 7.2 Hz, 1-C*H*$_b$), 2.32-2.20 (1 H, m, 2-C*H*), 2.14 (1 H, br s, O*H*) and 1.06 (3 H, d, *J* = 7.2 Hz, 2-C*H*$_3$); δ_C (100.59 MHz, $CDCl_3$) 156.93 (Ar 1'-*C*), 139.91 (Ar 4'-*C*), 138.48 (Ar 2'-*C*), 129.26 (Ar 5'-*C*), 121.95 (Ar 3'-*C*), 114.41 (Ar 6'-*C*), 72.83 (3-*C*H$_2$), 64.38 (1-*C*H$_2$), 35.41 (2-*C*H) and 13.30 (2-*C*H$_3$); ESI-MS m/z calcd. for $[M+Na]^+C_{10}H_{12}N_2NaO_6$: 279.0593, found 279.0569.

Attempted synthesis of (2*S*)-3-(2,4-dinitrophenoxy)-2-methylpropanoic acid (175)

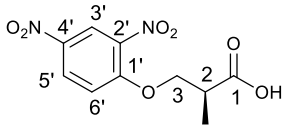

Compound **175** was prepared from 3-(2,4-dinitrophenoxy)-2-methylpropan-1-ol **174** (247 mg, 0.97 mmol) using the same procedure as for compound **167** to give a white solid (120 mg, 46.1%). R_f = 0.20 [1:2 (v/v) PE:EtOAc]; $[\alpha]_D^{20}$

0.0 (*c* 0.44 in $CHCl_3$); melting point 135-138 °C; IR ν_{max}/cm^{-1} 3084 (OH), 1698 (C=O), 1527 (N-O) and 1354 (N-O); δ_H (500.13 MHz; $CDCl_3$) 8.74 (1 H, d, *J* = 2.8 Hz, Ar 3'-*H*), 8.43 (1 H, dd, *J* = 9.0, 2.8 Hz, Ar 5'-*H*), 7.60 (1 H, br s, O*H*), 7.23 (1 H, d, *J* = 9.0 Hz, Ar 6'-*H*), 4.43 (1 H, dd, *J* = 9.0, 6.5 Hz, 3-CH_a), 4.31 (1 H, dd, *J* = 9.0, 6.0 Hz, 3-CH_b), 3.17-3.03 (1 H, m, 2-C*H*) and 1.40 (3 H, d, *J* = 7.0 Hz, 2-CH_3); δ_C (125.76 MHz, $CDCl_3$) 178.59 (*C*=O), 156.26 (Ar 1'-*C*), 140.40 (Ar 4'-*C*), 138.86 (Ar 2'-*C*), 129.12 (Ar 5'-*C*), 121.96 (Ar 3'-*C*), 114.52 (Ar 6'-*C*), 71.42 (3-CH_2), 39.22 (2-*C*H) and 13.58 (2-CH_3); ESI-MS m/z calcd. for $[M-H]^-C_{10}H_9N_2O_7$: 269.0410, found 269.0411.

6.32 Synthesis of the acyl-CoA ester of racemic 3-(2,4-dinitrophenoxy)-2-methylpropanoic acid

3-(2,4-Dinitrophenoxy)-2-methylpropanoyl-CoA (135)

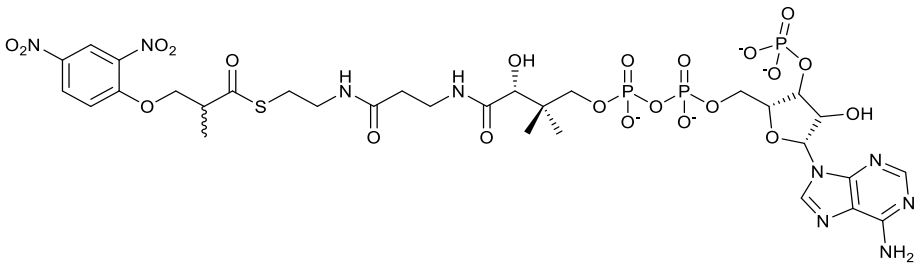

Compound **135** was prepared from 3-(2,4-dinitrophenoxy)-2-methylpropanoic acid (30 mg, 0.11 mmol) using the same procedure as for compound **49** to give a white solid (36 mg). δ_H (500.13 MHz, ^2H_2O) 8.74 (1 H, s, Ar-*H*), 8.59 (1 H, s, adenosine C*H*), 8.42 (1 H, dd, *J* = 9.5, 2.5 Hz, Ar-*H*), 8.34 (1 H, s, adenosine C*H*), 7.26 (1 H, d, *J* = 9.5 Hz, Ar-*H*), 6.15-6.06 (1 H, m, adenosine C*H*), 4.45-4.35 (2 H, m, CH_2), 4.18 (2 H, br s, adenosine CH_2), 3.96 (1 H, s, CoA(OHC*H*)), 3.85-3.74 (1 H, m, CoA(OCH_a)), 3.55-3.48 (1 H, m, CoA(OCH_b)), 3.40-3.25 (5 H, m, 2×CoA(CH_2) and CH_3C*H*), 2.99 (2 H, t, *J* = 6.5 Hz, CoA(SCH_2)), 2.33 (2 H, t, *J* = 6.5 Hz, CoA(CH_2)), 1.22 (3 H, d, *J* = 7.0 Hz, CHCH_3), 0.86 (3 H, s, CoA(CH_3)) and 0.72 (3 H, s, CoA(CH_3)); ESI-MS m/z calcd. for $[M+Na-2H]^-$ $C_{31}H_{42}N_9NaO_{22}P_3S$: 1040.1276, found 1040.1313.

6.33 Derivatisation of 2-methyldecanoic acid with a chiral amine

(2*R*)-2-methyl-*N*-[(1*S*)-1-phenylethyl]decanamide (179)

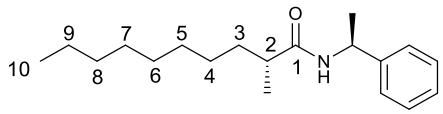

The amide **179** was synthesised using the protocol previously described.[1] Oxalyl chloride (31 µL, 0.37 mmol) and DMF (2 µL) were added to (2*R*)-2-methyldecanoic acid **184** (16 mg, 0.08 mmol) in DCM (1 mL). The mixture was stirred at room temperature for 45 min before the solvent was evaporated *in vacuo*. *S*-1-Phenylethylamine (31 µL, 0.24 mmol) was added to a solution of the crude intermediate in DCM (1 mL). The mixture was stirred at room temperature for 45 min before it was washed with HCl $_{aq.}$ (1.0 M, 3×3 mL). The organic layer was evaporated *in vacuo* to give a colourless gum (19 mg, 79.8%). The ^{1}H NMR spectrum of the product was consistent with previously reported data.[1] δ_H (500.13 MHz; $CDCl_3$) 7.37-7.21 (5 H, m, Ar-*H*), 5.61 (1 H, br d, *J* = 7.5 Hz, N*H*), 5.20-5.10 (1 H, m, NHC*H*), 2.19-2.08 (1 H, m, 2-*H*), 1.70-1.58 (1 H, m, 3-H_a), 1.48 (3 H, d, *J* = 7.0 Hz, ArCHCH_3), 1.40-1.33 (1 H, m, 3-H_b), 1.33-1.20 (12 H, m, 6×CH_2), 1.10 (3 H, d, *J* = 7.0 Hz, 2-CH_3) and 0.87 (3 H, t, *J* = 6.5 Hz, 10-*H*); δ_C (125.76 MHz, $CDCl_3$) 175.59 (*C*=O), 143.29 (Ar-*C*), 128.65 (Ar-*C*), 127.30 (Ar-*C*), 126.16 (Ar-*C*), 48.34 (NH*C*H), 41.71 (2-*C*), 34.40 (3-*C*), 31.85 (*C*H_2), 29.61(*C*H_2), 29.49 (*C*H_2), 29.25 (*C*H_2), 27.50 (*C*H_2), 22.65 (*C*H_2), 21.66 (ArCHCH_3), 17.84 (2-*C*H_3), and 14.08 (10-*C*).

(2*S*)-2-Methyl-*N*-[(1*S*)-1-phenylethyl]decanamide (180)

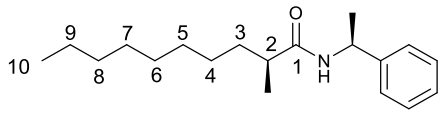

Compound **180** was prepared from (2*S*)-2-methyldecanoic acid **187** (15 mg, 0.08 mmol) using the same procedure as for compound **179** and as described by Darley *et al*.[1] to give a colourless gum (17 mg, 76.1%). The ^{1}H NMR spectrum of the product was consistent with previously reported data.[1] δ_H (500.13 MHz; $CDCl_3$) 7.35-7.21 (5 H, m, Ar-*H*), 5.62 (1 H, br d, *J* = 7.5 Hz, N*H*), 5.19-5.08 (1 H, m, NHC*H*), 2.19-2.09 (1 H, m, 2-*H*), 1.65-1.55 (1 H, m, 3-H_a), 1.48 (3 H, d, *J* = 7.0 Hz, ArCHCH_3), 1.39-1.31 (1 H, m, 3-H_b), 1.31-1.17 (12 H, m, 6×CH_2), 1.13 (3 H, d, *J* = 7.0 Hz, 2-CH_3) and 0.86 (3 H, t, *J* = 6.5

Hz, 10-*H*); δ_C (125.76 MHz, $CDCl_3$) 175.69 (*C*=O), 143.37 (Ar-*C*), 128.60 (Ar-*C*), 127.27 (Ar-*C*), 126.15 (Ar-*C*), 48.35 (NH*C*H), 41.67 (2-*C*), 34.43 (3-*C*), 31.85 (CH_2), 29.57(CH_2), 29.47 (CH_2), 29.20 (CH_2), 27.44 (CH_2), 22.63 (CH_2), 21.61 (ArCHCH_3), 17.84 (2-CH_3), and 14.09 (10-*C*).

7 References

1. Darley, D. J., Butler, D. S., Prideaux, S. J., Thornton, T. W., Wilson, A. D., Woodman, T. J., Threadgill, M. D., and Lloyd, M. D. (2009) Synthesis and use of isotope-labelled substrates for a mechanistic study on human α-methylacyl-CoA racemase 1A (AMACR; P504S). *Org. Biomol. Chem.* ***7***, 543-552.

2. Woodman, T. J., Wood, P. J., Thompson, A. S., Hutchings, T. J., Steel, G. R., Jiao, P., Threadgill, M. D., and Lloyd, M. D. (2011) Chiral inversion of 2-arylpropionyl-CoA esters by human α-methylacyl-CoA racemase 1A (P504S) – a potential mechanism for the anti-cancer effects of ibuprofen. *Chem. Commun.* ***47***, 7332-7334.

3. Yevglevskis, M., Lee, G. L., Threadgill, M. D., Woodman, T. J., and Lloyd, M. D. (2014) The perils of rational design – unexpected irreversible elimination of fluoride from 3-fluoro-2-methylacyl-CoA esters catalysed by α-methylacyl-CoA racemase (AMACR; P504S). *Chem. Commun.* ***50***, 14164-14166.

4. Timms, B. G. (2008) Prostate development: A historical perspective. *Differentiation* ***76***, 565-577.

5. Kumar, V. L., and Majumder, P. K. (1995) Prostate gland: Structure, functions and regulation. *Int. Urol. Nephrol.* ***27***, 231-243.

6. Aalberts, M., Stout, T. A., and Stoorvogel, W. (2014) Prostasomes: extracellular vesicles from the prostate. *Reproduction* ***147***, R1-R14.

7. Lonergan, P. E., and Tindall, D. J. (2011) Androgen receptor signaling in prostate cancer development and progression. *J. Carcinog.* ***10***, 20.

8. Pluta, R. M., Lynm, C., and Golub, R. M. (2012) Prostatitis. *JAMA* ***307***, 527-527.

9. Naber, K. G. (2001) Prostatitis. *Nephrol. Dial. Transplant.* ***16***, 132-134.

10. Rees, J., Abrahams, M., Doble, A., Cooper, A., and Prostatitis Expert Reference Group (PERG). (2015) Diagnosis and treatment of chronic bacterial prostatitis and chronic prostatitis/chronic pelvic pain syndrome: A consensus guideline. *Brit. J. Urol. Int.* ***116***, 509-525.

11. McVary, K. T. (2006) BPH: Epidemiology and comorbidities. *Am. J. Manag. Care* ***12***, S122-S128.

12. Platz, E. A., Kawachi, I., Rimm, E. B., Colditz, G. A., Stampfer, M. J., Willett, W. C., and Giovannucci, E. (1998) Physical activity and benign prostatic hyperplasia. *Arch. Intern. Med.* ***158***, 2349-2356.

13. National Guideline Clearinghouse. Guideline on the management of benign prostatic hyperplasia (BPH). Available from: http://www.guideline.gov/content.aspx?id=25635 [Accessed 20 September 2015].

14. Baade, P. D., Youlden, D. R., and Krnjacki, L. J. (2009) International epidemiology of prostate cancer: Geographical distribution and secular trends. *Mol. Nutr. Food Res.* ***53***, 171-184.

15. Cancer Research UK. Prostate cancer statistics. Available from: http://www.cancerresearchuk.org/health-professional/cancer-statistics/statistics-by-cancer-type/prostate-cancer#heading-One [Accessed 22 September 2015].

16. Siegel, R., Ma, J., Zou, Z., and Jemal, A. (2014) Cancer statistics, 2014. *CA: Cancer J. Clin.* ***64***, 9-29.

17. Kelly, B. D., Miller, N., Sweeney, K. J., Durkan, G. C., Rogers, E., Walsh, K., and Kerin, M. J. (2015) A circulating microRNA signature as a biomarker for prostate cancer in a high risk group. *J. Clin. Med.* ***4***, 1369-1379.

18. Bostwick, D. G., Burke, H. B., Djakiew, D., Euling, S., Ho, S. M., Landolph, J., Morrison, H., Sonawane, B., Shifflett, T., Waters, D. J., and Timms, B. (2004) Human prostate cancer risk factors. *Cancer* ***101***, 2371-2490.

19. Albertsen, P. C., Moore, D. F., Shih, W., Lin, Y., Li, H., and Lu-Yao, G. L. (2011) Impact of comorbidity on survival among men with localized prostate cancer. *J. Clin. Oncol.* ***29***, 1335-1341.

20. Stangelberger, A., Waldert, M., and Djavan, B. (2008) Prostate cancer in elderly men. *Rev. Urol.* ***10***, 111-119.

21. Grönberg, H. (2003) Prostate cancer epidemiology. *Lancet* ***361***, 859-864.

22. Crawford, E. D. (2003) Epidemiology of prostate cancer. *Urology* ***62***, 3-12.

23. Gann, P. H. (2002) Risk factors for prostate cancer. *Rev. Urol.* ***4***, S3-S10.

24. Steinberg, G. D., Carter, B. S., Beaty, T. H., Childs, B., and Walsh, P. C. (1990) Family history and the risk of prostate cancer. *Prostate* ***17***, 337-347.

25. Page, W. F., Braun, M. M., Partin, A. W., Caporaso, N., and Walsh, P. (1997) Heredity and prostate cancer: A study of World War II veteran twins. *Prostate* ***33***, 240-245.

26. Gronberg, H., Damber, L., and Damber, J. E. (1994) Studies of genetic factors in prostate cancer in a twin population. *J. Urol.* ***152***, 1484-1487; discussion 1487-1489.

27. Wright, A. S., Thomas, L. N., Douglas, R. C., Lazier, C. B., and Rittmaster, R. S. (1996) Relative potency of testosterone and dihydrotestosterone in preventing atrophy and apoptosis in the prostate of the castrated rat. *J. Clin. Invest.* ***98***, 2558-2563.

28. Zhou, Z. X., Lane, M. V., Kemppainen, J. A., French, F. S., and Wilson, E. M. (1995) Specificity of ligand-dependent androgen receptor stabilization:

Receptor domain interactions influence ligand dissociation and receptor stability. *Mol. Endocrinol.* ***9***, 208-218.

29. Heinlein, C. A., and Chang, C. (2004) Androgen receptor in prostate cancer. *Endocr. Rev.* ***25***, 276-308.

30. Isaacs, J. T. (1984) Antagonistic effect of androgen on prostatic cell death. *Prostate* ***5***, 545-557.

31. Tomlins, S. A., Rhodes, D. R., Perner, S., Dhanasekaran, S. M., Mehra, R., Sun, X. W., Varambally, S., Cao, X., Tchinda, J., Kuefer, R., Lee, C., Montie, J. E., Shah, R. B., Pienta, K. J., Rubin, M. A., and Chinnaiyan, A. M. (2005) Recurrent fusion of TMPRSS2 and ETS transcription factor genes in prostate cancer. *Science* ***310***, 644-648.

32. Rajput, A. B., Miller, M. A., De Luca, A., Boyd, N., Leung, S., Hurtado-Coll, A., Fazli, L., Jones, E. C., Palmer, J. B., Gleave, M. E., Cox, M. E., and Huntsman, D. G. (2007) Frequency of the TMPRSS2: ERG gene fusion is increased in moderate to poorly differentiated prostate cancers. *J. Clin. Pathol.* ***60***, 1238-1243.

33. Mehra, R., Tomlins, S. A., Shen, R., Nadeem, O., Wang, L., Wei, J. T., Pienta, K. J., Ghosh, D., Rubin, M. A., Chinnaiyan, A. M., and Shah, R. B. (2007) Comprehensive assessment of TMPRSS2 and ETS family gene aberrations in clinically localized prostate cancer. *Mod. Pathol.* ***20***, 538-544.

34. Hellerstedt, B. A., and Pienta, K. J. (2002) The current state of hormonal therapy for prostate cancer. *CA: Cancer J. Clin.* ***52***, 154-179.

35. Chan, J. M., Stampfer, M. J., Giovannucci, E., Gann, P. H., Ma, J., Wilkinson, P., Hennekens, C. H., and Pollak, M. (1998) Plasma insulin-like growth factor-I and prostate cancer risk: a prospective study. *Science* ***279***, 563-566.

36. Stattin, P., Bylund, A., Rinaldi, S., Biessy, C., Déchaud, H., Stenman, U.-H., Egevad, L., Riboli, E., Hallmans, G., and Kaaks, R. (2000) Plasma insulin-like growth factor-I, insulin-like growth factor-binding proteins, and prostate cancer risk: A prospective study. *J. Natl. Cancer Inst.* ***92***, 1910-1917.

37. Wu, J. D., Haugk, K., Woodke, L., Nelson, P., Coleman, I., and Plymate, S. R. (2006) Interaction of IGF signaling and the androgen receptor in prostate cancer progression. *J. Cell. Biochem.* ***99***, 392-401.

38. Dimakakos, A., Armakolas, A., and Koutsilieris, M. (2014) Novel tools for prostate cancer prognosis, diagnosis, and follow-up. *Biomed. Res. Int.* ***2014***, 1-9.

39. Montie, J. E. (1995) Staging of prostate cancer. Current TNM classification and future prospects for prognostic factors. *Cancer* ***75***, 1814-1818.

40. Humphrey, P. A. (2004) Gleason grading and prognostic factors in carcinoma of the prostate. *Mod. Pathol.* ***17***, 292-306.

41. Frydenberg, M., Stricker, P. D., and Kaye, K. W. (1997) Prostate cancer diagnosis and management. *Lancet* ***349***, 1681-1687.

42. Heidenreich, A., Bastian, P. J., Bellmunt, J., Bolla, M., Joniau, S., Van Der Kwast, T., Mason, M., Matveev, V., Wiegel, T., Zattoni, F., and Mottet, N. (2014) EAU guidelines on prostate cancer. Part 1: Screening, diagnosis, and local treatment with curative intent – update 2013. *Eur. Urol.* ***65***, 124-137.

43. Andriole, G., Djavan, B., Fleshner, N., and Schröder, F. (2006) The case for prostate cancer screening with prostate-specific antigen. *Eur. Urol. Suppl.* ***5***, 737-745.

44. Howrey, B. T., Kuo, Y.-F., Lin, Y.-L., and Goodwin, J. S. (2013) The impact of PSA screening on prostate cancer mortality and overdiagnosis of prostate cancer in the United States. *J. Gerontol. A Biol. Sci. Med. Sci.* ***68***, 56-61.

45. Vickers, A. J., Sjoberg, D. D., Ulmert, D., Vertosick, E., Roobol, M. J., Thompson, I., Heijnsdijk, E. A., De Koning, H., Atoria-Swartz, C., Scardino, P. T., and Lilja, H. (2014) Empirical estimates of prostate cancer overdiagnosis by age and prostate-specific antigen. *BMC Med.* ***12***, 1-7.

46. Shariat, S. F., Semjonow, A., Lilja, H., Savage, C., Vickers, A. J., and Bjartell, A. (2011) Tumor markers in prostate cancer I: Blood-based markers. *Acta Oncol.* ***50***, 61-75.

47. Luo, J., Zha, S., Gage, W. R., Dunn, T. A., Hicks, J. L., Bennett, C. J., Ewing, C. M., Platz, E. A., Ferdinandusse, S., Wanders, R. J., Trent, J. M., Isaacs, W. B., and De Marzo, A. M. (2002) α-Methylacyl-CoA racemase: A new molecular marker for prostate cancer. *Cancer Res.* ***62***, 2220-2226.

48. Zha, S., Ferdinandusse, S., Denis, S., Wanders, R. J., Ewing, C. M., Luo, J., De Marzo, A. M., and Isaacs, W. B. (2003) α-Methylacyl-CoA racemase as an androgen-independent growth modifier in prostate cancer. *Cancer Res.* ***63***, 7365-7376.

49. Obort, A. S., Ajadi, M. B., and Akinloye, O. (2013) Prostate-specific antigen: Any successor in sight? *Rev. Urol.* ***15***, 97-107.

50. Jiang, Z., Woda, B. A., Rock, K. L., Xu, Y., Savas, L., Khan, A., Pihan, G., Cai, F., Babcook, J. S., Rathanaswami, P., Reed, S. G., Xu, J., and Fanger, G. R. (2001) P504S: A new molecular marker for the detection of prostate carcinoma. *Am. J. Surg. Pathol.* ***25***, 1397-1404.

51. Honma, I., Torigoe, T., Hirohashi, Y., Kitamura, H., Sato, E., Masumori, N., Tamura, Y., Tsukamoto, T., and Sato, N. (2009) Aberrant expression and potency as a cancer immunotherapy target of α-methylacyl-coenzyme A racemase in prostate cancer. *J. Transl. Med.* ***7***, 103.

52. Molinie, V., Fromont, G., Sibony, M., Vieillefond, A., Vassiliu, V., Cochand-Priollet, B., Herve, J. M., Lebret, T., and Baglin, A. C. (2004) Diagnostic utility

of a p63/α-methyl-CoA-racemase (P504S) cocktail in atypical foci in the prostate. *Mod. Pathol.* ***17***, 1180-1190.

53. Wang, W., Sun, X., and Epstein, J. I. (2008) Partial atrophy on prostate needle biopsy cores: A morphologic and immunohistochemical study. *Am. J. Surg. Pathol.* ***32***, 851-857.

54. Trpkov, K., Bartczak-McKay, J., and Yilmaz, A. (2009) Usefulness of cytokeratin 5/6 and AMACR applied as double sequential immunostains for diagnostic assessment of problematic prostate specimens. *Am. J. Clin. Pathol.* ***132***, 211-220.

55. Herawi, M., and Epstein, J. I. (2007) Immunohistochemical antibody cocktail staining (p63/HMWCK/AMACR) of ductal adenocarcinoma and Gleason pattern 4 cribriform and noncribriform acinar adenocarcinomas of the prostate. *Am. J. Surg. Pathol.* ***31***, 889-894.

56. White, J. M., Jr., and O' Brien, D. P., III. (1990) Prostate examination. In: Walker, H. K., Hall, W. D., and Hurst, J. W. ed. 3rd edn. *Clinical methods: The history, physical and laboratory examinations.* Boston: Butterworths. Ch. 190. 1-3.

57. Woolf, S. H., and Rothemich, S. F. (1999) Screening for prostate cancer: The roles of science, policy, and opinion in determining what is best for patients. *Annu. Rev. Med.* ***50***, 207-221.

58. Ford, M. E., Havstad, S. L., Demers, R., and Cole Johnson, C. (2005) Effects of false-positive prostate cancer screening results on subsequent prostate cancer screening behavior. *Cancer Epidemiol. Biomarkers Prev.* ***14***, 190-194.

59. Shariat, S. F., and Roehrborn, C. G. (2008) Using biopsy to detect prostate cancer. *Rev. Urol.* ***10***, 262-280.

60. Kitajima, K., Kaji, Y., Fukabori, Y., Yoshida, K.-i., Suganuma, N., and Sugimura, K. (2010) Prostate cancer detection with 3 T MRI: Comparison of diffusion-weighted imaging and dynamic contrast-enhanced MRI in combination with T2-weighted imaging. *J. Magn. Reson. Imaging* ***31***, 625-631.

61. Haider, M. A., Van Der Kwast, T. H., Tanguay, J., Evans, A. J., Hashmi, A.-T., Lockwood, G., and Trachtenberg, J. (2007) Combined T2-weighted and diffusion-weighted MRI for localization of prostate cancer. *Am. J. Roentgenol.* ***189***, 323-328.

62. Epstein, J. I. (2010) An update of the Gleason grading system. *J. Urol.* ***183***, 433-440.

63. Egevad, L., Granfors, T., Karlberg, L., Bergh, A., and Stattin, P. (2002) Prognostic value of the Gleason score in prostate cancer. *Brit. J. Urol. Int.* ***89***, 538-542.

64. Dall'Era, M. A., Cooperberg, M. R., Chan, J. M., Davies, B. J., Albertsen, P. C., Klotz, L. H., Warlick, C. A., Holmberg, L., Bailey, D. E., Wallace, M. E., Kantoff, P. W., and Carroll, P. R. (2008) Active surveillance for early-stage prostate cancer. *Cancer* ***112***, 1650-1659.

65. Parker, C. (2004) Active surveillance: Towards a new paradigm in the management of early prostate cancer. *Lancet Oncol.* ***5***, 101-106.

66. Zincke, H., Oesterling, J. E., Blute, M. L., Bergstralh, E. J., Myers, R. P., and Barrett, D. M. (1994) Long-term (15 years) results after radical prostatectomy for clinically localized (stage T2c or lower) prostate cancer. *J. Urol.* ***152***, 1850-1857.

67. Abdollah, F., Sun, M., Schmitges, J., Thuret, R., Bianchi, M., Shariat, S. F., Briganti, A., Jeldres, C., Perrotte, P., Montorsi, F., and Karakiewicz, P. I. (2012) Survival benefit of radical prostatectomy in patients with localized

prostate cancer: estimations of the number needed to treat according to tumor and patient characteristics. *J. Urol.* ***188***, 73-83.

68. Evans, M., and Mason, M. (2007) Radical radiotherapy for prostate cancer. In: Waxman, J. ed. *Urological cancers in clinical practice*. London: Springer-Verlag. Ch. 1. 1-23.

69. Crawford, E. D. (2004) Hormonal therapy in prostate cancer: Historical approaches. *Rev. Urol.* ***6***, S3-S11.

70. Perlmutter, M. A., and Lepor, H. (2007) Androgen deprivation therapy in the treatment of advanced prostate cancer. *Rev. Urol.* ***9***, S3-S8.

71. Gomella, L. G., Singh, J., Lallas, C., and Trabulsi, E. J. (2010) Hormone therapy in the management of prostate cancer: Evidence-based approaches. *Ther. Adv. Urol.* ***2***, 171-181.

72. Armstrong, C. M., and Gao, A. C. (2015) Drug resistance in castration resistant prostate cancer: Resistance mechanisms and emerging treatment strategies. *Am. J. Clin. Exp. Urol.* ***3***, 64-76.

73. Kirby, M., Hirst, C., and Crawford, E. D. (2011) Characterising the castration-resistant prostate cancer population: A systematic review. *Int. J. Clin. Pract.* ***65***, 1180-1192.

74. El-Amm, J., and Aragon-Ching, J. B. (2013) The changing landscape in the treatment of metastatic castration-resistant prostate cancer. *Ther. Adv. Med. Oncol.* ***5***, 25-40.

75. Xu, J., Stolk, J. A., Zhang, X., Silva, S. J., Houghton, R. L., Matsumura, M., Vedvick, T. S., Leslie, K. B., Badaro, R., and Reed, S. G. (2000) Identification of differentially expressed genes in human prostate cancer using subtraction and microarray. *Cancer Res.* ***60***, 1677-1682.

76. Lloyd, M. D., Yevglevskis, M., Lee, G. L., Wood, P. J., Threadgill, M. D., and Woodman, T. J. (2013) α-Methylacyl-CoA racemase (AMACR): Metabolic enzyme, drug metabolizer and cancer marker P504S. *Prog. Lipid Res.* ***52***, 220-230.

77. Lloyd, M. D., Darley, D. J., Wierzbicki, A. S., and Threadgill, M. D. (2008) α-Methylacyl-CoA racemase – an 'obscure' metabolic enzyme takes centre stage. *FEBS J.* ***275***, 1089-1102.

78. Witkiewicz, A. K., Varambally, S., Shen, R., Mehra, R., Sabel, M. S., Ghosh, D., Chinnaiyan, A. M., Rubin, M. A., and Kleer, C. G. (2005) α-Methylacyl-CoA racemase protein expression is associated with the degree of differentiation in breast cancer using quantitative image analysis. *Cancer Epidemiol. Biomarkers Prev.* ***14***, 1418-1423.

79. Zhou, M., Chinnaiyan, A. M., Kleer, C. G., Lucas, P. C., and Rubin, M. A. (2002) α-Methylacyl-CoA racemase: A novel tumor marker over-expressed in several human cancers and their precursor lesions. *Am. J. Surg. Pathol.* ***26***, 926-931.

80. Jiang, Z., Fanger, G. R., Banner, B. F., Woda, B. A., Algate, P., Dresser, K., Xu, J., Reed, S. G., Rock, K. L., and Chu, P. G. (2003) A dietary enzyme: α-Methylacyl-CoA racemase/P504S is overexpressed in colon carcinoma. *Cancer Detect. Prev.* ***27***, 422-426.

81. Noske, A., Zimmermann, A. K., Caduff, R., Varga, Z., Fink, D., Moch, H., and Kristiansen, G. (2011) α-Methylacyl-CoA racemase (AMACR) expression in epithelial ovarian cancer. *Virchows Arch.* ***459***, 91-97.

82. Chen, Y. T., Tu, J. J., Kao, J., Zhou, X. K., and Mazumdar, M. (2005) Messenger RNA expression ratios among four genes predict subtypes of renal cell carcinoma and distinguish oncocytoma from carcinoma. *Clin. Cancer Res.* ***11***, 6558-6566.

83. Molinie, V., Balaton, A., Rotman, S., Mansouri, D., De Pinieux, I., Homsi, T., and Guillou, L. (2006) α-Methyl CoA racemase expression in renal cell carcinomas. *Hum. Pathol.* ***37***, 698-703.

84. Takahara, K., Azuma, H., Sakamoto, T., Kiyama, S., Inamoto, T., Ibuki, N., Nishida, T., Nomi, H., Ubai, T., Segawa, N., and Katsuoka, Y. (2009) Conversion of prostate cancer from hormone independency to dependency due to AMACR inhibition: Involvement of increased AR expression and decreased IGF1 expression. *Anticancer Res.* ***29***, 2497-2505.

85. Wilson, B. A., Wang, H., Nacev, B. A., Mease, R. C., Liu, J. O., Pomper, M. G., and Isaacs, W. B. (2011) High-throughput screen identifies novel inhibitors of cancer biomarker α-methylacyl coenzyme A racemase (AMACR/P504S). *Mol. Cancer Ther.* ***10***, 825-838.

86. Savolainen, K., Bhaumik, P., Schmitz, W., Kotti, T. J., Conzelmann, E., Wierenga, R. K., and Hiltunen, J. K. (2005) α-Methylacyl-CoA racemase from *Mycobacterium tuberculosis*. Mutational and structural characterization of the active site and the fold. *J. Biol. Chem.* ***280***, 12611-12620.

87. Heider, J. (2001) A new family of CoA-transferases. *FEBS Lett.* ***509***, 345-349.

88. Leutwein, C., and Heider, J. (2001) Succinyl-CoA: (*R*)-benzylsuccinate CoA-transferase: An enzyme of the anaerobic toluene catabolic pathway in denitrifying bacteria. *J. Bacteriol.* ***183***, 4288-4295.

89. Jonsson, S., Ricagno, S., Lindqvist, Y., and Richards, N. G. (2004) Kinetic and mechanistic characterization of the formyl-CoA transferase from *Oxalobacter formigenes*. *J. Biol. Chem.* ***279***, 36003-36012.

90. Schmitz, W., Albers, C., Fingerhut, R., and Conzelmann, E. (1995) Purification and characterization of an α-methylacyl-CoA racemase from human liver. *Eur. J. Biochem.* ***231***, 815-822.

91. Schmitz, W., Fingerhut, R., and Conzelmann, E. (1994) Purification and properties of an α-methylacyl-CoA racemase from rat liver. *Eur. J. Biochem.* ***222***, 313-323.

92. Kotti, T. J., Savolainen, K., Helander, H. M., Yagi, A., Novikov, D. K., Kalkkinen, N., Conzelmann, E., Hiltunen, J. K., and Schmitz, W. (2000) In mouse α-methylacyl-CoA racemase, the same gene product is simultaneously located in mitochondria and peroxisomes. *J. Biol. Chem.* ***275***, 20887-20895.

93. Schmitz, W., Helander, H. M., Hiltunen, J. K., and Conzelmann, E. (1997) Molecular cloning of cDNA species for rat and mouse liver α-methylacyl-CoA racemases. *Biochem. J.* ***326***, 883-889.

94. Ferdinandusse, S., Denis, S., Clayton, P. T., Graham, A., Rees, J. E., Allen, J. T., McLean, B. N., Brown, A. Y., Vreken, P., Waterham, H. R., and Wanders, R. J. (2000) Mutations in the gene encoding peroxisomal α-methylacyl-CoA racemase cause adult-onset sensory motor neuropathy. *Nat. Genet.* ***24***, 188-191.

95. Reichel, C., Bang, H., Brune, K., Geisslinger, G., and Menzel, S. (1995) 2-Arylpropionyl-CoA epimerase: Partial peptide sequences and tissue localization. *Biochem. Pharmacol.* ***50***, 1803-1806.

96. Reichel, C., Brugger, R., Bang, H., Geisslinger, G., and Brune, K. (1997) Molecular cloning and expression of a 2-arylpropionyl-coenzyme A epimerase: A key enzyme in the inversion metabolism of ibuprofen. *Mol. Pharmacol.* ***51***, 576-582.

97. Shieh, W. R., and Chen, C. S. (1993) Purification and characterization of novel "2-arylpropionyl-CoA epimerases" from rat liver cytosol and mitochondria. *J. Biol. Chem.* ***268***, 3487-3493.

98. Ferdinandusse, S., Denis, S., IJlst, L., Dacremont, G., Waterham, H. R., and Wanders, R. J. A. (2000) Subcellular localization and physiological role of α-methylacyl-CoA racemase. *J. Lipid Res.* ***41***, 1890-1896.

99. Van Veldhoven, P. P., Croes, K., Casteels, M., and Mannaerts, G. P. (1997) 2-Methylacyl racemase: A coupled assay based on the use of pristanoyl-CoA oxidase/peroxidase and reinvestigation of its subcellular distribution in rat and human liver. *Biochim. Biophys. Acta – Lipids Lipid Met.* ***1347***, 62-68.

100. Gavel, Y., and Von Heijne, G. (1990) Cleavage-site motifs in mitochondrial targeting peptides. *Protein Eng.* ***4***, 33-37.

101. Amery, L., Fransen, M., De Nys, K., Mannaerts, G. P., and Van Veldhoven, P. P. (2000) Mitochondrial and peroxisomal targeting of 2-methylacyl-CoA racemase in humans. *J. Lipid Res.* ***41***, 1752-1759.

102. Ferdinandusse, S., Denis, S., Faust, P. L., and Wanders, R. J. A. (2009) Bile acids: The role of peroxisomes. *J. Lipid Res.* ***50***, 2139-2147.

103. Baes, M., Gressens, P., Baumgart, E., Carmeliet, P., Casteels, M., Fransen, M., Evrard, P., Fahimi, D., Declercq, P. E., Collen, D., Van Veldhoven, P. P., and Mannaerts, G. P. (1997) A mouse model for Zellweger syndrome. *Nat. Genet.* ***17***, 49-57.

104. Steinberg, S. J., Raymond, G. V., Braverman, N. E., and Moser, A. B. (1993; updated 2012) Peroxisome biogenesis disorders, Zellweger syndrome spectrum. In: Pagon, R. A., Adam, M. P., Ardinger, H. H., Wallace, S. E., Amemiya, A., Bean, L. J. H., Bird, T. D., Fong, C. T., Mefford, H. C., Smith, R. J. H., and Stephens, K. ed. *GeneReviews [Internet]*. Seattle: University of Washington. 1-35.

105. Jansen, G. A., Mihalik, S. J., Watkins, P. A., Moser, H. W., Jakobs, C., Denis, S., and Wanders, R. J. (1996) Phytanoyl-CoA hydroxylase is present

in human liver, located in peroxisomes, and deficient in Zellweger syndrome: Direct, unequivocal evidence for the new, revised pathway of phytanic acid α-oxidation in humans. *Biochem. Biophys. Res. Commun.* ***229***, 205-210.

106. Ouazia, D., and Bearne, S. L. (2010) A continuous assay for α-methylacyl-coenzyme A racemase using circular dichroism. *Anal. Biochem.* ***398***, 45-51.

107. Li, X., Zheng, Q.-C., and Zhang, H.-X. (2012) Quantum chemical modeling of 1,1-proton transfer reaction catalyzed by a cofactor-independent α-methylacyl-CoA racemase. *Int. J. Quantum Chem.* ***112***, 619-624.

108. Sharma, S., Bhaumik, P., Schmitz, W., Venkatesan, R., Hiltunen, J. K., Conzelmann, E., Juffer, A. H., and Wierenga, R. K. (2012) The enolization chemistry of a thioester-dependent racemase: The 1.4 Å crystal structure of a reaction intermediate complex characterized by detailed QM/MM calculations. *J. Phys. Chem. B* ***116***, 3619-3629.

109. Kim, B. J., Kim, S. M., Cho, M. K., Yu, H. S., Lee, Y. S., Cha, H. J., and Ock, M. (2012) Expression and characterization of α-methylacyl CoA racemase from *Anisakis simplex* larvae. *Korean J. Parasitol.* ***50***, 165-171.

110. Mukherji, M., Schofield, C. J., Wierzbicki, A. S., Jansen, G. A., Wanders, R. J. A., and Lloyd, M. D. (2003) The chemical biology of branched-chain lipid metabolism. *Prog. Lipid Res.* ***42***, 359-376.

111. Wanders, R. J. A., Komen, J., and Ferdinandusse, S. (2011) Phytanic acid metabolism in health and disease. *Biochim. Biophys. Acta – Mol. Cell Biol. L.* ***1811***, 498-507.

112. Wierzbicki, A. S. (2007) Peroxisomal disorders affecting phytanic acid α-oxidation: A review. *Biochem. Soc. Trans.* ***35***, 881-886.

113. Wanders, R. J. A., and Waterham, H. R. (2006) Peroxisomal disorders: The single peroxisomal enzyme deficiencies. *Biochim. Biophys. Acta – Mol. Cell Res.* ***1763***, 1707-1720.

114. Van Veldhoven, P. P., Croes, K., Asselberghs, S., Herdewijn, P., and Mannaerts, G. P. (1996) Peroxisomal β-oxidation of 2-methyl-branched acyl-CoA esters: Stereospecific recognition of the 2*S*-methyl compounds by trihydroxycoprostanoyl-CoA oxidase and pristanoyl-CoA oxidase. *FEBS Lett.* ***388***, 80-84.

115. Kasaragod, P., Schmitz, W., Hiltunen, J. K., and Wierenga, R. K. (2013) The isomerase and hydratase reaction mechanism of the crotonase active site of the multifunctional enzyme (type-1), as deduced from structures of complexes with 3*S*-hydroxy-acyl-CoA. *FEBS J.* ***280***, 3160-3175.

116. Schmitz, W., and Conzelmann, E. (1997) Stereochemistry of peroxisomal and mitochondrial β-oxidation of α-methylacyl-CoAs. *Eur. J. Biochem.* ***244***, 434-440.

117. Battaile, K. P., McBurney, M., Van Veldhoven, P. P., and Vockley, J. (1998) Human long chain, very long chain and medium chain acyl-CoA dehydrogenases are specific for the *S*-enantiomer of 2- methylpentadecanoyl-CoA. *Biochim. Biophys. Acta – Lipid Lipid Met.* ***1390***, 333-338.

118. Ferdinandusse, S., and Houten, S. M. (2006) Peroxisomes and bile acid biosynthesis. *Biochim. Biophys. Acta – Mol. Cell Res.* ***1763***, 1427-1440.

119. Hoshita, N., Shefer, S., Cheng, F. W., Dayal, B., Batta, A. K., Tint, G. S., Salen, G., and Mosbach, E. H. (1978) Biosynthesis of chenodeoxycholic acid: Side-chain hydroxylation of 5β-cholestane-3α,7α-diol by subcellular fractions of guinea pig liver. *Lipids* ***13***, 961-965.

120. Ferdinandusse, S., Overmars, H., Denis, S., Waterham, H. R., Wanders, R. J. A., and Vreken, P. (2001) Plasma analysis of di- and

trihydroxycholestanoic acid diastereoisomers in peroxisomal α-methylacyl-CoA racemase deficiency. *J. Lipid Res.* ***42***, 137-141.

121. Savolainen, K., Kotti, T. J., Schmitz, W., Savolainen, T. I., Sormunen, R. T., Ilves, M., Vainio, S. J., Conzelmann, E., and Hiltunen, J. K. (2004) A mouse model for α-methylacyl-CoA racemase deficiency: Adjustment of bile acid synthesis and intolerance to dietary methyl-branched lipids. *Hum. Mol. Genet.* ***13***, 955-965.

122. Landoni, M. F., and Soraci, A. (2001) Pharmacology of chiral compounds: 2-Arylpropionic acid derivatives. *Curr. Drug Metab.* ***2***, 37-51.

123. Hawkey, C. J. (2001) COX-1 and COX-2 inhibitors. *Best Pract. Res. Clin. Gastroenterol.* ***15***, 801-820.

124. Mitchell, J. A., Akarasereenont, P., Thiemermann, C., Flower, R. J., and Vane, J. R. (1993) Selectivity of nonsteroidal antiinflammatory drugs as inhibitors of constitutive and inducible cyclooxygenase. *Proc. Natl. Acad. Sci. U.S.A.* ***90***, 11693-11697.

125. Dubois, N., Muller, N., Lapicque, F., Gillet, P., Netter, P., and Royer, R. J. (1993) Stereoselective protein binding of non-steroidal anti-inflammatory agents. Pharmacological implications. *Therapie* ***48***, 335-339.

126. Neupert, W., Brugger, R., Euchenhofer, C., Brune, K., and Geisslinger, G. (1997) Effects of ibuprofen enantiomers and its coenzyme A thioesters on human prostaglandin endoperoxide synthases. *Br. J. Pharmacol.* ***122***, 487-492.

127. Benoit, E., Delatour, P., Olivier, L., and Caldwell, J. (1995) (-)-*R*-fenoprofen: Formation of fenoprofenyl-coenzyme A by rat liver microsomes. *Biochem. Pharmacol.* ***49***, 1717-1720.

128. Brugger, R., Garcia Alia, B., Reichel, C., Waibel, R., Menzel, S., Brune, K., and Geisslinger, G. (1996) Isolation and characterization of rat liver

microsomal *R*-ibuprofenoyl-CoA synthetase. *Biochem. Pharmacol.* ***52***, 1007-1013.

129. Sevoz, C., Benoit, E., and Buronfosse, T. (2000) Thioesterification of 2-arylpropionic acids by recombinant acyl-coenzyme A synthetases (ACS1 and ACS2). *Drug Metab. Dispos.* ***28***, 398-402.

130. Mazaleuskaya, L. L., Theken, K. N., Gong, L., Thorn, C. F., FitzGerald, G. A., Altman, R. B., and Klein, T. E. (2015) PharmGKB summary: Ibuprofen pathways. *Pharmacogenet. genomics* ***25***, 96-106.

131. Qu, X., Allan, A., Chui, G., Hutchings, T. J., Jiao, P., Johnson, L., Leung, W. Y., Li, P. K., Steel, G. R., Thompson, A. S., Threadgill, M. D., Woodman, T. J., and Lloyd, M. D. (2013) Hydrolysis of ibuprofenoyl-CoA and other 2-APA-CoA esters by human acyl-CoA thioesterases-1 and -2 and their possible role in the chiral inversion of profens. *Biochem. Pharmacol.* ***86***, 1621-1625.

132. Hunt, M. C., and Alexson, S. E. (2008) Novel functions of acyl-CoA thioesterases and acyltransferases as auxiliary enzymes in peroxisomal lipid metabolism. *Prog. Lipid Res.* ***47***, 405-421.

133. Kirkby, B., Roman, N., Kobe, B., Kellie, S., and Forwood, J. K. (2010) Functional and structural properties of mammalian acyl-coenzyme A thioesterases. *Prog. Lipid Res.* ***49***, 366-377.

134. Menzel, S., Waibel, R., Brune, K., and Geisslinger, G. (1994) Is the formation of *R*-ibuprofenyl-adenylate the first stereoselective step of chiral inversion? *Biochem. Pharmacol.* ***48***, 1056-1058.

135. Leipold, D. D., Kantoci, D., Murray, E. D., Quiggle, D. D., and Wechter, W. J. (2004) Bioinversion of *R*-flurbiprofen to *S*-flurbiprofen at various dose levels in rat, mouse, and monkey. *Chirality* ***16***, 379-387.

136. Jamali, F., Berry, B. W., Tehrani, M. R., and Russell, A. S. (1988) Stereoselective pharmacokinetics of flurbiprofen in humans and rats. *J. Pharm. Sci.* ***77***, 666-669.

137. Porubek, D. J., Sanins, S. M., Stephens, J. R., Grillo, M. P., Kaiser, D. G., Halstead, G. W., Adams, W. J., and Baillie, T. A. (1991) Metabolic chiral inversion of flurbiprofen-CoA *in vitro*. *Biochem. Pharmacol.* ***42***, R1-R4.

138. Jacobs, E. J., Rodriguez, C., Mondul, A. M., Connell, C. J., Henley, S. J., Calle, E. E., and Thun, M. J. (2005) A large cohort study of aspirin and other nonsteroidal anti-inflammatory drugs and prostate cancer incidence. *J. Natl. Cancer Inst.* ***97***, 975-980.

139. Mahmud, S. M., Franco, E. L., Turner, D., Platt, R. W., Beck, P., Skarsgard, D., Tonita, J., Sharpe, C., and Aprikian, A. G. (2011) Use of non-steroidal anti-inflammatory drugs and prostate cancer risk: A population-based nested case-control study. *PLoS One* ***6***, e16412.

140. Ulrich, C. M., Bigler, J., and Potter, J. D. (2006) Non-steroidal anti-inflammatory drugs for cancer prevention: Promise, perils and pharmacogenetics. *Nat. Rev. Cancer* ***6***, 130-140.

141. Harris, R. E., Beebe-Donk, J., Doss, H., and Burr Doss, D. (2005) Aspirin, ibuprofen, and other non-steroidal anti-inflammatory drugs in cancer prevention: A critical review of non-selective COX-2 blockade (review). *Oncol. Rep.* ***13***, 559-583.

142. Daugherty, S. E., Shugart, Y. Y., Platz, E. A., Fallin, M. D., Isaacs, W. B., Pfeiffer, R. M., Welch, R., Huang, W.-Y., Reding, D., and Hayes, R. B. (2007) Polymorphic variants in α-methylacyl-CoA racemase and prostate cancer. *Prostate* ***67***, 1487-1497.

143. Carnell, A. J., Hale, I., Denis, S., Wanders, R. J., Isaacs, W. B., Wilson, B. A., and Ferdinandusse, S. (2007) Design, synthesis, and *in vitro* testing of α-methylacyl-CoA racemase inhibitors. *J. Med. Chem.* ***50***, 2700-2707.

144. Morgenroth, A., Urusova, E. A., Dinger, C., Al-Momani, E., Kull, T., Glatting, G., Frauendorf, H., Jahn, O., Mottaghy, F. M., Reske, S. N., and Zlatopolskiy, B. D. (2011) New molecular markers for prostate tumor imaging: A study on 2-methylene substituted fatty acids as new AMACR inhibitors. *Chemistry* ***17***, 10144-10150.

145. Carnell, A. J., Kirk, R., Smith, M., McKenna, S., Lian, L.-Y., and Gibson, R. (2013) Inhibition of human α-methylacyl CoA racemase (AMACR): A target for prostate cancer. *ChemMedChem* ***8***, 1643-1647.

146. Bhaumik, P., Schmitz, W., Hassinen, A., Hiltunen, J. K., Conzelmann, E., and Wierenga, R. K. (2007) The catalysis of the 1,1-proton transfer by α-methyl-acyl-CoA racemase is coupled to a movement of the fatty acyl moiety over a hydrophobic, methionine-rich surface. *J. Mol. Biol.* ***367***, 1145-1161.

147. Sattar, F. A., Darley, D. J., Politano, F., Woodman, T. J., Threadgill, M. D., and Lloyd, M. D. (2010) Unexpected stereoselective exchange of straight-chain fatty acyl-CoA α-protons by human α-methylacyl-CoA racemase 1A (P504S). *Chem. Commun.* ***46***, 3348-3350.

148. Chen, C. S., Shieh, W. R., Lu, P. H., Harriman, S., and Chen, C. Y. (1991) Metabolic stereoisomeric inversion of ibuprofen in mammals. *Biochim. Biophys. Acta* ***1078***, 411-417.

149. Kelly, S. M., Jess, T. J., and Price, N. C. (2005) How to study proteins by circular dichroism. *Biochim. Biophys. Acta* ***1751***, 119-139.

150. Sharp, T. R., Hegeman, G. D., and Kenyon, G. L. (1979) A direct kinetic assay for mandelate racemase using circular dichroic measurements. *Anal. Biochem.* ***94***, 329-334.

151. Noda, M., Matoba, Y., Kumagai, T., and Sugiyama, M. (2005) A novel assay method for an amino acid racemase reaction based on circular dichroism. *Biochem. J.* ***389***, 491-496.

152. Tanner, M. E., Gallo, K. A., and Knowles, J. R. (1993) Isotope effects and the identification of catalytic residues in the reaction catalyzed by glutamate racemase. *Biochemistry* ***32***, 3998-4006.

153. Bhaumik, P., Kursula, P., Ratas, V., Conzelmann, E., Hiltunen, J. K., Schmitz, W., and Wierenga, R. K. (2003) Crystallization and preliminary X-ray diffraction studies of an α-methylacyl-CoA racemase from *Mycobacterium tuberculosis*. *Acta Crystallogr. D Biol. Crystallogr.* ***59***, 353-355.

154. Rhee, K.-H., Lee, K. S., Priyadarshi, A., Kim, E. E., and Hwang, K. Y. (2005) Crystallization and preliminary X-ray crystallographic studies of fatty acid-CoA racemase from *Mycobacterium tuberculosis* H37Rv. *Acta Crystallogr. Sect. F Struct. Biol. Cryst. Commun.* ***61***, 1017-1019.

155. Acharya, K. R., and Lloyd, M. D. (2005) The advantages and limitations of protein crystal structures. *Trends Pharmacol. Sci.* ***26***, 10-14.

156. Swaminathan, G. J., Holloway, D. E., Colvin, R. A., Campanella, G. K., Papageorgiou, A. C., Luster, A. D., and Acharya, K. R. (2003) Crystal structures of oligomeric forms of the IP-10/CXCL10 chemokine. *Structure* ***11***, 521-532.

157. Lin, P.-Y., Cheng, K.-L., McGuffin-Cawley, J. D., Shieu, F.-S., Samia, A. C., Gupta, S., Cooney, M., Thompson, C. L., and Liu, C. C. (2012) Detection of α-methylacyl-CoA racemase (AMACR), a biomarker of prostate cancer, in patient blood samples using a nanoparticle electrochemical biosensor. *Biosensors* ***2***, 377-387.

158. Ouyang, B., Leung, Y.-K., Wang, V., Chung, E., Levin, L., Bracken, B., Cheng, L., and Ho, S.-M. (2011) α-Methylacyl-CoA racemase spliced variants

and their expression in normal and malignant prostate tissues. *Urology* ***77***, 249.e241-249.e247.

159. Shen-Ong, G. L., Feng, Y., and Troyer, D. A. (2003) Expression profiling identifies a novel α-methylacyl-CoA racemase exon with fumarate hydratase homology. *Cancer Res.* ***63***, 3296-3301.

160. Mubiru, J. N., Shen-Ong, G. L., Valente, A. J., and Troyer, D. A. (2004) Alternative spliced variants of the α-methylacyl-CoA racemase gene and their expression in prostate cancer. *Gene* ***327***, 89-98.

161. Mubiru, J. N., Valente, A. J., and Troyer, D. A. (2005) A Variant of the α-methyl-acyl-CoA racemase gene created by a deletion in exon 5 and its expression in prostate cancer. *Prostate* ***65***, 117-123.

162. Zheng, S. L., Chang, B.-l., Faith, D. A., Johnson, J. R., Isaacs, S. D., Hawkins, G. A., Turner, A., Wiley, K. E., Bleecker, E. R., Walsh, P. C., Meyers, D. A., Isaacs, W. B., and Xu, J. (2002) Sequence variants of α-methylacyl-CoA racemase are associated with prostate cancer risk. *Cancer Res.* ***62***, 6485-6488.

163. Levin, A. M., Zuhlke, K. A., Ray, A. M., Cooney, K. A., and Douglas, J. A. (2007) Sequence variation in α-methylacyl-CoA racemase and risk of early-onset and familial prostate cancer. *Prostate* ***67***, 1507-1513.

164. Wright, J. L., Neuhouser, M. L., Lin, D. W., Kwon, E. M., Feng, Z., Ostrander, E. A., and Stanford, J. L. (2011) AMACR polymorphisms, dietary intake of red meat and dairy and prostate cancer risk. *Prostate* ***71***, 498-506.

165. Lee, S. J., Joung, J. Y., Yoon, H., Kim, J. E., Park, W. S., Seo, H. K., Chung, J., Hwang, J. A., Hong, S. H., Nam, S., Park, S., Kim, J., Lee, K. H., and Lee, Y. S. (2013) Genetic variations of α-methylacyl-CoA racemase are associated with sporadic prostate cancer risk in ethnically homogenous Koreans. *Biomed. Res. Int.* ***2013***, 1-11.

166. FitzGerald, L. M., Thomson, R., Polanowski, A., Patterson, B., McKay, J. D., Stankovich, J., and Dickinson, J. L. (2008) Sequence variants of α-methylacyl-CoA racemase are associated with prostate cancer risk: A replication study in an ethnically homogeneous population. *Prostate* ***68***, 1373-1379.

167. Festuccia, C., Gravina, G. L., Mancini, A., Muzi, P., Cesare, E. D., Kirk, R., Smith, M., Hughes, S., Gibson, R., Lian, L. Y., Ricevuto, E., and Carnell, A. J. (2014) Trifluoroibuprofen inhibits α-methylacyl coenzyme A racemase (AMACR/P504S), reduces cancer cell proliferation and inhibits *in vivo* tumor growth in aggressive prostate cancer models. *Anticancer Agents Med Chem* ***14***, 1031-1041.

168. Almonacid, D. E., Yera, E. R., Mitchell, J. B. O., and Babbitt, P. C. (2010) Quantitative comparison of catalytic mechanisms and overall reactions in convergently evolved enzymes: Implications for classification of enzyme function. *PLoS Comput. Biol.* ***6***, e1000700.

169. Meng, E. C., Polacco, B. J., and Babbit, P. C. (2009) 3D motifs. In: Rigden, D. J. ed. *From protein structure to function with bioinformatics*. Netherlands: Springer Ch. 8. 187-216.

170. Huang, Q., Campo, M. A., Yao, T., Tian, Q., and Larock, R. C. (2004) Synthesis of fused polycycles by 1,4-palladium migration chemistry. *J. Org. Chem.* ***69***, 8251-8257.

171. Gangjee, A., Dubash, N. P., and Queener, S. F. (2000) The synthesis of new 2,4-diaminofuro[2,3-d]pyrimidines with 5-biphenyl, phenoxyphenyl and tricyclic substitutions as dihydrofolate reductase inhibitors. *J. Heterocycl. Chem.* ***37***, 935-942.

172. Newman, M. S., and Karnes, H. A. (1966) The conversion of phenols to thiophenols via dialkylthiocarbamates. *J. Org. Chem.* ***31***, 3980-3984.

173. Zonta, C., De Lucchi, O., Volpicelli, R., and Cotarca, L. (2007) Thione-thiol rearrangement: Miyazaki-Newman-Kwart rearrangement and others. In: Schaumann, E. ed. *Sulfur-mediated rearrangements II*. Berlin Heidelberg: Springer-Verlag Ch. 4. 131-161.

174. Brown, S., Bernardo, M. M., Li, Z.-H., Kotra, L. P., Tanaka, Y., Fridman, R., and Mobashery, S. (2000) Potent and selective mechanism-based inhibition of gelatinases. *J. Am. Chem. Soc.* ***122***, 6799-6800.

175. Aranapakam, V., Grosu, G. T., Davis, J. M., Hu, B., Ellingboe, J., Baker, J. L., Skotnicki, J. S., Zask, A., DiJoseph, J. F., Sung, A., Sharr, M. A., Killar, L. M., Walter, T., Jin, G., and Cowling, R. (2003) Synthesis and structure-activity relationship of α-sulfonylhydroxamic acids as novel, orally active matrix metalloproteinase inhibitors for the treatment of osteoarthritis. *J. Med. Chem.* ***46***, 2361-2375.

176. Grillo, M. P., and Benet, L. Z. (2002) Studies on the reactivity of clofibryl-*S*-acyl-CoA thioester with glutathione *in vitro*. *Drug Metab. Dispos.* ***30***, 55-62.

177. Horng, H., and Benet, L. Z. (2013) Characterization of the acyl-adenylate linked metabolite of mefenamic Acid. *Chem. Res. Toxicol.* ***26***, 465-476.

178. Mitsunobu, O., and Yamada, M. (1967) Preparation of esters of carboxylic and phosphoric acid *via* quaternary phosphonium salts. *Bull. Chem. Soc. Jpn.* ***40***, 2380-2382.

179. Camp, D., and Jenkins, I. D. (1989) The mechanism of the Mitsunobu esterification reaction. Part I. The involvement of phosphoranes and oxyphosphonium salts. *J. Org. Chem.* ***54***, 3045-3049.

180. Hughes, D. L., and Reamer, R. A. (1996) The effect of acid strength on the Mitsunobu esterification reaction: Carboxyl vs hydroxyl reactivity. *J. Org. Chem.* ***61***, 2967-2971.

181. Dixon, S. M., Li, P., Liu, R., Wolosker, H., Lam, K. S., Kurth, M. J., and Toney, M. D. (2006) Slow-binding human serine racemase inhibitors from high-throughput screening of combinatorial libraries. *J. Med. Chem.* ***49***, 2388-2397.

182. Henderickx, H. J. W., Duchateau, A. L. L., and Raemakers-Franken, P. C. (2003) Chiral liquid chromatography-mass spectrometry for high-throughput screening of enzymatic racemase activity. *J. Chromatogr. A* ***1020***, 69-74.

183. Yevglevskis, M., Lee, G. L., Sun, J., Zhou, S., Sun, X., Kociok-Kohn, G., James, T. D., Woodman, T. J., and Lloyd, M. D. (2016) A study on the AMACR catalysed elimination reaction and its application to inhibitor testing. *Org. Biomol. Chem.* ***14***, 612-622.

184. Yevglevskis, M., Bowskill, C. R., Chan, C. C. Y., Heng, J. H. J., Threadgill, M. D., Woodman, T. J., and Lloyd, M. D. (2014) A study on the chiral inversion of mandelic acid in humans. *Org. Biomol. Chem.* ***12***, 6737-6744.

185. Saccoccia, F., Angelucci, F., Boumis, G., Carotti, D., Desiato, G., Miele, A. E., and Bellelli, A. (2014) Thioredoxin reductase and its inhibitors. *Curr. Protein Pept. Sci.* ***15***, 621-646.

186. Barrett, S., Mohr, P. G., Schmidt, P. M., and McKimm-Breschkin, J. L. (2011) Real time enzyme inhibition assays provide insights into differences in binding of neuraminidase inhibitors to wild type and mutant influenza viruses. *PLoS One* ***6***, e23627.

187. Khajehpour, M., Troxler, T., and Vanderkooi, J. M. (2004) Probing the active site of trypsin with rose bengal: Insights into the photodynamic inactivation of the enzyme. *Photochem. Photobiol.* ***80***, 359-365.

188. Morgan, P. E., Dean, R. T., and Davies, M. J. (2002) Inhibition of glyceraldehyde-3-phosphate dehydrogenase by peptide and protein

peroxides generated by singlet oxygen attack. *Eur. J. Biochem.* ***269***, 1916-1925.

189. Kim, S. Y., Tak, J. K., and Park, J. W. (2004) Inactivation of NADP(+)-dependent isocitrate dehydrogenase by singlet oxygen derived from photoactivated rose bengal. *Biochimie* ***86***, 501-507.

190. Copeland, R. A. (2005) Evaluation of enzyme inhibitors in drug discovery. A guide for medicinal chemists and pharmacologists. New Jersey: John Wiley & Sons. 271.

191. Rydzik, A. M., Leung, I. K. H., Kochan, G. T., Thalhammer, A., Oppermann, U., Claridge, T. D. W., and Schofield, C. J. (2012) Development and application of a fluoride-detection-based fluorescence assay for γ-butyrobetaine hydroxylase. *ChemBioChem* ***13***, 1559-1563.

192. Sun, X., Xu, Q., Kim, G., Flower, S. E., Lowe, J. P., Yoon, J., Fossey, J. S., Qian, X., Bull, S. D., and James, T. D. (2014) A water-soluble boronate-based fluorescent probe for the selective detection of peroxynitrite and imaging in living cells. *Chem. Sci.* ***5***, 3368-3373.

193. Torimura, M., Kurata, S., Yamada, K., Yokomaku, T., Kamagata, Y., Kanagawa, T., and Kurane, R. (2001) Fluorescence-quenching phenomenon by photoinduced electron transfer between a fluorescent dye and a nucleotide base. *Anal. Sci.* ***17***, 155-160.

194. Yevglevskis, M. (2014) Targeting AMACR to treat castrate-resistant prostate cancer (PhD thesis). The University of Bath.

195. Fang, X., and Wang, R. The K_i calculator for fluorescence-based competitive binding assays. Available from: http://sw16.im.med.umich.edu/software/calc_ki/ [Accessed 08 February 2016].

196. Nikolovska-Coleska, Z., Wang, R., Fang, X., Pan, H., Tomita, Y., Li, P., Roller, P. P., Krajewski, K., Saito, N. G., Stuckey, J. A., and Wang, S. (2004) Development and optimization of a binding assay for the XIAP BIR3 domain using fluorescence polarization. *Anal. Biochem.* ***332***, 261-273.

197. Yevglevskis, M., Lee, G. L., Nathubhai, A., Petrova, Y., James, T. D., Threadgill M. D., Woodman, T. J., and Lloyd, M. D. (2016) A convenient colorimetric assay for α-methylacyl-CoA racemase (AMACR; P504S) and characterization of inhibitors, manuscript in preparation.

198. Sigler, K., Knotkova, A., and Kotyk, A. (1978) Effect of inhibitors on acid production by baker's yeast. *Folia Microbiol.* ***23***, 409-422.

199. Chafaa, S., Meullemeestre, J., Schwing, M.-J., Vierling, F., Böhmer, V., and Vogt, W. (1993) (*o*-Hydroxyphenyl)methylphosphonic acids: Spectrophotometric determination of their pK_a values and of the deprotonation sequence. *Helv. Chim. Acta* ***76***, 1425-1434.

200. Cheng, Y., and Prusoff, W. H. (1973) Relationship between the inhibition constant (K_I) and the concentration of inhibitor which causes 50 per cent inhibition (I_{50}) of an enzymatic reaction. *Biochem. Pharmacol.* ***22***, 3099-3108.

201. Gao, L. B., Wang, J. Z., Yao, T. W., and Zeng, S. (2012) Study on the metabolic mechanism of chiral inversion of *S*-mandelic acid *in vitro*. *Chirality* ***24***, 86-95.

202. Kitz, R., and Wilson, I. B. (1962) Esters of methanesulfonic acid as irreversible inhibitors of acetylcholinesterase. *J. Biol. Chem.* ***237***, 3245-3249.

203. Cornish-Bowden, A., and Eisenthal, R. (1974) Statistical considerations in the estimation of enzyme kinetic parameters by the Direct Linear Plot and other methods. *Biochem. J.* ***139***, 721-730.

204. Eisenthal, R., and Cornish-Bowden, A. (1974) The Direct Linear Plot. A new graphical procedure for estimating enzyme kinetic parameters. *Biochem. J.* ***139***, 715-720.

205. Cornish-Bowden, A. (2001) Detection of errors of interpretation in experiments in enzyme kinetics. *Methods* ***24***, 181-190.

206. Babbitt, P. C., and Gerlt, J. A. (1997) Understanding enzyme superfamilies. Chemistry as the fundamental determinant in the evolution of new catalytic activities. *J. Biol. Chem.* ***272***, 30591-30594.

207. Gerlt, J. A., and Babbitt, P. C. (1998) Mechanistically diverse enzyme superfamilies: The importance of chemistry in the evolution of catalysis. *Curr. Opin. Chem. Biol.* ***2***, 607-612.

208. Powers, V. M., Koo, C. W., Kenyon, G. L., Gerlt, J. A., and Kozarich, J. W. (1991) Mechanism of the reaction catalyzed by mandelate racemase. 1. Chemical and kinetic evidence for a two-base mechanism. *Biochemistry* ***30***, 9255-9263.

209. Cardinale, G. J., and Abeles, R. H. (1968) Purification and mechanism of action of proline racemase. *Biochemistry* ***7***, 3970-3978.

210. Ahmed, S. A., Esaki, N., Tanaka, H., and Soda, K. (1986) Mechanism of α-amino-ε-caprolactam racemase reaction. *Biochemistry* ***25***, 385-388.

211. Traidej, M., Marquart, M. E., Caballero, A. R., Thibodeaux, B. A., and O'Callaghan, R. J. (2003) Identification of the active site residues of *Pseudomonas aeruginosa* protease IV: Importance of enzyme activity in autoprocessing and activation. *J. Biol. Chem.* ***278***, 2549-2553.

212. Lopez-Llano, J., Campos, L. A., and Sancho, J. (2006) α-Helix stabilization by alanine relative to glycine: Roles of polar and apolar solvent exposures and of backbone entropy. *Proteins* ***64***, 769-778.

213. Baneyx, F. (1999) Recombinant protein expression in *Escherichia coli*. *Curr. Opin. Biotech.* ***10***, 411-421.

214. Kopanic, J. L., Al-Mugotir, M., Zach, S., Das, S., Grosely, R., and Sorgen, P. L. (2013) An *Escherichia coli* strain for expression of the connexin45 carboxyl terminus attached to the 4th transmembrane domain. *Front. Pharmacol.* ***4***, 106.

215. Baneyx, F., and Mujacic, M. (2004) Recombinant protein folding and misfolding in *Escherichia coli*. *Nat. Biotechnol.* ***22***, 1399-1408.

216. Tan, J., Ramanan, R., Ling, T., Mustafa, S., and Ariff, A. (2012) The role of lac operon and lac repressor in the induction using lactose for the expression of periplasmic human interferon-α2b by *Escherichia coli*. *Ann. Microbiol.* ***62***, 1427-1435.

217. Weng, Y.-P., Hsu, F.-C., Yang, W.-S., and Chen, H.-P. (2006) Optimization of the overexpression of glutamate mutase S component under the control of T7 system by using lactose and IPTG as the inducers. *Enzyme Microb. Technol.* ***38***, 465-469.

218. Rosano, G. L., and Ceccarelli, E. A. (2014) Recombinant protein expression in *Escherichia coli*: Advances and challenges. *Front. Microbiol.* ***5***, 1-17.

219. Structural Genomics Consortium, Architecture et Fonction des Macromolécules Biologiques, Berkeley Structural Genomics Center, China Structural Genomics Consortium, Integrated Center for Structure and Function Innovation, Israel Structural Proteomics Center, Joint Center for Structural Genomics, Midwest Center for Structural Genomics, New York Structural GenomiX Research Center for Structural Genomics, Northeast Structural Genomics Consortium, Oxford Protein Production Facility, Protein Sample Production Facility, Max Delbrück Center for Molecular Medicine, Riken

Structural Genomics/Proteomics Initiative, and Spine Complexes. (2008) Protein production and purification. *Nat. methods* ***5***, 135-146.

220. Liu, X., Dai, Q., Austin, L., Coutts, J., Knowles, G., Zou, J., Chen, H., and Huo, Q. (2008) A one-step homogeneous immunoassay for cancer biomarker detection using gold nanoparticle probes coupled with dynamic light scattering. *J. Am. Chem. Soc.* ***130***, 2780-2782.

221. Wang, X., Ramström, O., and Yan, M. (2011) Dynamic light scattering as an efficient tool to study glyconanoparticle-lectin interactions. *Analyst* ***136***, 4174-4178.

222. Erickson, H. P. (2009) Size and shape of protein molecules at the nanometer level determined by sedimentation, gel filtration, and electron microscopy. *Biol. Proced. Online* ***11***, 32-51.

223. Greenfield, N. J. (2006) Using circular dichroism spectra to estimate protein secondary structure. *Nat. protoc.* ***1***, 2876-2890.

224. Kelly, S. M., and Price, N. C. (1997) The application of circular dichroism to studies of protein folding and unfolding. *Biochim. Biophys. Acta* ***1338***, 161-185.

225. Kelly, S. M., and Price, N. C. (2000) The use of circular dichroism in the investigation of protein structure and function. *Curr. Protein Pept. Sci.* ***1***, 349-384.

226. Huang, C.-W., Chen, Y.-H., Chen, Y.-H., Tsai, Y.-C., and Lee, H.-J. (2009) The interaction of Glu294 at the subunit interface is important for the activity and stability of goose δ-crystallin. *Mol. Vis.* ***15***, 2358-2363.

227. Le, W.-P., Yan, S.-X., Zhang, Y.-X., and Zhou, H.-M. (1996) Acid-induced folding of yeast alcohol dehydrogenase under low pH conditions. *J. Biochem.* ***119***, 674-679.

228. Matulis, D., and Lovrien, R. (1998) 1-Anilino-8-naphthalene sulfonate anion-protein binding depends primarily on ion pair formation. *Biophys. J.* ***74***, 422-429.

229. Kamen, D. E., and Woody, R. W. (2001) A partially folded intermediate conformation is induced in pectate lyase C by the addition of 8-anilino-1-naphthalenesulfonate (ANS). *Protein Sci.* ***10***, 2123-2130.

230. Qadeer, A., Rabbani, G., Zaidi, N., Ahmad, E., Khan, J. M., and Khan, R. H. (2012) 1-Anilino-8-naphthalene sulfonate (ANS) is not a desirable probe for determining the molten globule state of chymopapain. *PLoS One* ***7***, e50633.

231. Ali, V., Prakash, K., Kulkarni, S., Ahmad, A., Madhusudan, K. P., and Bhakuni, V. (1999) 8-Anilino-1-naphthalene sulfonic acid (ANS) induces folding of acid unfolded cytochrome c to molten globule state as a result of electrostatic interactions. *Biochemistry* ***38***, 13635-13642.

232. Sun, S., and Toney, M. D. (1999) Evidence for a two-base mechanism involving tyrosine-265 from arginine-219 mutants of alanine racemase. *Biochemistry* ***38***, 4058-4065.

233. Choi, S. Y., Esaki, N., Yoshimura, T., and Soda, K. (1992) Reaction mechanism of glutamate racemase, a pyridoxal phosphate-independent amino acid racemase. *J. Biochem.* ***112***, 139-142.

234. Nagar, M., and Bearne, S. L. (2015) An additional role for the Brønsted acid-base catalysts of mandelate racemase in transition state stabilization. *Biochemistry* ***54***, 6743-6752.

235. Rudnick, G., and Abeles, R. H. (1975) Reaction mechanism and structure of the active site of proline racemase. *Biochemistry* ***14***, 4515-4522.

236. Dakoji, S., Shin, I., Battaile, K. P., Vockley, J., and Liu, H. W. (1997) Redesigning the active-site of an acyl-CoA dehydrogenase: New evidence supporting a one-base mechanism. *Bioorg. Med. Chem.* ***5***, 2157-2164.

237. Tu, C., Silverman, D. N., Forsman, C., Jonsson, B. H., and Lindskog, S. (1989) Role of histidine 64 in the catalytic mechanism of human carbonic anhydrase II studied with a site-specific mutant. *Biochemistry* ***28***, 7913-7918.

238. Roy, A., and Taraphder, S. (2006) Proton transfer pathways in the mutant His-64-Ala of human carbonic anhydrase II. *Biopolymers* ***82***, 623-630.

239. Mikulski, R., West, D., Sippel, K. H., Avvaru, B. S., Aggarwal, M., Tu, C., McKenna, R., and Silverman, D. N. (2013) Water networks in fast proton transfer during catalysis by human carbonic anhydrase II. *Biochemistry* ***52***, 125-131.

240. Heilbron, I., Jones, E. R. H., and Sondheimer, F. (1949) Researches on acetylenic compounds. Part XV. The oxidation of primary acetylenic carbinols and glycols. *J. Chem. Soc.*, 604-607.

241. Horne, G., and Potter, B. V. L. (2001) Synthesis of the enantiomers of 6-deoxy-*myo*-inositol 1,3,4,5-tetrakisphosphate, structural analogues of *myo*-inositol 1,3,4,5-tetrakisphosphate. *Chemistry* ***7***, 80-87.

242. Mills, S. J., and Potter, B. V. L. (1996) Synthesis of D- and L-*myo*-inositol 1,4,6-trisphosphate, regioisomers of a ubiquitous second messenger. *J. Org. Chem.* ***61***, 8980-8987.

243. Pelletier, G., Bechara, W. S., and Charette, A. B. (2010) Controlled and chemoselective reduction of secondary amides. *J. Am. Chem. Soc.* ***132***, 12817-12819.

244. Laemmli, U. K. (1970) Cleavage of structural proteins during the assembly of the head of bacteriophage T4. *Nature* ***227***, 680-685.

245. Malik, S. S., and Shrivastava, T. (2013) Protein characterization using modern biophysical techniques. In: Ashraf, G. M., and Sheikh, I. A. ed. *Advances in protein chemistry*. Foster City: OMICS Group eBooks. 10-11.

246. Johnson, K. A., and Goody, R. S. (2011) The original Michaelis constant: Translation of the 1913 Michaelis-Menten paper. *Biochemistry **50***, 8264-8269.

247. Michaelis, L., and Menten, M. L. (1913) Die kinetik der invertinwirkung. *Biochem. Z. **49***, 333-369.

248. Lineweaver, H., and Burk, D. (1934) The determination of enzyme dissociation constants. *J. Am. Chem. Soc. **56***, 658-666.

249. Ferrié, L., Reymond, S., Capdevielle, P., and Cossy, J. (2006) Total synthesis of (-)-spongidepsin. *Org. Lett. **8***, 3441-3443.

250. Fürstner, A., Kattnig, E., and Lepage, O. (2006) Total syntheses of amphidinolide X and Y. *J. Am. Chem. Soc. **128***, 9194-9204.

251. Clough, J. M., Dube, H., Martin, B. J., Pattenden, G., Reddy, K. S., and Waldron, I. R. (2006) Total synthesis of myxothiazols, novel bis-thiazole β-methoxyacrylate-based anti-fungal compounds from myxobacteria. *Org. Biomol. Chem. **4***, 2906-2911.

8 Appendices

8.1 Appendix 1: Protein sequences of MCR and human AMACR

```
MCR             MAGPLSGLRVVELAGIGPGPHAAMILGDLGADVVRIDRPSSVDGISRDAMLRNRRIVTAD
AMACR           --MALQGISVVELSGLAPGPFCAMVLADFGARVVRVDRPGSRYDVSR--LGRGKRSLVLD

MCR             LKSDQGLELALKLIAKADVLIEGYRPGVTERLGLGPEECAKVNDRLIYARMTGWGQTGPR
AMACR           LKQPRGAAVLRRLCKRSDVLLEPFRRGVMEKLQLGPEILQRENPRLIYARLSGFGQSGSF

MCR             SQQAGHDINYISLNGILHAIGRGDERPVPPLNLVGDFGGGSMFLLVGILAALWERQSSGK
AMACR           CRLAGHDINYLALSGVLSKIGRSGENPYAPLNLLADFAGGGLMCALGIIMALFDRTRTGK

MCR             GQVVDAAMVDGSSVLIQMMWAMRATGMWTDTRGANMLDGGAPYYDTYECADGRYVAVGAI
AMACR           GQVIDANMVEGTAYLSSFLWKTQKSSLWEAPRGQNMLDGGAPFYTTYRTADGEFMAVGAI

MCR             EPQFYAAMLAGLGLDAAELPPQNDRARWPELRALLTEAFASHDRDHWGAVFANSDACVTP
AMACR           EPQFYELLIKGLGLKSDELPNQMSMDDWPEMKKKFADVFAKKTKAEWCQIFDGTDACVTP

MCR             VLAFGEVHNEPHIIERNTFYEANG---GWQPMPAPRFSRTASSQPRPPAATIDIEAVLTD
AMACR           VLTFEEVVHHDHNKERGSFITSEEQDVSPRPAPLLLNTPAIPSFKRDPFIGEHTEEILEE

MCR             WDG----------------------
AMACR           FGFSREEIYQLNSDKIIESNKVKASL
```

8.2 Appendix 2: Kinetic analyses of wild-type AMACR with *R*-2-methyldecanoyl-CoA **44**

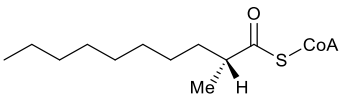

44

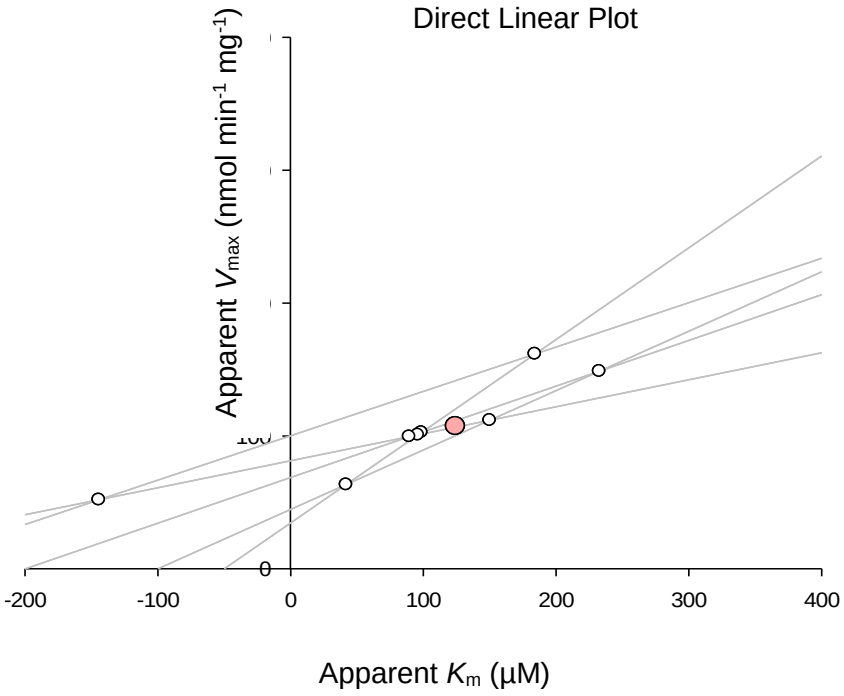

Kinetic parameters from Direct Linear Plot: K_m = 124 μM, V_{max} = 107 nmol min^{-1} mg^{-1}

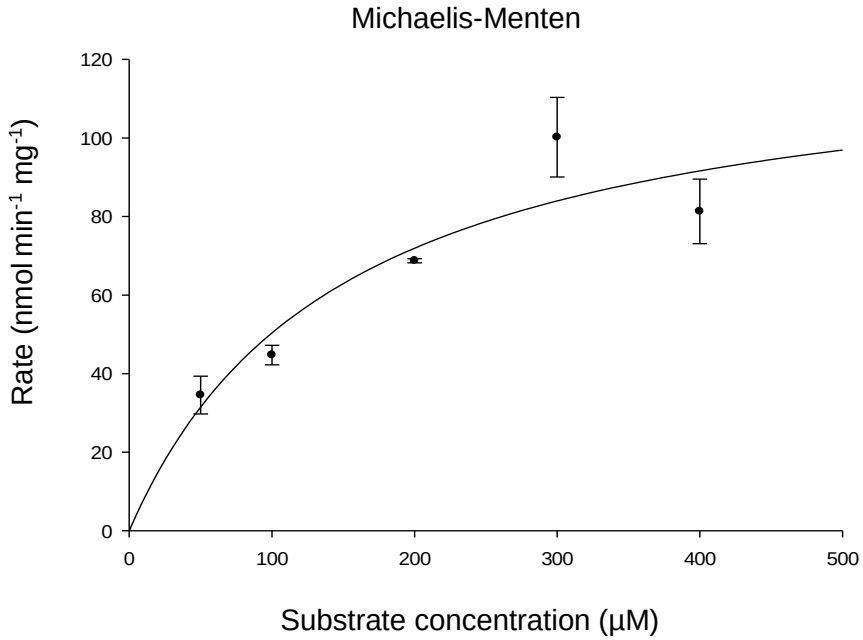

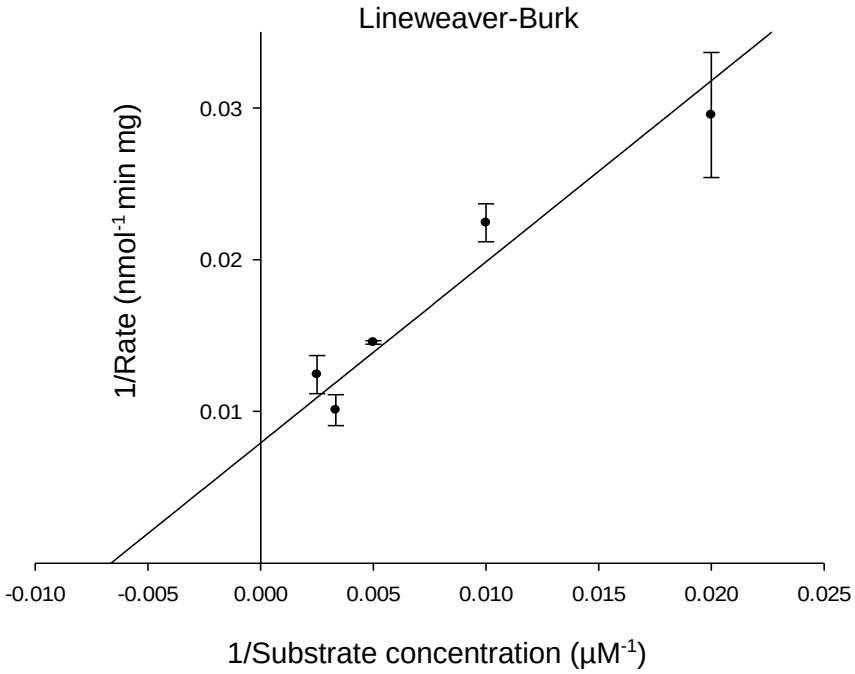
Lineweaver-Burk
1/Rate (nmol-1 min mg)
0.03
0.02
0.01
-0.010
-0.005
0.000
0.005
0.010
0.015
0.020
0.025
1/Substrate concentration (µM-1)

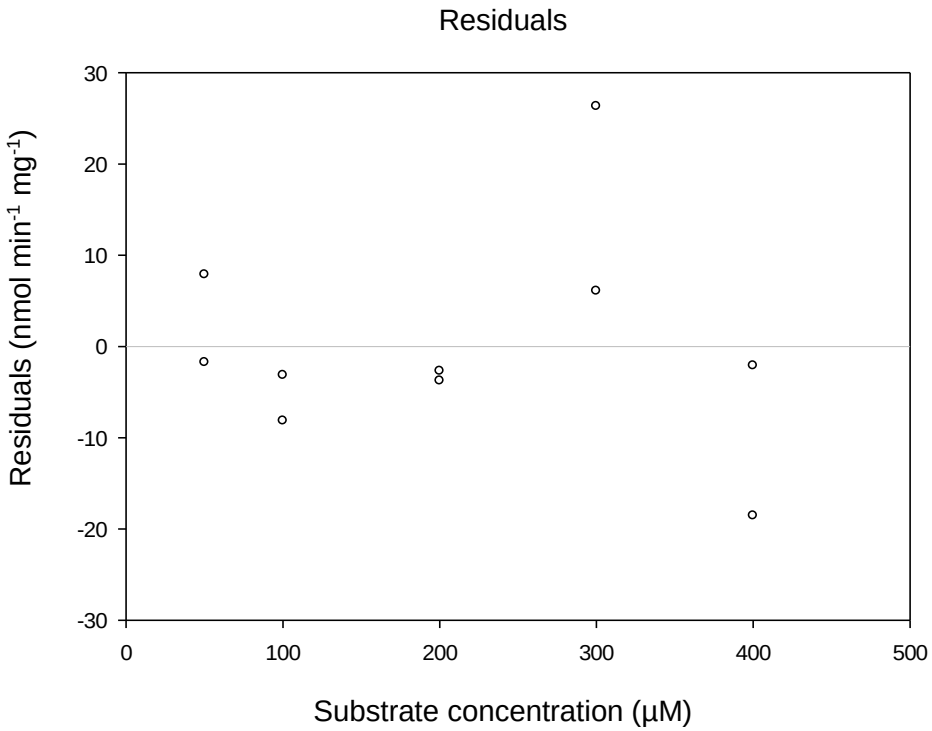
Residuals
Residuals (nmol min-1 mg-1)
30
20
10
0
-10
-20
-30
0
100
200
300
400
500
Substrate concentration (µM)

Kinetic parameters (Michaelis-Menten Plot)

	Value	±Std. Error	95% Conf. Interval
V_{max} (nmol min^{-1} mg^{-1})	126.0946	22.6514	73.8592 to 178.3300
K_m (µM)	150.4509	67.7755	-5.8431 to 306.7449

Goodness of Fit

Degrees of Freedom	8
AICc	58.214
R^2	0.797
Sum of Squares	1,241.410
Sy.x	12.457
Runs Test p Value	0.256

Data

Number of x values	5
Number of replicates	2
Total number of values	10
Number of missing values	0

8.3 Appendix 3: Kinetic analyses of wild-type AMACR with *S*-2-methyldecanoyl-CoA **38**

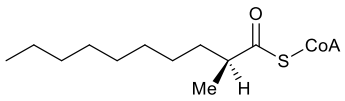

38

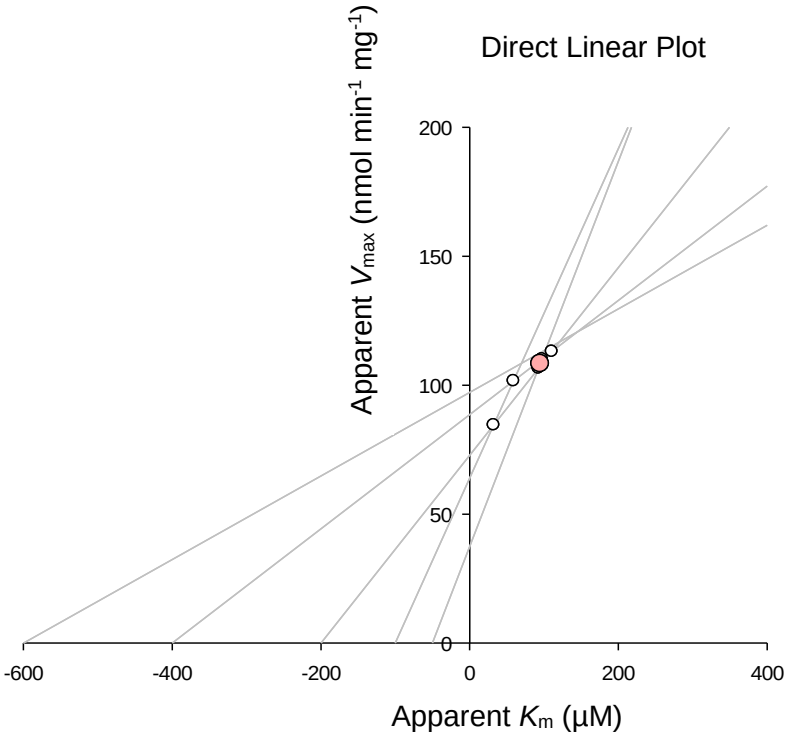

Kinetic parameters from Direct Linear Plot: K_m = 95 µM, V_{max} = 108 nmol min^{-1} mg^{-1}

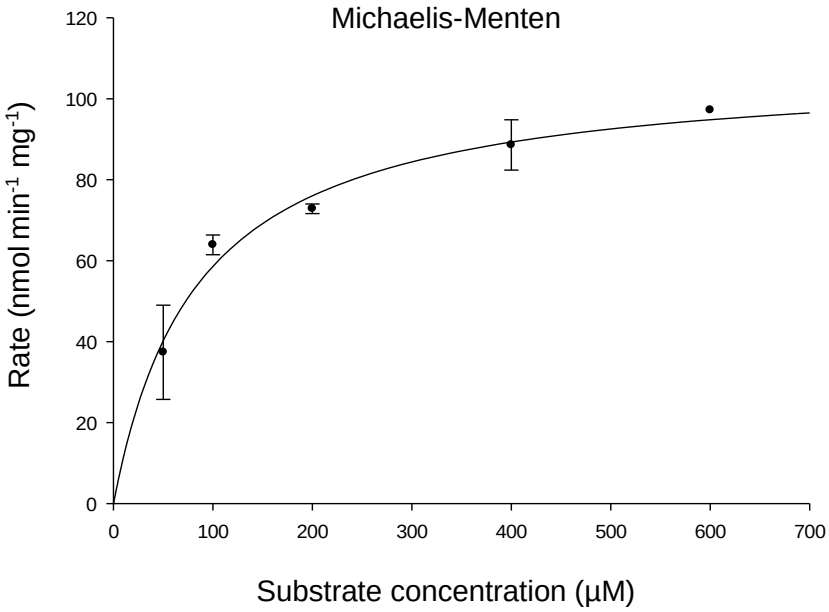

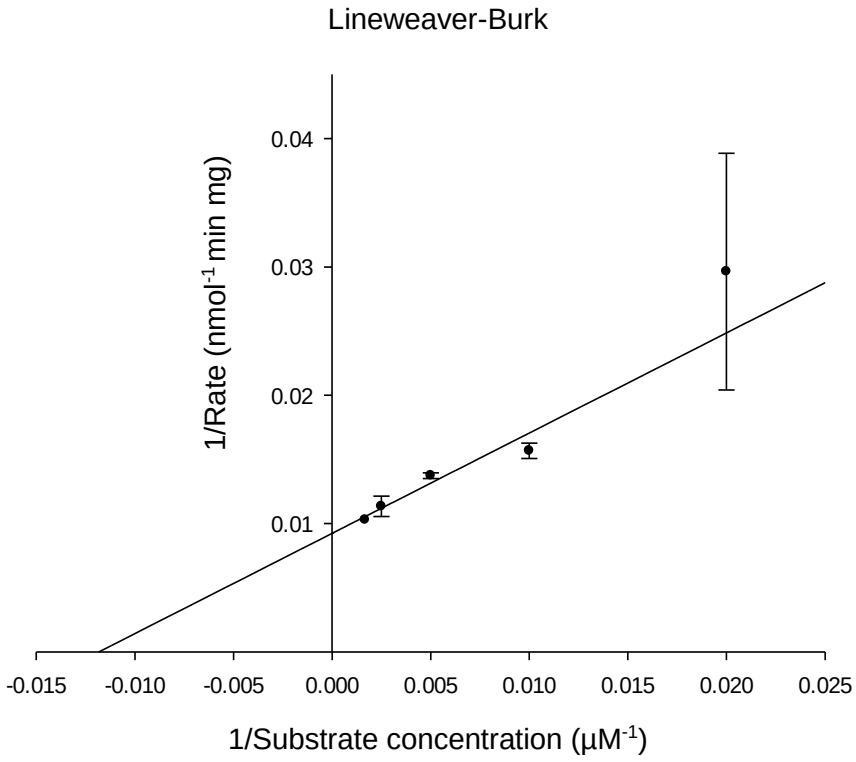
Lineweaver-Burk
1/Rate (nmol-1 min mg)
0.04
0.03
0.02
0.01
-0.015
-0.010
-0.005
0.000
0.005
0.010
0.015
0.020
0.025
1/Substrate concentration (µM-1)

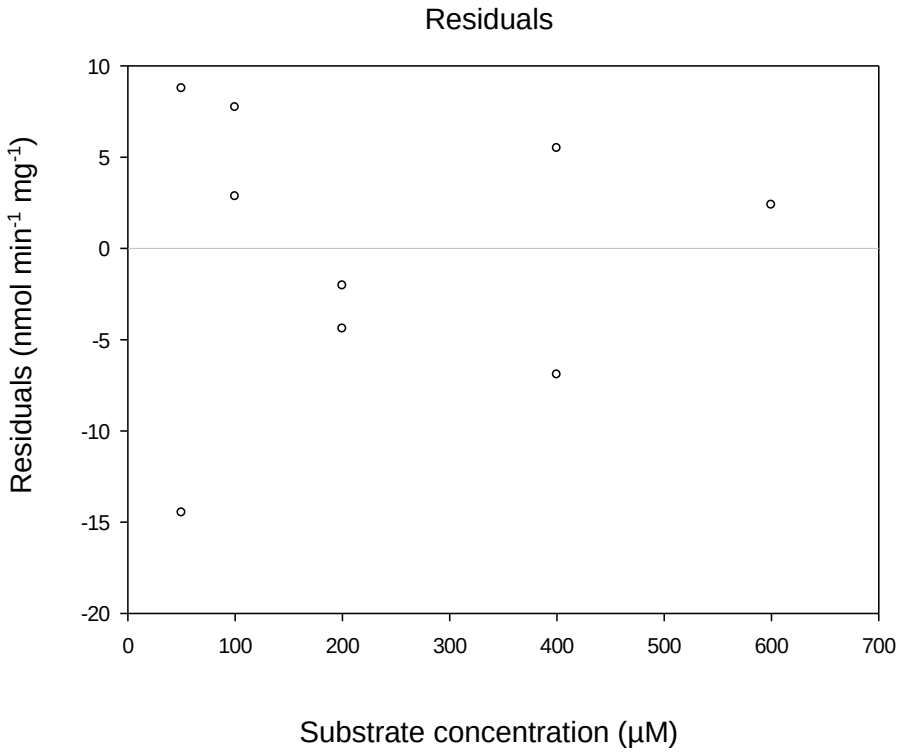
Residuals
Residuals (nmol min-1 mg-1)
10
5
0
-5
-10
-15
-20
0
100
200
300
400
500
600
700
Substrate concentration (µM)

Kinetic parameters (Michaelis-Menten Plot)

	Value	±Std. Error	95% Conf. Interval
V_{max} (nmol min^{-1} mg^{-1})	108.1721	8.4738	88.1344 to 128.2098
K_m (µM)	84.4831	21.6391	33.3136 to 135.6527

Goodness of Fit

Degrees of Freedom	7
AICc	46.238
R^2	0.885
Sum of Squares	461.656
Sy.x	8.121
Runs Test p Value	0.130

Data

Number of x values	5
Number of replicates	2
Total number of values	9
Number of missing values	1

8.4 Appendix 4: Kinetic analysis of the M184A mutant with *S*-2-methyldecanoyl-CoA **38**

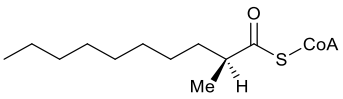

38

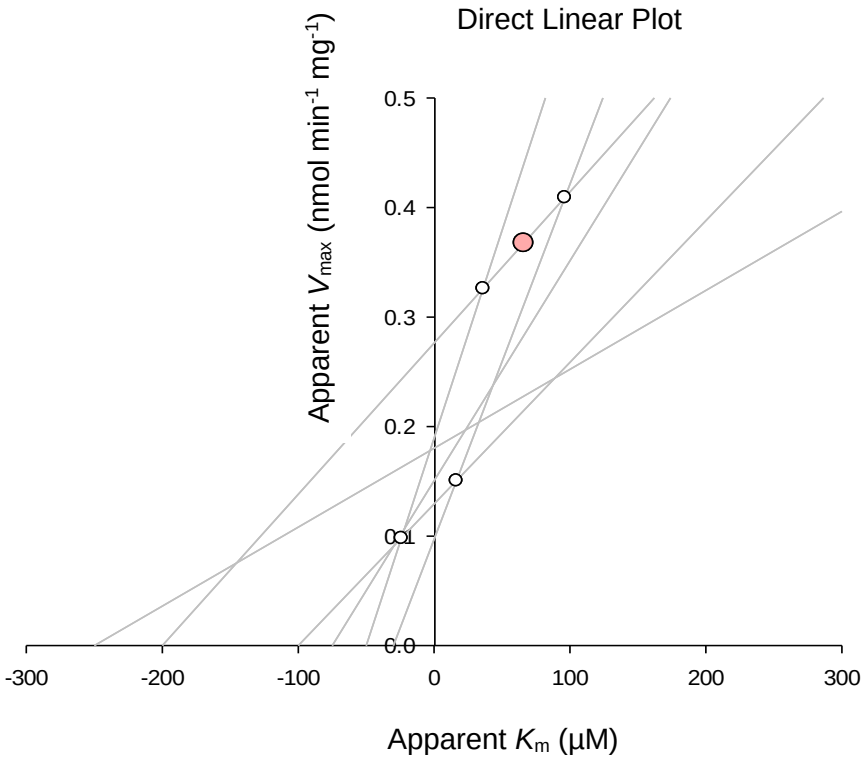

Direct Linear Plot failed to converge to give K_m and V_{max} values.

8.5 Appendix 5: Kinetic analyses of wild-type AMACR with 3-(2,4-dinitrophenoxy)-2-methylpropanoyl-CoA **135** substrate

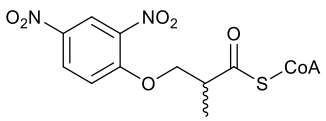

135

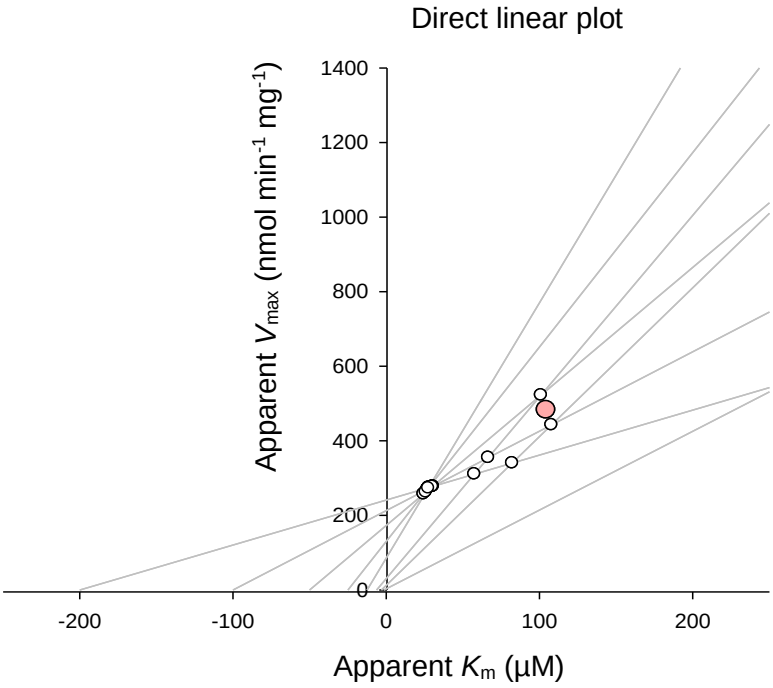

Kinetic parameters from Direct Linear Plot: K_m = 27 µM, V_{max} = 274 nmol min^{-1} mg^{-1}, manually obtained from Direct Linear Plot as the data does not converge

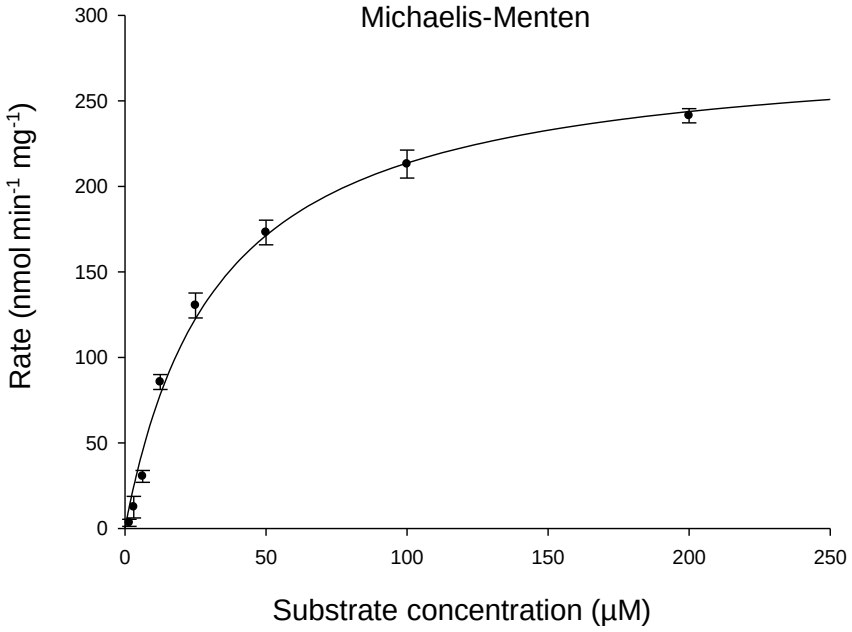

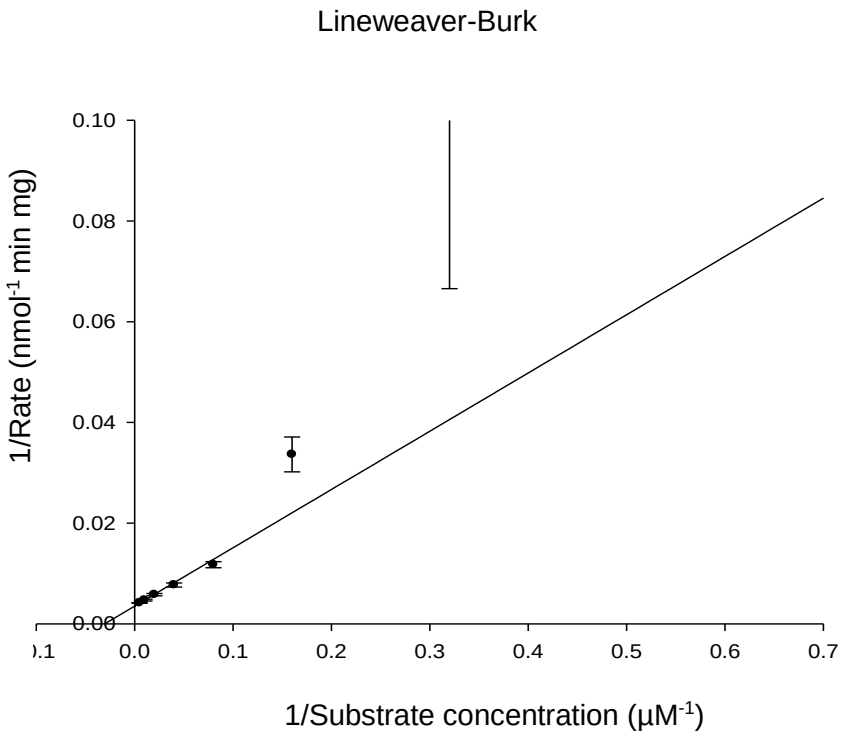
Lineweaver-Burk
0.10
0.08
0.06
0.04
0.02
0.00
1/Rate (nmol-1 min mg)
.1
0.0
0.1
0.2
0.3
0.4
0.5
0.6
0.7
1/Substrate concentration (µM-1)

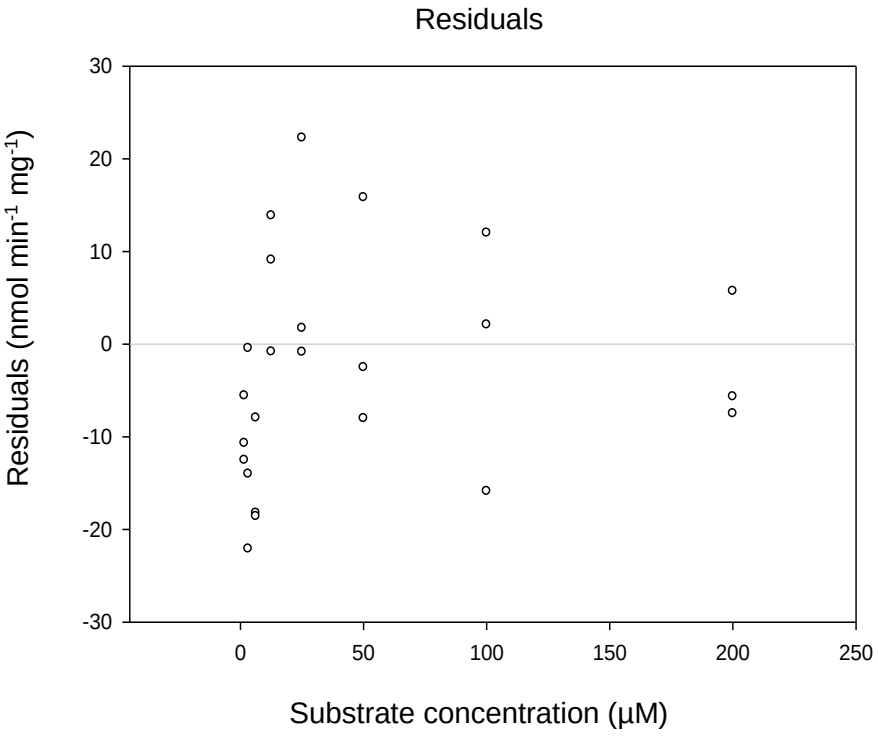
Residuals
30
20
10
0
-10
-20
-30
Residuals (nmol min-1 mg-1)
0
50
100
150
200
250
Substrate concentration (µM)

Kinetic parameters (Michaelis-Menten Plot)

	Value	±Std. Error	95% Conf. Interval
V_{max} (nmol min^{-1} mg^{-1})	283.7937	9.8534	263.3584 to 304.2288
K_m (µM)	32.8497	3.3143	25.9761 to 39.7233

Goodness of Fit

Degrees of Freedom	22
AICc	125.687
R^2	0.982
Sum of Squares	3,344.267
Sy.x	12.329
Runs Test p Value	0.042

Data

Number of x values	8
Number of replicates	3
Total number of values	24
Number of missing value	0

8.6 Appendix 6: Kinetic analyses of the H122L mutant with 3-(2,4-dinitrophenoxy)-2-methylpropanoyl-CoA **135** substrate

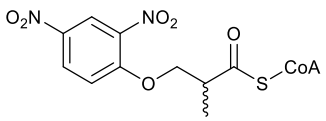

135

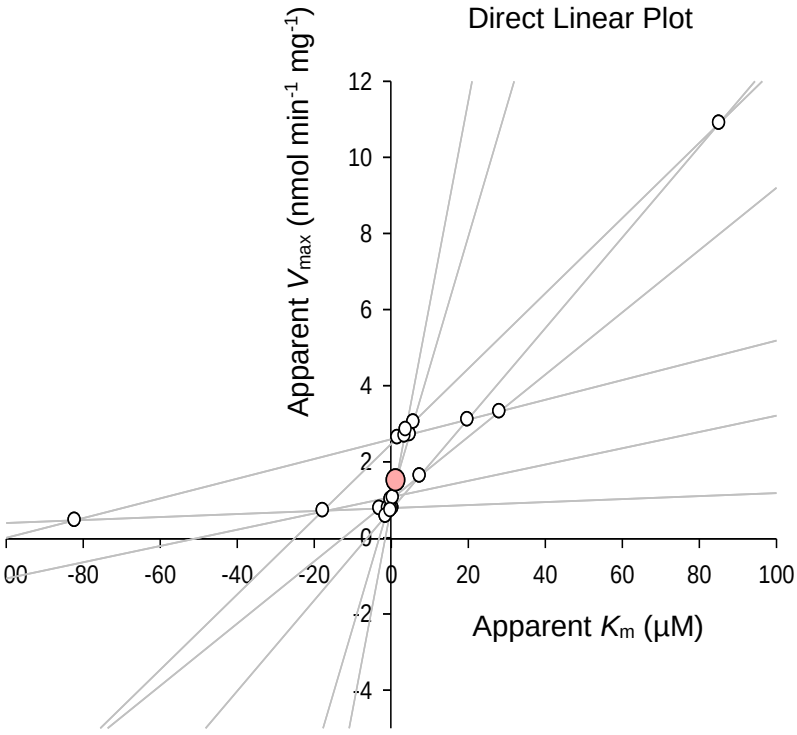

Kinetic parameters from Direct Linear Plot: K_m = 1.3 µM, V_{max} = 1.5 nmol min^{-1} mg^{-1}.

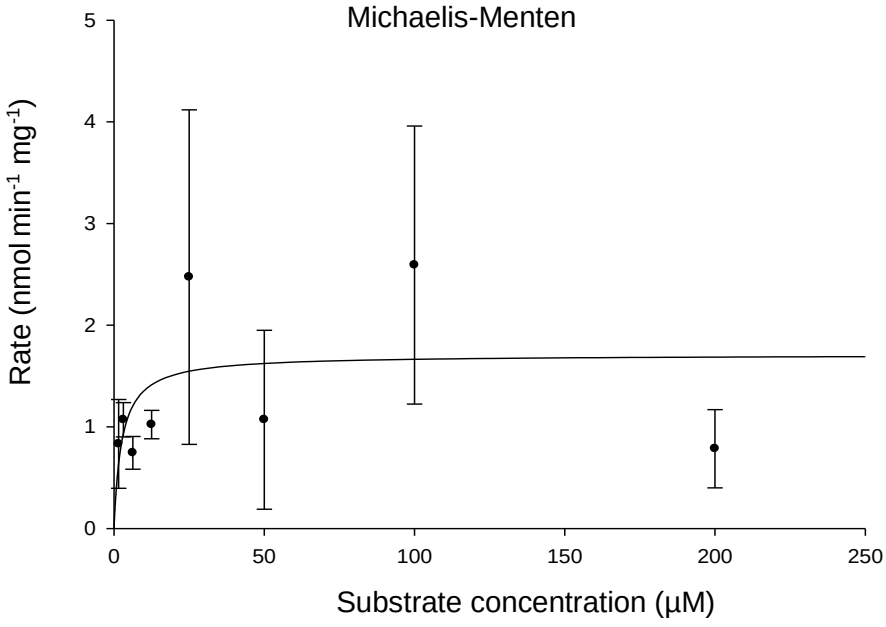

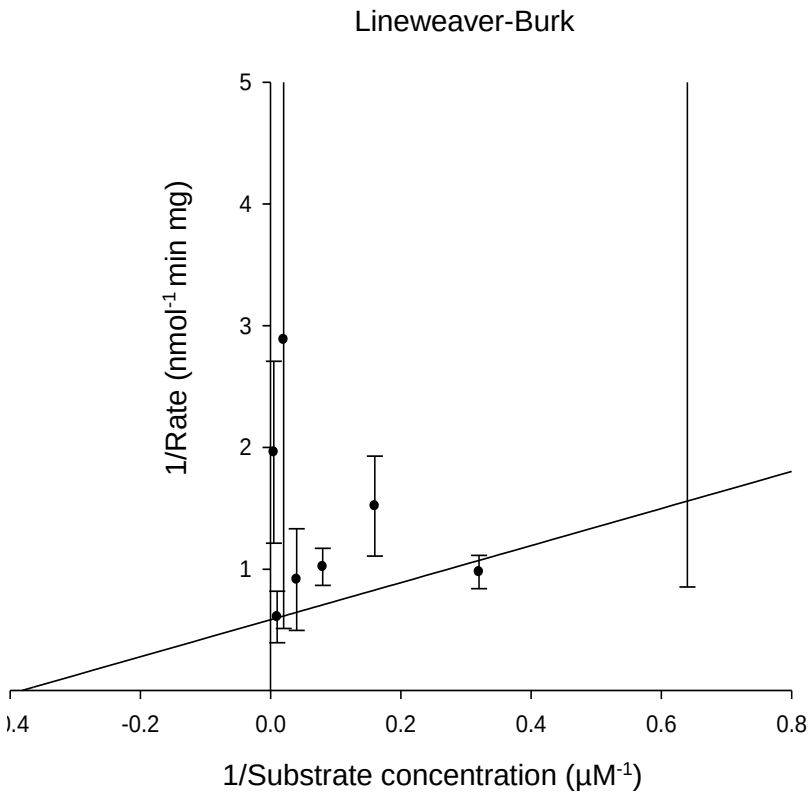
Lineweaver-Burk
1/Rate (nmol-1 min mg)
1/Substrate concentration (µM-1)
5
4
3
2
1
-0.4
-0.2
0.0
0.2
0.4
0.6
0.8

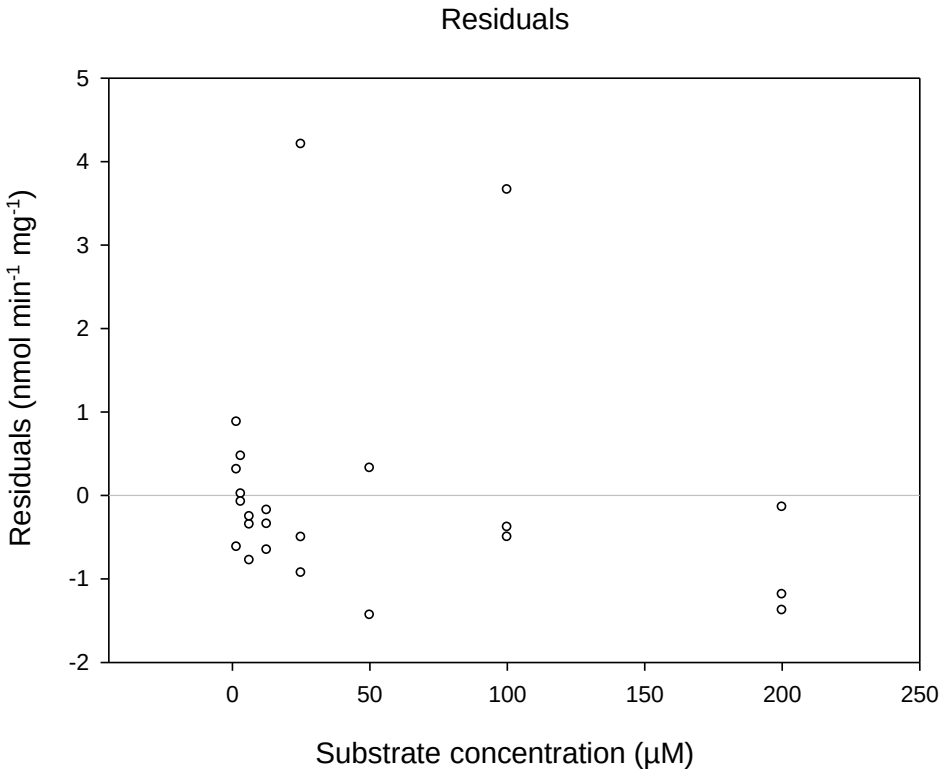
Residuals
Residuals (nmol min-1 mg-1)
Substrate concentration (µM)
5
4
3
2
1
0
-1
-2
0
50
100
150
200
250

Kinetic parameters (Michaelis-Menten Plot)

	Value	±Std. Error	95% Conf. Interval
V_{max} (nmol min^{-1} mg^{-1})	1.7078	0.4764	0.7171 to 2.6985
K_m (µM)	2.5984	3.7145	-5.1265 to 10.3232

Goodness of Fit

Degrees of Freedom	21
AICc	20.533
R^2	5.784e-2
Sum of Squares	40.954
Sy.x	1.396
Runs Test p Value	0.188

Data

Number of x values	8
Number of replicates	3
Total number of values	23
Number of missing values	1

8.7 Appendix 7: Kinetic analyses of the D152N mutant with 3-(2,4-dinitrophenoxy)-2-methylpropanoyl-CoA **135** substrate

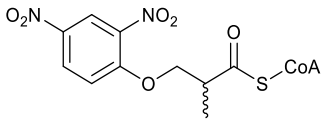

135

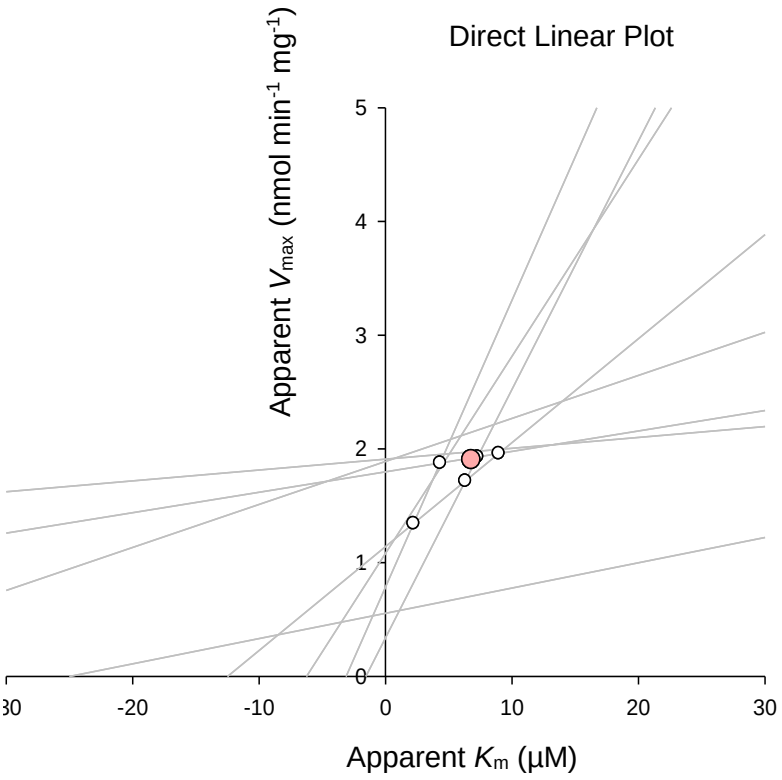

Kinetic parameters from Direct Linear Plot: K_m = 6.8 µM, V_{max} = 1.9 nmol min^{-1} mg^{-1}

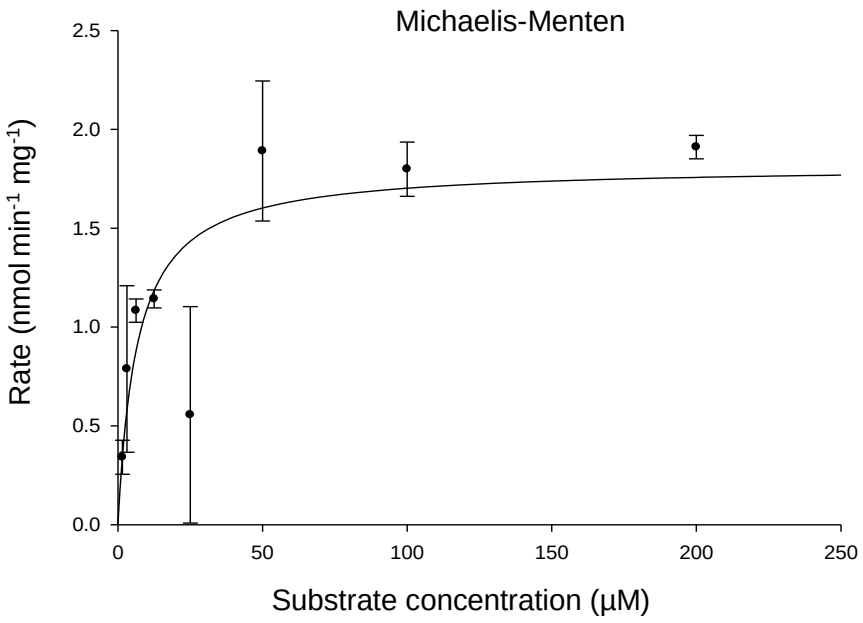

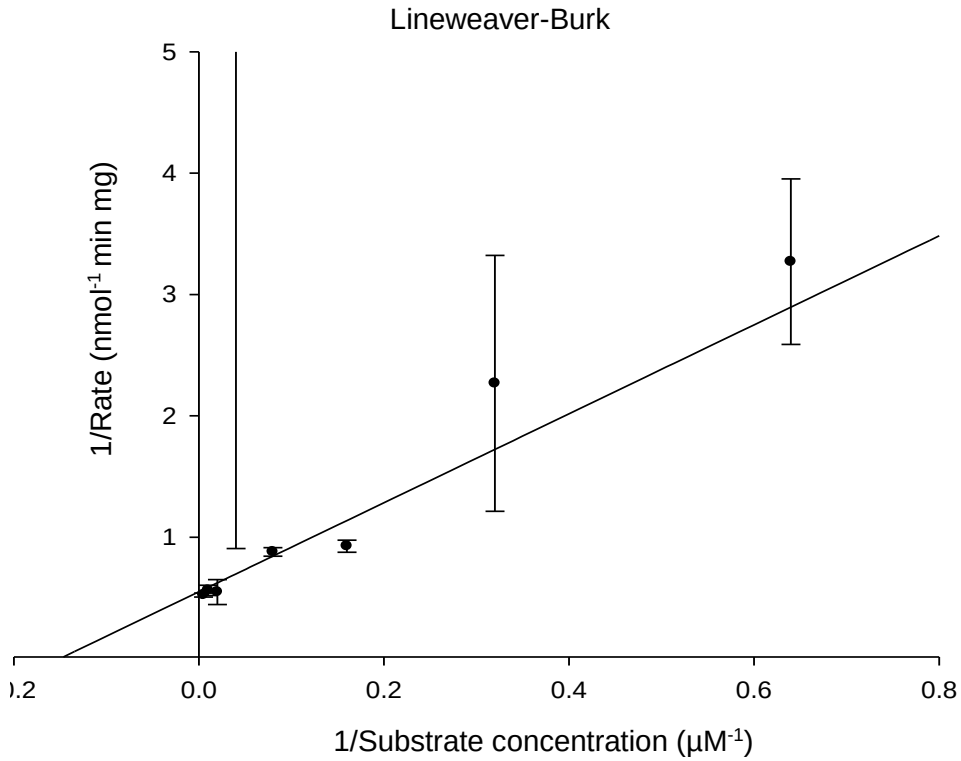
Lineweaver-Burk
1/Rate (nmol-1 min mg)
5
4
3
2
1
0.2
0.0
0.2
0.4
0.6
0.8
1/Substrate concentration (µM-1)

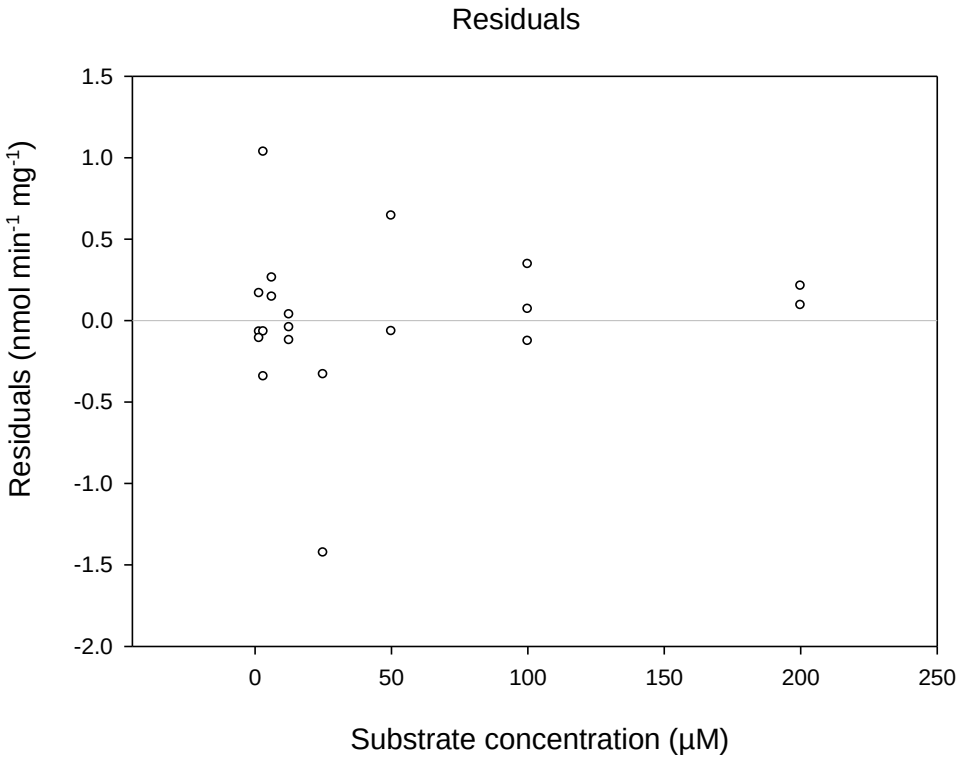
Residuals
Residuals (nmol min-1 mg-1)
1.5
1.0
0.5
0.0
-0.5
-1.0
-1.5
-2.0
0
50
100
150
200
250
Substrate concentration (µM)

Kinetic parameters (Michaelis-Menten Plot)

	Value	±Std. Error	95% Conf. Interval
V_{max} (nmol min^{-1} mg^{-1})	1.8156	0.2184	1.3568 to 2.2745
K_m (µM)	6.6551	3.2337	-0.1388 to 13.4490

Goodness of Fit

Degrees of Freedom	18
AICc	-24.188
R^2	0.528
Sum of Squares	4.101
Sy.x	0.477
Runs Test p Value	0.323

Data

Number of x values	8
Number of replicates	3
Total number of values	20
Number of missing values	4

8.8 Appendix 8: Kinetic analyses of the M184A mutant with 3-(2,4-dinitrophenoxy)-2-methylpropanoyl-CoA **135** substrate

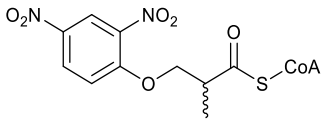

135

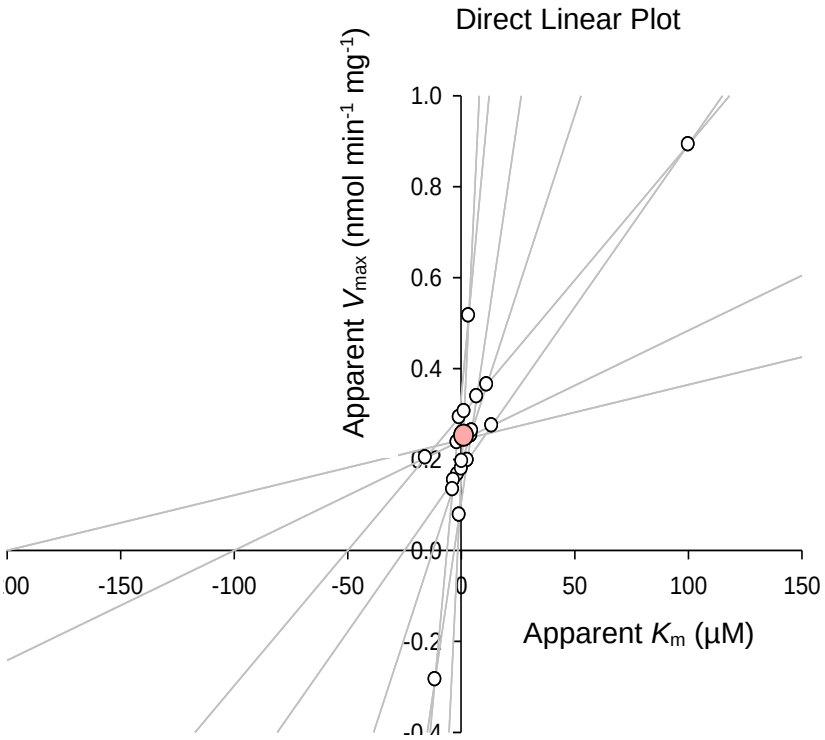

Kinetic parameters from Direct Linear Plot: K_m = 1.3 µM, V_{max} = 0.3 nmol min^{-1} mg^{-1}

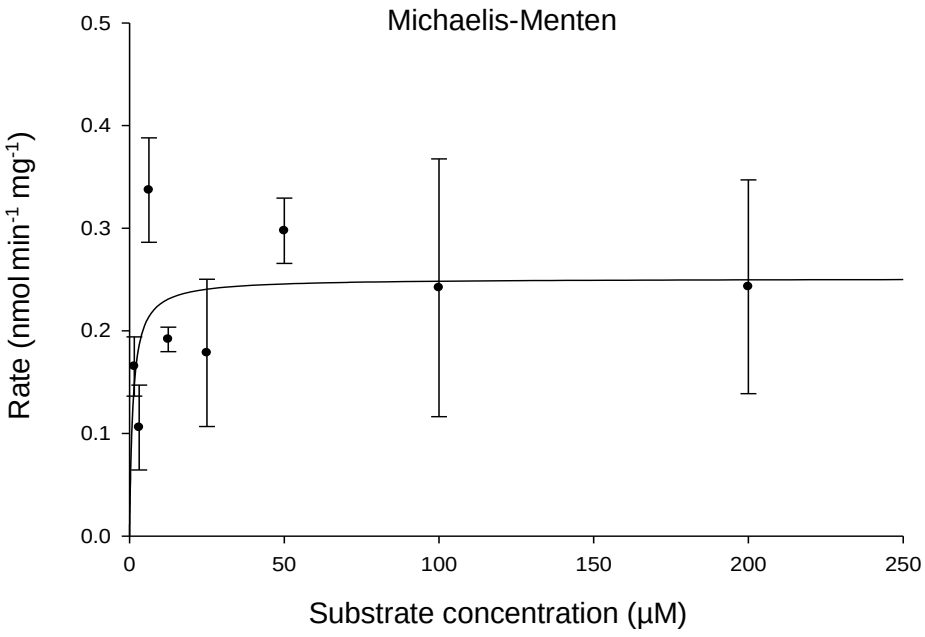

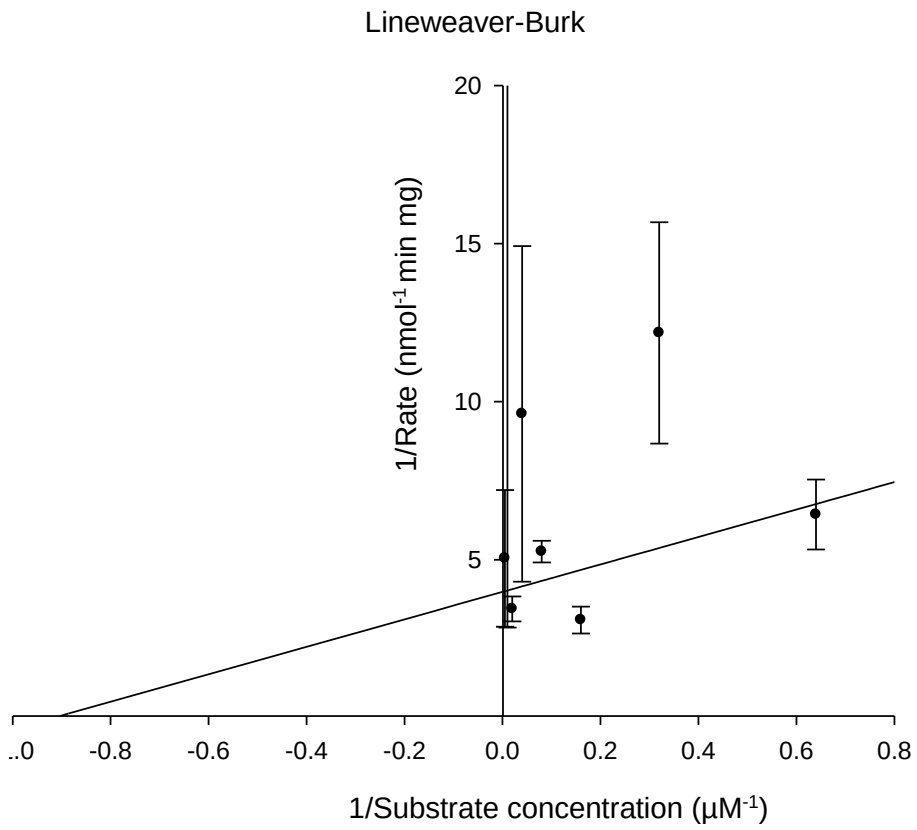
Lineweaver-Burk
20
15
10
5
1/Rate (nmol-1 min mg)
..0
-0.8
-0.6
-0.4
-0.2
0.0
0.2
0.4
0.6
0.8
1/Substrate concentration (µM-1)

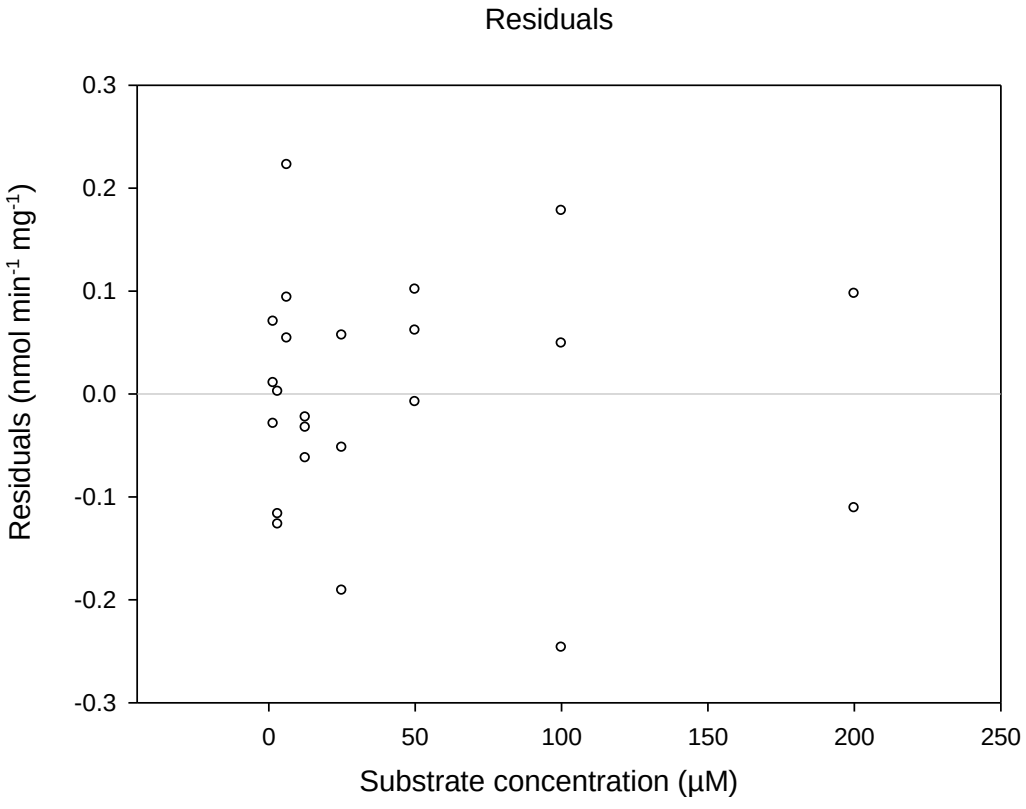
Residuals
0.3
0.2
0.1
0.0
-0.1
-0.2
-0.3
Residuals (nmol min-1 mg-1)
0
50
100
150
200
250
Substrate concentration (µM)

Kinetic parameters (Michaelis-Menten Plot)

	Value	±Std. Error	95% Conf. Interval
V_{max} (nmol min^{-1} mg^{-1})	0.2510	0.003488	0.1785 to 0.3236
K_m (µM)	1.0899	1.0740	-1.1436 to 3.3234

Goodness of Fit

Degrees of Freedom	21
AICc	-94.517
R^2	8.926e-2
Sum of Squares	0.275
Sy.x	0.115
Runs Test p Value	0.419

Data

Number of x values	8
Number of replicates	3
Total number of values	23
Number of missing values	1

8.9 Appendix 9: Kinetic analyses of the E237A mutant with 3-(2,4-dinitrophenoxy)-2-methylpropanoyl-CoA **135** substrate

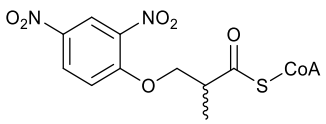

135

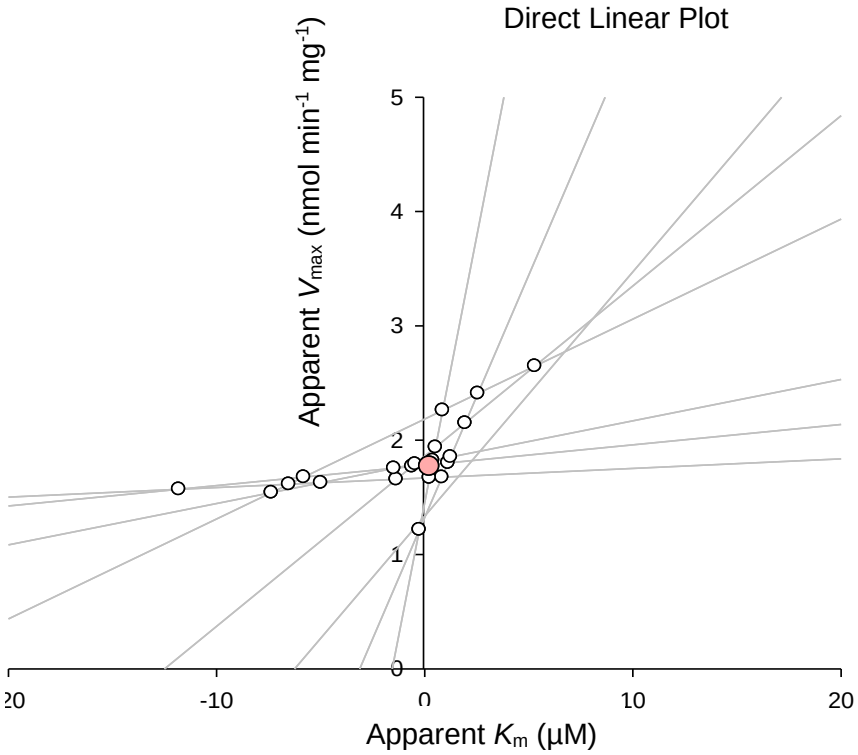

Kinetic parameters from Direct Linear Plot: K_m = 0.2 µM, V_{max} = 1.8 nmol min^{-1} mg^{-1}

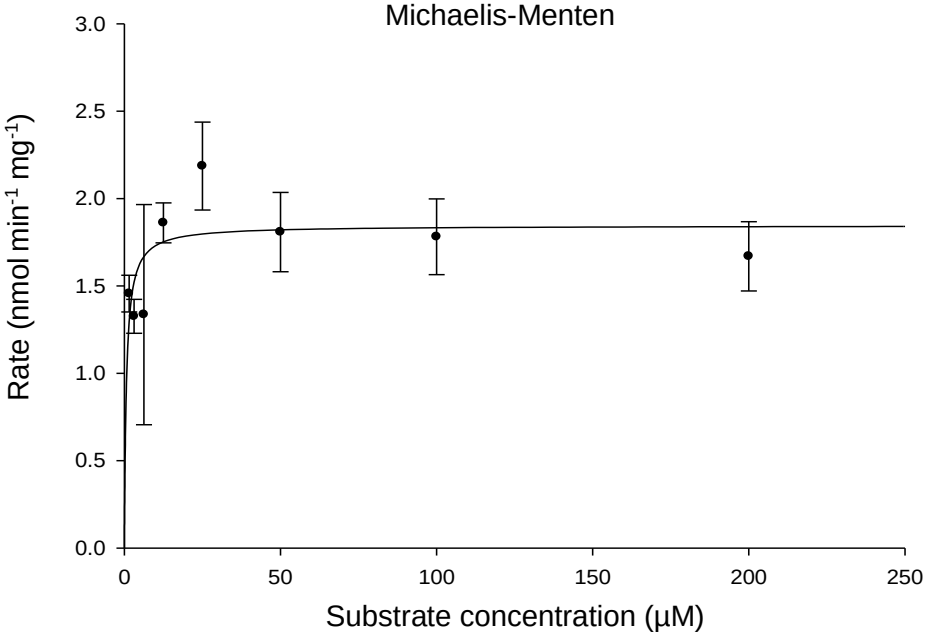

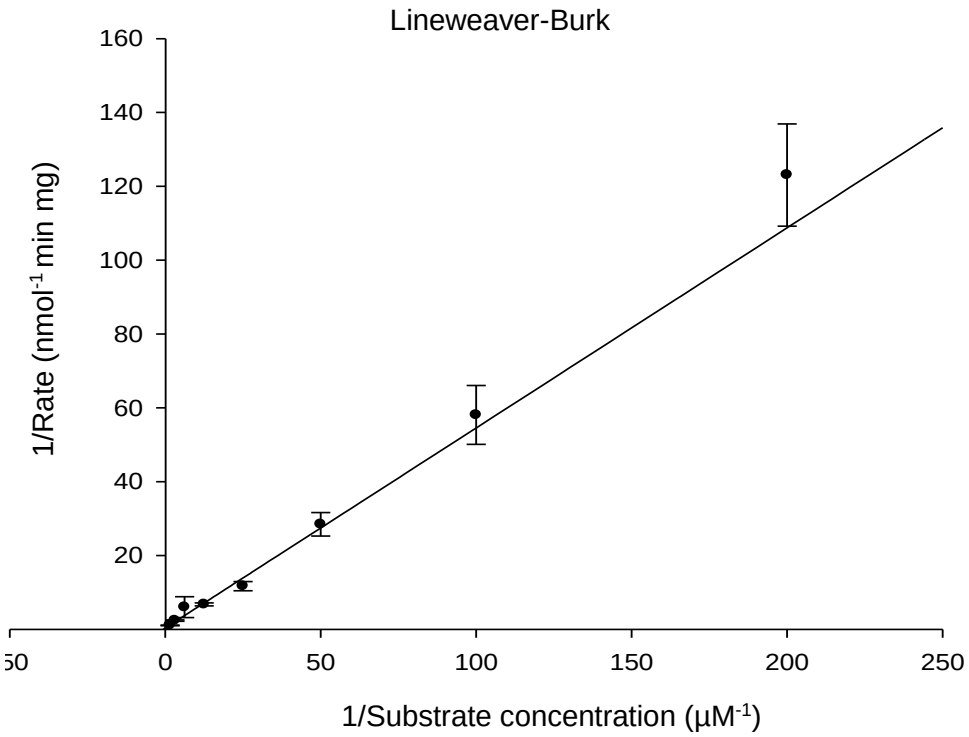
Lineweaver-Burk
160
140
120
100
80
60
40
20
1/Rate (nmol-1 min mg)
50
0
50
100
150
200
250
1/Substrate concentration (µM-1)

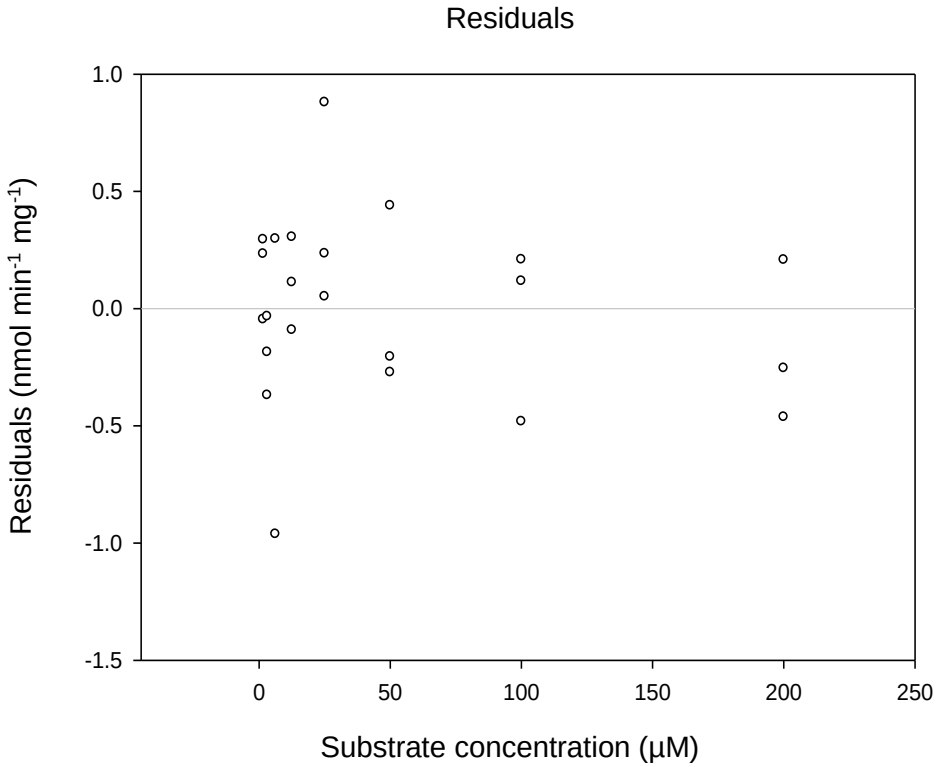
Residuals
1.0
0.5
0.0
-0.5
-1.0
-1.5
Residuals (nmol min-1 mg-1)
0
50
100
150
200
250
Substrate concentration (µM)

Kinetic parameters (Michaelis-Menten Plot)

	Value	±Std. Error	95% Conf. Interval
V_{max} (nmol min^{-1} mg^{-1})	1.8450	0.1098	1.6166 to 2.0734
K_m (µM)	0.6633	0.3738	-0.1141 to 1.4407

Goodness of Fit

Degrees of Freedom	21
AICc	-38.137
R^2	0.182
Sum of Squares	3.195
Sy.x	0.390
Runs Test p Value	0.264

Data

Number of x values	8
Number of replicates	3
Total number of values	23
Number of missing values	1

8.10 Appendix 10: Kinetic analyses of the E237Q mutant with 3-(2,4-dinitrophenoxy)-2-methylpropanoyl-CoA **135** substrate

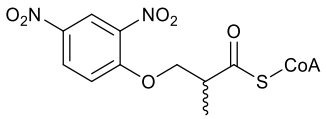

135

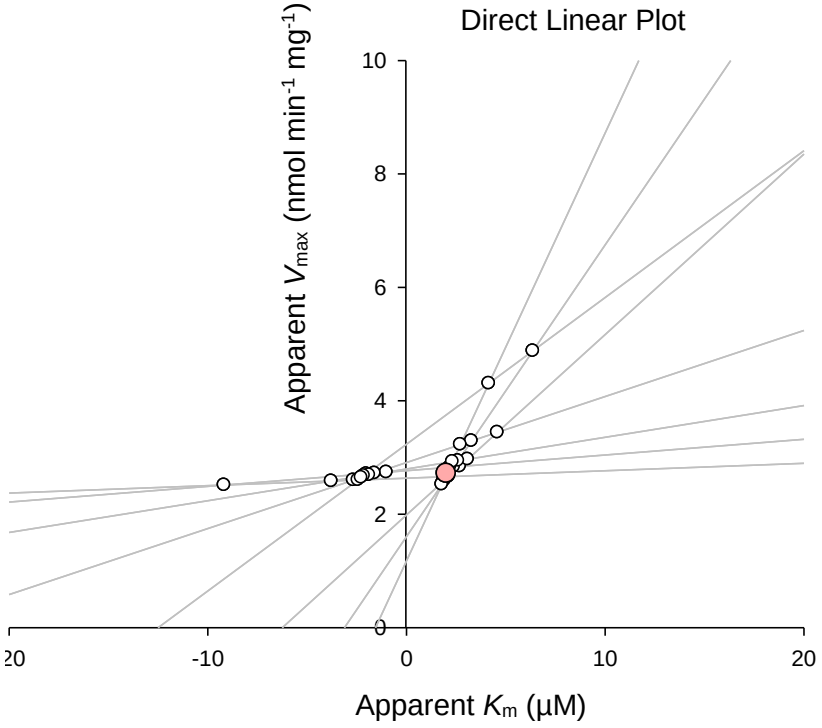

Kinetic parameters from Direct Linear Plot: K_m = 2.0 µM, V_{max} = 2.7 nmol min^{-1} mg^{-1}

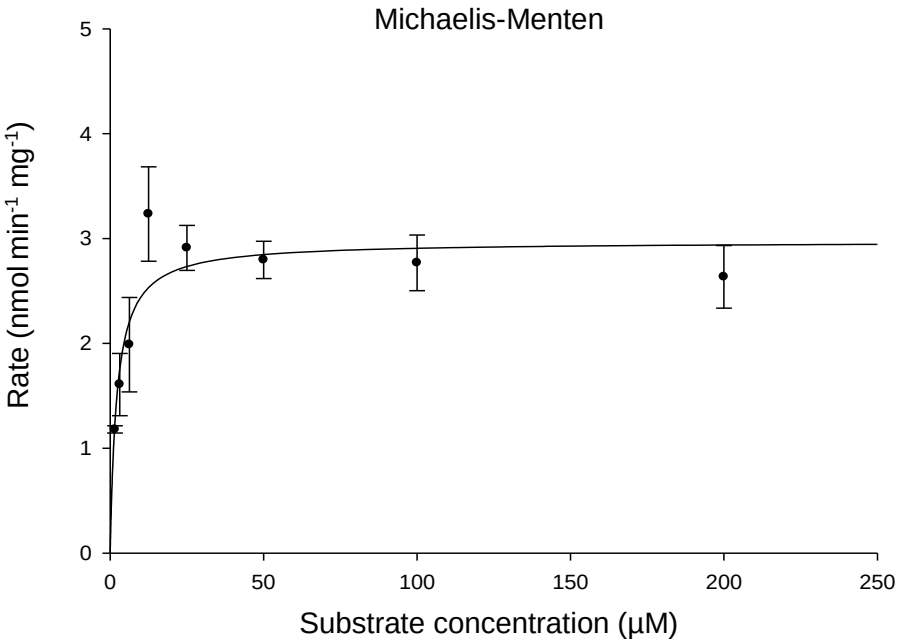

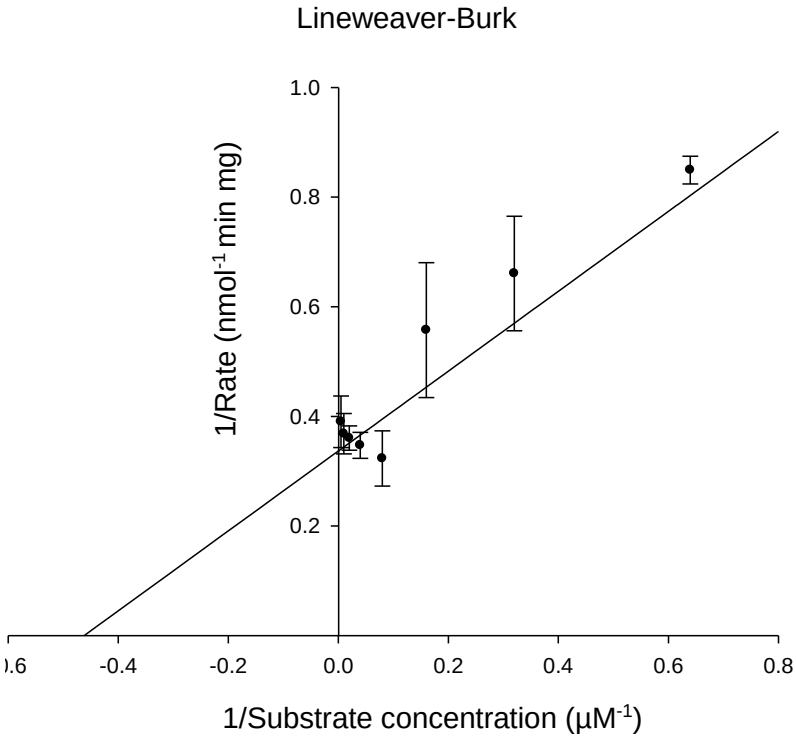
Lineweaver-Burk
1/Rate (nmol-1 min mg)
1.0
0.8
0.6
0.4
0.2
.6
-0.4
-0.2
0.0
0.2
0.4
0.6
0.8
1/Substrate concentration (µM-1)

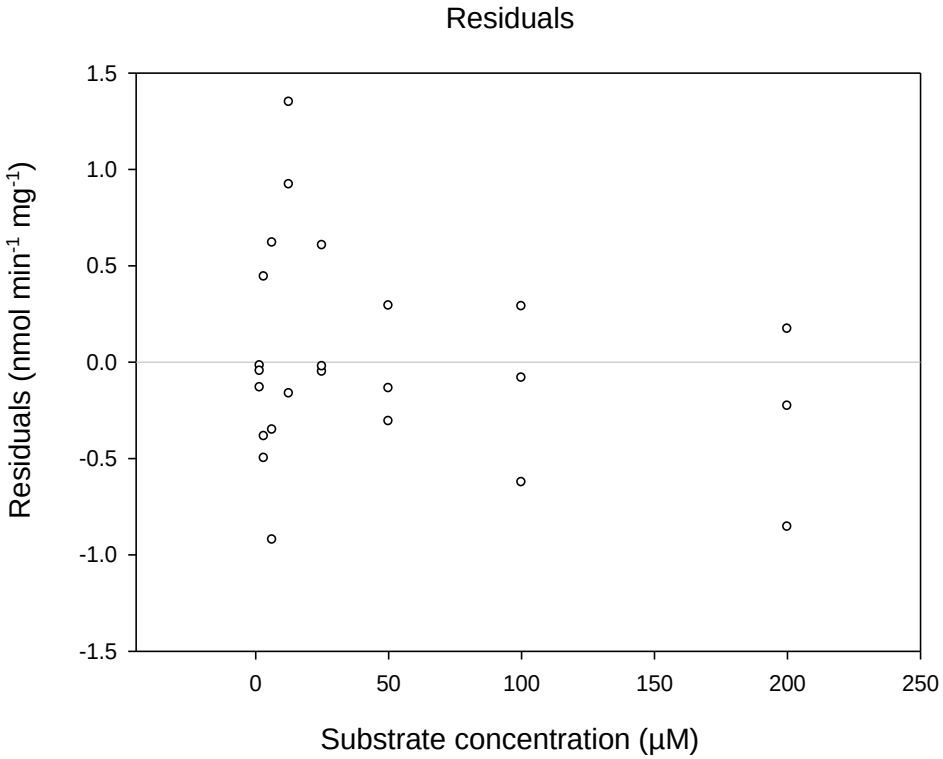
Residuals
Residuals (nmol min-1 mg-1)
1.5
1.0
0.5
0.0
-0.5
-1.0
-1.5
0
50
100
150
200
250
Substrate concentration (µM)

Kinetic parameters (Michaelis-Menten Plot)

	Value	±Std. Error	95% Conf. Interval
V_{max} (nmol min^{-1} mg^{-1})	2.9701	0.1740	2.6094 to 3.3309
K_m (µM)	2.1647	0.7059	0.7006 to 3.6287

Goodness of Fit

Degrees of Freedom	22
AICc	-24.058
R^2	0.570
Sum of Squares	6.525
Sy.x	0.545
Runs Test p Value	0.501

Data

Number of x values	8
Number of replicates	3
Total number of values	24
Number of missing values	0

8.11 Appendix 11: List of presentations at conferences

Oral presentations

- 11 November 2015: 12th CR@B (Cancer Research at Bath) symposium, the University of Bath
- 9 June 2015: Faculty of science graduate school afternoon of research presentations, the University of Bath (2-minute lightning talk and poster)
- 29 April 2015: 26th Society of Chemical Industry (SCI) postgraduate symposium, the University of Sheffield
- 21 November 2014: RSC's protein and peptide science group (PPSG) early stage researcher meeting 2014, London
- 3 June 2014: Faculty of science graduate school afternoon of research presentations, the University of Bath
- 8 May 2013: Postgraduate 6-month research symposium, the University of Bath

Poster presentations

- 28 June-3 July 2015: European school of medicinal chemistry, Urbino, Italy
- 19 May 2015: RSC Chemical biology and bioorganic chemistry postgraduate symposium, the University of Bristol
- 22 April 2015: 11th CR@B symposium, the University of Bath
- 9 March 2015: SET for Britain, House of Commons, Westminster
- 18 February 2015: RSC organic division south-west regional meeting, the University of Reading
- 25-29 January 2015: 12th Winter conference on medicinal and bioorganic chemistry, Colorado, the United States of America
- 21 November 2014: RSC's PPSG early stage researcher meeting 2014, London
- 12 November 2014: 10th CR@B symposium, the University of Bath

8.12 Appendix 12: List of publications

1. Lee, G. L., Yevglevskis, M., Cozier, G., Thompson, A. S., Woodman T. J., and Lloyd, M. D. (2016) Active site residues of α-methylacyl-CoA racemase (AMACR; P504S) and their role in racemisation and elimination reactions, manuscript in preparation.

2. Yevglevskis, M., Lee, G. L., Nathubhai, A., Petrova, Y., James, T. D., Threadgill M. D., Woodman, T. J., and Lloyd, M. D. (2016) A convenient colorimetric assay for α-methylacyl-CoA racemase (AMACR; P504S) and characterization of inhibitors, manuscript in preparation.

3. Yevglevskis, M., Lee, G. L., Sun, J., Zhou, S., Sun, X., Kociok-Kohn, G., James, T. D., Woodman, T. J., and Lloyd, M. D. (2016) A study on the AMACR catalysed elimination reaction and its application to inhibitor testing, *Org. Biomol. Chem.* **14**, 612-622.

4. Lloyd, M. D., Woodman, T. J., Yevglevskis, M. Threadgill, M. D., and Lee, G. L. (2015) Methods (AMACR). UK Pat., 1200139240; World Pat., WO2015114383.

5. Yevglevskis, M., Lee, G. L., Threadgill, M. D., Woodman, T. J., and Lloyd, M. D. (2014) The perils of rational design – unexpected irreversible elimination of fluoride from 3-fluoro-2-methylacyl-CoA esters catalysed by α-methylacyl-CoA racemase (AMACR; P504S), *Chem. Comm.* **50**, 14164-14166.

6. Lloyd, M. D., Yevglevskis, M., Lee, G. L., Wood, P. J., Threadgill, M. D., and Woodman, T. J. (2013) α-Methylacyl-CoA racemase (AMACR): Metabolic enzyme, drug metabolizer and cancer marker P504S, *Prog. Lipid Res.* **52**, 220-230.